Author:
Kingston, Edward James

Title:
Advances in the deep-hole drilling technique for residual stress measurement

ADVANCES IN THE DEEP-HOLE DRILLING TECHNIQUE FOR RESIDUAL STRESS MEASUREMENT

BY

Edward James KINGSTON

A thesis submitted to the University of Bristol
in accordance with the requirements of
the degree of Doctor of Philosophy in the
Department of Mechanical Engineering
In the Faculty of Engineering

July 2003

Structural Integrity Research Team
Department of Mechanical Engineering
University of Bristol
Bristol BS8 1TR
United Kingdom

45,800

ABSTRACT

Most engineering components contain defects (e.g. cavities and cracks) which are usually generated during the manufacture process. During the service life of the component it is possible that the defects could grow leading to ultimate failure of the component. For safety critical engineering components, such as those used in nuclear power plant systems, rail track systems and aerospace systems, ultimate failure is not permitted. To eliminate failure, the structural integrity of the component is assessed using knowledge of both the applied and residual stress distributions present. The applied stress distributions are calculated, whereas the residual stress distributions are measured using methods like the deep-hole drilling technique.

The deep-hole drilling residual stress measurement technique was investigated to increase its accuracy and reliability in measuring the residual stress distributions present within components. It is a semi-invasive technique that involves drilling a small hole through the component and then the accurate diameter measurement thereof. A cylinder of material containing the hole is then extracted from the component causing the hole to deform due to the relaxation of the residual stresses present. The hole diameter is then re-measured and the change is used to determine the pre-existent residual stress distribution.

The applicability of the technique was extended through modifications made to the machining processes, to include both thicker and thinner components. The accuracy of the measurements recorded and analysis thereof were improved. A portable machine was made to carry out "on-site" deep-hole drilling residual stress measurements on large components.

Calibration experiments were carried out on components containing various known stress distributions to test the accuracy and modifications of the technique, and its applicability to different materials.

Finally, an extensive set of residual stress measurements were undertaken on different components varying in geometry and material composition to test the accuracy and reliability of the technique in comparison with alternative measurement methods.

ACKNOWLEDGEMENTS

There are a number people who have assisted me during the completion of this research to whom I would like to now express my thanks.

My sincere gratitude is expressed to my supervisors, Professor David Smith who has provided continuous advice with unceasing encouragement and understanding during the course of this research.

Dr. Chris Truman has also provided encouragement and support in the absence of Professor Smith for which I thank him.

I would like to express my gratitude to the Mechanical Engineering workshop and in particular Ian Milnes and Guy Pearn, who have provided technical expertise and help regarding the use and manufacture of the experimental equipment.

To all the members of Structural Integrity Research Team (SIRT), I would like to thank you for providing a dynamic and friendly atmosphere in which to work.

Finally, I would like to thank my family and especially my partner Caroline, for their love, encouragement and unreserved support throughout this work. I should also acknowledge Caroline's patience during this work.

AUTHOR'S DECLARATION

I declare that the work in this dissertation was carried out in accordance with the Regulations of the University of Bristol. The work is original except where indicated by special reference in the text and no part of the dissertation has been submitted for any other degree. Any views expressed in the dissertation are those of the author and in no way represent those of the University of Bristol. The dissertation has not been presented to any other University for examination either in the United Kingdom or overseas.

Edward James KINGSTON

July 2003

PUBLICATIONS

The following publications have presented research carried out during this project.

George D., Kingston E. and Smith D. J. – 2000 – **'Residual Stress Measurement In Thick Section Components'.** American Society Of Mechanical Engineers, Pressure Vessels And Piping Division (Publication), Vol. 410-1, Pp 275-282.

George, D., Kingston, E. and Smith, D. J. – 2002 – **'Measurement Of Through-Thickness Stresses Using Small Holes'.** Journal Of Strain Analysis, Vol. 37, No. 2, Pp 125-139

Thomas, A., Ehrlich, R., Kingston, E., and Smith, D. J. – 2002 – **'Measurement Of Residual Stresses In Steel Nozzle Intersections Containing Repair Welds'.** American Society Of Mechanical Engineers, Pressure Vessels And Piping Division (Publication) PVP, Vol. 434, Pp 67-72

Smith, D. J., Kingston, E., Thomas, A. and Ehrlich R. – 2002 – **'Residual Stress Measurements After Repair Welding'.** Third International HIDA And Integrity Conference On Integrity Of High Temperature Repair Welds, Lisbon, Portugal

Kingston, E. and Smith, D.J. – 2003 – **'Measurement Of Residual Stresses In Steel Cylinders And Nozzles Containing Repair Welds'.** Proceedings Of The Seventh International Colloquium On Asset Management Of Aged Plant And Materials: Assessment Methods, South Africa, Edited By R. K. Penny, EMAS Publishing Ltd, Sheffield, Pp 185-205.

Kingston, E., Smith, D.J., Thomas, A. and Ehrlich, R. – 2003 – **'Measurement Of Residual Stresses In Ferritic Steels'.** Proceedings of the 2nd International Conference On Integrity Of High Temperature Welds, IOM.

Wimpory R.C., May P.S., O'Dowd N.P., Webster G.A., Smith D.J. and Kingston E. – 2003 – **'Measurement Of Residual Stresses In T-Plate Weldments'**. Journal Of Strain Analysis, Vol. 38, No. 4, Pp 349-365

Kingston E.J., Stefanescu D., Mahmoudi A.H., Truman C.E. And Smith D.J. – 2004 – **'Novel Applications Of The Deep-Hole Drilling Technique For Measuring Through-Thickness Residual Stress Distributions'**. Journal Of Testing And Evaluation. ASTM International. Paper submitted.

CONTENTS

ACRONYMS

2D	Two-dimensional
3D	Three-dimensional
CHD	Centre-hole drilling
DHD	Deep-hole drilling
EDM	Electro-discharge machining
EMI	Electro-magnetic interference
FE	Finite element
FFT	Fast Fourier transform
HAZ	Heat affected zone
ID	Internal diameter
ICHD	Incremental centre-hole drilling
LR	Layer removal
LVDT	Linear variable differential transformer
MAG	Metal active gas
MIG	Metal inert gas
MMA	Manual metal arc
ND	Neutron diffraction
NPL	National Physical Laboratory
NSS	Neutron strain scanning
OD	Outside diameter
PSD	Power spectral density
PWHT	Post weld heat treatment
pwr1	Partial weld repair 1
pwr2	Partial weld repair 2
TDC	Top dead centre
TIG	Tungsten inert gas
XRD	X-ray diffraction

NOMENCLATURE

The following lists the symbols used in the main text.

$A[z]$	A parameter representing uniform expansion of the reference hole
a_r	Hole radius
$B[z]$	A parameter representing eccentric deformation of the reference hole
C_p	Specific heat capacity
d	Diameter of the deformed reference hole
d_0	Diameter of the initial reference hole
d_e	Equivalent diameter
E	Young's modulus
$f[\theta], g[\theta], h[\theta]$	Angular functions
h	Heat film coefficient
h_0	Gauge height of the core
h_i	Increment in trepanned depth
H_{Mech}	Axial distortion due to residual stress release
$H_{Thermal}$	Axial distortion due to thermal expansion
H_{Total}	Total core axial distortion
k	Thermal conductivity
l	Length of surface to fluid contact
$[M_{2D}]^*$, $[M_{3D}]^*$	Pseudo-inverses of matrices $[M_{2D}]$ and $[M_{3D}]$
$[M_{2D}]$, $[M_{3D}]$	2D and 3D compliance matrix
Nu	Nusselt number
P	Applied load
Pr	Prandtl number
Re	Reynolds number
r_o, r_t	Outer and transition radii
$[S]$	Sensitivity matrix
t	Thickness

T_0	Initial temperature of the core
T_{Ave}	Average temperature of the core
T_f, T_s	Temperature of fluid and surface respectively
u	Velocity
u_{rr}, $u_{\theta\theta}$	Radial and hoop distortion
$\overline{u_{rr}}$	Normalised radial distortion
w	Width
x, y	Co-ordinates in the plane normal to the axis of the reference hole
z	Position through thickness

$\hat{\sigma}$	Optimised stress vector
$\dot{q}$	Heat flux
θ	Angle round hole from axis of applied stress
ν	Poisson's ratio
ψ	Principal stress direction
α	Coefficient of thermal expansion
ρ	Density
μ	Dynamic viscosity
σ_1, σ_2, σ_3	Principal stresses
δd_{err}	Error in measured diameter
σ_{ind}	Induced stress
σ_{nom}	Nominal stress
σ_r, σ_θ	Radial and hoop stress
ε_{rr}, $\varepsilon_{\theta\theta}$	Radial and hoop strain
σ_{xx}, σ_{yy}	Evaluated stresses in the plane normal to the reference hole axis
σ_{zz}	Evaluated stresses along the reference hole axis

LIST OF FIGURES

Chapter 1: INTRODUCTION

It is well known that most engineering components contain defects. The defects are usually generated during the components' manufacture and take the form of cavities, cracks, etc. Impossible to eliminate, the presence of the defects are accepted and consequently incorporated into the design.

Incorporation into the design requires assessment of the defects' impact on the components' structural integrity. Assessment of the components' structural integrity requires information on the stresses exerted on the defect during the component's life. For each component, the stresses exerted are a combination of in-service stresses and residual stresses. The in-service stresses are the stresses generated during use of the component and can easily be calculated using general theories of mechanics. The residual stresses however, are the stresses generated by the interaction of adjacent regions of material undergoing elastic and plastic strain. The residual stresses usually originate during the manufacture of the component. The methods of prediction of residual stresses are at present unreliable and so residual stress measurements are undertaken in order to a) provide information for the structural integrity calculations, and b) provide a comparison for the improvement/validation of the predictions. There are many available techniques for the measurement of residual stresses, this research project however is only focused on the Deep-hole Drilling (DHD) technique already under development here at the University of Bristol.

The DHD technique relies on a 5 stage process, see Figure 1.1. For illustration purposes only, Figure 1.1 shows for each stage a section through the wall thickness of a welded component. In stage 1 - reference bushes are glued to the front and rear of the component at the measurement location. Stage 2 – a small diameter reference hole (less than 4mm) is gundrilled through the component and reference bushes. Stage 3 – the diameter of the reference hole is measured through the component and reference bushes. Stage 4 – a cylinder of material (outside diameter less than 20mm)

containing the reference hole is machined from the component. Stage 5 – the diameter of the reference hole is re-measured through the component and reference bushes.

The diameter of the reference hole measured in stage 3 is the diameter when residual stresses are present. During stage 4 the residual stresses are cut away, hence the diameter of the reference hole measured in stage 5 is the diameter when residual stresses are not present. The differences between the measured diameters at stages 3 and 5 enable the residual stresses to be calculated.

The main objective of this project was to undertake research and development of the DHD technique to increase its accuracy, to miniaturise the technique and to introduce a portable system.

At the start of this research project the DHD technique was limited in its application to components in the range of 20mm to 100mm thick. The limited application was empirical due to the scope of application of the DHD technique to components in the range of 20mm to 100mm thick in previous research (Bonner [1996a] and George [2000a]). One limiting factor is the ratio of sampling volume to component thickness. Therefore in order to decrease the sampling volume and hence have the ability to measure thinner components, refinement/miniaturisation of the machining processes used for the manufacture of the sampling volume was investigated. It was also anticipated that through the miniaturisation of the sampling volume, improvements in resolution and hence accuracy of the DHD technique would be achieved.

In addition to miniaturisation there was the development of a portable DHD machine. The machine would be capable of carrying out the DHD technique away from the laboratory and hence would include portable miniaturised machining processes. The machine would be computer interfaced to provide automatic control and datalogging throughout the process.

Throughout this research project, calibration studies were undertaken to provide validation of the areas of investigation, namely miniaturisation, accuracy and portability. Residual stress measurements on real components were also undertaken to test the refinements made to the DHD technique and to highlight new areas for development.

Chapter 2 presents an overview of background information concerning the definition, nature, origin and measurement of residual stresses. Similar content has been discussed in the literature reviews of Bonner [1996a] and George [2000a], however new literature has been added to expand and compound these earlier reviews.

Chapter 3 describes in detail the "state of the art" of the laboratory based DHD technique. The detailed description includes the refinements made and implemented during the course of this research. The chapter describes the laboratory DHD equipment, its use through the 5 stage process, the calculation of 2D and 3D residual stress distributions and then highlights the sources of measurement error.

Chapters 4 and 5 then present the research undertaken to improve the DHD technique. Chapter 4 reviews alternative equipment and machining processes to test their suitability for the present and future DHD techniques. The experiments carried out to test the abilities of the most applicable processes and conclusions made are described. Modifications to the present processes for the improvement of the DHD technique in the immediate future are also described. Chapter 5 presents the modifications made to the analysis used by the DHD technique. The full use of all measurement data is investigated and refinements to the analysis are discussed. The refinements to the analysis are presented with reference to the use of simulations, modelling and experimentation.

As with all practical techniques, modifications and refinements require calibration and validation studies. Hence Chapter 6 presents the experiments carried out for that purpose on specimens with known and controlled stress distributions. The experiments were undertaken using different specimen materials and different stress distributions providing an increased breadth to the previous studies made in earlier research.

The last experiment presented in Chapter 6 was heavily steered towards validating the use of the DHD technique for a particular application on real components. It is for this reason, the application on real components, that the DHD technique is being developed. Therefore Chapter 7 presents the application and testing of the DHD technique on real components and the measurements of residual stress therein. Again, to give the tests an increased breadth, measurements were conducted on components of varying size, geometry, material and residual stress origin.

The knowledge and in-depth understanding of all the refinements, modifications and applications of the laboratory based DHD technique allowed for the ultimate development of a portable DHD machine and fulfilment of the last project objective. Chapter 8 presents the portable DHD machine and its application on real components for calibration/validation thereof.

Chapter 9 discusses the position and comparison of the DHD technique in relation to the most widely used residual stress measurement techniques available. The main structure of the Thesis finishes with Chapter 10 presenting the conclusions made throughout the course of the research and the avenues for future work.

Chapter 2: LITERATURE REVIEW

2.1 Introduction

The literature reviewed in this chapter is aimed at providing an overview of background information concerning the definition, nature, origin and measurement of residual stresses. It is not intended that this overview be a complete and exhaustive discussion on the subject of residual stresses since this would be far too long. Rather this overview is aimed at providing information on the subjects relevant to this thesis.

Similar content has been discussed in the literature reviews of Bonner [1996a] and George [2000a], however new literature has been added to expand and compound these earlier reviews.

2.2 Definition of Residual Stresses

Residual stresses are defined as the self-equilibrating internal stresses that remain in a body after manufacture and processing in the absence of external forces or thermal gradients. At equilibrium, without external load, both the resultant force and moment of the free body must be equal to zero.

Residual stresses arise from misfits in the natural shape between material regions (as in shot-peening), different parts (such as shrink-fit components), or different phases (as is the case for composites).

Residual stresses can be classified as either macro or micro stresses and both may be present within a component at any one time. Macro residual stresses, which are often referred to as *Type I* residual stresses, vary within the body of the component

over a range much larger than the grain size. *Type I* residual stresses equilibrate over macroscopic dimensions (i.e. the scale of the component). Micro residual stresses, which result from differences within the microstructure of a material, can be sub-classified as *Type II or III*. *Type II* residual stresses are micro residual stresses that operate at the grain size level, whereas *Type III* operate at the atomic level. *Type II* residual stresses equilibrate over a number of grain dimensions (i.e. 3-10 × grain size). *Type III* residual stresses, on the other hand, exist over atomic dimensions and balance within a grain (i.e. < grain size). The different types of residual stresses are shown schematically in Figure 2.1.

One or a superposition of these three types define all the possible residual stress states. However from an engineering point of view, macro residual stresses have more importance than micro residual stresses because any modification to equilibrium also modifies the external dimensions of the body.

2.3 Nature and Origins of Residual Stresses

In practice, it is unlikely that any manufactured component would be entirely free from defects (e.g. cavities, cracks) introduced during the manufacturing process. Impossible to eliminate, the presence of the defects are accepted and consequently incorporated into the design.

As the design of engineering components becomes less conservative, hence more efficient, there is an increasing interest in how residual stresses affect the mechanical properties and performance of a component. This is because structural failure can be caused by the combined effect of residual and applied stresses on the defects.

Residual stresses however, can be beneficial as well as detrimental to the structural integrity of a component or material. The performance of materials and components can be improved markedly by the intelligent use of residual stresses. A common example is thermally toughened glass in which rapid cooling of the glass from an elevated temperature generates compressive surface stresses counterbalanced by interior tensile stresses [Withers and Bhadeshia, 2001a]. The surface compressive

stress (~100MPa) means that the surface flaws that would otherwise cause failure at very low levels of applied stress experience in-plane compression. While the interior experiences counterbalancing tensile stresses, this region is largely defect free and so the inherent strength of the glass is sufficient to prevent failure. Of course, once a crack does penetrate to the interior it can grow rapidly and catastrophically to give the characteristic "mosaic" pattern.

Residual stresses develop from a number of sources and can be present in the unprocessed raw material, introduced during manufacturing or can arise from in-service loading [Withers and Bhadeshia, 2001b; Rudd, 1992 and Borland, 1994]. The most common source is from manufacturing and maintenance processes involving machining, forming, elasto-plastic loading, heat treating and joining. These processes will be briefly reviewed in the following sub-sections.

2.3.1 Machining (Grinding, turning, drilling, milling)

Grinding, turning, drilling and milling are all chip-forming (i.e. material separation) machining methods with similar residual stress generation methodologies [Scholtes, 1987]. The cutting energy used in these processes result in a temperature increase and plastic deformation. Four factors can be distinguished as the generators of residual stresses:

- Chip formation tends to give rise to tensile residual stresses.
- Plastic deformation involving a smearing of the material in the plane of the workface tends to give compressive residual stresses.
- Localised temperature increase that momentarily causes an expansion, which is constrained by the bulk material. The resulting thermal stresses may exceed the yield stress at the actual elevated temperature and, therefore the workface of the component will be upset. During the subsequent cooling, tensile residual stresses are created.
- The material phase may change due to the rapid heating and cooling, causing compressive residual stresses.

The total resulting residual stress depends on the balance between these four factors, however compressive residual stresses are usually the overall result [Schajer et al,

1996 and Bainbridge, 1969]. The intensity of the residual stresses generated depend upon the machining parameters (i.e. cutting speed, depth of cut, feed rate, tool sharpness) and the mechanical and thermal properties of the tool and component.

As an example; during the grinding of steel, residual stress values between 600MPa in tension and compression, acting at depths of less than 100μm, have been reported [Scholtes, 1991]. After turning however, the affected depths have been found to be larger at up to 200μm.

2.3.2 Forming (rolling, shot-peening, drawing, extrusion)

Rolling is a process in which the thickness of the material is reduced (plastically deformed) by passing between a pair of revolving rollers, usually cylindrical in shape, for producing flat products such as sheets or strips. The magnitude of the residual stresses generated is dependent on the material yield stress, the material thickness, the roll size and the degree of reduction [Baldwin, 1949]. Specifically, cold rolling is carried out for special purposes such as the production of a good surface finish or special mechanical properties.

The primary objective of shot-peening is not to shape the component but to strengthen it. In shot-peening, shots made of steel, ceramic, glass, or other materials are jettisoned at the surface by air jet or centrifugal forces. It results in the localised plastic deformation of the outer surface, which elongates relative to the interior. Studies [Noyan and Cohen, 1981] show that the interior constrains the outer surface causing high local compressive residual stresses near the surface, balanced by tensile residual stresses in the interior. The process is well understood and fairly accurate methods are used to calculate the residual stresses by finite element (FE) analysis [Mcguid et al, 1999; Schiffner, 1999, and Mori and Osada, 1994].

Drawing and extrusion are similar processes in which a cylinder or billet of material is either pulled (drawn) or pushed (extruded) through an appropriately shaped die to create the desired cross-sectional dimensions and/or shape. The processes may be repeated with reducing sized dies (up to 50% reduction) to obtain the desired component. Total reductions of more than 90% from start to finish have been found

to double the tensile strength of the component when compared with its as-received state [Gong]. Drawing generates tensile residual stresses at the surface and compressive residual stresses at the core of the produced component. The magnitudes of these residual stresses can be of the order of ±600MPa [Gerhardt and Tekkaya, 1987].

2.3.3 Elasto-plastic loading (bending, tension, compression)

Following other manufacturing processes, straightening of the final component is often carried out in order to meet the required component tolerances. Elasto-plastic loading is carried out for the straightening process, which includes bending, tension and compression. These procedures involve the plastic deformation in local areas of the component and bring about the generation of residual stresses [Noyan and Cohen, 1987]. Figure 2.2 illustrates how after bending partially into the plastic regime, residual stresses are generated due to elastic recovery. The most common straightening procedures depend on bending and are usually carried out in several small steps. Stretching (tension) of components is less frequent because it is difficult to get the same productivity as for bending [Horn, 1991].

2.3.4 Heat treating

Heat treatment procedures can cause residual stresses (thermal stresses) even without crystalline structural change [Noyan and Cohen, 1987; Ericsson and Hildenwall, 1981 and Mayr 1987]. For example; if a material is cooled sufficiently fast, cooling will not be accompanied by microstructural transformation changes. Under these conditions, the surface cools much more quickly than the core at first. At this point the specific volume of the core is much greater than that of the surface, and the reduction in volume at the surface (due to lower temperature) is resisted by the greater volume in the core, resulting in the surface being in tension and the core in compression.

During heat treatment there is also the possibility of the formation of transformational stresses as well as thermal stresses due to a crystalline structural change [Ericsson and Hildenwall, 1981 and Mayr, 1987]. Upon cooling of the

component, if a non-uniform phase transformation of the material occurs, non-uniform crystalline packing densities may develop. This can cause the core to be in residual compression and the surface to be in residual tension simultaneously.

2.3.5 Joining (welding, soldering, brazing, adhering)

Welding residual stresses are the result of the fluctuating inhomogeneous temperature distributions arising during the welding process in and around the weld seam. Heating, as well as the cooling period, is of importance. The main source of residual stresses is the impeded shrinkage processes, which occur when heated and cooled regions are neighboured, see Figure 2.3. Other less important factors can influence the final distribution; for example, residual stresses remaining in the parent material due to previous processing, like preparatory machining, preheating, original welding, or the parameters of the final welding process itself.

The main sources of residual stresses arising from welding and their relative importance are reviewed below:

Shrinkage

As mentioned earlier the principal origin of residual stresses in welded components is the localised shrinkage of cooling weld material opposed by colder adjacent material. In the case of a weld seam, starting from the stress free state of the molten weld pool, tensile thermal stresses build up during the cooling period, which reach the temperature-dependent yield strength of the material. Consequently, at the end of the cooling process, tensile residual stresses exist in the weld seam.

If shrinkage is not opposed, thermal stresses relax completely and no residual stresses remain after cooling.

Quenching

Particularly in the case of thick plates, considerable temperature differences build up between the surface and core of a component during cooling [Macherauch and

Wohlfahrt, 1977]. The resulting thermal stresses may exceed the yield strength of the material and plastic deformation will occur. Obviously, these inhomogeneous plastic deformations lead to the development of residual stresses, compressive near the surface and tensile in the core.

Phase transformation

Residual stresses as a result of phase transformations during welding processes occur if, during the cooling down period of the heated weld seam, phase transformation processes connected with volume changes occur locally. For example, in the case of steels, transformation from austenite to ferrite, bainite or martensite is connected with a characteristic volume increase. Consequently, compressive residual stresses occur in transformed regions, balanced by tensile residual stresses in the adjacent regions.

It is possible to shift the phase transformation temperature by alloying the specimen. Alloying can however result in the increased [Macherauch and Wohlfahrt, 1977] or decreased [Parlane, 1981] magnitude of residual stresses, hence the choice of alloying requires careful consideration.

Superimposition of shrinkage, quenching and phase transformation

In most cases however, residual stresses are generated during welding due to the combination of shrinkage, quenching and, if present, phase transformations. The simplest way to view the combination of their effects is with a linear superimposition, as shown in Figure 2.4. It can be seen that the maximum tensile residual stress usually occurs just offset from the weld centreline.

Experiments by Macherauch and Wohlfahrt [1977] showed a good agreement with the linear superimposition model. However, more recent work by Macherauch and Klaus [1986] showed only a limited understanding of the sources of welding residual stresses. Additional sources (minor sources) of residual stress generation during the welding process are presented by Darbyshire [1985] and Parlane [1981].

The development of welding residual stresses inside the component is still more complex, being continually modified during the actual process. A controlled study of this problem is therefore an extremely difficult exercise due to the many number of variable parameters influencing the outcome.

2.4 Measuring residual stresses

Due to the many variables involved in the generation of residual stresses, modelling and prediction methods are often unreliable, hence, individual residual stress measurements are usually carried out. The characteristically non-uniform, high stress gradient nature of residual stresses require that either the induced stress field is well understood and predictable, or many residual stress measurements must be performed [Toten et al, 2002]. A number of procedures and techniques have been applied to determine the residual stresses existent in a component. The measurement techniques invariably measure strains rather than stresses, and the residual stresses are then deduced using the appropriate material parameters such as Young's modulus and Poisson's ratio. These strain measurement techniques can be classified into three different categories:

- Non-destructive. The measurements are carried out without causing any damage to the component (e.g. x-ray diffraction and neutron diffraction),
- Semi-destructive. Whereby only a small/finite amount of material is removed from the component during measurement (e.g. centre-hole drilling, deep-hole drilling),
- Destructive. Large quantities of material are removed from the component during the measurement process, sometimes to the extent of total destruction (e.g. Sachs and layer removal).

Most material removal techniques remove macroscopically sized regions of material over which micro-residual stresses (i.e. *Type II* and *Type III* stresses) average to zero so that only macro-residual stresses are recorded. Hence micro-residual stress measurements are generally restricted to the non-invasive technique.

The different widely available measurement techniques are discussed in more detail below.

2.4.1 Non-destructive techniques

Non-invasive techniques measure a dimension of the crystal lattice structure of the material or some physical parameter affected by the crystal lattice dimensions. Work by Hutchings [1990] showed that specific lattice planes in metallic crystalline structures distort under applied loading and this is directly proportional to the induced stress.

X-ray diffraction

This measurement technique is relatively straightforward and equipment readily available, both laboratory based and portable. During measurement the component is irradiated with high energy x-rays that penetrate the surface, the crystal planes diffract some of these x-rays, according to Bragg's law:

$$\lambda = 2d \sin\theta \tag{2.1}$$

where λ is the radiation wavelength, d is the spacing between reflecting crystal planes and θ is the angle of incidence and diffraction of the x-ray radiation from these planes.

A detector is moved around the component to detect the angular positions where diffracted x-rays are located and records their intensity. The locations of the peaks enable the user to evaluate the stress within the component.

The strains obtained by this technique are very localised to the extent of being only associated with the surface region. In practice, the x-ray diffraction technique can measure stresses at depths up to 5um in titanium, 15um in steel and 50um in aluminium [Kandil et al, 2001]. Measurements can be made at greater depths when combined with layer removal, however the depth can only practically be extended to

a maximum of 1mm. Also, with layer removal the technique becomes classified as semi-invasive.

One of the major disadvantages with XRD is the limitation imposed on the test sample geometry. The geometry has to be such that an x-ray can both hit the measurement area and still be diffracted to the detector without hitting any obstructions.

Errors can arise when investigating rough surfaces (e.g. welds) using the conventional focusing optics due to changes in sample "heights".

Synchrotron (or hard) x-rays

Synchrotron (or hard) x-rays are available at central facilities, such as the European Synchrotron Research Facility in Grenoble and the SRS in Daresbury.

Synchrotrons provide very intense beams of high energy x-rays, typically as much as a million times more intense than conventional x-rays. Synchrotrons have a much higher depth penetration than conventional x-rays, for example: 50mm compared to 50μm in aluminium [Withers and Bhadeshia, 2001a and Kandil et al, 2001]. The increased penetration depth means that synchrotrons are capable of providing high spatial resolution, three-dimensional maps of the strain distribution to millimetre depths. Very fast data acquisition times (< 1s) are possible at large depths [Withers and Bhadeshia, 2001b].

Neutron-diffraction

Like x-rays, the neutron diffraction technique relies on elastic deformations within a polycrystalline material that causes changes in the spacing of the lattice planes from their stress free state [Webster and Webster, 1985]. Measurements are carried out in much the same way as with x-ray diffraction, with a detector moving around the sample, locating the positions of high intensity diffracted beams according to Bragg's law (Equation 2.1).

There are essentially two neutron diffraction techniques, namely, conventional $\theta/2\theta$ scanning and time of flight. $\theta/2\theta$ scanning uses a continuous beam from a reactor source and monitors the shift $\Delta\theta$ in a single diffraction peak according to:

$$\varepsilon = \frac{\Delta d}{d} = -\cot\theta.\Delta\theta \tag{2.2}$$

Whereas time of flight uses a pulsed beam from a spallation source and monitors the incident/diffracted wavelength, lambda, at a constant Bragg angle, θ.

Neutrons have the advantage over x-rays in that for wavelengths comparable to the atomic spacing, their penetration into materials is typically many centimetres. Also, by restricting the irradiated region and the field of view of the detector by slits or radial collimators, it is possible to record diffracted intensities from only a small volume (~1mm^3) at these large depths. Neutrons are able to provide high spatial resolution 3D strain maps at depths from 0.2mm to 100mm in aluminium or 25mm in steel [Kandil et al, 2001].

However, copmpared to toher techniques, the cost of neutron diffraction is high and the availability low. Neutron diffraction is carried out at central facilities, including ISIS (Didcot), ILL (Grenoble), Saclay (Paris) and Chalk River (Canada), with beam-time allocated under peer review.

Ultrasonic methods

Ultrasonic methods utilise the sensitivity of the speed of ultrasound waves travelling through a material to the stress levels within it [Green, 1973]. Stress is measured by inducing a sound wave at a frequency of several megahertz into the component and measuring the time of flight or some other speed related parameter. The changes in speed provide a measure of the average stress along the entire wave path, hence the method is only applicable to the measurement of macro residual stresses. Spatial resolution is also restricted by the degree of texture (grain alignment) in the material. The acousto-elastic coefficients necessary for the analysis are usually calculated using calibration tests [Thompson et al, 1996].

The equipment is portable and cheap to apply; hence the method is well suited to routine inspection procedures and industrial studies of large components [Green, 1973 and Bray et al, 1997].

Magnetic methods

The principle of the magnetic methods makes use of changes in the magnetic properties of a material when subjected to varying stress states, due to magnetostriction and the consequent magnetoelastic effect [Buttle et al, 2000]. Hence the method is only applicable to ferromagnetic materials.

The stress induced anisotropy leads to the rotation of an induced magnetic field away from the direction applied [Abuku, 1977 and Buttle et al, 2000]. A sensor coil can monitor these small rotations in the plane of the component surface. Incidentally, when no rotation is observed, the principal axes of the applied magnetic field and stress are parallel. By rotating the induction and sensor coils, both the principal stress directions and their relative sizes can be measured.

Although the stress dependence of the magnetic parameters is quite strong, there are many other variables, such as hardness, texture, grain size, etc., which also affect the measurement. For this reason a combination of magnetic techniques is required so that the effect of these others variables can be eliminated. The method also requires calibration of the magnetic parameter against known stress levels.

The main advantages of the magnetic method is that the equipment is portable, quick to apply and can measure stresses at depths of 6-10mm. However the method is restricted to ferromagnetic materials and is sensitive to other microstructural features.

Piezo-spectroscopic (Raman)

The Raman effect involves the interaction of light with matter. Incident laser light causes the bonds between atoms to vibrate. Analysis of the scattered light, known as Raman spectrum, reveals vital information about a component's state and chemical

structure. Raman or fluorescence luminescence lines shift linearly with variations in hydrostatic stress. The spectral shifts can be easily and accurately measured and by using optical microscopy, it is even possible to analyse regions of just a few microns in size.

The method is effectively a surface strain measurement technique, but with optically transparent materials it is even possible to obtain sub-surface information. The method is particularly useful for studying fibre composites, providing basic residual stress information from fibre centres to fibre ends [Qing and Clarke, 1993, Qing et al, 1994 and Schadler and Galiotis, 1995].

2.4.2 Semi-destructive techniques.

Centre-Hole Drilling

The centre-hole drilling technique was first proposed by Mather [1934] and is based on the measurement of the change in surface strain caused by the relief of stresses during the machining of a shallow hole in a component. The principle is that removal of stressed material results in the surrounding material readjusting its stress state to attain stress equilibrium. The measured surface strains allow for the back calculation of the previously existing residual stresses. The formulae and calculations derived for the back calculation process were developed from a combination of experimental and Finite Element analyses [Schajer, 1988a and 1988b].

The surface strains are usually measured using a strain gauge rosette attached concentrically around the hole axis [Schajer, 1988a, Schajer and Tootoonian, 1997 and Grant et al, 2002]. Within the rosette are positioned three strain gauges, radially aligned around the rosette's centre (hole axis) with a relative angular spacing of 45 degrees. The use of the three strain gauge rosette permits measurement of a bi-axial residual stress state. For a linear, elastic, isotropic material, it can be shown that the strain relaxation measured at any of the strain gauges can be related to the principal residual stresses using:

$$\varepsilon_r = A(\sigma_{max} + \sigma_{min}) + B(\sigma_{max} - \sigma_{min})\cos 2\alpha \quad (2.3)$$

where ϵ is the measured strain relaxation, σ_{max} is the maximum principal stress, σ_{min} is the minimum principal stress, A and B are calibration constants, and α is the angle measured anti-clockwise from the maximum principal stress direction to the axis of the strain gauge.

Although the strain gauge rosette is the most widely used measurement apparatus, a number of other measurement apparatus have also been developed, such as moiré interferometry and laser interferometry [Li, 1997, Makino and Nelson, 1997 and Nelson et al, 1997].

Even though it is possible to measure the variation in stress with depth by incrementally deepening the hole [Schajer, 1988b], the practical measurement depth is limited to the diameter of the drilled hole. The method does suffer from limited strain sensitivity and potential errors and uncertainties related to the dimensions of the hole (e.g. diameter, concentricity, profile, depth), surface roughness, flatness and specimen preparation.

The centre-hole drilling method is the most widely used due to being cheap, quick and easily available, both in the lab and on-site.

Ring coring

Similar in principle to the centre-hole drilling technique, ring coring is based on the measurement of released strain caused by a disruption to the original stress field. However in this case, strain release is caused by the machining of a shallow ring (i.e. trepanning) around a strain gauge rosette to produce a relatively stress free island of material [Wolf and Sauer, 1974 and Keil, 1993]. The subsequent strain release, as measured by the central rosette, is then used to calculate the original stress state.

Kellar et al [1989] presented a general process for obtaining good results up to a depth of 25mm. The outside diameter of the trepanned groove was approximately

18mm, making it a more invasive method than the centre-hole drilling method, however, an increase in measurement accuracy was found at these greater depths [De Angelis and Sampietri, 1990]. Misra and Peterson [1982] pointed out that there is also the potential for greater precision in the ring-coring method when compared to the centre-hole drilling method due to the amount of residual stresses released from machining. In the ring-coring method 90% of the residual stresses are released, whereas in the centre-hole drilling method only 25% of the residual stresses are released.

Deep-Hole drilling

Deep-hole drilling, the method investigated for this research project, is very similar in principle to the ring-core method. Distortions are measured during disruption of the original stress field by the machining of a ring (i.e. trepanning) around a central strain gauge. In this case however, the central strain gauge is a hole drilled deep (i.e. length/diameter > 4) into the component. The diameter of the drilled hole is measured before and after trepanning and the difference used to calculate the original stress state. Upon completion of the trepanning process, a cylinder (core) of relatively stress free material containing the coaxial hole is extracted from the component.

Initial studies and development of the deep-hole drilling technique were carried out by Zhadanov and Gonchar [1978], Beaney [1978], and Jesensky and Vargova [1981].

Zhadanov examined residual stresses in steel welds in which 8mm diameter holes were drilled and cores of 40mm diameter were trepanned. The cores were incrementally trepanned in order to measure their change in axial length at each stage. Both the changes in diameter and axial length were used to then calculate the triaxial residual stress state.

Beaney [1978] proposed gundrilling, using a 1/8 inch drill bit, as the most suitable method of introducing the very smooth and straight gauge hole. The gauge hole diameter was then measured at 0, 45 and 90 at each 2mm in depth along its entire

length. The hole diameter was measured using strain gauges fixed onto two parallel beams fixed together and drawn along the side walls of the hole. Changes in diameter would cause changes in beam deflection, which were then measured by the attached strain gauges. The core was trepanned using the electro-chemical machining (ECM) process. Beaney's methodology was updated and improved by Procter and Beaney [1987], whos most notable introduction was the use of non-contacting capacitance gauges instead of strain gauged beams to measure the hole diameter.

Jesensky and Vargova [1981] measured residual stresses in steel weldments. The method proposed used two blind holes drilled from opposite surfaces with strain gauges attached inside the holes and on the surfaces. The method provided measurements of the triaxial stress state within the weldments following the extraction of 32mm diameter cores.

More recently, improvements of the deep-hole drilling technique have been introduced by Leggatt et al [1996], Bonner [1996a], and George [2000a].

Leggatt et al [1996] assessed the deep-hole drilling technique through a calibration test using a rectangular steel bar, 875mm long, 100mm deep and 52mm wide. The rectangular bar was subjected to four-point elastic-plastic bending after which the deep-hole drilling technique was used to assess the residual stresses introduced. An analytical solution to the residual stress state was also calculated for comparison.

Focussed research studies on the deep-hole drilling technique have been carried out solely at the University of Bristol over the past decade. Bonner [1996a] and George [2000a] had therefore generated the most recent improvements of the technique on which this research project has extended. Therefore a lengthy, in depth review of these works will not be discussed here. Rather, throughout this thesis, earlier work is referenced and discussed where appropriate.

2.4.3 Destructive techniques

Sachs method

Named after its inventor, Sachs [1927] proposed the measurement of residual stresses from the partial relaxation of strain during the incremental removal of several layers of material from a component. During application, strain gauges are positioned on either the inside or outside face of a component aligned in the hoop and axial directions. Obviously the positioning of strain gauges on the inside of the component is only applicable to tubes or other hollow shaped components. The machining process is then started from the opposite face to that the strain gauges are on and incrementally stepped towards the strain gauge face. For example, if the strain gauges are on the inside diameter of a tube, layers will be removed from the outside diameter first. Each increment in machining removes an axisymmetric layer from the component until no more strain relaxation is recorded.

Sachs [1927] showed that the calculations to convert the relaxed strains into residual stresses remained simple if the geometry of the component was axisymmetric. Ueda et al [1975] demonstrated that the Sachs method should also only be used in cases where the residual stresses have a rotational symmetry and are uniform in the axial direction.

Therefore the application of the Sachs method is most suited to tubes and cylinders.

Curvature and Layer removal

The curvature and layer removal methods are often used for measuring the presence of residual stresses in simple component geometries. Similar in principle to the Sachs method, the strain of the test component is measured during the deposition or removal of layers of material.

Curvature and layer removal measurements are frequently used to determine the stresses imposed on a component from coatings and layers [Perry et al, 1996, Clyne and Gill, 1996 and Kuroda et al, 1987]. The deposition/removal of a layer or coating

can induce/release stresses, which cause the component to curve. The resulting changes in curvature during deposition/removal make it possible to calculate the corresponding variations in stress as a function of layer/component thickness.

The curvature of the component can be measured using a variety of methods, including optical microscopy, laser scanning, strain gauges or profilometry, depending on the resolution and range of measurement required. The measurements are usually carried out on narrow strips of material (width/length < 0.2) to avoid multiaxial curvature and mechanical instability.

The methods are generally quick and require only simple calculations to relate the curvature to the residual stress state.

2.5 Concluding remarks

Most engineering components contain residual stresses, having been introduced during manufacturing processes like machining, forming, elasto-plastic loading, heat treating and joining.

Residual stresses can beneficial as well as detrimental to the structural integrity of an engineering component and so the intelligent management of residual stresses can markedly improve the performance of a component.

The generation of residual stresses is at present difficult to model analytically and so residual stress measurements are heavily relied upon.

There are many methods available for the measurement of residual stresses in engineering components. No single method can provide the full range of measurement capabilities. Therefore it is important to consider the individual application and the desired results before selecting. In many cases the complementary use of more than one method is desirable.

The selection of any one measurement method can depend upon the type of residual stress to be measured (e.g. macro or micro), the depth of measurement (e.g. surface or sub-surface), the damage caused during measurement (e.g. non-invasive, semi-invasive or invasive) and the availability of the measurement facilities.

The University of Bristol has been the sole research centre for the Deep-Hole Drilling technique over the past decade. Hence my predecessors, Bonner [1996a] and George [2000a], have carried out the most recent research on the DHD technique on which this research project has extended.

Chapter 3: THE DEEP-HOLE DRILLING TECHNIQUE

3.1 INTRODUCTION

This chapter presents the "state of the art" of the DHD technique as used for the measurement of residual stresses, and includes all the modifications and refinements made therein. The aforementioned modifications and refinements are highlighted and discussed in detail in Chapters 4 and 5.

The first two sections describe the equipment and its use to carry out the DHD technique. The following two sections present the analyses used to calculate the 2D or 3D residual stresses from the measurements recorded. The final section describes possible sources of error within the calculated residual stress results.

3.2 EQUIPMENT

The equipment used in the DHD technique comprises of six major components, numbered 1 to 6 in Figure 3.1. The components are (1) a reference frame, (2) a specimen table, (3) a gundrill system, (4) a hole diameter measurement system, (5) an electro-discharge machining (EDM) and measurement system, and (6) a PC control and data logging system. Each component is detailed below.

3.2.1 Reference Frame

The reference frame is a modified milling machine bed with 3 orthogonal axes of movement, as shown in Figure 3.2. All 3 axes have manual feed, but only the machining z-axis has the extra option of engaging an automatic feed. Upon the reference frame is fixed a plate with a keyway onto which components (3) - (5) can

in-turn be located. The orientation of the keyway is such that all the processes are carried out along the reference frame's horizontal z direction.

3.2.2 Specimen Table

The specimen table comprises of a steel framework with a flat, horizontal top surface onto which specimens may be clamped, as shown in Figure 3.3. The specimen table is positioned next to the reference frame and orientated such that the reference frame's z-axis passes through its centre.

3.2.3 Gundrill System

The gundrilling system is used for the manufacture of the precision reference hole and consists of a gundrill head, an oil pump and filtration reservoir, and a gundrill bit and guides. The gundrill head, as shown in Figure 3.4, provides rotation of the drill bit and is capable of spindle speeds up to 5500rpm. At the same time a pump and filtration reservoir can supply cutting/coolant oil to the gundrill head at high pressure, up to 65bar. The cutting oil passes through a 360° rotary pressure fitting connected to the back of the chuck and then down a central hole within the chuck before arriving at the drill bit.

Two different diameters of gundrill can be used. For standard applications (i.e. specimen thicknesses greater than 20mm or in components that are likely to contain low residual stress gradients) a gundrill of 3.18mm diameter is used. This thesis also explored for non-standard applications using a gundrill of 1.5mm diameter. The specialised gundrill bit, as shown in Figure 3.5, is characterised by three features:

i. It has a central hole passing through its entire length providing a clear path for the delivery of cutting oil to the tip,
ii. Its exterior incorporates a straight flute designed to ease the escape of cutting oil and swarf,
iii. Its tip has an off-axis point with the result that its rotation produces self-centralising forces.

These features combine to provide a hole with a very straight axis and a highly uniform specific diameter. The gundrill manufacturer claims an axis deviation of less than 0.1μm per mm of depth and a diameter tolerance of ±13μm.

Guides are fixed and aligned between the gundrill head and the specimen. The guides are used to support the gundrill bit, preventing bending and chattering during the drilling process.

A chip box is used for the collection and containment of swarf and used cutting oil exiting the newly drilled reference hole.

3.2.4 Hole Diameter Measurement System

Measurement of the reference hole diameter is undertaken using an air probe, the manipulation of which is provided by a purpose built frame, as shown in Figure 3.6.

Compressed air is externally filtered and regulated to a working pressure of 2.965bar before entering a pressure transducer. Within the pressure transducer the compressed air is fed into a chamber passed a diaphragm, which is sensitive to very small changes in pressure, before exiting through a pipe to the air probe. The air probe consists of an end-capped steel tube through which the compressed air is fed. The air exits to atmosphere through two diametrically opposite holes in the tube wall of the air probe tip, see Figure 3.7. The flow of the compressed air through the air probe is restricted by the proximity of the side walls of the reference hole (i.e. the reference hole diameter). The variable diameter, and hence flow restriction, creates a variable back-pressure exerted on the diaphragm within the pressure transducer. The movement of the diaphragm, due to the variable back-pressure, is measured using a linear variable differential transformer (LVDT). The output from the LVDT is then converted into a diameter measurement to be recorded. The conversion of the diameter measurements is calibrated using rings of a known internal diameter (ID) supplied with the air probe. Two calibration rings are also shown in Figure 3.7.

The air probe is controlled and manipulated by a purpose built frame, see Figure 3.6, comprising of two sections, a rotation section and a feed section. The rotation

section mainly consists of a base plate with keyway to be orientated and fixed onto the reference frame, a stepper motor and planetary gear box to provide rotation and an axle to transmit that rotation to the feed section. The feed section mainly consists of two linear ball splines to provide smooth and accurate movement, a lead screw with anti-backlash nut to provide accurate movement and positioning of the air probe, a stepper motor with encoder to manipulate the lead screw and the connector for the air probe.

3.2.5 EDM and Measurement System

EDM is used to coaxially trepan around the reference hole producing a stress free cylindrical core. The EDM head is shown in Figure 3.8.

EDM removes material by means of repetitive spark discharges between the electrode tool and specimen. A constant spark gap between the electrode and work-surface is maintained by a servo-controlled mechanism within the EDM head. Each spark produces a localised temperature in the order of 12000°C vaporising the specimen material on contact and forming a small crater on the work-surface. Once vaporised, dielectric fluid carries the specimen material away. The dielectric fluid is supplied to the specimen work-surface through the centre of the tubular electrode and exits down the outside of the electrode. Flushing the work-surface with the dielectric fluid also helps to eliminate the risk of fire. The dielectric is then recycled through a pump and filtration reservoir.

The electrode comprises of a copper tube, which is held and rotated by the chuck mounted on the front of the EDM head. The rotation of the electrode results in even wear of both the electrode and specimen.

During the trepanning process the depth of machining is recorded using an LVDT mounted on the EDM head. This is illustrated in Figure 3.8.

Changes in the length of the reference hole are monitored during the trepanning process (if the rear face is accessible). A rod connected to the front bush passes through the reference hole and protrudes out of the rear face. The

distortion/movement of the core is transmitted via the rod to the rear face at which point it is recorded by an LVDT.

During the trepanning process heat is created and transmitted to the specimen due to the nature of EDM. Therefore in order to take this heat input into account six K-type thermocouples are glued onto the front and rear surfaces of the specimen to measure its temperature rise. The thermocouples used are shielded to eliminate electro-magnetic interference (EMI) from the EDM process. The glue used is thermal bonding epoxy, which provides thermal conduction but electrical insulation between the specimen and the thermocouples. The effect of this heating on the measurement of the axial deformation of the core is explained in Section 5.4.

3.2.6 Control and Datalogging System

Equipment communication, control and datalogging are all provided by a PC through onboard serial ports and an analogue to digital converter. Control of the PC is provided by dedicated software written "in-house". The control and datalogging system is shown in Figure 3.9.

3.3 Measurement Process

Use of the equipment described above to carry out the different stages of the DHD technique is now presented below.

3.3.1 Preparation of the Specimen

The specimen is placed upon the specimen table. The gundrill head is then fixed upon the reference frame and is used to "clock" the specimen ensuring the correct orientation and alignment before clamping.

For each measurement location reference bushes are adhered to the front and rear of the specimen as shown schematically in Figure 3.10. The reference bushes are manufactured from standard workshop materials with similar machining

characteristics to that of the specimen material. The reference bushes serve several functions:

i. Provide sacrificial material to encompass any "bell-mouthing"[1] from gundrilling,
ii. Provide a reference between repeated measurements of the hole diameter,
iii. Minimise the near hole entrance and exit effects for the hole diameter measurements,
iv. Provide a mount for the fixation of the protruding rod and the LVDT used during the trepanning process.

The measurement location is degreased before the adhesion of the front reference bush. Two different sizes of front reference bush are used depending upon the diameter of core produced during the trepanning process. A "10mm" front bush is used for gundrill diameters of 3.18mm. A "5mm" front bush is used for gundrill diameters of 1.5mm. The adhesive used is a two-part adhesive resistant to both heat and chemical attack. The front reference bush is held in place and in the correct orientation by a fixture mounted in the gundrill head, whilst the adhesive cures.

Before the outer front bush and the rear reference bush are adhered to the specimen, a total of six K-type thermocouples are bonded to the specimen, three to the front face and three to the rear face. The thermocouples are positioned at a radius of 15mm from the axis of the reference hole and at 120° to each other. The thermocouple measurements are used to differentiate between the thermal and mechanical axial distortions of the core during the EDM process.

The outer front bush and the rear bush are adhered to the specimen using the same two-part adhesive. Both bushes are held in place and in the correct orientation (i.e. concentric to the front reference bush) whilst the adhesive cures. The outer front bush acts as a reference onto which the fixtures used during the measurement process

[1] "Bell Mouthing" is a term used to describe the region that occurs at the entrance and exit of a drilled hole where the diameter is usually larger than the nominal hole diameter. This occurs as a result of insufficient drill stiffness and drill guidance.

can be attached without applying any undue external stress on the measurement location.

At this point the general preparations are finished and the specimen is ready for the commencement of the measurement process.

3.3.2 Gun Drilling

Preparation for the gundrilling process entails the fixation of the gundrill guides between the specimen and gundrill head, and the chip box to the outer front bush.

For standard applications a 3.18mm diameter gundrill is used. The standard gundrilling process takes place at approximately 5000rpm with a feed rate of approximately 12mm/min as provided by the reference frame. The cutting oil is supplied to the gundrill tip at a pressure of 55bar.

Research presented in Chapter 4 examined and developed for specialised applications the use of a 1.5mm diameter reference hole, which requires a 1.5mm diameter gundrill used at a spindle speed of 10000rpm and supplied with cutting oil at a pressure of 100 bar. Unfortunately the laboratory based equipment at the University is unable to provide these machining parameters and so gundrilling of the 1.5mm diameter reference holes is contracted out after the initial reference bush preparations. After the 1.5mm reference hole is manufactured the specimen is re-orientated and fixed on the specimen table to complete the rest of the DHD technique.

On completion of drilling, the gundrill head and all fixtures are removed in preparation for the measurement of the reference hole diameter.

3.3.3 Hole Diameter Measurement

The hole diameter measurement system is located and fixed upon the reference frame next.

Once the air probe system has reached its working pressure, it is allowed to stand to warm-up/stabilise. The air probe is then calibrated using the calibration rings supplied. The rings are threaded in turn onto the air probe and positioned at the correct depth and angle for the specified calibration diameter. The output of the diaphragm LVDT is then modified to display the correct measurement. The calibration of the air probe is set by the two rings at each end of the linear measurement range of the air probe. The rest of the rings are then used to fully define the calibration curve for which a 3rd order polynomial regression is found. An example of the calibration readings and the polynomial regression is shown in Figure 3.11. The readings of the air probe are transferred into diameter measurements using the equation of the polynomial regression.

After calibration, the datalogging and control system takes over with the computer automatically controlling all movements of the air probe, unless otherwise stated below. The air probe is first rotated anti-clockwise to a datum marking the first angle of measurement (usually at 0° to the weld). The air probe is then manually fed through the entire length of the reference hole and both reference bushes in order to record the start and finish positions for the following diameter measurements. From the start position the air probe is then stepped at 0.2mm increments through the entire length of the hole and both reference bushes. After each 0.2mm incremental movement, the air probe measurement system is allowed to settle for 1 second before the diameter measurement is recorded to file and the air probe moved again. When the finish position has been reached, the air probe is rotated through 10°, manually returned to the start position and automatically stepped through the hole again. The air probe is manually returned to the start position after each rotation in order to check that it fits down the hole at that angle and will not be damaged during the coming measurement. The process continues until the diameter of the hole at a total of 18 angles has been measured and recorded.

The hole diameter measurement system is then removed from the reference frame in preparation for the trepanning operation.

3.3.4 Electro-Discharge Machining

The EDM head is located and fixed upon the reference frame next.

Preparation for the trepanning process entails the attachment of a container to the outer front bush for the collection, containment and recycling of used dielectric. The specimen is also electrically grounded in order to create the charged gap needed between the specimen and electrode for the sparks to cross. The six thermocouples previously attached during specimen preparation are now connected to a thermocouple reader for use in recording the temperature of the core during trepanning. A seventh thermocouple is also inserted into the dielectric flow line to record the dielectric temperature during trepanning.

Next, the measurement device for recording the axial distortion of the reference hole is set-up.

The LVDT is set-up as shown in Figure 3.12. First, a small diameter rod is threaded through the reference hole and fixed to the front reference bush using its end-bolt. A bracket to hold the LVDT is then glued to the rear bush. The position of the LVDT is such that the protruding rod ends within the LVDT and acts as its magnetic core (armature). The LVDT is allowed to warm-up/stabilise, after which it is ready for use without repeated calibration.

With the set-up now complete, the trepanning process is started. The computerised data logging system automatically records the axial distortion of the reference hole, the through-thickness position of the EDM head and the temperatures of the seven thermocouples at operator specified time increments.

Trepanning finishes when the electrode tip reaches the glue line between the rear reference bush and the specimen. At this point there is no electrical conduction between the glue and the electrode and hence no more sparking. The result at the end of the EDM process is a deep-hole core with the reference hole at its axis. Figure 3.13 shows a resultant "10mm" diameter deep-hole core.

The EDM system is removed, and the hole diameter measurement system is relocated.

3.3.5 Hole Diameter Re-measurement

Re-measurement of the reference hole is conducted in the same manner as described earlier in Section 3.3.3.

3.4 Measurement Analysis

As with many residual stress measurement processes, the DHD technique calculates the residual stress distribution using measurements of distortion between a stressed and unstressed state. The equations used for the conversion of distortions into stresses rely upon the understanding of the following lemma[2] [Bonner, 1996a]. The lemma concerns the equivalence of imposed stress fields and prescribed displacement states, see Figure 3.14.

In general, the imposition of a stress system, S, on a region of material, R, resulting in elastic behaviour in that material, will produce the same stress field in a bounded sub-region of R, say R', as does the imposition of the same displacements on the boundary of R' as were caused by the system S.

The displacements measured during the many stages of the DHD technique are used for the calculation of the residual stress distribution throughout the thickness of a specimen. However the residual stress distribution can be calculated as a 2D or 3D distribution. The 2D residual stress distribution acting in the plane normal to the reference hole axis is calculated using only the hole diameter measurements. The 3D residual stress distribution is calculated using both the hole diameter measurements and the axial strain measurements. The 3D calculations are therefore extensions of the 2D calculations and as such the 2D calculations are considered to be the standard. The standard calculations have been defined and developed for many years, most

[2] Used in mathematics, a lemma descibes a minor theorem, of interest primarily because it serves in the proof of a major theorem.

notably by Leggatt et al [1996], Bonner [1996a] and more recently by Garcia-Granada et al [1998].

3.4.1 2D In-plane Residual Stress Analysis

The term "in-plane residual stresses" is used to describe the residual stresses acting in a plane normal to the axis of the reference hole. As such, the following analysis applies to the displacement measurements obtained from the in-plane directions only (i.e. the reference hole diameter measurements).

For the development of the analysis, the core thickness is considered to be divided into a number of blocklengths, each bounded by two parallel planes normal to the reference hole axis, as shown in Figure 3.15. The diameter measurements obtained at 0.2mm increments through the thickness of the specimen are assumed to be the average diameter of the reference hole within each blocklength. The following further assumptions are made:

i. The material properties of the specimen are isotropic,
ii. A state of plane stress exists on all planes normal to the axis of the reference hole,
iii. The state of stress was uniform within each blocklength before the reference hole was drilled,
iv. The behaviour of each blocklength is completely unaffected by the presence of other blocklengths,
v. As a result of the EDM process, the stresses within the core are completely relaxed in a linear-elastic manner.

Adoption of these assumptions allows the calculation of the residual stresses to be based around the repeated analysis of many independent blocklengths, the combination of which make up the specimen thickness. Each independent blocklength can then be reduced to the simple case of an infinite plate containing a hole, subjected to a uniform uniaxial stress, see Figure 3.16.

The theory of Elasticity [Timoshenko and Goodier, 1951] gives the radial and hoop distortions, u_{rr} and $u_{\theta\theta}$, at any point in a plate containing a circular hole as

$$u_{rr}(r,\theta)=\frac{\sigma a_r}{E}\left\{\left[(1+\nu)\frac{a_r}{2r}+(1-\nu)\frac{r}{2a_r}\right]+\left[(1+\nu)\frac{r}{2a_r}\left(1-\frac{a_r^4}{r^4}\right)+\frac{2a_r}{r}\right]\cos 2\theta\right\} \quad (3.1a)$$

$$u_{\theta\theta}(r,\theta)=-\frac{\sigma r}{2E}\left[\left(1+\frac{a_r^2}{r^2}\right)^2+\nu\left(1-\frac{a_r^2}{r^2}\right)^2\right]\sin 2\theta \quad (3.1b)$$

where a_r is the hole radius, E is the Young's modulus of the material, ν is the Poisson's ratio, and r and θ are polar co-ordinates with θ being the angle measured from the axis of the applied stress, σ.

In the case of the DHD technique, the radial distortion is measured at the hole edge, i.e. where $r = a_r$. Therefore Equation 3.1a reduces to

$$u_{rr}(\theta)=\frac{\sigma a_r}{E}(1+2\cos 2\theta) \quad (3.2)$$

Equation 3.2 can be re-written to give the normalised radial distortion at the hole edge as

$$\frac{u_{rr}(\theta)}{a_r}=\frac{\sigma}{E}(1+2\cos 2\theta) \quad (3.3)$$

(Note: The term "normalised radial distortion" and not "strain" is used because the radial and hoop strains in polar co-ordinates, ϵ_{rr} and $\epsilon_{\theta\theta}$, at any point in a plate are given by [Timoshenko and Goodier, 1951]

$$\varepsilon_{rr}(r,\theta)=\frac{\partial u_{rr}}{\partial r} \quad (3.4a)$$

$$\varepsilon_{\theta\theta}(r,\theta)=\frac{1}{r}\frac{\partial u_{\theta\theta}}{\partial\theta}+\frac{u_{rr}}{r} \tag{3.4b}$$

Equation 3.4 shows that the normalised radial distortion measured during the DHD technique is not equal to the radial or hoop strain. Rather, the normalised radial distortion is one of two non-zero terms used in the calculation of hoop strain.)

For a stress of σ_{xx} acting in the x-direction, the normalised radial distortion that occurs at the hole edge, which is equivalent to the normalised diametral distortion measured during the DHD technique, is then given by

$$\frac{u_{rr}(\theta)}{a_r}=\frac{d(\theta)-d_0(\theta)}{d_0(\theta)}=\varepsilon_{\theta\theta}(\theta)-\frac{1}{a_r}\frac{\partial u_{\theta\theta}}{\partial\theta}=\frac{\sigma_{xx}}{E}(1+2\cos 2\theta) \tag{3.5}$$

where $d_0(\theta)$ and $d(\theta)$ are the diameters of the reference hole measured before and after trepanning respectively.

For a stress of σ_{yy} acting in the y-direction (i.e. at $\theta=\theta+90°$), the normalised radial distortion that occurs at the hole edge is given by

$$\frac{u_{rr}(\theta)}{a_r}=\frac{d(\theta)-d_0(\theta)}{d_0(\theta)}=\frac{\sigma_{yy}}{E}(1-2\cos 2\theta) \tag{3.6}$$

The case of a shear stress of σ_{xy} acting in the x-y plane can be represented by a direct stress of σ_{xy} acting at both $\theta=\theta+45°$ and $\theta=\theta-45°$. The normalised radial distortion that occurs at the hole edge in this case is given by

$$\frac{u_{rr}(\theta)}{a_r}=\frac{d(\theta)-d_0(\theta)}{d_0(\theta)}=\frac{\sigma_{xy}}{E}(1+2\cos 2[\theta+45°])-\frac{\sigma_{xy}}{E}(1+2\cos 2[\theta-45°]) \tag{3.7}$$

Equation 3.7 can be simplified, using trigonometric equivalencies, to

$$\frac{u_{rr}(\theta)}{a_r} = \frac{d(\theta) - d_0(\theta)}{d_0(\theta)} = \frac{\sigma_{xy}}{E}(-4\sin 2\theta) \tag{3.8}$$

The principle of superposition is then employed to combine the effects of individual uniaxial stresses σ_{xx}, σ_{yy} and σ_{xy} and evaluate the general case of uniform 2D plane stresses acting on a circular hole as

$$\frac{u_{rr}(\theta)}{a_r} = \frac{d(\theta) - d_0(\theta)}{d_0(\theta)} = \frac{1}{E}\left[\sigma_{xx}(1 + 2\cos 2\theta) + \sigma_{yy}(1 - 2\cos 2\theta) + \sigma_{xy}(-4\sin 2\theta)\right] \tag{3.9}$$

where θ is the angle around the reference hole from the x-axis.

The principle of superposition states that if the displacements at all points in an elastic body are proportional to the forces producing them, that is the body is linearly elastic, the effect (i.e. stresses and displacements) on such a body of a number of forces acting simultaneously is the sum of the effects of the forces applied separately [Megson, 1996].

It is important to remember that the distortions measured during the DHD technique are those resulting from the relaxation of the initial stress state. Hence the stresses calculated are equal and opposite to those that initially existed and Equation 3.9 becomes

$$\frac{u_{rr}(\theta)}{a_r} = \frac{d(\theta) - d_0(\theta)}{d_0(\theta)} = -\frac{1}{E}\left[\sigma_{xx}(1 + 2\cos 2\theta) + \sigma_{yy}(1 - 2\cos 2\theta) + \sigma_{xy}(-4\sin 2\theta)\right] \tag{3.10}$$

The equation for the normalised radial distortion is linear with respect to the unknown stresses σ_{xx}, σ_{yy} and σ_{xy}, and therefore can be expressed as

$$\overline{u_{rr}(\theta)} = -\frac{1}{E}\left[\sigma_{xx} f(\theta) + \sigma_{yy} g(\theta) + \sigma_{xy} h(\theta)\right] \tag{3.11}$$

where $\overline{u_{rr}(\theta)}$ is the normalised radial distortion, and $f(\theta)$, $g(\theta)$ and $h(\theta)$ are known from Equation 3.10 so long as θ is also known.

During the DHD technique a total of 18 angles and hence normalised radial distortion measurements are recorded. Equation 3.11 can be re-written as

$$\begin{bmatrix} \overline{u_{rr}(\theta_1)} \\ \overline{u_{rr}(\theta_2)} \\ \vdots \\ \overline{u_{rr}(\theta_{18})} \end{bmatrix} = -\frac{1}{E} \begin{bmatrix} f(\theta_1) & g(\theta_1) & h(\theta_1) \\ f(\theta_2) & g(\theta_2) & h(\theta_2) \\ \vdots & \vdots & \vdots \\ f(\theta_{18}) & g(\theta_{18}) & h(\theta_{18}) \end{bmatrix} \bullet \begin{bmatrix} \sigma_{xx} \\ \sigma_{yy} \\ \sigma_{xy} \end{bmatrix} \tag{3.12a}$$

or

$$\overline{u_{rr}} = -\frac{1}{E}[M_{2D}] \bullet \sigma \tag{3.12b}$$

With 3 unknown stresses and 18 measured normalised radial distortions the equation is over specified and the M_{2D} matrix is non-square. Therefore for matrix inversion a pseudo-inverse matrix is used and an optimum stress vector is calculated using a least squares, 2θ, sinusoidal theoretical fit to the normalised radial distortion data, see Figure 3.17. The optimum stress vector is

$$\hat{\sigma} = -E[M_{2D}]^{*} \bullet \overline{u_{rr}} \tag{3.13}$$

where $[\mathrm{M}_{2\mathrm{D}}]^{*} = \left([\mathrm{M}_{2\mathrm{D}}]^{T} \bullet [\mathrm{M}_{2\mathrm{D}}]\right)^{-1} \bullet [\mathrm{M}_{2\mathrm{D}}]^{T}$ is the pseudo-inverse of matrix $[M_{2D}]$, and $\hat{\sigma}$ is the optimum stress vector that best fits the measured normalised radial distortions, $\overline{u_{rr}}$. $[\mathrm{M}_{2\mathrm{D}}]^{T}$ is the transpose of matrix $[\mathrm{M}_{2\mathrm{D}}]$.

Having determined the in-plane residual stresses σ_{xx}, σ_{yy} and σ_{xy}, the in-plane principal stresses σ_1 and σ_2 can be obtained using

$$\sigma_1, \sigma_2 = \frac{\sigma_{xx} + \sigma_{yy}}{2} \pm \sqrt{\left(\frac{\sigma_{xx} - \sigma_{yy}}{2}\right)^2 + \sigma_{xy}^2} \tag{3.14}$$

The in-plane principal stress direction, ψ, is given by

$$\psi = \frac{1}{2}\tan^{-1}\left(\frac{2\sigma_{xy}}{\sigma_{xx} - \sigma_{yy}}\right) \tag{3.15}$$

3.4.2 3D Residual Stress Analysis

In order to obtain a 3D residual stress distribution, information about the axial distortion of the reference hole needs to be recorded and combined with the air probe diameter measurements. Hence the need for the LVDT during the trepanning process. However, the axial distortion recorded H_{total}, is a combination of both mechanical and thermal axial distortions, and can be written as,

$$H_{total} = H_{mech} + H_{thermal} \tag{3.16}$$

The mechanical axial distortion H_{mech}, is the distortion associated with the release of residual stresses and the thermal axial distortion $H_{thermal}$, is due to the heat input from the EDM process.

As yet, the temperature distribution through the thickness at each increment in time and electrode position is undetermined. Therefore in order to estimate the thermal axial distortion of the core during trepanning, and hence eliminate it from Equation 3.16, the following assumptions are made:

i. Within the core, uniform temperature distributions exist across the planes normal to the reference hole axis,
ii. At each position through the thickness, the temperatures experienced by the local parent material surrounding the core are the same as those experienced by the core.

Using these assumptions, an estimate of the thermal axial distortion of the core at each increment, *i*, in trepanned depth can be calculated using the following equation

$$H_{thermal_i} = h_o \alpha (T_{Ave_i} - T_o) \tag{3.17}$$

where h_o is the original gauge height (i.e. specimen wall thickness plus height of front and rear reference bushes), α is the coefficient of thermal expansion, T_{Ave_i} is the current average temperature of the core and T_o is the original temperature of the core.

During the trepanning process the temperatures of the front and rear faces are measured using the six thermocouples attached around the outside of the core. The temperature of the dielectric is also measured using a seventh thermocouple inserted into the dielectric flow. The average temperature of the core T_{Ave_i}, at each trepanned depth can be estimated by the following equation

$$T_{Ave_i} = aT_{Fr} + bT_{Rr} + cT_{Di} \tag{3.18}$$

where T_{Fr}, T_{Rr} and T_{Di} are the average measured front, rear and dielectric temperatures respectively. The coefficients *a*, *b* and *c* have been calculated from a combination of controlled experiments and FE analyses. The controlled experiments, FE analyses and coefficient derivations are discussed in Section 5.4.

Hence, having estimated the thermal axial distortion, rearrangement of Equation 3.16 gives the accumulated mechanical distortion of the core at each trepanned depth as,

$$H_{mech_i} = H_{total_i} - H_{thermal_i} \tag{3.19}$$

The incremental mechanical axial strain ε_{zzi} of the core at each increment in trepanned depth (h_i - h_{i-1}) is given by

$$\varepsilon_{zz_i} = \frac{\left(H_{mech_i} - H_{mech_{i-1}}\right)}{\left(h_i - h_{i-1}\right)} \tag{3.20}$$

The estimate of the mechanical axial strain can be combined with the in-plane normalised radial distortions to determine an estimate of the complete 3D residual stress distribution. The calculation of the 3-D residual stresses is provided by the following equations

$$\epsilon_{zz} = -\frac{1}{E}\left\{\sigma_{zz} - \nu\left(\sigma_{xx} + \sigma_{yy}\right)\right\} \tag{3.21}$$

$$\overline{u_{rr}(\theta)} = -\frac{1}{E}\left[\sigma_{xx}\left(1+2\cos 2\theta\right)+\sigma_{yy}\left(1-2\cos 2\theta\right)+\sigma_{xy}\left(-4\sin 2\theta\right)+\sigma_{zz}\left(-\nu\right)\right] \tag{3.22}$$

(Note again the presence of the minus signs in both equations to represent the release of residual stresses in both cases.)

Both equations are linear with respect to the unknown stresses σ_{xx}, σ_{yy}, σ_{xy} and σ_{zz}, and therefore can be expressed as

$$\begin{bmatrix} \overline{u_{rr}(\theta_1)} \\ \overline{u_{rr}(\theta_2)} \\ \vdots \\ \overline{u_{rr}(\theta_{18})} \\ \varepsilon_{zz} \end{bmatrix} = -\frac{1}{E}\begin{bmatrix} f(\theta_1) & g(\theta_1) & h(\theta_1) & -\nu \\ f(\theta_2) & g(\theta_2) & h(\theta_2) & -\nu \\ \vdots & \vdots & \vdots & \vdots \\ f(\theta_{18}) & g(\theta_{18}) & h(\theta_{18}) & -\nu \\ -\nu & -\nu & 0 & -1 \end{bmatrix} \bullet \begin{bmatrix} \sigma_{xx} \\ \sigma_{yy} \\ \sigma_{xy} \\ \sigma_{zz} \end{bmatrix} \tag{3.23a}$$

or

$$\Delta = -\frac{1}{E}\left[M_{3D}\right] \bullet \sigma \tag{3.23b}$$

Again, using pseudo-inverse matrices, the optimum stress vector is found to be

$$\hat{\sigma} = -E\left[M_{3D}\right]^{*} \bullet \Delta \tag{3.24}$$

The in-plane principal stresses are given by Equation 3.14, with their direction being given by Equation 3.15. The DHD technique is usually applied such that the axis of the reference hole is along the axis of the third principal stress (i.e. $\sigma_3 = \sigma_{zz}$). If the axis of the reference hole isn't parallel with the axis of the third principal stress, then the stresses calculated (i.e. σ_{xx}, σ_{yy} and σ_{xy}) will be comprised of components of all three principal stress directions, x, y and z.

3.5 Sources of Measurement Error

The accuracy of the DHD technique is heavily dependent upon the accuracy of the measuring devices used. For the 2D analysis the calculated residual stresses are only dependent upon the accuracy of the reference hole diameter measurements made by the air probe. For the 3D analysis the calculated residual stresses are dependent not only on the air probe, but also on the LVDT measuring the axial deformation of the core and the thermocouples measuring the temperature of the specimen. These experimental sources of measurement error used in the DHD analyses are discussed below.

3.5.1 2D Residual Stress Errors

It is known [George, 2000a] that the air probe is unable to measure the diameter of the reference hole accurately at the hole entrance and exit faces (i.e. the front and rear surfaces). Therefore the calculated residual stresses at these depths is also inaccurate. The reason for these inaccuracies is that the air probe uses a square profile surrounding the air exit holes in the tip of the air probe to aid measurement. Figures 3.18a and 3.18b show the tips of the 1.5mm and 3.16mm diameter air probes respectively, highlighting the square profiles and their dimensions. The dimensions of the air probe tips were measured using a Mondo shadow graph machine. The air probes are unable to measure the diameters accurately until the whole of the square profile is inside the hole. Therefore the 3.16mm diameter air probe is unable to measure the reference hole diameter accurately within about 0.7mm of the entrance or exit of the hole. The 1.5mm diameter air probe however is unable to measure the reference hole diameter accurately within about 0.4mm of the entrance or exit of the

hole. Figure 3.19 shows a schematic of an air probe entering the reference hole and the reasons for the distances above.

Previous calibration experiments [George, 2000a] have found that the air probe diameter measurements are accurate to within approximately ±0.5μm. Therefore the deformation of the reference hole is accurate to within 1μm due to the compounded error from both the before and after EDM diameter measurements. To calculate the associated error of the residual stresses, the deformation error is input into the 2D analysis (Equation 3.13) as the deformation at each of the 18 angles, giving

$$\begin{Bmatrix} \delta\sigma_{xx} \\ \delta\sigma_{yy} \\ \delta\sigma_{xy} \end{Bmatrix} = -E \begin{bmatrix} f(\theta_1)' & f(\theta_2)' & \cdots & f(\theta_n)' \\ g(\theta_1)' & g(\theta_2)' & \cdots & g(\theta_n)' \\ h(\theta_1)' & h(\theta_2)' & \cdots & h(\theta_n)' \end{bmatrix} \begin{Bmatrix} \frac{\delta d_{err}}{d_0} \\ \frac{\delta d_{err}}{d_0} \\ \vdots \\ \frac{\delta d_{err}}{d_0} \end{Bmatrix} \tag{3.25}$$

where $\delta\sigma_{xx}$, $\delta\sigma_{yy}$ and $\delta\sigma_{xy}$ are the calculated errors in residual stress, δd_{err} is the deformation error, and $f(\theta_n)'$, $g(\theta_n)'$ and $h(\theta_n)'$ are the terms of the pseudo-inverse matrix $[M_{2D}]^*$.

Instead of inputting the deformation error through the full version of Equation 3.25, an exact and easier calculation of the error can be made by the following simplification to

$$\delta\sigma_{xx} = -E\frac{\delta d_{err}}{d_0}\left(f(\theta_1)' + f(\theta_2)' + \ldots + f(\theta_n)'\right) \tag{3.26}$$

However, when the pseudo-inverse matrix $[M_{2D}]^*$ was calculated, it was found that

$$\left(f(\theta_1)' + f(\theta_2)' + \ldots + f(\theta_n)'\right) = 0.5 \tag{3.27}$$

Therefore Equation 3.26 can be simplified further to enable the calculation of the residual stress error using

$$\delta\sigma_{xx} = -0.5E\frac{\delta d_{err}}{d_0} \tag{3.28}$$

The calculation of the error for the other residual stresses can be inferred from the calculation for $\delta\sigma_{xx}$.

As an example, for a compounded deformation error of ±1μm, an original reference hole diameter of 3.18mm and a Young's modulus, E, of 200GPa, the error of the calculated residual stresses is about ±31MPa.

The error calculated with Equation 3.28 is the maximum possible error due to the air probe measurements. In practice however, the error in air probe measurement is unlikely to occur for all n angles of diameter measurement. Therefore, because of the over-specified M matrix and the consequential least squares fit to the normalised radial distortion data, the practical error in residual stress will be lower. This practical reduction in error by over-specification is the reason for measuring the deformation at more angles than is needed (i.e. 18 angles instead of 3) to calculate the residual stresses.

Another source of error in the air probe measurements is the misalignment in depth between measurements of the reference hole diameter from before and after EDM. For example, the diameter of the reference hole before EDM at a depth of 5mm could be compared with the diameter of the reference hole after EDM at a depth of 6mm. The misalignment in depth produces a deformation error due to the comparison of different diameters from before and after EDM, see Figure 3.20. The effect of the misalignment error is exaggerated when steps in diameter occur. The steps in diameter could arise from scratches, cavities or being at depths near the entrance and exit surfaces of the reference hole (i.e. the measured diameter inside and outside of the hole). The use of gundrilling to manufacture the reference hole helps to reduce the presence of scratches. Unfortunately, cavities and measuring at

depths near the entrance and exit surfaces of the reference hole are inevitable. Therefore by keeping the increment in depth at which the air probe is stepped down the reference hole to a small value the error in misalignment is also small. However a compromise is made between the depth increment being infinitely small (i.e. misalignment error = 0) and the time taken to measure the diameter of the hole being practical (i.e. less than infinity). Currently the increment in depth is 0.2mm and so the maximum error in depth misalignment is ±0.1mm. The effect of the misalignment error results in the calculation of "noisey" residual stresses. The calculated residual stresses would then require smoothing to reduce the magnitude of the noise and determine a residual stress trend line. The overall effect of the smoothing operation is beneficial, however damping of the measured residual stress gradients and peaks does occur.

3.5.2 3D Residual Stress Errors

The analyses used for the calculation of the 3D residual stresses are prone to errors due to the estimation of various parameters. The errors discussed here are those arising from the measurement apparatus alone and not the estimated parameters. The estimated parameters are discussed further in Section 5.4.

The errors associated with the air probe are also applicable to the 3D residual stress calculations. However the 3D residual stress calculations also include measurements taken from the deformation LVDT and the thermocouples.

Calibration of the deformation LVDT allowed for the calculation of a linear best-fit equation to the measured data. The resulting best-fit linear equation calculates the deformation of the LVDT with a maximum error of ±0.7μm. Calibration of the deformation LVDT is discussed later in Section 4.3.2.

Calibration of the thermocouples also allowed for the calculation of a linear best-fit equation to the measured data. The resulting best-fit linear equation calculates the temperature measured by the thermocouples with a maximum error of ±0.5°. Calibration of the thermocouples is also discussed later in Section 4.4.3.

Experience has found that when the EDM takes place near the front and rear surfaces of the specimen, the front and rear temperature measurements are dominated by localised effects from the EDM tool rather than the temperature of the core. Therefore when using the 3D analysis, the calculated thermal distortions and hence through-thickness residual stresses within 5mm of the front and rear surfaces are inaccurate. The calculated 3D residual stresses are therefore always omitted at these depths to avoid confusion.

Chapter 4: ADVANCES IN THE DHD PROCESSES

4.1 Introduction

The previous chapter presented the "state of the art" condition of the DHD technique. The description included the modifications and refinements carried out to the DHD equipment, process and analysis during this research project. This chapter highlights and discusses the modifications and refinements made to the DHD equipment and process to achieve that "state of the art". The modifications and refinements carried out on the DHD analysis are discussed in Chapter 5.

The first section describes a review of various machining processes with respect to their suitability for the requirements of the present and future DHD technique. The following sections then concentrate on the refinements of the preferred machining processes and experimental set-up that have improved the DHD technique. The final section discusses and concludes the topics presented within the chapter.

4.2 Alternative Machining Processes

As previously mentioned, the main objective of this project was to undertake research and development of the DHD technique to increase its accuracy, to miniaturise the technique and to introduce a portable system. Miniaturisation of the DHD technique requires more intricate machining to be achieved from the present machining processes. At present, the gundrilling system can successfully manufacture the standard 3.18mm diameter reference holes, but is unable to meet the specifications needed to manufacture the specialised 1.5mm diameter reference holes. The required spindle speed (10000rpm) and cutting oil pressure (100bar) are approximately double the capacity of the present gundrilling system. The extraction of smaller diameter cores to suit the smaller diameter reference holes is within the

capabilities of the EDM system and would only require the use of a suitable sized electrode.

Therefore investment would be needed to increase the capabilities of the gundrilling system and also the DHD technique. Before the committal of investment though, the assumption that gundrilling was still the most suitable process to manufacture the reference holes was questioned. Therefore a review was undertaken of alternative machining processes for carrying out the DHD technique. The review was made with the use of available literature on machining and machine tools ([Boothroyd and Knight, 1989], [ASM, 1989] and [Hall-Stephens, 2001]). The review was aimed at finding the most suitable machining process or processes for carrying out the manufacture of the reference hole and the core. Advances in portability would certainly be aided by the use of a single machining process for carrying out both operations.

The review is presented below which looks at both the "conventional" and "non-conventional" machining processes available. The review then leads into experimental trials using the most suitable process or processes found before finalising with a discussion and conclusions.

4.2.1 Conventional Machining Processes

All conventional machining processes rely on the relative movement between the cutting tool and work-surface for the removal of material. The different machining processes are then categorised by the design, and relative axes of movement of both machine and tool. Gundrilling for example, is a specialised variant of the conventional drilling process requiring a specialised drill bit and machine. The following section discusses other adaptations of machining tool and process for use in the different machining stages of the DHD technique.

Split-point Drill Bits

Increased accuracy from the use of basic drilling machinery and procedures can be implemented through the use of split-point drill bits. Originally developed for the

manufacture of small diameter, deep-holes in automotive crankshafts, the use of split-point drill bits has now become more widespread. The design of a split-point drill bit is very similar to that of a standard twist drill bit, however identification is provided by the tip profile, as shown in Figure 4.1. The main identification points are the presence of a secondary cutting edge and the reduced width of chisel edge. The additional cutting edge and reduced chisel width improve the centring capability of the drill.

Peck Drilling

Frequent drill bit retraction from the work surface to clear chips is known as peck drilling and is the recognised method for the manufacture of small diameter, deep-holes using standard twist drill bits. With small diameter hole drilling, the removal of chips is restricted by the greater ratio of web thickness to diameter of the drill bits used. Alternatively, if instead of chips, metal powder is formed, packing could occur, causing the drill bit to break. Both problems may be alleviated by peck drilling through frequent drill bit retraction, clearing of the hole and the application of a lubricant.

Air-turbine Drilling Machine

For the manufacture of small diameter holes, high spindle speeds are needed to maintain the correct cutting speed between the cutting edge and the work-surface. Vibration of the drill bit and hence drilling machine needs to be kept to a minimum for the maintenance of high tolerances. Standard drilling machines use large, heavy electric motors to supply the rotary motion of the drill bit. Air-turbine drilling machines however use high pressure air to turn a turbine and provide the rotary motion for the drill bit. Air turbine drilling machines typically provide very high spindle speeds, little vibration but low torque. Air-turbine drills are commonly used for an alternative residual stress measurement technique called centre-hole drilling (CHD).

Reaming

Reaming is a machining process that can be used after initial hole manufacture in which a rotary tool takes a light cut from around the hole edge to improve its accuracy and surface roughness. The depth of hole to be reamed is usually limited to be less than or equal to the length of the cutting edges on the tool. For a 3.18mm diameter reamer the depth of hole should be limited to 31mm and for a 1.5mm diameter reamer the depth of hole should be limited to 21mm. Within these limits, diameter tolerances of less than 25μm and surface finishes of 1μm can be achieved. Reaming holes at depths greater than the above-specified limits compromises accuracy.

Honing

Honing is a machining process that can also be used after initial hole manufacture. Honing is a controlled, low-speed sizing and surface finishing process in which material is removed by an abrasive rotary tool. Surface finishes of less than 1μm can be achieved with a standard honing process.

Trepanning

Tools are available for performing a trepanning operation under the classification of a conventional machining process. The tools usually consist of a fly cutter mounted on a twist drill, as shown in Figure 4.2. The central drill bit acts as both driver and pilot by drilling a central hole at the same time as trepanning. Tools without the central drill bit do exist, however rigidity during the process is more difficult to maintain and there is a greater likelihood of tool chatter and loss of dimensional control. A normal drilling head can be used to provide the rotation of the tool. Unfortunately, the trepanning tool is limited in its use to sheet material where the clearance of chips is unrestricted by the small depth of cut.

4.2.2 **Non-conventional Machining Processes**

The non-conventional machining processes mentioned below utilise a variety of different energy sources for removing work piece material. Schematics of the

different processes are shown in Figure 4.3 (Source: [Boothroyd and Knight, 1989]), grouped according to the energy source used. Three processes use a mechanical action, namely ultrasonic machining, abrasive-jet machining, and water-jet machining (including abrasive water-jet machining). Four of the processes use an electro-thermal action, namely electron-beam machining, laser-beam machining, plasma-beam machining and EDM. The remaining two processes use a chemical action, namely chemical machining and electro-chemical machining (including electro-chemical grinding).

Ultrasonic Machining

During ultrasonic machining the process of material removal is by the abrasive action of a grit-loaded slurry circulating between the work-surface and the tool, which vibrates at ultrasonic frequencies. The tool is gradually fed into the work piece to produce a cavity corresponding to the shape of the tool. Hole diameters ranging from as small as 0.076mm to an upper limit of 75mm can be drilled. Machining depths of 50mm or more are possible, but depths are usually of the order of 5mm or less. Tolerances of ±0.25mm and surface finishes of 25μm can routinely be obtained. Ultrasonic machining can be used on most materials whether electrically conductive, non-conductive, metallic, ceramic, or composite and is particularly effective on hard, brittle materials.

Abrasive-jet Machining

As the name suggests, abrasive-jet machining removes material through the chipping action of an abrasive jet. The abrasive jet is formed from the mixing of micro-abrasive particles and a pressurised inert gas before exiting at high velocity through a small nozzle directed at the work-surface. Tolerances of ±0.12mm and surface finishes ranging between 0.25 and 1.25μm can be obtained. Mechanical and thermal damage is limited during the process due to the relatively low overall machining forces generated and the cooling effect of the jet. The process is well suited to hard, brittle materials and performing intricate cutting, drilling, polishing, and etching operations. When cutting and drilling however, the process is restricted to metal foils and thin sections of ceramics and glass.

Water-jet Machining

Similar in principal to abrasive-jet machining, material is removed through the erosion effects of a high velocity, small diameter water-jet. Mechanical and thermal damage is negligible. Tolerances depend on the material being cut, but are generally within ±0.1 to 0.2mm. Tapering does occur, increasing with material thickness, which can be up to 100mm. Water-jet machining is mainly used for the machining of soft, non-metallic materials in sheet form, often in multi-layer stacks. However, abrasive particles can be added to the water-jet enabling it to be used on hard, metallic materials; used in this form the process is known as abrasive water-jet machining.

Electron-beam Machining

In electron-beam machining, material removal is by means of a focussed beam of high-velocity electrons that strike the work-surface. The kinetic energy of the electrons is converted into heat that is sufficient to cause rapid vaporisation/melting of the work-surface material. To eliminate scattering of the electron beam the work is done in a vacuum chamber and a magnetic lens is used for focusing. Being another non-contacting process, forces exerted on the work-surface are eliminated allowing for the machining of brittle/fragile materials. Thermal damage (i.e. the heat affected zone (HAZ)) is confined to a circumferential layer of less than 0.025mm thick due to the extremely high energy density of the beam and the short duration of application. Multiple pulses can be used for the penetration of thick specimens. Multiple deflection coils can be used to move the beam around to cut holes of any shape.

Laser-beam Machining

Laser-beam machining removes material by means of a high-energy, coherent beam of light vaporising/melting the work-surface upon which it is focussed. The process is non-contacting and so mechanical damage and tool wear are non-existent. However, due to the vaporising/melting action of the laser-beam a small HAZ is inevitable. Holes produced using this process are generally tapered and are only

approximately round. Again, multiple pulses can be used for the penetration of thick specimens.

Plasma-beam Machining

Plasma-beam machining utilises a high temperature plasma beam focussed on the work-surface causing rapid vaporisation/melting of the material. Any gas heated to extremely high temperatures dissociates into free electrons, ions, and neutral atoms and this condition is known as plasma. Materials up to 200mm in thickness can be penetrated, however the tolerance of cut increases with increasing thickness (e.g. ±0.8mm for 25mm thickness). Significant HAZ is also produced varying between 0.7 and 5mm in thickness.

EDM

The method of material removal by EDM was described earlier in Section 3.2.5. EDM can create holes with a diameter as small as 0.3mm. With efficient flushing, deep-holes can be created with diameter to depth aspect ratios of 1:100. Surface finishes of the order of 0.25μm and better can be achieved.

Chemical Machining

In chemical machining a strong acid or alkaline solution is used to selectively dissolve material away, resulting in controlled material removal. A chemically resistant coating is selectively applied to the material protecting the areas not to be machined. Dimensional tolerances at depth are difficult to maintain using this process. Hard, brittle materials are well suited to this process.

Electro-chemical Machining

ECM is the metal removal process in which electrolytic action is used to dissolve the work-surface material. High-current, low-voltage electricity is connected across the electrode and component whilst the machining surface is constantly flushed by electrolytic fluid. The action of the current flowing through the electrolyte between electrode and work-surface dissolves the material. The current flows across the

smallest gap between electrode and work-surface, and therefore shaped cavities can be formed using an appropriately shaped electrode. The whole process is non-contacting and so no mechanical damage occurs. Thermal damage from the flowing current is kept to a minimum due to the cooling effect of the electrolyte. ECM is mainly applied to difficult-to-machine materials, such as those used in high temperature applications.

ECM was used previously for the trepanning operation during the DHD technique. The ECM process was found to be highly volatile, it removed excessive quantities of material and extracted cores with low dimensional tolerances. Therefore during the research carried out by George [2000a] a switch to EDM was made.

4.2.3 Experimental Reference Hole Manufacture

After assessing the various machining processes available, it was decided that the manufacture of a satisfactory reference hole would only be possible by either conventional machining processes or EDM. However the process of core extraction would still only be possible by EDM. Therefore if conventional machining processes were used to carry out the manufacture of the reference hole and EDM used for core extraction, a double machining process would still occur for the DHD technique. The only improvements to the DHD technique would arise from the use of EDM throughout. Therefore an investigation of the EDM process was undertaken experimentally by the manufacture and measurement of through-holes in a 100 x 50 x 20mm thick stainless steel block.

EDM Trials

During the DHD technique, when carrying out the trepanning process, the surface finish of the resulting cut is compromised due to the required speed of operation. If the EDM machine is to be used for the manufacture of the reference hole however, then the balance between surface finish and speed for this operation needs to be redressed. The programme of trials is presented below.

- Hole 1 was manufactured using a non-rotating electrode with the block submerged in a dielectric tank. A tubular, copper electrode of diameter 3.18mm was used with the machine settings appropriate for a high surface finish.

After approximately 3mm in machining depth, a build up of debris on one side of the electrode occurred. The debris reduced the localised spark gap, hence sparking and erosion between the debris and the specimen then occurred resulting in a disfigured hole entrance. The manufacture of hole 1 was therefore aborted.

- Hole 2 was manufactured in the same manner as hole 1, except that some of the machine settings were changed to increase the flushing of the work surface.

The process took a considerable amount of time due to the fine erosion of the material needed for the high surface finish, but it completed without fault. Visual inspection of hole 2 revealed however, that it tapered very badly when increasing in depth from start to finish of the EDM. The taper was also uneven, because the hole started off circular and finished as an ellipse. A possible cause could have again been the gradual uneven build-up of debris on the electrode.

- Hole 3. In order to further increase the flushing of the work surface and also decrease the process time, a roughing cut was introduced for the manufacture of hole 3. First, an initial through-hole was made with a tubular, copper electrode of diameter 2.4mm and machine settings to suit a fast, low surface finish cut. The 2.4mm electrode was then replaced by a 3.18mm tubular, copper electrode and the machine settings changed back to suit a cut with a high surface finish.

The process completed without fault and in a considerably shorter period of time. The initial rough hole permitted double sided flushing of the work surface during the second stage of the manufacture. Visual inspection of hole 3 still revealed tapering, from a larger diameter at the EDM start to a smaller diameter at the finish, however the extent of tapering was much reduced and the hole appeared to remain circular. The probable cause of tapering in hole 3 is a common problem caused by continued sparking and hence erosion between the sides of the electrode and the hole walls as the electrode is advanced.

- Hole 4. A change in EDM machine to one that could rotate the electrode was implemented at this stage. The EDM machine used was the one used horizontally during the DHD technique. In order to carry out the trial a number of changes to the EDM machine's normal use were implemented. The machine was mounted vertically on the 3-axis milling machine bed instead of horizontally, flushing was supplied by external jets instead of at high pressure through the centre of the electrode, and electrode guides were used for alignment and to eliminate electrode wobble.

The same two-stage procedure incorporating a 2.4mm diameter roughing-cut, followed by a 3.18mm diameter finishing-cut was used. The finishing cut however was only performed to a depth of 18mm allowing inspection of the size of the roughing cut over the last 2 mm.

The roughing cut was of a sufficiently small diameter such that any evidence of its previous existence was completely removed by the finishing cut. The diameter of the rest of hole 4 was measured at 4 angles (i.e. 0°, 45°, 90° and 135°) and at 0.25mm steps, the results are shown in Figure 4.4. The measured diameter of the hole was outside of the calibration range of the air probe and so the results shown do have a level of uncertainty about them. However, uncertainty or not, the results do show a tapering of hole 4 with a starting diameter of approximately 3.332mm and a diameter of 3.306mm at a depth of 7.8mm. What was encouraging about the results was that the diameter measurements between each angle were very close indicating that the hole was circular.

- For hole 5, the process of manufacture was the same as for hole 4, but a new finishing electrode was made with a backed-off tip profile to limit the tapering effect. The electrode consisted of a 3mm diameter shaft onto which larger diameter tips could be fixed, the design of the electrode is shown in Figure 4.5. For the manufacture of hole 5, a 3.06mm diameter tip was used on the finishing electrode.

The resulting diameter of the completed hole was too small to be measured by the air probe and therefore the profile of the hole is unknown.

- For hole 6, the machine settings and process of manufacture remained unchanged, but a larger, 3.08mm diameter tip was used on the finishing electrode.

Again the resulting diameter of the completed hole was too small to be measured by the air probe. However, a "Flex-hone" was used to enlarge the hole diameter to allow its measurement, the results are shown Figure 4.6. Honing using a "Flex-hone" was previously found to uniformly increase the diameter of a hole without changing the surface roughness (George [2000a]). The diameter measurements of hole 6 remained within the calibration range and show a non-circular hole, bowing out in the centre, with a widely distributed range of diameter.

- For hole 7, the machine settings and process of manufacture remained unchanged, but a larger 3.11mm diameter tip was used on the finishing electrode.

During the finishing stage it was noted that the larger electrode diameter had little effect on the roughed-out hole, only sparking at the start and finish of the depth. Inspection of the equipment revealed that the electrode guides had enlarged and become very sloppy resulting in a larger than normal roughing cut. Hole 7 was measured using the air probe and the results are shown in Figure 4.7. The diameter measured was out of calibration range throughout the depth and therefore there is again some uncertainty in the measurements. The hole has a bowed profile becoming smaller and non-circular toward the start and finish depths.

- The EDM of hole 8 was carried out outside of the University at a specialist EDM company. The stainless steel block used for hole 8 was of the same material as that used for holes 1 – 7, but 100mm thick instead of 20mm.

An initial through-hole of about 1mm diameter was introduced using a tubular brass electrode on a conventional EDM machine. The block was then transferred to a "state of the art" wire-EDM machine for the final sizing operation. The initial hole was used as the starting hole to thread the wire through. The block was then submerged in dielectric and the wire proceeded to spiral out to make a final hole diameter of 3.18mm.

Hole 8 was measured using the air probe and the results are shown in Figure 4.8. The measured hole diameter shows a bowed profile becoming smaller and non-circular towards the start and finish depths. The bowed profile is again consistent with the problem of inadequate dielectric flushing within the hole.

4.2.4 Manufacturing Discussion and Conclusions

Although the conventional machining processes (e.g. peck drilling with a split-point drill bit followed by a reaming/honing operation) were reviewed and found theoretically capable of manufacturing the reference holes, the abilities of gundrilling were still unsurpassed.

During the EDM trials, many problems and sources of machining error were encountered with the manufacture of the reference holes (e.g. inadequate flushing, electrode wear, unguided electrodes). To alleviate the problems, changes to the EDM process were instigated and even a trial on a "state of the art" precision wire-EDM machine was carried out. Unfortunately none of the changes dramatically improved the successful manufacture of an adequate reference hole. Also, the repeatability of the EDM process across differing materials is thought to be highly variable. Therefore EDM was found to be incapable of reliably and repeatedly manufacturing the precision reference holes required for the DHD technique. However, despite the downfalls of EDM to produce the tolerances needed for the reference hole, it is still the best machining process for the rough trepanning operation.

Therefore in conclusion, a double machining operation is still required for the DHD technique. Gundrilling to manufacture the precision reference hole and EDM to carry out the trepanning operation.

4.3 Core Miniaturisation

Having found that gundrilling and EDM presented themselves as the best machining operations to carry out the DHD technique, any improvements made to achieve the miniaturisation objective could then be tailored accordingly.

As mentioned previously, at the start of this research project the range of specimen thicknesses that the DHD technique had been successfully applied was between 20 – 100mm. It was apparent that there was a relatively large gap in the thickness application between the two most widely used residual stress measurement techniques (i.e. CHD and X-ray diffraction (XRD)) and that of the DHD technique. The gap accounts for specimen thicknesses in the range of 3.2 – 20mm, see Figure 4.9. Therefore the miniaturisation objective of this research project was implemented to reduce the gap and hence increase the range of specimen thicknesses over which the DHD technique could be applied.

Previous research [George, 2000a] highlighted the effect of core diameter on the accuracy of residual stress measurements using the DHD technique. George showed empirically that for an accurate residual stress measurement the core diameter should be less than half the specimen thickness. Therefore to fulfil the miniaturisation objective, the diameter of the extracted core should be reduced in order to adhere to the core diameter to thickness ratio of 1:2.

George [2000a] used an electrode with a 22mm ID for the standardised extraction of a core with a 20mm OD. George introduced the use of an electrode with a 12mm ID for the specialised extraction of a core with a 10mm outside diameter (OD) where the specimen thicknesses were less than 30mm. Both the "20mm" and "10mm" cores contained a 3.18mm diameter reference hole at their centres. Miniaturisation required the standardised extraction of the smaller "10mm" cores and the specialised extraction of core with a 5mm OD. In order to achieve these requirements, several aspects of the DHD technique needed to be re-assessed and re-designed.

4.3.1 Front Reference Bush Re-design

For the standard operation, the OD of the front reference bush would need to be reduced from less than 20mm to less than 10mm. The design of the "20mm" front bush is shown in Figure 4.10. The key feature of the reference bush is the external micro screw thread needed for the calibration of the capacitance gauges. The capacitance gauges, which have now been replaced by an LVDT, were used for the measurement of the axial deformation of the core during the EDM process. The manufacture of the micro screw thread on the front bush was not a standard workshop operation and required great skill and time for accurate reproduction. The cap to screw onto the micro screw thread was even more difficult to manufacture due to accessibility to the internal workface for machining. New reference bushes were manufactured for each DHD measurement, but the screw cap was used repeatedly. For the manufacture of smaller diameter front bushes, the prospect of successfully reproducing the micro screw thread on the front bush let alone inside a cap was impractical. Therefore a new design of front bush was made and is shown in Figure 4.11.

The main features of the new design are:

i. 9mm maximum OD,
ii. Wasted external profile,
iii. Standard M6 internal screw thread.

With a 9mm maximum OD the new front bush was small enough to fit within the EDM electrode and remain intact during the EDM process. The wasted external profile serves as a bearing surface on which alignment tools are used to improve the concentricity of the different machining processes. The bearing surface of the "20mm" front bush had been its internal bore. Standardising the internal screw thread of the new front bush allowed for a more efficient and practical manufacturing process. However, the relatively coarse screw thread now made the calibration of the capacitance gauges impossible. This factor was considered during the re-design process and was one of the reasons why the capacitance gauges were replaced with an LVDT. The main benefit of using the LVDT is that there is no need for

calibration every time it is set-up for a measurement and therefore no need for a calibration micro screw thread.

The extraction of the "5mm" cores is aided by the gundrilling of 1.5mm diameter reference holes. Unfortunately the 1.5mm diameter reference holes are too small for the use of the LVDT and protruding rod set-up during the trepanning operation. Therefore the front reference bushes used for the "5mm" cores are just cylinders of material with an OD of less than 5mm.

4.3.2 Measurement of Axial Deformation

Originally capacitance gauges performed the measurement of the axial deformation of the core during the EDM process. As mentioned in Section 4.3.1, the capacitance gauges were replaced by an LVDT to aid the manufacture of the smaller diameter front reference bushes. This was not the only reason however, as other benefits were produced as a result.

The calibration procedure for the LVDT and hence the core's axial deformation was improved. The set-up of the capacitance gauges was similar to that of the LVDT. This can be seen by comparing Figures 3.12 and 4.12. However, the capacitance gauges needed re-calibrating every time they were used. Calibration of the capacitance gauges was difficult and usually took at least an hour each time. The LVDT however, was calibrated immediately after purchase and only requires checking annually. Calibration of the LVDT was more accurate having been carried out using a barrel micrometer with a 0.5μm resolution. Figure 4.13 shows the calibration curve of the LVDT and the calibration coefficients, which calculates the deformation of the LVDT with a maximum error of ±0.7μm. Calibration of the capacitance gauges was provided by their repeated movement back and forth by the rotation of the screw cap through ±90°. The ±90° rotation was estimated by eye and was therefore highly prone to errors.

Also, as shown in Figure 4.12, the capacitance gauges were attached to the rod protruding through the reference hole from the front bush. Therefore the weight of the capacitance gauges on the rod would transmit a bending moment to the front

bush. The transmitted bending moment increased the likelihood of detachment of either the front bush and/or the core during the EDM process. The LVDT however, is attached to the rear bush and not the protruding rod, therefore no undue forces or moments are transmitted to the front bush. The bracket attaching the LVDT to the rear bush was specifically designed for use during the DHD technique and is shown in Figure 4.14. The design of the bracket enables the axial alignment of the LVDT with the reference hole and hence alignment of the protruding rod within the LVDT. The bracket design also allows for movement of the LVDT along its axis for datum finding.

4.3.3 EDM Electrode Re-design

The machining of a smaller diameter core would obviously be carried out with a smaller diameter electrode. Ordinary copper tubing was previously used for the manufacture of the "20mm" electrodes and any imperfections in straightness and diameter were taken out when the electrode was turned-down to the correct size. Unfortunately, when standardising the extraction of "10mm" cores, even for great depths, it was found that the manufacture of extra long "10mm" electrodes using the same practice was fruitless. With the reduced diameter and hence reduced bending moment of inertia, the electrodes would buckle under the bending moment applied by the turning tool. Therefore alternative electrode designs were temporarily used where the main shaft of the electrode was manufactured from aluminium and a copper tip was screwed onto the end, see Figure 4.15. The main aluminium shaft had a wasted profile ensuring that arcing between the electrode and specimen only occurred at the tip. The controlled arcing increases the efficiency of the EDM process, decreases the time taken, and improves the average diameter tolerance along the entire length of the core. However, problems were encountered with wear of the electrode. The screw thread holding on the tip would wear and the tip fall off inside the component or complete wear of the tip leaving just the aluminium main shaft. The problems encountered with long the bi-metallic electrodes were solved with the out-sourcing of precision copper electrodes requiring little machining.

4.3.4 EDM Chuck Re-design

Reducing the electrode diameter by half also meant that the material removed from the trepanned hole was also approximately halved. The reduced material removal resulted in a smaller hole for the dielectric to pass down to flush the work-surface. The smaller hole produced a greater back-pressure and caused the dielectric to flow not down the centre of the electrode but out the back of the chuck around the outside of the electrode. The work-surface as a result had little flushing to cool the cutting process and subdue the volatile nature of spark erosion. The reduced flushing also increased the wear of the electrode, increased the build up of removed material debris, and caused arcing between the side of the electrode and the debris thus lowering the machining tolerances and producing a non-circular, non-concentric core. The EDM chuck was redesigned from that of a standard adjustable 3-jaw chuck (similar to an electric drill chuck), see Figure 4.16, to produce a fully enclosed, non-adjustable chuck, as shown in Figure 4.17. The tolerances of the fit of the electrodes within the chuck are such that there is no gap for the dielectric to escape, only pass down the centre of the electrode as desired. The chuck re-design successfully abated the by-pass of the dielectric fluid and restored adequate flushing to the work-surface.

4.3.5 Reduced Reference Hole Diameters

The design changes described in the previous sections were all implemented to standardise the extraction of "10mm" cores and make "20mm" core extraction obsolete. The extraction of "10mm" cores allows DHD measurements to be made on specimen thicknesses down to 20mm. The diameter of the reference hole at 3.18mm means that the "10mm" core wall thickness is approximately 3.5mm. Decreasing the core diameter further creates another potential error. The error would occur with misalignment between the gundrill and EDM machining axes or wandering of either of the tool tips. The trepanned hole must not intersect with the reference hole otherwise data would be lost in the proximity of the breakthrough.

Errors after further core diameter reductions could also occur due to the nature of EDM. EDM was chosen for the trepanning operation for many reasons, one of them

being its relatively stress free machining characteristics. Research by Rebelo et al [1998] and Wong et al [1995] have shown that residual stresses are generated by EDM in the sub-surface layer of the material machined. Tensile residual stresses of the order of 600MPa can be generated in steels at depths of up to 100μm falling to 0MPa at 300μm. Therefore, if the wall thickness of the extracted core becomes too small, the tensile residual stresses generated during the EDM process will have a more than negligible effect.

Due to the errors highlighted above, decreasing the core diameter further also required decreasing the diameter of reference hole. Gundrills are readily available for drilling holes down to a diameter of 0.74mm, however the air probes to measure the very small reference holes are very specialist and are made to order. An air probe and calibration rings to measure a reference hole of 1.5mm diameter were made. The intricate manufacture of the very fragile air probe took 3 attempts and cost 10 times that of a 3.18mm diameter air probe. Unfortunately, when the diameter of the air probe was halved, so too was the calibration range and hence the required tolerance of the gundrilled hole increased. Calibration/validation experiments using the 1.5mm air probe are discussed in Section 6.2. Reducing the reference hole diameter to 1.5mm enabled the use of a "5mm" electrode and the extraction of a "5mm" core. The redesign of the EDM machine and tooling for "10mm" core extraction was sufficient for use with "5mm" core extraction. Extraction of a "5mm" core enables the DHD technique to be applied to specimen thicknesses down to 10mm. DHD residual stress measurements have been successfully carried out with the extraction of a "5mm" core and are presented in Sections 7.2.1 and 7.4.1. Figure 4.18 shows the comparative sizes of a "10mm" and "5mm" core.

4.3.6 Miniaturisation Discussion and Conclusions

The changes presented above were implemented for the benefit of increasing the range of application of the DHD technique. However other benefits are also experienced as a result.

Reducing the diameter of the extracted core directly reduces the amount of material removed from the component. This in turn enables more DHD measurements to be

taken from the same component as the proximity between measurements could be reduced. High localised stresses (stress concentrations) in materials caused by holes are well documented and form the basis on which the proximity is calculated. The general rule of thumb used is that the perimeter of the next core should be at a minimum distance of 3 times the diameter away from the previous extracted core, see Figure 4.19. Hence the distance between DHD measurements reduces by 3 times the reduction in core diameter.

Another benefit of core diameter reduction is the reduction in sampling volume for the residual stress measurement. As mentioned earlier, the residual stresses acting on the reference hole are released during trepanning, that is the residual stresses acting within the core are released. The release of the residual stresses then causes the core to deform to a new state of equilibrium with near zero residual stresses. The smaller the core diameter, the closer the proximity of stress-free surfaces and hence a more stress-free final state. The actual residual stress release to an approximately stress-free final state will be an average release from one equilibrium state to another. Therefore the deformation of the reference hole will be the projection of this average release. If the core diameter is reduced there is a reduced sampling volume over which the average will be taken and a more accurate measurement will be made. This is especially important when measuring steep stress gradients where the upper and lower bound of residual stresses contained within the core are very different.

Yet another benefit is the reduction in time taken to extract a smaller core due to the reduction in material excavated. A reduction in core diameter by half also reduces the volume of material excavated and time taken by approximately half.

On the other hand, the changes also aided in increasing the penetration of the DHD technique. The gundrills and air probes were already capable at large penetration depths. The limiting factor to the penetration of the DHD technique was due to the EDM process and the flushing of the work-surface with adequate dielectric. Therefore the redesign of the EDM chuck to improve its flushing capabilities allowed for the increase in penetration of the DHD technique. Following the changes, DHD residual stress measurements have been successfully carried out at penetration depths of 430mm and are presented in Section 7.2.5.

Therefore through the changes highlighted above, the range of application of the DHD technique has been increased from 20 – 100mm to 10 – 430mm. The increased range is reflected in Figure 4.20, which is an updated version of Figure 4.9.

4.4 Other Refinements

Not all the refinements made to the DHD process were directly related to specific objectives. The refinements described below for example were for the general development of the DHD technique. The refinements were implemented to simplify the set-up procedures of the technique, to increase the automation of the technique, to increase the accuracy of the technique and to increase the efficiency of the technique.

4.4.1 Cleaner Gunrilling Operation

During the gundrilling operation the high pressure cutting oil containing swarf exits the drilled reference hole by passing up the single flute of the gundrill. On exiting the front reference bush the cutting oil is no longer contained by the walls of the reference hole and is free to spray in any direction. The previous method of containment of the cutting oil has been from the encasement of the gundrilling set-up with polythene sheeting. The polythene sheeting would then contain and collect the oil spray before redirecting it to designated containers. The pool of oil within the containers would then be poured back into the pump and filtration system to repeat the cycle. Unfortunately, the polythene encasement was always a "Heath Robinson" structure and the cutting oil would escape, contaminating the equipment, experimental set-up, clothing and general working environment. This arrangement was therefore wholly unprofessional and unsatisfactory.

The solution in cleaning up the gundrilling operation was the simple introduction of a chip box containing a "grommet", as used by the gundrill manufacturers and sub-contractors. The "grommet" is a plastic disc, approximately 15mm diameter and 2mm thick, with a kidney shaped hole at its centre. The size of "grommet" used is such that the kidney shaped hole is the exact size to fit over the main shaft of the gundrill. The "grommet" then prevents any further flow of the cutting oil up the

gundrill's single flute passed its position. The "grommet" therefore redirects the spent cutting oil outwards, parallel to its face, from the centre of the drill. The radial spray of cutting oil is then contained using the chip box and redirected to the designated containers. The set-up of the chip box and "grommet" is shown in Figure 4.21.

The use of the chip box and "grommet" is not only cleaner and more professional but also quicker to set-up and take-down.

4.4.2 Reference Hole Diameter Measurement

As mentioned in Section 3.2.4, the measurement of the diameter of the reference hole is provided by the use of an air probe. The back-pressure of the air supplied to the air probe deforms a diaphragm which is measured using an LVDT. Previous to this research, the electronics used to power and measure the LVDT were connected to the PC datalogger via an analogue to digital (A/D) converter. The connection between the LVDT electronics and the A/D converter was not recognised within the technical specifications of the LVDT electronics and was therefore carried out "in-house". Unfortunately the signal to noise ratio through the connection was very low, hence the diameter measurements recorded by the PC were heavily prone to noise induced errors. However, with being noise induced errors, the calculated residual stress profiles were good, just very erratic. Therefore smoothing operations were carried out on the residual stress profiles to average out the noise and improve the results.

During this research, the accuracy of the recorded diameter measurements and hence calculated residual stresses was improved by the addition of new LVDT electronics with a dedicated signal connection. The signal was passed between the LVDT electronics and the PC through a dedicated communication serial link. The commands and communication protocols were programmed into the existing software for the air probe datalogging and control procedures. The signal was now communicated digitally in a 7-bit data format and the noise errors were eradicated.

4.4.3 Core Temperature Measurement

The use of thermocouples during the EDM process was instigated prior to this research project. The six thermocouples measuring the front and rear temperature of the specimen were recorded manually. The increment in time between each measurement varied from every minute for the first 5 minutes and then increasing to 2, 4 and 8 minutes before reaching and remaining constant at 15 minutes after the first hour. The varied increments in time were due to the rate of change of temperature of the specimen. For the initial 45 minutes of the EDM process the flow of heat through the specimen is considered to be transient. Therefore the measurements are taken more regularly to record the rapid increase in temperature of the specimen. After 45 minutes the flow of heat through the specimen reaches a steady-state where the heat input is in approximate equilibrium with the heat loss. Therefore the rate of increase in temperature of the specimen becomes very slow and 15 minute increments are more than adequate to fully record the profile. The manual recording of the thermocouple temperatures at the start of the EDM process was heavily intensive and therefore during this research project an automatic thermocouple recorder was acquired. The automatic thermocouple recorder was able to be connected to a PC that provided datalogging, control and power.

The thermocouples used to measure the temperature of the specimen were K-type with a fibreglass shield. The ends of the two constituent conductors were spot-welded together and to the specimen in a single operation at the desired locations. Spot-welding was used to achieve a sound electrical connection between the two conductors and a sound thermal connection to the specimen. Unfortunately the spot-weld also made a sound electrical connection between the thermocouples and the specimen. This became a problem when the thermocouples were connected to the automatic datalogger. During the EDM process, large amounts of power are transmitted through the specimen via the sparks providing material erosion. Therefore the mV temperature signals of the thermocouples are negligible when compared to the power of the EDM system and hence during spark erosion the thermocouples recorded a large amount of noise.

In order to overcome the measurement of noise, the spot-welding of the thermocouples to the specimen was replaced with gluing. The glue used to adhere the thermocouples to the specimen was a thermal bonding epoxy normally used to adhere heat sinks to electrical components/circuits. The properties of the thermal bonding epoxy are ideal. The epoxy is electrically insulating and highly thermally conductive allowing the thermocouples to have a sound thermal connection to the specimen without the electrical connection.

It was found however that this did not fully overcome the problem of noise. The source of the reduced noise was then thought to originate from EMI from the specimen, which was then amplified by the specimen table. Therefore the fibreglass shielded thermocouples were replaced with stainless steel shielded thermocouples. The stainless steel shielding provides a Faraday Cage around the thermocouple tip eliminating the effects of EMI and the measurement of noise.

Calibration of the thermocouples was carried out using a furnace and high precision thermometer (accuracy ±0.04°C). The shielded thermocouples were connected to the automatic recorder and inserted into the furnace along with the calibrated thermocouple. The furnace temperature was then stepped up in 5°C increments from room temperature (i.e. 20°C) up to 70°C. 70°C corresponds to 1.5 times the maximum temperature ever recorded by the thermocouples during EDM. After each increment in temperature the furnace was allowed to reach a steady, uniform temperature throughout, ensuring that the shielded thermocouples and the calibrated thermocouple were at the same temperature. During the whole calibration procedure the temperature of all thermocouples was recorded every 30 seconds. Analysis of all the temperature measurements allowed for a calibration curve to be plotted and the accuracy of the thermocouples identified. The calibration curve is shown in Figure 4.22, which plots the temperature measured by the automatic recorder against the exact temperature measured by the calibrated thermocouple. The calibration coefficients therefore allow for the automatically recorded temperatures to be converted into accurately calibrated temperatures. The calibration coefficients calculate the temperature of the thermocouples with a maximum error of ±0.5°.

Chapter 5: STRAIN ANALYSIS OF THE DHD TECHNIQUE

5.1 Introduction

The previous chapters have presented a "state of the art" description of the DHD technique and the modifications and refinements made to the DHD equipment therein. This chapter highlights and discusses the modifications and refinements carried out on the DHD analysis to couple with those of the equipment to achieve the "state of the art" condition of the DHD technique.

The first section describes an analysis to investigate the dominant frequencies of variation within the measured normalised radial distortions. The second section reviews previous research regarding the refinement of the 2D residual stress calculations and its implementation thereof. The last section develops an improved analysis of the core temperature during EDM for use in the 3D residual stress calculations.

5.2 Power Spectral Density

The DHD analysis presented in Section 3.4 describes how the experimental measurements of reference hole diameter are converted into residual stresses. The basic equation developed for the DHD analysis is Equation 3.10 and is repeated below for reference.

$$\frac{u_{rr}(\theta)}{a_r} = \frac{d(\theta)-d_0(\theta)}{d_0(\theta)} = -\frac{1}{E}\left[\sigma_{xx}(1+2\cos 2\theta)+\sigma_{yy}(1-2\cos 2\theta)+\sigma_{xy}(-4\sin 2\theta)\right]$$

The equation shows that the measured normalised radial distortion is a periodic function with a frequency of 2. Hence, when inverted, the optimum stress vector is calculated from a theoretical 2θ least squares fit to the measured normalised radial distortions. Further analysis of the measured normalised radial distortions does show them to be evenly distributed about the 2θ fit, see Figure 5.1. Therefore it could be argued that Equation 3.10 should contain extra terms of a higher frequency (e.g. 3θ, 4θ, 5θ, etc) so that the curve passes through an increased number of data points, increasing the accuracy of the analysis and ultimately the accuracy of the measurement technique.

Therefore work was undertaken to investigate the measured normalised radial distortions using power spectral density (PSD) analysis. The power spectral density analysis makes use of the Fast Fourier Transform (FFT) to analyse the data. The FFT converts the time domain normalised radial distortion measurements into a frequency domain representation, see Figure 5.2. The frequency domain representation is a complex number with real and imaginary parts. The PSD is the square of both parts resulting in an amplitude squared representation of the frequencies present within the data.

The normalised radial distortion measurements are calculated from the reference hole diameter measurements made by the air probe from 0° - 170° at 10° intervals. Above 170° the diameter measurements are repeated (i.e. 0° = 180°, 20° = 190°, etc). Therefore the only possible frequencies within the normalised radial distortion measurements are even numbered frequencies from 2 to 18 due to diameter measurement repetition.

The normalised radial distortion measurements from all residual stress components can be tested using the PSD analysis. For example, the PSD analysis for a 48mm thick, butt-welded pipe is shown in Figure 5.3. The 48mm thick, butt-welded pipe is discussed later in Section 7.2.4. The graph shows the PSD calculated for every 1mm in depth through the thickness of the pipe and has been normalised with respect to a frequency of 2. When compared to a frequency of 2, it can be seen that for the majority of the thickness any other frequencies present within the normalised radial

distortion measurements have an amplitude squared of less than 5%. In other words, the presence of the 2θ signal is more than 20 times larger than any other signal.

Even at 5% though, it can be said that there is still a presence of other frequencies. In order to check the source of the other frequencies, the impact of experimental error and noise on an idealised set of normalised radial distortion measurements was analysed. A random normalised radial distortion error (maximum value of $\pm 1.6 \times 10^{-4}$) was superimposed onto the idealised normalised radial distortion measurements and the PSD analysis repeated. The random normalised radial distortion error is analogous with the error of the air probe diameter measurements. Figure 5.4 shows the 2θ least squares fit, the idealised set of normalised radial distortion measurements and the idealised plus random error normalised radial distortion measurements for a depth of 23mm.

Figure 5.5 shows the through thickness PSD results for the pipe using the idealised plus random error normalised radial distortion measurements. Again it can be seen that for the majority of the thickness the amplitude squared is comparatively low for frequencies other than 2. However frequencies can be found with amplitude squared values as high as 10% which can only be accountable to the diameter measurement errors.

Therefore the general idealisation of the measured normalised radial distortions to Equation 3.10 is justified. Any suggested appearance of frequencies other than 2θ in the measured normalised radial distortions can be accounted for by experimental error.

5.3 Parameter Updating

Section 3.4 described the standard analysis used during the DHD technique for the calculation of residual stresses. Previous research by Garcia-Granada et al [1998] presented refinements to the analysis using FE analyses to model the deformation of the reference hole when subjected to a uniform applied stress. The outcome of the

research was the proposed introduced of parameters *A(z)* and *B(z)* into the standard 2D equation (Equation 3.10) to refine the analysis for thick components.

The initial research by Garcia-Granada et al [1998] was carried out on plates measuring 50mm square of varying thickness subjected to a constant uniaxial stress of 100MPa. The research presented here examines the effects of varying the square dimensions of the plate and the effects of varying the magnitudes of biaxial stress applied.

5.3.1 Basic Model Generation and Analysis

A 3D FE analysis was used to model a 50mm square by 20mm thick plate containing a 3.18mm diameter reference hole at its centre. The axis of the reference hole was through the thickness of the plate, see Figure 5.6.

The 3D solid elements used to model the plate are classified as 20-noded quadratic brick elements (C3D20). During node generation, the spacing between adjacent nodes in the plane normal to the hole axis was increased as the distance from the hole edge increased. The spacing between adjacent nodes through the thickness of the plate was also modified. The node concentration was increased towards the front and rear surfaces of the plate to account for near surface affects. The spacing of the nodes was varied so that the resolution of the analysis was optimised. The increased spacing was automatically set using the "BIAS" parameter available in ABAQUS. The value entered for the "BIAS" parameter is the ratio of spacing between adjacent nodes.

Once generated, the plate was subjected to a fully elastic stress/displacement analysis assuming material properties of E = 210GPa and ν = 0.3. The uniform stress was applied as a distributed load normal to the reference hole axis at the edges of the plate.

The data file produced from the analysis recorded the deformation of the nodes around the hole edge through the thickness of the plate. The deformations were recorded in Cartesian co-ordinates x and y. Equation 3.10 however requires the input

of reference hole deformations in Polar co-ordinates and at specific angles. Therefore the deformations were transformed from Cartesian co-ordinates into Polar co-ordinates. The deformation of the hole from a perfect circle into a perfect ellipse was used to transform the co-ordinate system. Figure 5.7 shows the deformation of the hole from a circle into an ellipse as calculated by the model.

The equation for an ellipse is

$$\frac{x^2}{a^2} + \frac{y^2}{b^2} = 1 \qquad (5.1)$$

where a and b are the semi-major and semi-minor axes.

Rearrangement of Equation 5.1 into the form defining a straight line (i.e. $y = mx + c$) enabled the perfect elliptical shape of the deformed reference hole to be verified. Rearrangement gives

$$y^2 = \frac{-b^2}{a^2} x^2 + b^2 \qquad (5.2)$$

Plotting the shape of the deformation hole using Equation 5.2 and fitting a straight line through the points enabled the calculation of a and b, and the verification of the elliptical shape with a calculated coefficient of regression, $r^2 = 1$. Figure 5.8 shows the plotted data and the values of a, b and r^2.

The points around the elliptical hole edge for diameter measurement are defined in Cartesian co-ordinates by Equation 5.2 and in Polar co-ordinates by the following

$$x = r\sin\theta \quad \text{and} \quad y = r\cos\theta \qquad (5.3)$$

where r is the radius and θ is the angle anti-clockwise from the x-axis.

The combination and rearrangement of Equations 5.2 and 5.3 give the deformed diameter of the hole ($d = 2r$) at any angle θ as

$$d = 2\sqrt{\frac{a^2 b^2}{a^2 \sin^2\theta + b^2 \cos^2\theta}} \tag{5.4}$$

The initial and deformed diameters were then used to calculate the normalised radial distortions of the reference hole and then compared with those predicted by the theoretical analysis of Equation 3.10.

Garcia-Granada et al [1998] proposed that there would be discrepancies in normalised radial distortion at the surfaces of the plate near to the reference hole entrance and exit. The theoretical analysis had no allowances for these surface effects and so Garcia-Granada et al [1998] proposed the introduction of parameters *A(z)* and *B(z)* into Equation 3.10 to become

$$\varepsilon_{rr}(\theta, z) = -\frac{A(z)}{E}\left[\sigma_{xx}\left(1 + 2B(z)\cos 2\theta\right) + \sigma_{yy}\left(1 - 2B(z)\cos 2\theta\right) + \sigma_{xy}\left(-4B(z)\sin 2\theta\right)\right] \tag{5.5}$$

A(z) represents a measure of the uniform expansion of the reference hole and *B(z)* the eccentricity of the reference hole.

Garcia-Granada et al [1998] calculated the values of parameters *A(z)* and *B(z)* using curve fitting to the reference hole normalised radial distortion data. However, parameter updating was now used to calculate the values of *A(z)* and *B(z)* at each position through the plate. The following equations were used to perform the updating procedure [Greening, 1999].

$$\begin{Bmatrix} \delta\varepsilon(\theta_1) \\ \delta\varepsilon(\theta_2) \\ \vdots \\ \delta\varepsilon(\theta_n) \end{Bmatrix} = \begin{bmatrix} \dfrac{\delta\varepsilon(\theta_1)}{\delta A} & \dfrac{\delta\varepsilon(\theta_1)}{\delta B} \\ \dfrac{\delta\varepsilon(\theta_2)}{\delta A} & \dfrac{\delta\varepsilon(\theta_2)}{\delta B} \\ \vdots & \vdots \\ \dfrac{\delta\varepsilon(\theta_n)}{\delta A} & \dfrac{\delta\varepsilon(\theta_n)}{\delta B} \end{bmatrix} \begin{Bmatrix} \delta A \\ \delta B \end{Bmatrix} \tag{5.6a}$$

or

$$\{\delta\varepsilon\} = [S]\{\delta P\} \tag{5.6b}$$

where $\{\delta\varepsilon\}$ is the difference between the FE normalised radial distortion and the theoretical normalised radial distortion (i.e. $\{\delta\varepsilon\} = \{\varepsilon_{FE}\} - \{\varepsilon_{Theory}\}$), [S] is the sensitivity matrix and $\{\delta P\}$ is the change in updated parameter. The sensitivity matrix describes the sensitivity of a change in normalised radial distortion to a change in *A(z)* and *B(z)*.

Inversion of Equation 5.6 using the pseudo-inverse of the sensitivity matrix, $[S]^* = \left([S]^T \bullet [S]\right)^{-1} \bullet [S]^T$, gives

$$\{\delta P\} = [S]^* \bullet \{\delta\varepsilon\} \tag{5.7}$$

Equation 5.7 gives the change in *A(z)* and *B(z)* that corresponds to the difference in normalised radial distortion between the FE and theoretical calculations. The change in *A(z)* and *B(z)* is then applied to Equation 5.5 and the updating procedure repeated. The repetition of the updating procedure increases the resolution of the calculated parameter change and improves the normalised radial distortion matching through convergence. Figure 5.9 shows the convergence of the updated theoretical normalised radial distortion towards the FE normalised radial distortion due to repeated analyses.

A MATLAB routine was created to automatically perform the updating procedure, which is shown in Appendix A.

5.3.2 Size Dependent Analyses

The basic FE model generated, applied a 100MPa tensile load to a 50mm square, 20mm thick plate. The theoretical analysis however was developed for an infinitely square, thin plate. Therefore an initial set of models were generated of a 100MPa load applied to a 20mm thick plate with varying square dimension.

Figure 5.10 shows the results of the analysis of the normalised radial distortions using parameter updating. It can be seen that parameter *A(z)* remains approximately constant at a value near 1 throughout the thickness of the plate. Parameter *B(z)* however is approximately 1 near the surfaces of the plate and exponentially decreases to a value of 0.92 at the centre of the plate. Both parameters show a symmetric variance about the centre of the plate as expected. It can also be seen that both parameters converge to a set of final values as the square dimension of the plate increases to 300mm square. The convergence showed that the ratio of dimensions of the plate is critical. The dimension of the plate modelled by Garcia-Granada et al was 50mm square and 20mm thick and is shown to have the largest difference to the final converged set of parameter values. Therefore the basic FE model used for all further analyses was 300mm square and 20mm thick.

5.3.3 Load Dependent Analysis

The size trials were carried out using an applied tensile stress in the x-direction of 100MPa. However this is not a full representation of the stresses experienced by real engineering components. Therefore further models were generated with uniaxial and bi-axial loading of varying magnitudes to more effectively represent the loading cases experienced by real engineering components.

Figure 5.11 shows the results of the parameter updating analysis carried out for parameter *A(z)*. It can be seen that parameter *A(z)* remains approximately constant between depths of 0.3 – 19.7mm for all stress configurations. Figure 5.11 also shows that as the stress becomes increasingly equi-biaxial the average value of *A(z)* increases. When the stress configuration is equi-biaxial, regardless of magnitude, the average value of *A(z)* is the same at 0.9988. Conversely, the minimum average value of parameter *A(z)* (*A(z)* = 0.9905) was found with the maximum uni-axial stress configuration (i.e. σ_{xx} = 700MPa and σ_{yy} = 0MPa). Parameter *A(z)* does represent a measure of the uniform expansion of the hole and so the above findings are not unexpected. Uniform expansion of the hole occurs when the stress configuration is equi-biaxial.

Figure 5.12 shows the results of the parameter updating analysis carried out for parameter *B(z)*. It can be seen that for the majority of stress configurations parameter *B(z)* decreases from an average value of 1.0000 at the surface of the plate to an average value of 0.9048 at mid-thickness. Parameter *B(z)* is shown to be symmetrical about mid-thickness as expected. The average value of *B(z)* increases as the stress configuration becomes increasingly uni-axial. Parameter B does represent a measure of the eccentricity of the hole and so the above findings are again not unexpected.

Figure 5.12 also shows that there is a line at $B(z) = 1$. The line is in fact more than one set of data, occurring when equi-biaxial stress configurations are applied to the plate. The equi-biaxial stress configurations uniformly expand the hole and hence are not a function of eccentricity and *B(z)*. Therefore during the updating procedure, the value of normalised radial distortion is insensitive to changes in *B(z)*, and so *B(z)* is not changed from its initial value of 1.

5.3.4 Parameter Implementation

Following completion of their work, Garcia-Granada et al [1998] did not fully implement their findings into Equation 3.10, rather parameters *A(z)* and *B(z)* were assumed to be equal to 1 and a maximum error of about 15% was accepted. The maximum error occurred for the shear stress at the surfaces of the plate. During this research however, equations for parameters *A(z)* and *B(z)* have been found and are presented below.

For implementation into Equation 3.10 parameter *A(z)* can be assumed to be constant throughout the thickness of the specimen with an averaged magnitude of 0.9967. The air probe diameter measurements are not considered to be accurate within 0.7mm of the surface of the plate, see Section 3.5.1, therefore the maximum error in using an averaged parameter *A(z)* between the depths of 0.7mm – 19.3mm is 0.0063 or 0.6%.

The relatively large range in value of parameter *B(z)* through the thickness of the plate eliminated the effective use of a constant value as suggested for parameter *A(z)*

and therefore a regression fit was needed. The symmetrical shape of parameter *B(z)* allowed for the reduction in quantity of data by half. Parameter *B(z)* was therefore reduced as shown in Figure 5.13 and a 5 parameter, double exponential decay was found to best fit the data.

$$B = B_0 + ae^{-bz} + ce^{-dz} \tag{5.8}$$

where B_0, a, b, c and d are the coefficients of the fit.

An average profile of updated parameter *B(z)* was calculated for the regression fit. The coefficients for the average profile were found to be

$$B_0 = 0.9012$$
$$a = 0.0605$$
$$b = 3.1600$$
$$c = 0.0383$$
$$d = 0.2543$$

Figure 5.13 shows the regression fit to the data which resulted in a coefficient of regression, $r^2 = 0.99984$. Over- or under-estimation of parameter *B(z)* due to the use of an average produces an error band of +0.0066 and -0.0024 (or +0.66% and -0.13%). The reason for the unequal error band is that a mean value of *B(z)* was used to calculate the regression and not a median value. The mean was used so that the calculated value of *B(z)* implemented in the analysis would give the least error for most of the time.

In order to calculate the values of *B(z)* for the symmetrical data and for depths within the reference bushes, the application of the fit needs care. If the depth of the reference hole deformation measurement is within the bushes then $B(z) = 1$. However if the depth of the reference hole deformation measurement is within the component, taking into account for the symmetrical data, then

$$B(z) = B_0 + ae^{-b\left(\frac{t}{2} - \left|z - \frac{t}{2}\right|\right)} + ce^{-d\left(\frac{t}{2} - \left|z - \frac{t}{2}\right|\right)} \tag{5.9}$$

where t is the thickness of the component.

5.3.5 Discussion

The original theoretical analysis centres around the loading of an infinitely large, thin plate under plane stress conditions. The original analysis developed Equation 3.10 which when compared to the refined equation (Equation 5.5) shows that theoretically parameters $A(z)$ and $B(z)$ are equal to 1. For the refined analysis of the relatively thick plate, the values of $A(z)$ and $B(z)$ tended to 1 at the surfaces of the plate where only a state of plane stress can exist, which is in agreement with the theoretical analysis.

When using $A(z) = B(z) = 1$ throughout the thickness of the component, the maximum error occurs at mid-thickness where $B(z)$ is a minimum (i.e. $B(z) \approx 0.9048$) and not at the surfaces where $B(z) = 1$ as Garcia-Granada et al suggested. At mid-thickness the plate material behaves more like plane strain conditions, not plane stress on which the analysis is built, hence the location of maximum error. Empirically, using $A(z) = 1$ creates a maximum error of 0.33%, and using $B(z) = 1$ creates maximum errors of 4.76% and 0% for biaxial and equi-biaxial stress cases respectively.

5.4 Core Temperature Estimation

The measurement and analysis used to calculate the in-plane residual stresses (i.e. σ_{xx}, σ_{yy} and σ_{xy}) is well understood and accurate. However the measurement and analysis used to calculate the out-of-plane residual stress, σ_{zz}, is still in development. During this project investigations have been carried out to improve the methodology used for the calculation of σ_{zz}.

As mentioned in Section 3.4.2, to calculate both the in- and out-of-plane residual stresses, σ_{xx}, σ_{yy}, σ_{xy} and σ_{zz}, the analysis uses both the measurement of the reference hole diameter deformation and the measurement of the axial deformation of the core.

The measurement of the reference hole diameter deformation is performed by the air probe and known to be accurate. The area of investigation was therefore concentrated on the measurement of the axial deformations of the core.

The axial deformations of the core are measured during the EDM process. The measured axial deformations are caused by the release of the residual stresses and the thermal expansion of the core. For the accurate calculation of the residual stresses the deformation due to thermal expansion needs to be identified and eliminated from the measurements. In order to identify the thermal expansion of the core, thermocouples are attached to the front and rear faces of the specimen around the measurement location. The thermocouples record the temperature of the specimen during the EDM process and the measurements are used to estimate the temperature and hence thermal expansion of the core. The thermal expansion of the core is estimated using Equation 3.17, which is shown below for reference.

$$H_{thermal_i} = h_o \alpha \left(T_{Ave_i} - T_o\right)$$

The accuracy of the calculated thermal expansion, $H_{thermal}$, depends upon the value of average core temperature, T_{Ave_i}, used. Previous research [George, 2000a] introduced the use of the average front and rear thermocouple measurements for T_{Ave_i}, be used. However this was thought to be inaccurate and an improved method of estimating the average core temperature was investigated using a combination of experiments and FE analyses.

5.4.1 Experiments

The experiments were carried out to replicate the EDM process on real components during the DHD technique. A cylindrical stainless steel sample was manufactured for the experiment to act as the component for measurement. The cylindrical shape was chosen for the benefit of the FE simulations, the reasons for which are discussed later. The sample had an outside diameter of 150mm and a thickness of 60mm, see Figure 5.14. The sample was manufactured with great care so that any residual stresses introduced were negligible. Without residual stresses, any through-thickness

deformations of the core during the EDM process were accountable to thermal expansion alone.

The sample was orientated and fixed on the specimen table so that the axis of the reference hole would coincide with the axis of the sample. Wooden inserts were packed between the clamps and the sample to provide thermal insulation from the surrounding structures and prevent unpredictable heat loss. Extra thermocouples were attached to the sides of the sample and inserted into the dielectric flow to increase data collection during the EDM process. A single thermocouple was used to also record the room temperature. The increased data collection, helped to set the boundary conditions for the FE analysis and its validation thereof. The final experimental set-up is shown in Figure 5.15.

The sample was subjected to the DHD technique by manufacturing a 3.18mm diameter reference hole and extracting a "20mm" core. The deformations of the reference hole diameter were unnecessary for the purposes of this experiment and so were not measured.

The EDM process was undertaken using the standard machine settings and progressed at a rate of about 8mm/hr. The core deflection and temperatures were recorded every 30 seconds throughout the experiment. The copious amounts of data were reduced to best fit lines to ease manipulation. Figures 5.16 and 5.17 show the temperatures and core deflection recorded during the experiment, respectively.

5.4.2 Finite Element Analysis

The measurements of temperature and core deflection during the experiment show the effects of the EDM process on the outside of the sample. The objective of the experiment was to provide the boundary conditions for FE simulations and show the effects of the EDM process on the inside of the sample. ABAQUS was used to simulate the EDM process.

Basic Model Generation

The cylindrical samples used for the experiments allowed for a simplified 2D axi-symmetric model to be developed. The use of cylindrical samples also eliminated the analysis of complex heat transfer paths found at the corners of samples.

Figure 5.18 shows the axi-symmetric model generated for the simulation of the experiment. As well as the stainless steel sample, the front and rear bushes, and the glue were included and are identified in Figure 5.18. Also shown is the axis of symmetry used for the model which was the axis of the reference hole. The axi-symmetric solid elements used throughout the model are classified as 4-noded bilinear displacement and temperature elements (CAX4T).

A higher element density was used within and immediately around the core to increase the resolution of the analysis in these areas where higher temperature and displacement gradients would be encountered.

Having built the element mesh, the boundary conditions were then applied using a mixture of experimental and theoretical values. The boundary conditions applied to the mesh were the heat input at the electrode tip, Q, and the air and dielectric film heat transfer coefficients, h_a and h_d respectively. The areas of application of the boundary conditions are shown in Figure 5.19.

The progression of the electrode through the sample during the EDM process is very slow and therefore the heat flow can be considered to be steady-state. So to simulate the progression of the EDM process, independent models were analysed for every 5mm increment in depth assuming a steady-state heat flow. The model was modified for each increment in depth by removing elements and updating the boundary conditions. The temperature and displacement results from each analysis were then compared with those of the experiment.

Discrepancies between the results of the model and the experiments lead to model refinements and re-analysis. The basic model underwent 4 stages of boundary

condition refinement before achieving its present state. The applied boundary conditions and their refinements are discussed below.

Boundary Conditions

The EDM machine settings remained constant during the experiment providing a constant power to the electrode from start to finish. Therefore the heat input from the EDM process was modelled as a constant concentrated heat flux at the node corresponding to the position of the electrode tip. It was assumed that sparking and hence heat input did not occur along the sides of the electrode.

The cooling effect of the air and dielectric were modelled using a fluid film layer. For a film layer the heat flow between the surface and the fluid passing over is calculated using

$$\dot{q} = -h(T_f - T_s) \tag{5.10}$$

where T_f is the fluid temperature, T_s is the surface temperature, h is the film heat transfer coefficient and $\dot{q}$ is the heat flux.

ABAQUS uses Equation 5.10 to perform the thermal analysis, taking values of h and T_f from the user and generating T_s within the analysis itself. For air cooling, T_f was measured during the experiment and an average value of h (h = 7.1W/m^{2}K) was referenced [W1]. For the dielectric, T_f was measured during the experiment and h was calculated using the Dittus-Boelter equation ([Bsebsu and Bede, 2002] and [W2]).

$$\mathrm{Nu} = 0.023\,\mathrm{Re}^{0.8}\,\mathrm{Pr}^{0.4} \tag{5.11}$$

where Nu, Re and Pr are the Nusselt, Reynolds and Prandtl numbers respectively.

$$\mathrm{Nu} = \frac{hl}{k} \tag{5.12}$$

$$\mathrm{Re} = \frac{\rho u d_e}{\mu} \tag{5.13}$$

$$\mathrm{Pr} = \frac{\mu C_p}{k} \tag{5.14}$$

where h is the film heat transfer coefficient, l is the length of surface to fluid contact, k is the thermal conductivity, ρ is the density, u is the velocity, d_e is the equivalent flow diameter, μ is the dynamic viscosity, and C_p is the specific heat capacity.

The values used for the calculations were either attained from the dielectric technical data sheet or measured during the experiment.

The main variable used to refine the boundary conditions and hence the model was the heat transfer coefficient for the dielectric. Most of the variables used in the calculation of the heat transfer coefficient are mechanical properties of the dielectric fluid and hence non-variable. The only other variables available for change in Equation 5.11 are the velocity, u, and length of surface contact, l, of the dielectric fluid. However, the incremental change in length of surface contact of the dielectric fluid is linked to the incremental change in depth of trepanning. Therefore the length of surface contact is a function of the trepanned depth and hence not variable. Therefore the velocity of dielectric fluid flushing the work-surface was the major factor controlling the successful modelling of the EDM process.

The flow rate of the dielectric pump and filtration system was measured before the EDM process was started. The measured value corresponded to the maximum flow rate possible during EDM. This was because, as the electrode progressed through the sample the filtration system became increasingly clogged with eroded material and the efficiency of the pump system decreased. Also, the progression of the electrode through the sample also increased the depth for the supply of dielectric to the work-surface which the decreasingly efficient pump system could not provide. Therefore the velocity of dielectric decreased during the experiment decreasing the coefficient of heat transfer and the cooling effect of the dielectric.

Results

The initial analysis performed used constant boundary conditions throughout the EDM process (i.e. Q, h_a and h_d all remained constant). Figure 5.20 shows the front and rear temperatures during the EDM process for both the experiment and the FE analysis. It can be seen that there was a constant increase in the experimental temperatures of the sample during EDM. However the FE model shows a decrease in temperature of the sample during EDM. It is evident that for the FE with a constant h_d, the dielectric provides more cooling as the area of contact with the sample increases due to the increased machining depth.

After 4 stages of model refinement, accounting for the reduced efficiency of the dielectric cooling, the temperatures of the FE model show an improved agreement with those of the experiment. Figure 5.21 shows the front and rear temperatures during the EDM process for both the experiment and the FE analysis. It can be seen that further refinements to the modelled temperatures and hence the FE analysis were still required, however at this stage an initial analysis of the results was performed.

The FE modelled temperature distributions through the core were calculated for each 5mm increment in trepanned depth. The calculated temperature distributions are shown in Figure 5.22. It can be seen that the distributions are all similar in shape, with increasing temperatures from the front to a maximum at the position of the electrode tip before decreasing slightly towards the rear bush. The average temperature was calculated for each distribution. Figure 5.23 shows the average, front and rear thermocouple temperatures from the FE model, as well as the corresponding dielectric temperature measured during the experiments and used in the FE analysis. The following equation was then fitted to the data linking the average core temperature to the front, rear and dielectric temperatures.

$$T_{Ave} = aT_{Fr} + bT_{Rr} + cT_{Di} \tag{5.15}$$

where T_{Ave}, T_{Fr}, T_{Rr} and T_{Di} are the average, front, rear and dielectric temperatures respectively. a, b and c are unknown coefficients.

Equation 5.15 can be expanded to encompass all the incremental measurements into matrix form.

$$\begin{bmatrix} T_{Ave}(5mm) \\ T_{Ave}(10mm) \\ \vdots \\ T_{Ave}(55mm) \end{bmatrix} = \begin{bmatrix} T_{Fr}(5mm) & T_{Rr}(5mm) & T_{Di}(5mm) \\ T_{Fr}(10mm) & T_{Rr}(10mm) & T_{Di}(10mm) \\ \vdots & \vdots & \vdots \\ T_{Fr}(55mm) & T_{Rr}(55mm) & T_{Di}(55mm) \end{bmatrix} \begin{bmatrix} a \\ b \\ c \end{bmatrix} \tag{5.16a}$$

or

$$T_{Ave} = [T_M] \bullet C \tag{5.16b}$$

where $C = [a \quad b \quad c]^T$.

Equation 5.16 is over specified and hence inversion using the pseudo-inverse matrix of $[T_M]$ allows for the calculation of a, b and c from a least squares fit giving

$$\hat{C} = [T_M]^{\dagger} \bullet T_{Ave} \tag{5.17}$$

Using Equation 5.17 the unknown coefficients a, b and c were calculated as

$$\hat{C} = \begin{bmatrix} a \\ b \\ c \end{bmatrix} = \begin{bmatrix} 0.7372 \\ 0.1557 \\ 0.0756 \end{bmatrix} \tag{5.18}$$

5.4.3 Implementation

Having carried out FE analyses to define Equation 5.15 using the temperature measurements of the experimental EDM process, the Equation was then implemented to predict the axial thermal distortion measured during the experiment. Therefore the experimentally measured front, rear and dielectric fluid temperatures were entered into Equation 5.15 to calculate the average core temperature which was then used to calculate the axial thermal distortion. Figure 5.23 shows a comparison

between the average core temperature predicted using Equation 5.15 and that predicted using the previous method (i.e. average of front and rear temperatures). Also shown are the front, rear and dielectric temperatures measured during the experiment. It can be seen that the temperatures predicted by Equation 5.15 were for the majority of the sample thickness less than the temperatures predicted by the previous method. At most depths, the temperatures predicted by Equation 5.15 were also calculated to be less than the temperatures measured at the front and rear surfaces of the sample.

The axial thermal distortion of the core was then calculated using both predictions of the average core temperature. Figure 5.24 shows a comparison of the axial thermal distortions calculated using the two methods and that measured during the experiment. It can be seen that the axial thermal distortions calculated using both methods were similar in shape to that measured. The axial thermal distortion calculated using Equation 5.15 however was found to be the most accurate, remaining approximately parallel throughout the majority of the thickness of the sample.

5.4.4 Discussion and Conclusion

Following omission of the axial thermal distortions within 5mm of the front and rear surfaces due to their already inherent error, see Chapter 3, the offset/error between the predicted and measured axial thermal distortions using Equation 5.15 was found to be +6μm.

The FE analyses and experiments were carried out to estimate the average core temperature during the EDM process for a 60mm thick specimen and Equation 5.15 was developed. The equation however is still applicable to thicker or thinner specimens due to the input of real experimental temperature measurements. The front, rear and dielectric temperature measurements recorded during the EDM process for each specimen are input into Equation 5.15 to apply boundary conditions. The input of the temperature boundary conditions should result in the widespread applicability of the equation.

As mentioned earlier, further refinements to the FE analysis are still required increasing the accuracy of the predicted temperatures and decrease the error in axial thermal distortion.

Chapter 6: CALIBRATION EXPERIMENTS

6.1 Introduction

All experimental processes pass through validation procedures before widespread confidence and acceptance of them is gained. The validation procedures provide important information on the processes concerning accuracy, repeatability, reliability, and possible errors. Various different calibration studies have already been undertaken during the many years of development of the DHD technique (Bonner [1996] and George [2000a]). The complementary studies undertaken here are specific to the progression of the DHD technique towards miniaturisation, and the widening of its application.

The first set of calibration studies presented investigates the area of miniaturisation through the use of a 1.5mm diameter reference hole for the measurement of stress. The second set of calibration studies presented investigates the measurement of steep stress gradients, in this case a step change. The third set of calibration studies investigates the use of the DHD technique on a non-metallic material.

6.2 Smaller Reference Holes

The previous calibration studies (Bonner [1996] and George [2000a]) have involved the measurement of stresses in specimens for which the values and distributions are well defined and easily predicted using theory. However for some of the cases, slight variants in stress to those predicted by theory have been measured and later argued to be the result of inaccuracies in the practical application of the loads. Therefore, for the course of the calibration studies presented in this section, the load application and induced stress distributions have been taken back to the basics of the uniaxial loading of a plate in a servo-hydraulic test machine.

6.2.1 Test Parameters

Previous to this research the DHD technique was applicable (empirically) to specimens down to a thickness of 20mm and calibration studies have been undertaken to this extent. Therefore, for the course of these calibration studies specimens of 20mm thickness and less were tested.

For the measurement of the induced stress distribution within the specimen, a reference hole was manufactured through the thickness, normal to the loading direction, see Figure 6.1. Introduction of the hole however induces a stress concentration field around it, as shown in Figure 6.2. The stress experienced at the hole edge increases to 3 times the nominal stress. The stress then exponentially decreases to equal the nominal stress at a distance of 3 times the hole diameter, away from the hole axis. Studies by Lin and Chou [1995] on the centre-hole drilling measurement technique, have shown that there is negligible error in the stresses measured due to local yielding during drilling of the stress concentrating hole when the levels of residual stresses present are less than 65% of the yield strength. It is hoped that this is also applicable to the deep-hole drilling technique, however further work would have to be carried out to confirm as such.

The term "nominal stress" is defined as the stress experienced by the specimen due to the applied load acting over the reduced cross-sectional area dissecting the hole, see Figure 6.2. The nominal stress can therefore be calculated using the following equation.

$$\sigma_{nom} = \frac{P}{(w - d_0)t} \tag{6.1}$$

where P is the applied axial load, d_0 is the diameter of the reference hole, and w and t are the width and thickness of the specimen respectively. To accurately measure the induced nominal stress within the specimen, strain gauges were attached to the sides of the specimen in alignment with the reference hole, see Figure 6.1. Therefore the specimen had to be of a certain thickness such that the strain gauges did not pick up the stress concentration and measure the applied load and induced nominal stress

incorrectly. For a reference hole of 3.18mm diameter, the width of the specimen had to be at least 19.08mm. A width of 30mm was chosen.

The stress measured using the DHD technique however was not the nominal stress, as measured using the strain gauges, but the stress induced in the specimen as if the reference hole was not present. The induced stress can be calculated using the following equation

$$\sigma_{ind} = \frac{P}{wt} \tag{6.2}$$

In order to convert the strain gauge measured nominal stress into the DHD measured induced stress, Equations 6.1 and 6.2 were combined to give

$$\sigma_{ind} = \left(1 - \frac{d_0}{w}\right)\sigma_{nom} \tag{6.3}$$

The stresses now referred to throughout this section for the uniaxially loaded specimens will be the induced stresses as measured by the DHD technique and not the nominal stresses.

With the width of the specimens being fixed at 30mm and the loading limit of the tensile testing machine in mind, it was evident that the specimen material would have to be aluminium. The use of aluminium with its relatively low Young's modulus (70GPa), when compared to stainless steel (200GPa), would give a more appreciable hole deformation better suited to the range and resolution of the air probe.

Unfortunately, as well as a lower Young's modulus, aluminium also has a lower yield stress. Therefore the applied load and induced stress was restricted in order that plastic deformation would not occur at the hole edge due to the stress concentrations.

The measurement procedure carried out for the calibration studies was essentially that used in the DHD technique described in Chapter 3. The diameter of the

reference hole was measured in a stressed and unstressed state and the resulting hole deformation converted first into normalised radial distortions and then into stresses. However, there were slight differences to the measurement procedure. During preparation, 10mm diameter aluminium reference bushes were attached to both the front and rear of the specimen and the outer front bush was not used. The hole was drilled in an unstressed state, the load was then applied and the hole diameter measured. Then instead of using a trepanning operation to release the stresses, the applied load was simply taken off and the hole diameter re-measured.

6.2.2 Tests and Results

Specimen 1 (t=20mm, d_0=3.18mm)

The first test specimen was 20mm thick with a reference hole diameter of 3.18mm. Testing on this size of specimen provided a benchmark to assess the procedure because the DHD technique is known to work for such specimen thicknesses [George, 2000a].

Figure 6.3 shows the stress distribution for an induced stress of 57MPa, comparing the predicted distribution based on the strain gauge values and the measured distribution using the DHD technique. The measured stress distribution was not as expected (i.e. a square wave), only reaching the predicted uniform peak value in the central 10mm of the specimen. It can also be seen that the supposedly stress free reference bushes did experience some of the induced stress. Although not shown, all the initial load conditions produced similar shaped stress distributions. Therefore it was assumed that the glue lines between the specimen and the reference bushes were the cause of the distribution inaccuracies by transmitting some of the strain experienced by the specimen to the bushes. Therefore the reference bushes were removed and the specimen reloaded at 28MPa and 57MPa.

Figures 6.4 and 6.5 show the revised stress distributions for induced stresses of 28MPa and 57MPa. The figures compare the predicted distributions based on the strain gauge values and the measured distributions using the DHD technique. For

both load conditions the measured stress distributions were now as expected, uniform throughout the thickness.

For an induced stress of 28MPa in the load direction, as predicted by the strain gauges, the DHD technique measured a stress distribution with an average value of 26MPa. All the stress values were within +5 and –14MPa of that predicted. The measured stress distribution in the direction normal to the load averaged at –2MPa with all the stress values being within +4 and –8MPa of that predicted at 0MPa.

For an induced stress of 57MPa in the load direction, the DHD technique measured a stress distribution with an average value of 56MPa. All the stress values were within ±9MPa of that predicted. The measured stress distribution in the direction normal to the load averaged at 3MPa with all the stress values being within +10 and –3MPa of that predicted at 0MPa.

Specimen 2 (t=10mm, d_0=3.18mm)

A 10mm thick specimen with a 3.18mm diameter reference hole was made after the successful application of the DHD technique on specimen 1. For this test, reference bushes were attached to prevent bell-mouthing of the reference hole during its manufacture and then removed.

Figures 6.6 – 6.8 show the stress distributions for the 30, 59 and 74MPa induced stresses, comparing the predicted distributions based on the strain gauge values and the measured distributions using the DHD technique. All three loading conditions show measured stress distributions that are approximately uniform, the greatest discrepancies occurring in the centre of the specimen.

For an induced stress of 30MPa in the load direction, the DHD technique measured a stress distribution with an average value of 31MPa. All the stress values were within +10 and –7MPa of that predicted. The measured stress distribution in the direction normal to the load averaged at 2MPa with all the stress values being within +12 and –10MPa of that predicted at 0MPa.

For an induced stress of 59MPa in the load direction, the DHD technique measured a stress distribution with an average value of 70MPa. All the stress values were within +25 and –1MPa of that predicted. The measured stress distribution in the direction normal to the load averaged at 12MPa with all the stress values being within +28 and –8MPa of that predicted at 0MPa.

For an induced stress of 74MPa in the load direction, the DHD technique measured a stress distribution with an average value of 86MPa. All the stress values were within +24 and +2MPa of that predicted. The measured stress distribution in the direction normal to the load averaged at 13MPa with all the stress values being within +31 and –1MPa of the predicted stress at 0MPa.

Specimen 3 ($t=10mm$, $d_0=1.5mm$)

Another 10mm thick specimen was made this time for use with a 1.5mm diameter reference hole. Again, reference bushes were attached to prevent bell-mouthing of the reference hole during its manufacture and then removed.

Figures 6.9 – 6.11 show the stress distributions for the 30, 61 and 92MPa induced stresses, comparing the predicted distributions based on the strain gauge values and the measured distributions using the DHD technique. All three loading conditions show measured stress distributions that are approximately uniform, the greatest discrepancies occurring near the rear face of the specimen.

For an induced stress of 30MPa in the load direction, the DHD technique measured a stress distribution with an average value of 32MPa. All the stress values were within +17 and –18MPa of that predicted. The measured stress distribution in the direction normal to the load averaged at 0MPa with all the stress values being within ±12MPa of that predicted at 0MPa.

For an induced stress of 61MPa in the load direction, the DHD technique measured a stress distribution with an average value of 62MPa. All the stress values were within +16 and –27MPa of that predicted. The measured stress distribution in the direction

normal to the load averaged at 0MPa with all the stress values being within +14 and −16MPa of that predicted stress at 0MPa.

For an induced stress of 92MPa in the load direction, the DHD technique measured a stress distribution with an average value of 90MPa. All the stress values were within +18 and −33MPa of that predicted. The measured stress distribution in the direction normal to the load averaged at -1MPa with all the stress values being within +18 and −22MPa of that predicted at 0MPa.

Specimen 4 (t=5mm, d_0=1.5mm)

A 5mm thick specimen was made for use with a 1.5mm diameter reference hole. Again reference bushes were attached to prevent bell-mouthing of the reference hole during its manufacture and then removed.

Figures 6.12 – 6.14 show the stress distributions for the 31, 62 and 92MPa induced stresses, comparing the predicted distributions based on the strain gauge values and the measured distributions using the DHD technique. All three loading conditions show measured stress distributions that are approximately uniform.

For an induced stress of 31MPa in the load direction, the DHD technique measured a stress distribution with an average value of 31MPa. All the stress values were within +21 and −24MPa of that predicted. The measured stress distribution in the direction normal to the load averaged at 0MPa with all the stress values being within +17 and −22MPa of that predicted at 0MPa.

For an induced stress of 62MPa in the load direction, the DHD technique measured a stress distribution with an average value of 64MPa. All the stress values were within +17 and −19MPa of that predicted. The measured stress distribution in the direction normal to the load averaged at -2MPa with all the stress values being within +18 and −30MPa of that predicted at 0MPa.

For an induced stress of 92MPa in the load direction, the DHD technique measured a stress distribution with an average value of 94MPa. All the stress values were within

+18 and –17MPa of that predicted. The measured stress distribution in the direction normal to the load averaged at 2MPa with all the stress values being within ±19MPa of that predicted at 0MPa.

6.2.3 Discussion and Conclusions

Overall, excellent agreement was found between the predicted stress distribution based on the strain gauge values and the measured stress distribution using the DHD technique. A summary of the measurements is shown in Figure 6.15. With the exception of specimen 2, all the DHD measured stress distributions were within ±2MPa of that predicted. Specimen 2 was within the ±2MPa bracket for the smallest stress tested (i.e. 30MPa), however at the large stresses (i.e. 59MPa and 74MPa) the DHD measured stresses were larger by approximately 12MPa. This error could be accounted for by the ±0.5μm error of the air probe, which does equate to an error of ±11MPa, see Equation 3.28.

The results of the tests show excellent agreement when comparing the average stress values. However the variance in stress about the average values were large and a maximum of –33MPa was measured for specimen 3. The reason for this is most probably due to the use of the old air probe LVDT electronics during the tests and so the measurement of erratic noise, see Section 4.4.2. Therefore the measured noise was averaged out to show excellent average agreement but was still present when calculating the variance. It should be noted that the variance was the largest for the 1.5mm diameter reference holes where the ratio of noise to diameter signal would also be the largest.

The overall success of these calibration experiments suggest that the DHD technique can measure stress distributions using 1.5mm diameter reference holes and within specimens down to a thickness of 5mm.

6.3 Step Changes In Stress

All previously undertaken calibration studies have involved the application and then measurement of stresses with a uniform or gradual gradient stress distribution. Presented here are calibration studies that tested the accuracy of the DHD technique in determining residual stresses with a step change in the stress distribution. Tested in particular was the ability of the air probe in picking up the exact transition point of the step change.

6.3.1 Test Parameters

Shrink fit specimens, as shown in Figure 6.16, were used to provide the step change stress distribution. During manufacture the outside diameter of the core is larger than the inside diameter of the annulus preventing the two pieces to be combined. However utilising thermal expansion/contraction of the two pieces, the annulus can be placed over the core producing the shrink fit specimen.

Due to the interference diameters, the annulus experiences tensile hoop stresses while the core experiences compressive hoop stresses, producing a stress step change at the transition. The idealised hoop stress is shown in Figure 6.16. The stress distributions can be predicted using the Lamé equations shown below.

$$\sigma_r = j - \frac{k}{r^2} \tag{6.4a}$$

$$\sigma_\theta = j + \frac{k}{r^2} \tag{6.4b}$$

where $\sigma_{r,\theta}$ are the radial and hoop stresses respectively, r is the radius, and j and k are constants evaluated using boundary conditions relevant to the specimen.

For a shrink fit specimen in which the core is solid, Equation 6.4 predicts that at the centre of the core (i.e. where r = 0) both the radial and hoop stress distributions approach infinity which cannot be the case. Therefore Equation 6.4 is used to

calculate the stress distributions in the annulus (i.e. where $r \geq r_t$) only and the stress distributions within the core are given as

$$\sigma_{cr} = \sigma_{c\theta} = -p = \text{constant} \tag{6.5}$$

where p is the interface pressure.

For an annulus of outer radius r_o, and a transition radius of r_t, the following two boundary conditions apply:

i. At $r = r_t$, $\sigma_{ar} = -p$

ii. At $r = r_o$, $\sigma_{ar} = 0$

Using the above boundary conditions, the constants j and k are found to be

$$j = \frac{pr_t^2}{r_o^2 - r_t^2} \tag{6.6a}$$

$$k = \frac{pr_t^2 r_o^2}{r_o^2 - r_t^2} \tag{6.6b}$$

Combining Equations 6.4 and 6.6, the radial and hoop stress distributions are given by

$$\sigma_{ar} = \frac{pr_t^2(r^2 - r_o^2)}{r^2(r_o^2 - r_t^2)} \tag{6.7a}$$

$$\sigma_{a\theta} = \frac{pr_t^2(r^2 + r_o^2)}{r^2(r_o^2 - r_t^2)} \tag{6.7b}$$

In order to assess the possibility of specimen manufacture, the following equations were used to calculate the interference needed at differing transition radii for given interface pressures. Using the analogy of strain compatibility

$$\delta = \delta_c + \delta_a \tag{6.8}$$

where δ is the interference, and δ_c and δ_a are the changes in radius of the core and annulus respectively.

For a thin specimen, the equations for the core and annulus hoop strains are respectively

$$\varepsilon_{c\theta} = -\frac{\delta_c}{r_t} = \frac{1}{E}(\sigma_{c\theta} - \nu\sigma_{cr}) \tag{6.9a}$$

$$\varepsilon_{a\theta} = \frac{\delta_a}{r_t} = \frac{1}{E}(\sigma_{a\theta} - \nu\sigma_{ar}) \tag{6.9b}$$

where $\varepsilon_{c\theta}$ and $\varepsilon_{a\theta}$ are the core and annulus hoop strains, E is the Young's modulus, and ν is the Poisson's ratio.

The core's radial and hoop stresses are compressive and equal in magnitude to the interface pressure. At the transition, the annulus's radial stress is also negative and equal in magnitude to the interface pressure and the hoop stress is given by Equation 6.7b. Combining and rearranging Equations 6.8 and 6.9 gives

$$\delta = \delta_c + \delta_a = \frac{-r_t p(1-\nu)}{E} + \frac{r_t(\sigma_{a\theta} - \nu p)}{E} \tag{6.10}$$

Equation 6.10 can be simplified to give

$$\delta = \frac{r_t(\sigma_{a\theta} - p)}{E} \tag{6.11}$$

For the practicality of manufacture it was decided that the core was to be cooled in liquid nitrogen (approx. -190°C) contracting its size and enabling the room temperature annulus to be placed over. Therefore the following equation was used to assess the possible range of thermal contractions of the core and hence size of specimens to be manufactured.

$$\delta r = \alpha r_0 \delta T \tag{6.12}$$

where δr is the change in radius, α is the coefficient of thermal expansion, r_0 is the original radius, and δT is the change in temperature.

Figure 6.17 shows the findings of Equations 6.11 and 6.12. The figure shows the interference needed and the possible thermal contractions of the core for a fixed maximum stress and outer annulus radius but differing transition radii. Figure 6.17 shows that as the transition radius increases with respect to the outer annulus radius, the difference between the interference needed and the thermal contractions also increases. An increase in the difference eases the manufacture of the specimen.

The radial dimensions of the specimen were chosen depending on the value of maximum residual stress induced to prevent yielding. The thickness of the specimens was chosen to be 30mm, enabling attachment of all the bushes required for the DHD technique to be carried out.

6.3.2 Tests and Results

Specimen 1 (r_t=20mm, r_o=35mm, σ_{max}=150MPa)

Specimen 1 was chosen to have a transition radius of 20mm, an outside radius of 35mm and a maximum residual stress of 150MPa. Figure 6.18 shows the predicted residual stress distribution.

The purpose of these calibration studies was to test the accuracy of the DHD technique in measuring the residual stress distribution induced within the shrink fit specimens. However, although predicted theoretically, the residual stress distributions induced in the specimens are prone to errors due to manufacturing tolerances. Therefore the residual stress distributions induced in specimen 1 were measured using the Sachs boring technique to test the manufacturing capabilities.

The Sachs boring technique is carried out by incrementally boring from the centre to the outside of an axi-symmetric component. After each increment in boring the

release of residual stresses is measured by strain gauges adhered to the outside of the component. After the final increment in boring, the full set of strain gauge measurements are then combined and analysed to calculate the residual stress distribution along the axis of the component.

Therefore to carry out the Sachs boring technique an initial central hole of 1mm radius was made in specimen 1 enabling access for the cutter to start the incremental cuts. However the presence of this initial hole caused a redistribution of the residual stresses within the core. Therefore the residual stress distributions within the core described by Equation 6.5 were incorrect. The correct equations for a specimen comprising of two annular discs (inner radius r_i) were reformed from Equations 6.4a and 6.4b with a different set of boundary conditions, namely

i.) At $r = r_i$, $\sigma_{cr} = 0$

ii.) At $r = r_t$, $\sigma_{cr} = -p$

Equation 6.5 now becomes

$$\sigma_{cr} = \frac{pr_t^2(r_i^2 - r^2)}{r^2(r_t^2 - r_i^2)} \tag{6.13a}$$

$$\sigma_{c\theta} = \frac{pr_t^2(r^2 + r_i^2)}{r^2(r_i^2 - r_t^2)} \tag{6.13b}$$

The incremental cuts were made from the centre of the core outwards toward the core-annulus interface. When the cutter reached the core-annulus interface the last sliver of core material came free and rotated with the cutter. With the core material reduced to a sliver, no interfacial pressure could be exerted and hence the annulus was left in its original stress free state. Therefore only the radial and hoop residual stresses within the core were measured.

Figure 6.19 shows the residual stress distributions, comparing the re-predicted distributions using Equations 6.7 and 6.13, and the measured distributions using the Sachs boring method. Overall there is excellent agreement between the re-predicted and measured stress distributions. The measured radial and hoop stresses were found

to be less than the predicted stresses throughout the core, with a maximum error of -21MPa. The accuracy of the Sachs boring method is generally quoted as ±20MPa for aluminium [Lacarac, 2000] and so the error present from this experiment was acceptable. Therefore manufacture of the specimens with the correct stress distribution was deemed possible and therefore used for the calibration of the DHD technique.

Specimen 2 (r_i=40mm, r_o=50mm, σ_{max}=150MPa)

Due to the difficulties encountered during the manufacture of specimen 1, different dimensions were chosen for specimen 2. Specimen 2 was chosen to have a transition radius of 40mm, an outside radius of 50mm and a maximum residual stress of 150MPa. Figure 6.20 shows the predicted residual stress distribution. By increasing the radii of the parts the gap size between the cooled core and room temperature annulus was increased, enabling easier assembly.

It was assumed that specimen 2 contained the residual stress distribution as predicted and so the first validation measurement using the DHD technique was carried out. The location of the deep-hole measurement and hence the reference hole was chosen to be along the central axis of the specimen as shown in Figure 6.21. With such a location and axis, only the radial stress was measured, in two planes 90° apart, also shown in Figure 6.21. The diameter of electrode chosen for extraction of the core was 10mm ensuring accurate results from a thickness of 30mm. Due to the inaccuracies associated with the reference bushes on the previous uni-axially loaded plate specimens, the reference bushes were removed immediately after EDM. Therefore the reference hole was free to completely relax during EDM and the diameter measurements were then carried out.

Figure 6.22 shows the measured and predicted residual stress distributions. It can be seen that the measured stress distributions are approximately equi-biaxial and uniform throughout the thickness. The measured residual stress distributions have average values of -29MPa and -27MPa and all the stress values are within +11 and -0MPa of that predicted at 33MPa.

After the DHD technique and the extraction of the core, the specimen was left with a 12mm diameter hole in its centre. The specimen was therefore then used for Sachs boring with the central hole enabling access of the cutter. The residual stress distribution was again predicted using Equations 6.7 and 6.13 for a specimen comprising of two annular discs.

Figure 6.23 shows the residual stress distributions, comparing the re-predicted distributions using Equations 6.7 and 6.13 and the measured distributions using the Sachs boring technique. Overall there is good agreement between the re-predicted and measured stress distributions. The measured radial and hoop stresses were found to be predominantly less than the re-predicted stresses throughout the core, with a maximum error of -17MPa. Again, this error is within the error band of the Sachs boring method and so the residual stress distribution induced within the specimen was as expected.

Specimen 3 (r_i=40mm, r_o=50mm, σ_{max}=75MPa)

The dimensions of specimen 3 were the same as those of specimen 2, with a transition radius of 40mm and an outside radius of 50mm. However for specimen 3 a maximum residual stress of 75MPa was decided. Figure 6.24 shows the predicted residual stress distribution. Again it was assumed that specimen 3 contained the residual stress distribution as predicted and so the DHD technique was carried out. The axis of the reference hole was chosen to be along the radial axis of the specimen as shown in Figure 6.25. The axis of the reference hole was such that both the hoop and axial residual stresses were measured.

The diameter of electrode chosen for extraction of the core was again 10mm, however due to the method of assembly of the specimen a problem was foreseen during the EDM stage. The core and annulus are held together by the stresses induced by the interference fit, however when the specimen is trepanned the stresses are released and the core would fall apart. To avoid this problem a threaded bar was placed through the reference hole and bolts on each end were used to hold the core together during the EDM stage, as shown in Figure 6.26. Also, the residual stress distribution is axi-symmetric due to the geometry of the specimen and so the

measurements need only be taken for one half of the depth. Therefore the core was trepanned just over half way with the rest of the depth providing support. After the trepanning stage, glue was forced down the sides of the core to hold it in place before the threaded bar and the bolts were removed and the reference hole re-measured. Again the residual stress measurements were taken without reference bushes.

Figure 6.27 shows the measured and predicted residual stress distributions. Again the shape of the measured stress distributions is similar to that predicted. The hoop stress rises from a value of 46MPa at the front face to a peak value of 84MPa at the transition (values of 59MPa and 75MPa were predicted, respectively). The steep transition in hoop stress is clearly indicated at a depth of 10mm and occurs over a distance of only 0.6mm. The hoop stress then fluctuates about an average value of -8MPa between the depths of 10mm and 70mm (a value of -16MPa was predicted). At depths greater than 70mm (where the stresses have not been released by trepanning) the hoop stresses fluctuate about 0MPa as expected.

6.3.3 Discussion and Conclusions

Contrary to the predictions for thin specimens, the measurement carried out on specimen 3 showed that it was subject to axial residual stresses. This was only apparent from specimen 3 due to the radial axis of the reference hole and hence the axes measured. The axial stresses are the result of the friction between the sides of the core and annulus as the core expands when warming back up to room temperature. As the sides of the core and annulus touch, the axial expansion of the core forces the annulus to expand axially as well, producing a compressive residual stress on the outside face of the core and a tensile residual stress on the inside face of the annulus. Both residual stresses would reduce to zero at positions remote from the faces. The tensile residual stresses within the annulus can be seen, with the maximum tensile stress occurring near the interface and then decreasing towards the outer surface. Unfortunately the DHD technique didn't detect the compressive residual stress within the core although the magnitude would be small and therefore could be concealed by the error band.

The shrink fit measurements demonstrated the ability of the DHD technique to accurately measure residual stress distributions. The DHD measurements carried out for specimen 2 accurately identified the equi-biaxial radial residual stress distribution along the axis of the specimen. Also, the DHD measurements carried out for specimen 3 accurately identified the step change in the hoop residual stress distribution. The immediate transition from tension to compression was measured to occur over a distance of 0.8mm. This suggests that the practical depth resolution of the standard DHD technique (i.e. 3.18mm diameter reference hole and "10mm" core) is about 0.8mm. This value approximately correlates with the diameter of air exit holes in the tip of the air probe and suggests that the practical depth resolution of the specialised DHD technique (i.e. 1.5mm diameter reference hole and "5mm" core) could be about 0.4mm.

6.4 Graphite Components

The ability of the DHD technique to measure residual stresses within porous components, particularly graphite, was investigated. The graphite tested was the specific reactor graphite used to encase the nuclear control rods within the nuclear reactor. It has been found that with continued exposure to radiation, residual stresses develop and ultimately lead to the fracture of the graphite. Having been developed for and used on steel components, initial investigations were undertaken into the applicability of the DHD technique to reactor graphite. The following section describes the simple calibration/validation experiments carried out on a "cold" sample of reactor graphite.

6.4.1 Test Parameters

The test plan for the graphite was similar to the uni-axial aluminium bars mentioned earlier, however the applied loading would be compressive instead of tensile. Compressive loading was chosen due to the ease of specimen manufacture, ease of applying the loads and the lower risk of uncontrolled fracture. The test plan therefore involved the application of a known compressive load and measurement thereof using a reference hole. For the purpose of these tests it was decided that use of the proven 3.18mm diameter reference hole was the most suitable. As with the

uni-axial aluminium specimens, a minimum dimension for the graphite specimen of 19.08mm was required in order to eliminate the effect of stress concentrations due to the hole.

A cubical graphite specimen, 30 x 30 x 30mm, was manufactured with a central 3.18mm diameter reference hole, see Figure 6.28. The reference hole was made using a split-point drill bit and then reamed to attain the dimensional tolerance and surface finish. Gundrilling was not used due to the porous structure of the graphite and contamination thereof due to the high pressure cutting oil.

The machine used to apply the compressive loads was developed at the University of Bristol [Holmes, 2003]. The machine was developed to investigate the contact surface of reactor graphite under variable compressive loads using ultrasound. The machine basically consisted of two steel plates, one static and one moveable. The specimen is placed between the two plates and the moveable plate is pushed up trapping the specimen and applying the compressive load, see Figure 6.29. The movement of the plate is provided by four inter-connected hydraulic pistons. The inter-connections ensure equal loading is applied. The loading is measured using pressure transducers mounted above each piston. Calibration of the pressure transducers was carried out using calibrated servo-hydraulic testing machines here at the University.

The test parameters were set using a combination of the mechanical properties of the graphite and the limits of the testing machine. For the graphite, the compressive strain limit before fracture is 0.5% and the Young's modulus is 9.48GPa. Therefore the maximum compressive stress before fracture of the graphite was found to be 47MPa. The loading limit of each of the 4 pressure transducers used in the machine is 5kN. Therefore, for a 30mm cube the maximum compressive stress the machine can apply is 22MPa. The loading limit was therefore governed by the machine and not the graphite. Three tests were carried out.

6.4.2 Tests and Results

Test 1

Test 1 investigated the repeatability and reliability of the diameter measurements using the air probe.

There was uncertainty in the ability of the air probe to accurately measure the diameter of the reference hole within the graphite. There was the possibility of air leakage through the porous structure of the graphite reducing the effect of a changing back-pressure due to the hole diameter.

There was also the possibility that with repeated movement of the air probe through the reference hole to complete each angular measurement, the hole would wear. The wear would be misinterpreted as hole deformation due to stress release and be the source of large stress measurement errors.

Therefore test 1 involved the repeated measurement of the reference hole diameter at zero load. Figure 6.30 shows the measured diameter of the reference hole at 0° for measurement sets 1 and 2 (0° was the future loading direction). Figure 6.31 shows the measured diameter of the reference hole at 90° for measurement sets 1 and 2. Both figures show that there was good repeatability between the measurement sets. This indicates that there was negligible wear during the measurement process. The measured variations in reference hole diameter are consistent with small scratches or pores and the lack of evidence of air probe measurement saturation indicate that air leakage did not occur.

All 18 angles of reference hole diameter measurement from sets 1 and 2 were then compared and analysed using the DHD technique. Figure 6.32 shows the calculated stress error associated with the negligible difference in measured reference hole diameter between measurement sets 1 and 2. The calculated residual stress error was found to average at –0.07MPa with a standard deviation of 0.7MPa.

Test 2

Finding that the repeatability of the reference hole diameter measurement was good, the first test under load was undertaken. The graphite specimen was subjected to a compressive stress of –9.7MPa and the reference hole diameter was measured.

The applied stresses were calculated by comparison of the diameters measured during tests 1 and 2 (i.e. in the unstressed and stressed states, respectively). The calculated applied stresses are shown in Figure 6.33. The average stress measured at 0° was -9.5MPa, which shows excellent agreement with the applied stress of –9.7MPa. There is however a slight gradient to the measured applied stress, ranging from -11.7MPa at the front of the block to -7.3MPa at the rear. Further analysis of the pressure transducer measurements did show that there was a very small discrepancy between the front and rear applied loads. The average stress measured at 90° was –1.2MPa showing good agreement with the applied stress at 90° of 0MPa.

Test 3

Following the success of test 2, the graphite block was subjected to an increased compressive stress of –19.2MPa and the reference hole diameter was re-measured.

Figure 6.34 shows the measured applied stress responsible for the deformations. The average stress measured was –22.9MPa, which shows good agreement with the applied stress. Again there is a slight gradient to the measured applied stress, which could be again due to a small discrepancy between the front and rear applied loads. The average stress measured at 90° was –2.5MPa showing good agreement with the applied stress at 90° of 0MPa.

6.4.3 Discussion and Conclusions

The initial calibration tests performed on the reactor graphite showed very promising results. The air probe was able to repeatedly measure the reference hole diameter with negligible error, suggesting negligible wear and porosity effects. Also, the

stresses measured using the reference hole deformations were in good agreement at +0.2MPa and –3.7MPa of that applied.

The experimental error due to the uneven loading of the specimen occurred as a result of the comparatively large size of the compressive testing machine. The large size of the machine meant that the four inter-connected hydraulic pistons were remotely located from the graphite sample. Therefore the small graphite sample acted like a pivot point allowing for the discrepancies between the applied loads of the inter-connected pistons. Further testing should be carried out with a specifically designed machine to apply the load evenly throughout the specimen.

Chapter 7: APPLICATION OF THE DHD TECHNIQUE

7.1 Introduction

During this research project the DHD technique and the refinements thereof were applied to real engineering components to measure the residual stresses present. This chapter presents the measurements, which are categorised into three sections depending upon component shape and material composition.

The first section presents the measurements carried out on components with a simple geometry, i.e. plates, pipes and cylinders. The second section presents the measurements carried out on more geometrically complex components, i.e. nozzle-pipe intersections and T-section butt welds. The third section presents the measurements carried out on components manufactured from aluminium and titanium alloys.

The sections present the measurements of residual stress carried out to test the abilities of the DHD technique. Although categorised with respect to geometry and material composition, the measurements provided a wide spectrum of challenges for the DHD technique.

The measurements tested the sensitivity of the DHD technique to near surface residual stresses and high stress gradients. Measurements were also carried out on thin components to investigate the critical size of core extracted and hence sampling volume. The already large penetration depths of the DHD technique were tested and extended. The accessibility of the DHD technique was examined with respect to different component geometries. The effects of geometry on the distribution of residual stresses generated and measured using the DHD technique were tested.

Having been initially developed for steels, the applicability of the DHD technique to alternative materials was also investigated. The overall assessment of the ability of the DHD technique to carry out the tests was made possible with the comparison of residual stress measurements provided by other techniques.

7.2 Simple Geometry

Of the 11 components measured, 5 were of a simple geometry, i.e. 2 plates, 2 pipes and a cylinder. The measurements carried out on these components provided tests of the sensitivity, sampling volume, geometry effects, and penetration depth of the DHD technique.

7.2.1 Shot-peened Component

The National Physical Laboratory (NPL) co-ordinated an intercomparison exercise for the development of a set of guidelines for the reliable measurement of residual stresses using the X-ray diffraction (XRD) and CHD techniques [Lord et al, 2002]. Twenty laboratories participated in the exercise by measuring the residual stresses present within the same components using their "in-house" XRD or CHD techniques. The University of Bristol participated in the exercise and was supplied with a shot-peened component for incremental centre-hole drilling (ICHD). Having completed the ICHD measurement for the intercomparison exercise, the component was subjected to further "in-house" testing using the DHD technique.

Component Design

The shot-peened component consisted of a 100mm square plate with a thickness of 25mm, see Figure 7.1. The plate was manufactured from a martensitic CCr spring steel. One half of the front surface of the plate was shot-peened with 4.5mm diameter balls to introduce compressive residual stresses into the surface layers. The remainder of the plate was left in the as-received (nominally stress-free) condition.

Measurement Location

The DHD measurement location was through the centre of the shot-peened area through the thickness of the plate, see Figure 7.1. The axis notation used for this measurement location is also shown in Figure 7.1. To measure the surface layer residual stresses, a 1.5mm diameter reference hole and a 5mm diameter core was used to carry out the DHD measurement. The 1.5mm diameter reference hole was manufactured using a two stage operation. The initial hole was made using a split-point drill bit before being reamed to the correct size.

Results

Figure 7.2 shows the measured normalised radial distortions of the reference hole, following core extraction, in the xx and yy directions. The normalised radial distortions were then converted into residual stresses using a Young's modulus, E, of 200GPa. The measured residual stress distributions for σ_{xx}, σ_{yy} and σ_{xy} are shown in Figure 7.3. The residual stresses are shown as functions of depth through the plate from the shot-peened surface.

The residual stresses were found to be equi-biaxial through the thickness of the plate as expected. The results show that compressive residual stresses are experienced at depths up to 1mm below the shot-peened surface. At 1mm the compressive residual stresses convert to tensile and reach a maximum value of 60MPa at a depth of about 2.5mm. The tensile residual stresses then decrease to 0MPa at a depth of 10mm and remain at 0MPa thereafter.

Discussion

The introduction of residual stresses using shot-peening has only a surface/sub-surface effect. Therefore it was assumed that high residual stress gradients were present within the sub-surface layers of the plate. High stress gradients are most accurately measured with the DHD technique by using small cores. Hence the use of a 1.5mm diameter reference hole and a 5mm core for this DHD measurement. Also, the 1.5mm air probe is able to accurately measure the deformation of the reference

hole at depths closest to the surface of the plate where the maximum residual stresses are present, refer to Section 3.5.1.

The facilities at the University at the time of measurement were such that manufacture of the 1.5mm reference hole was only capable by using a split-point drill bit and reamer. The surface of the reference hole produced was therefore very rough when compared to gundrilling. Increases in roughness of the reference hole increases the likelihood of erratic residual stress results due to depth misalignments, refer to Section 3.5.1. This was the case for this measurement and a smoothing operation was carried out to produce the results shown in Figures 7.2 and 7.3. The smoothing operation averaged the calculated residual stress values for every 0.6mm data block.

The calculated residual stresses were as expected, compression at surface, tension in the sub-surface layers and zero stress throughout the rest of the thickness.

As mentioned the shot-peened plate was supplied to the University for the measurement of residual stresses using the University's "in-house" CHD technique. Also, prior to the supply of the specimen, XRD residual stress measurements were undertaken by NPL. Therefore it is instructive to compare these measurements [Lord et al, 2002] with those carried out using the DHD technique. Figure 7.4 shows the results of the residual stress measurements carried out using the DHD, CHD and XRD techniques. It can be seen that there are large discrepancies between the measurements at the surface of the plate (DHD measures –155MPa, XRD measures –535MPa and CHD measures –855MPa). Unlike XRD and CHD, DHD is not accurate at the surfaces of specimens and so no information can be inferred for DHD at these depths. For XRD and CHD however there is a large (320MPa) discrepancy between their measurements and so the accuracy for these measurements is also questionable. Within the sub-surface layers the residual stresses measured using DHD and CHD do show some agreement. The transition from compressive to tensile residual stresses occurs within 1mm of the surface. The peak tensile residual stress experienced is about 60MPa. In order to improve measurement comparisons the DHD measurement should be repeated with a 1.5mm diameter gundrilled reference hole.

7.2.2 Partial Depth Welded Plate

A single DHD residual stress measurement was carried out on a thin plate containing a partial depth weld. The plate was supplied by DSM Services.

Component Design

The plate was approximately 500mm square, 20.5mm thick and made of stainless steel, see Figure 7.5. A partial depth multi-pass weld was introduced along the centre of the plate. The weld was triangular in shape and penetrated to a depth of approximately 17mm. As a result of the introduction of the weld and hence residual stresses, the plate had folded-in by approximately 7° about the weld axis.

Measurement Location

The location of the DHD measurement was mid-weld length and 3mm in from the edge of the weld towards its centre-line, see Figures 7.5 and 7.6. The axis notation used for the measurement location is also shown in Figure 7.5. The DHD measurement was carried out to characterise the residual stresses through the thickness of the plate in the HAZ region adjacent to the weld. The DHD technique was carried out using a 3.18mm reference hole and a 10mm core.

Results

Figure 7.7 shows the measured normalised radial distortions of the reference hole, following core extraction, in the transverse and longitudinal directions. The normalised radial distortions were then converted into residual stresses using a Young's modulus, E, of 200GPa. The measured residual stress distributions are shown in Figure 7.8. The residual stresses are shown for the directions transverse and longitudinal to the weld as well as the associated in-plane shear. The residual stresses are shown as functions of depth through the plate from the welded surface.

The transverse and longitudinal residual stresses were found to be similar in shape. Both tensile at the front of the plate (i.e. at depth = 0mm) then decreasing to a minimum at a depth of about 13mm before increasing again towards the back face.

The longitudinal stress was tensile throughout the thickness. The transverse stress however was only tensile near the front and rear surfaces. For the majority of the thickness (i.e. full depth of the weld) the longitudinal stress was the largest by an average of about 175MPa. For the last 4mm in depth however, the transverse stress became the largest.

The transverse stress had a tensile value of 140MPa at the front, decreasing to a compressive value of –130MPa at about 13mm before turning back into tensile at the rear at a value of 230MPa. The transitions from tension to compression occur at 6.5mm and 16mm.

The longitudinal stress had a tensile value of 250MPa at the front, decreasing to a value of 30MPa at about 13mm before increasing again to a value of 195MPa at the rear surface.

It can be seen that the magnitude of the in-plane shear stresses is small, hence the principal stresses are approximately equal to the transverse and longitudinal residual stresses.

Discussion

During measurement of the reference hole diameter both before and after EDM, a large change in diameter was noticed between depths of 14 – 18mm, see Figure 7.9. The larger diameter coincides with the bottom of the weld and so could be due to a cavity between the weld and parent material or the transition from weld to parent material affecting the gundrill and swarf. The larger diameter is still within the calibration range of the air probe and so the measured diameter should be accurate. The step in diameter and so possible depth misalignment does reveal itself as a small erratic peak in the residual stress results at these depths.

7.2.3 Butt-welded pipe, 19mm wall thickness

A 19mm thick butt-welded pipe was supplied for the measurement of residual stresses using the DHD technique. The measurement was undertaken as part of a

European project called TRAINSS [Bouchard, 2002]. The overall aim of the project was to train its industrial members in the technique of neutron strain scanning (NSS) and to compare NSS with other techniques. NSS is another name for the neutron diffraction (ND) technique.

Component design

The component consisted of a butt-welded 316H stainless steel pipe with dimensions of 830mm long, 432mm OD and an average wall thickness of 19.6mm, see Figure 7.10.

The fully circumferential weld was introduced using a combination of tungsten inert gas (TIG) and manual metal arc (MMA) welding. TIG welding was used to provide the initial weld root pass. The weld was situated at 65mm and 50mm from nozzles A and B respectively. The weld had a width of approximately 30mm on the outer surface of the pipe.

During the life of the pipe many DHD residual stress measurements have been carried out. George [2000a] presented the DHD measurements carried out on the original weld at locations 1 – 3. After locations 1 – 3 and before locations 4 and 5, which were carried out during this research, two partial depth repair welds of different lengths were introduced.

A short repair (approximately 20° arc length) was introduced circumferentially centred at 70° from top dead centre (TDC) of the pipe. A long repair (approximately 60° arc length) was introduced circumferentially centred at 240° from TDC. The circumferential positions of the repairs were chosen to minimise their interactions with each other and with nozzles A and B. Both repair welds were introduced offset from the centreline of the original weld by approximately 12mm and penetrated to a depth of approximately 14mm. The repair welds were deposited using the MMA welding process. The repair welds were not subjected to post weld heat treatment (PWHT).

Measurement Location

DHD measurements were carried out to characterise the through-thickness residual stress distributions in the HAZ adjacent to both the short and long repairs. Measurement location 4 was at 70° from TDC, corresponding to the circumferential mid-length of the repair, see Figure 7.10. At the mid-length position, the entrance of the reference hole was located 1.5mm in from the edge of the repair towards the weld centreline. Measurement location 5 was in the same position as location 4 but with respect to the long repair, i.e. mid-length of the long repair (240° from TDC) and 1.5mm in from the edge, see Figure 7.10. The axis notation used for these measurement locations is also shown in Figure 7.10. The axis of the reference hole at each location was along the radial line of the pipe. Both DHD measurements were carried out using a 3.18mm reference hole and a 10mm core.

Results

Figures 7.11 and 7.12 show the measured normalised radial distortions of the reference hole, following core extraction, in the transverse and longitudinal directions for locations 4 and 5 respectively. The normalised radial distortions were then converted to residual stresses using a Young's modulus, E, of 195.6GPa as supplied by the TRAINSS project participants. The residual stress distributions for locations 4 and 5 are shown in Figures 7.13 and 7.14 respectively. The residual stresses are shown in the transverse, longitudinal and associated in-plane shear directions. The residual stresses are shown as functions of depth through the pipe thickness from the outer surface. The transverse and longitudinal residual stresses were approximately equi-biaxial through the thickness of the pipe for both locations. Both the transverse and longitudinal residual stresses were predominantly tensile through the thickness of the pipe.

For location 4, the transverse residual stresses increase from a value of -5MPa at the outer surface of the pipe to a maximum of 265MPa at a depth of 16mm before decreasing to 170MPa at the inner surface. The longitudinal residual stresses increase from a value of -20MPa at the outer surface of the pipe to a maximum of 285MPa at a depth of 13mm before decreasing to 135MPa at the inner surface.

For location 5, the transverse residual stresses increase from a value of 5MPa at the outer surface of the pipe to a maximum of 260MPa at a depth of 17.5mm before decreasing to 185MPa at the inner surface. The longitudinal residual stresses increase from a value of -35MPa at the outer surface of the pipe to a maximum of 265MPa at a depth of 16mm before decreasing to 145MPa at the inner surface.

It can be seen that the magnitude of the in-plane shear stresses is small, hence the principal stresses are approximately equal to the transverse and longitudinal residual stresses.

Discussion

The thickness of the pipe at 19.6mm dictated that a 10mm core was extracted for both DHD measurements. The first and second cores (i.e. locations 1 and 2) extracted from the pipe during earlier research had a diameter of 20mm and were found to give inaccurate results when compared to other technique measurements and FE analyses [George, 2000a]. George then carried out a third DHD measurement with the extraction of a 10mm diameter core and found the results to then be in good agreement with those predicted.

It is instructive to compare the residual stresses measured at the two locations. Therefore, Figure 7.15 shows the transverse residual stresses measured at locations 4 and 5 and Figure 7.16 shows the longitudinal residual stresses measured at locations 4 and 5. It can be seen that the longitudinal residual stresses experienced by the two different length repairs are the same, the transverse residual stresses however are similar but not the same. The transverse residual stresses experienced in the longer repair weld (i.e. location 5) are lower by about 70MPa towards mid-thickness. The 70MPa difference is slightly greater than the compounded error of both measurements and so cannot be accounted for by measurement error alone, the effect of the length of repair weld must also be involved.

At location 4, both ND and DHD residual stress measurements were carried out through the thickness of the pipe. The ND measurements were carried out by

Edwards et al [2001] and further discussed by Bouchard [2002]. Figure 7.17 shows the comparison between the ND and the DHD measurements. It can be seen that there is excellent agreement between the two measurement methods, giving credibility to both the measurements and the methods.

7.2.4 Butt-welded pipe, 48mm wall thickness

A 48mm thick butt-welded pipe was supplied for the measurement of residual stresses using the DHD technique. The measurement was undertaken as part of an ongoing European project called INTEGRITY. The overall aim of the project is to understand the impact of weld repairs on the integrity of high temperature steel components.

Component design

The component consisted of three sections butt-welded together to form a pipe with dimensions 1000mm long, 358mm OD and a wall thickness of 48mm, see Figure 7.18. The sections were all manufactured from P91, a high strength martensitic steel.

The original welds were introduced using a combination of TIG and MMA welding. TIG welding was used to provide the initial weld root pass. On completion of the welds the pipe was subjected to PWHT.

Following PWHT and in order to investigate the impact of repair welds, two different partial weld repair procedures were carried out. They're termed partial weld repairs because only part of the original weld and adjacent base material is removed and repaired. Repairs "pwr1" and "pwr2" were carried out separately on the two butt welds and are shown in Figure 7.18.

Weld repair type "pwr1" consisted of removing the original weld material and HAZ up to a depth of about 50% from the outer surface. The material is removed from the complete circumference of the original weld before being repaired.

Preparation for the second weld repair "pwr2" involved removing about half of the outer surface of original weld and its associated HAZ. The material is removed up to a depth of about 50% from the outer surface and from the complete circumference of the original weld before being repaired.

The weld repairs were introduced using a combination of metal inert gas (MIG) and metal active gas (MAG) processes. Neither of the weld repairs were subjected to PWHT.

Measurement Location

As yet only the residual stresses generated within "pwr1" have been measured. The measurement location was on the centre-line of the repair at an arbitrary position around the circumference. The axis notation used for this measurement location is shown in Figure 7.18. A 3.18mm diameter reference hole was gundrilled through the wall thickness along the radial line of the pipe and a 10mm core extracted. The hole location and axis is shown in Figure 7.18.

Results

Figure 7.19 shows the measured normalised radial distortions of the reference hole, following core extraction, in the transverse and longitudinal directions. The normalised radial distortions of the reference hole following core extraction were converted to residual stresses using a Young's modulus, E, of 206GPa. The residual stress distributions for "pwr1" are shown in Figure 7.20. The residual stresses are shown in the transverse, longitudinal and associated in-plane shear directions. The residual stresses are shown as functions of depth through the pipe thickness from the outer surface.

The transverse and longitudinal residual stresses are similar in shape, both tensile from the outer surface up to a depth of about 38mm before transforming into and remaining compressive thereafter.

The transverse residual stress starts at a value of 115MPa at the outer surface and then rises to a maximum of 240MPa at a depth of 4mm. The transverse residual stress then decreases gradually to 0MPa at 38mm before decreasing rapidly to a maximum compressive stress of –185MPa at the inner surface.

The longitudinal residual stress starts at a value of 135MPa at the outer surface and then rises to a maximum of 265MPa at a depth of 4mm. The longitudinal residual stress then decreases gradually to 190MPa at 32mm before decreasing rapidly to a maximum compressive stress of –230MPa at the inner surface.

It can be seen that the magnitude of the in-plane shear stresses is small, hence the principal stresses are approximately equal to the transverse and longitudinal residual stresses.

Discussion

The diameter of the reference hole in the front reference bush and over the first 4mm in depth of the component was measured to be very large and outside of the calibration range of the air probe, see Figure 7.21. At these depths therefore, the accuracy of the measured diameter and hence calculated residual stresses cannot be specified.

The gundrilled reference hole for this measurement was comparatively rough and so the calculated residual stress results were affected by a small amount of noise due to depth misalignment errors. Therefore a residual stress smoothing operation was carried out to produce the results shown. The smoothing operation averaged the residual stress values for every 1mm data block.

The transverse and longitudinal residual stresses were found to gradually decrease from their initial maximums near the outer surface up to a depth of about 32mm. After this depth the stress gradients of both the transverse and longitudinal residual stresses increased greatly. The depth of the partial weld repair was up to 50% (i.e. 24mm) and could be considered to be the main contributory to this change in stress gradient.

CHD measurements were undertaken on the outer surface and along the centre-line of "pwr1" [Thomas, 2002b]. Figure 7.22 shows the results in comparison to the DHD measurements. It can be seen that there is good agreement between the different measurements, again providing credibility to both the measurements and the methods.

7.2.5 Steel Roll

A single DHD residual stress measurement was carried out on a mini mock-up steel roll.

Component Design

The mini mock-up consisted of a cylindrical roll of overall length 780mm with a step in diameter from 380mm to 433mm at a distance of 300mm from the small end. Figure 7.23 shows the design of the roll for clarification. The mini mock-up was forged from a solid martensitic steel billet and achieved a final weight of approximately 830kg. Therefore the term "mini" is used here very loosely. The real rolls supplied to the milling industry vary in size from 80 – 460 tonnes. The residual stresses present within the roll are as a result of a surface hardening process carried out during final stages of manufacture.

Measurement Location

The location of the DHD measurement was along a radial line through the centre of the larger diameter step (i.e. 433mm OD) and at mid-length along the step, see Figure 7.23. The axis notation used for this measurement location is also shown in Figure 7.23. Due to the axi-symmetric design of the roll the entrance of the reference hole around the circumference was chosen arbitrarily. Extra long, hardened tip gundrills were used to drill the 3.18mm diameter reference hole through the diameter of the roll in a single pass. The copper electrode used for the EDM process had an increased diameter of 15mm due to its practical manufacture at extended lengths. The manufacture of electrodes at extended lengths was discussed earlier in Section

4.3.3. Therefore the outside diameter of the core extracted from the roll was approximately 15mm.

Results

Figure 7.24 shows the measured normalised radial distortions of the reference hole, following core extraction, in the hoop and axial directions. The normalised radial distortions of the reference hole following core extraction were converted to residual stresses using a Young's modulus, E, of 210GPa. The measured residual stress distributions are shown in Figure 7.25. The residual stresses are shown in the hoop, axial and associated in-plane shear directions. The residual stresses are shown as functions of depth through the roll from the outer surface.

The hoop and axial residual stresses are approximately equi-biaxial and compressive for the first 30mm in depth. Once tensile, the hoop and axial residual stresses separate and reach individual plateaux with the axial residual stress being the largest throughout.

The hoop residual stress starts at a compressive –340MPa at the outer surface and then increases passing through 0MPa at 38mm. At 70mm the hoop residual stress reaches 70MPa and then remains constant up to a depth of 360mm. After 360mm the hoop residual stress then decreases reaching 5MPa at the final measured depth of 390mm.

The axial residual stress starts at a compressive –350MPa at the outer surface and then increases passing through 0MPa at 33mm. At 85mm the axial residual stress reaches a maximum of 135MPa before decreasing to a plateau at 105MPa between the depths of 133 – 295mm. Thereafter the axial residual stress increases to another maximum of 130MPa at 345mm before decreasing to 50MPa at the final measured depth of 390mm.

It can be seen that the magnitude of the in-plane shear stresses is small, hence the principal stresses are approximately equal to the transverse and longitudinal residual stresses.

Discussion

It can be seen that the residual stresses were not recorded at depths over 390mm. The reference hole and the core were successfully manufactured completely through the roll producing reference hole deformations also completely through. The missing data is because the feed section of the air probe machine has a usable length of only 390mm. Therefore the air probe machine was unable to feed the air probe to depths greater than 390mm to measure the reference hole deformations. The residual stresses therefore could have been measured at depths greater 390mm for the sake of a longer feed section.

However, the axi-symmetric design and manufacture of the roll enables the assumption of a symmetric residual stress profile along the radial line of the roll. Therefore the missing data from depths greater than 390mm can be superimposed by mirroring the measured residual stresses from the first half of the roll. Figure 7.26 shows the measured and superimposed residual stress profiles. It can be seen that the superimposed data does agree with the measured data up to the final measured depth of 390mm. Therefore the assumption and the measured data are credible.

At a total thickness of 433mm, the use of the 15mm core instead of the 10mm core was easily justified and the impact on the results negligible. The modifications to the EDM head mainly regarding the enclosed chuck design were of vital importance to the success of this DHD measurement. When carrying out EDM at these great depths, adequate flushing becomes paramount.

7.3 Complex Geometry

Of the 11 components measured, 4 were of a complex geometry, i.e. 3 nozzle-pipe intersections and a T-section butt-weld. The measurements carried out on these components provided tests of the effects of accessibility and geometry on the DHD technique.

7.3.1 Nozzle-pipe T-section (S4)

Residual stress measurements were carried out on a stainless steel nozzle-pipe T-section mock-up using the DHD technique. A previous DHD measurement had been carried out on the mock-up in the as-welded state [George, 2000a]. The mock-up was then subjected to a thermal ageing process prior to the new measurement.

Component Design

The component consisted of a nozzle-pipe T-section mock-up, fabricated to represent the design of a superheater header for a steam power generation system. The mock-up consisted of a 429mm OD pipe of length about 550mm and wall thickness about 64mm. Joined to the pipe was a 274mm OD nozzle of length about 161mm and minimum wall thickness about 34mm. Figure 7.27 shows the design of the mock-up. The nozzle was welded to the side of the pipe with most of the weld preparation having been carried out on the nozzle and only a small amount of machining of the pipe.

Prior to the residual stress measurement carried out during this project the mock-up was subjected to a thermal ageing process carried out in a furnace at 550°C for a total of 19,644 hours.

Measurement Location

The measurement location was situated at the join between the nozzle and pipe at the saddle position. The saddle position is the position where the angle of intersection of the nozzle and pipe is most shallow. The new measurement location was 180° around the circumference of the weld from the previous location measured before thermal ageing, see Figure 7.27. The axis notation used for this measurement location is also shown in Figure 7.27. The axis of the reference hole was at an angle of 69° to the surface of the pipe. A 3.18mm diameter reference hole and 10mm core were used for the DHD measurement.

Results

Figure 7.28 shows the measured normalised radial distortions of the reference hole, following core extraction, in the transverse and longitudinal directions. The normalised radial distortions of the reference hole following core extraction were converted to residual stresses using a Young's modulus, E, of 200GPa. The measured residual stress distributions are shown in Figure 7.29. The residual stresses are shown in the transverse, longitudinal and associated in-plane shear directions. The residual stresses are shown as functions of depth through the pipe from the outer surface.

It can be seen that the residual stresses are approximately equi-biaxial throughout the thickness of the mock-up. Therefore both the transverse and longitudinal residual stresses start at a maximum tensile stress of 250MPa at the outer surface of the pipe decreasing to 0MPa at a depth of about 25mm. The now compressive residual stresses continue to decrease to a value of –50MPa at a depth of 48mm. After 48mm, the transverse residual stress increases to 0MPa at the inner surface of the pipe while the longitudinal residual stress remains constant at –50MPa.

Discussion

As already mentioned, a previous DHD measurement had been carried out on the mock-up in the as-welded state [George, 2000a], whereas the measurement at location 2 was carried out after a thermal ageing process. The locations of measurements 1 and 2 were essentially identical and therefore a direct comparison and assessment of the effect of ageing can be made. Figure 7.30 shows the residual stresses measured for locations 1 and 2. It can be seen that the absolute magnitudes of the residual stresses were reduced by the thermal ageing process.

7.3.2 Nozzle-Pipe T-sections (P22 Ferritic Steel, T4 and T5)

Two P22 ferritic steel nozzle-pipe T-sections were supplied for the measurement of residual stresses using the DHD technique. The measurements were undertaken as part of the European INTEGRITY project [Thomas et al, 2002a].

Component Design

The two nozzle-pipe T-sections were extracted from an ex-service steam pipe manifold system. The manifold had been exposed to service conditions for over 200,000 hours at a nominal temperature of 540°C and an internal pressure of 124bar. The manifold was cut to produce the two steel nozzle-pipe T-sections, labelled T4 and T5. Each T-section consisted of a 380mm OD pipe of length about 800mm and wall thickness about 65mm. Joined to the pipe was a 170mm OD nozzle of length about 420mm and wall thickness about 28mm. For each T-section the nozzle was joined to the pipe by a full penetration weld in the nozzle. The arrangements of each T-section and original weld are shown in Figure 7.31.

Two types of partial weld repair ("pwr1" and "pwr2") were introduced into the T-sections. Both partial weld repairs were the same as those discussed earlier in Section 7.2.4 except that the weld electrodes were matching P22 steel. Type "pwr1" repair weld was introduced into component T4 and type "pwr2" repair weld was introduced into component T5. Each repair weld was finished with an extra surface layer that was later removed by grinding. Neither of the weld repairs was subjected to PWHT.

Measurement Location

Two sets of DHD measurements were obtained, one for each of "pwr1" and "pwr2". The most easily accessible locations for the DHD measurements were at the saddle positions of each T-section. At each saddle position the whole weld region was polished and etched in order to locate the edge of each repair weld. After etching the entrance of each reference hole was easily located at the HAZ between the repair weld and the original base material. The hole location and axes notations used for these measurements are also shown in Figure 7.31. For each T-section a 3.18mm diameter reference hole was gun-drilled through the wall thickness along the radial line of the pipe and a 10mm core was extracted.

Results

Figures 7.32 and 7.33 show the measured normalised radial distortions of the reference hole, following core extraction, in the transverse and longitudinal directions for "pwr1" and "pwr2" respectively. The normalised radial distortions of the reference hole following core extraction were converted to residual stresses using a Young's modulus, E, of 210GPa. The residual stress distributions for "pwr1" and "pwr2" are shown in Figures 7.34 and 7.35 respectively. The residual stresses are shown in the transverse, longitudinal and associated in-plane shear directions. The measured residual stresses for both "pwr1" and "pwr2" were essentially very similar. For both types of weld repair, the transverse and longitudinal residual stresses were tensile for depths up to about 18mm below the outer surface. For the rest of the thickness of the T-sections the residual stresses remain compressive.

For "pwr1" the residual stresses are equi-biaxial for the majority of the thickness of the T-section. The transverse and longitudinal stresses start at a tensile value of 215MPa and decrease to become 0MPa at about 19mm. Once compressive the transverse and longitudinal stresses separate. The transverse residual stress decreases to a maximum compressive value of –35MPa at 43mm before increasing again to reach -5MPa at the inner surface. The longitudinal residual stress decreases to a maximum compressive value of –60MPa at 34mm before increasing again to reach -0MPa at the inner surface.

For "pwr2", the transverse residual stress starts at a tensile value of 210MPa and decreases to become 0MPa at about 18mm. The transverse residual stress then continues to decrease to a maximum compressive value of –40MPa at 55mm before increasing again to reach -25MPa at the inner surface. Whereas the longitudinal residual stress starts at a tensile value of 155MPa and decreases to become a maximum compressive value of –40MPa at a depth of 21mm, passing through 0MPa at about 16mm. At depths greater than 21mm the longitudinal residual stress increases again reaching 0MPa at the inner surface.

Discussion

In order to provide information on the effect of weld repairs on residual stresses it is instructive to directly compare the measurements made on "pwr1" and "pwr2". Therefore the transverse residual stresses of "pwr1" and "pwr2"are compared in Figure 7.36 and the longitudinal residual stresses of "pwr1" and "pwr2" are compared in Figure 7.37. It is shown that the transverse residual stresses are identical for "pwr1" and "pwr2", whereas the longitudinal residual stresses are only similar. The main discrepancy occurs at the outer surface where the axis of the reference hole is closest to the HAZ. At this point the longitudinal residual stresses of "pwr2" are lower than those of "pwr1" by about 60MPa.

Also shown in Figures 7.36 and 7.37 are CHD measurements carried out on "pwr1" and "pwr2" at the locations of the DHD measurements [Thomas et al, 2002a]. The CHD measurements were carried out outside of the University and correspond to residual stresses at 1mm below the surface. The measurements carried out using both techniques are in close agreement providing credibility to both measurement sets and techniques.

7.3.3 Butt welded T-section (low carbon ferritic steel)

A steel butt welded T-section was supplied by Imperial College London for the measurement of residual stresses using the DHD technique.

Component Design

The component consisted of two 100mm thick plates butt welded together to form a T-section, see Figure 7.38. The web and flange plates were manufactured from steel BS EN 10025 Grade S355 J2G3. This is a low carbon ferritic steel, which represents a group of materials commonly used in the offshore and power generation industries.

Partial penetration butt welds were used to manufacture the T-section. The welds were deposited using the MMA welding procedure. An alternating depositioning sequence was used for all the samples to minimise distortion during the welding process. The welding was carried out with an Oerlikon Tenacito 38R welding

electrode, which is also in common use in the offshore industry. To prevent cracking during welding, heating blankets were used to ensure that the temperature of the plates never dropped below 250° C.

The manufactured T-section was then cut into slices for residual stress measurement. A 100mm thick slice of the T-section was prepared for the DHD technique.

Measurement Locations

The axis of the reference hole was through the thickness of the flange plate at the point of intersection with the weld root. This location was chosen in order to measure the residual stresses generated in the HAZ between the weld and the original flange plate material. The measurement process was attempted twice for which the measurement locations are shown in Figure 7.38. At each measurement location a reference hole of 3.18mm diameter was gundrilled and a 10mm core extracted.

The first attempt (location 1) was carried out from the welded side of the component which required modifications to the standard set-up. Access of the machining heads to the welded side and measurement location 1 was restricted by the proximity of the web. Therefore an extended outer front bush configuration was used, enabling the machining heads to operate at a distance from the component.

The gundrills were of sufficient length to drill through the component when used in the distant gundrilling head. However the normal EDM electrode was too short for the trepanning operation. Manufacture of an extended copper electrode proved difficult. Therefore an alternative electrode design was used consisting of a tubular aluminium shaft onto which a copper tip was screwed. The manufacturing difficulties and alternative electrode design were discussed earlier in Section 4.3.3.

At location 1, the trepanning process was stopped when the EDM head had travelled through a distance of 105mm and presumably through the thickness of the component, allowing for a more than average amount of electrode wear. However, upon retraction of the electrode it was found that the electrode had worn considerably and that the trepanned depth was only 55mm. Therefore it was presumed that the

wear had started at the electrode tip progressing slowly through the copper before greatly increasing in speed when into the aluminium. Therefore another aluminium/copper electrode was made with an extended copper tip.

The trepanning process was resumed with the new electrode and the wear of the electrode inspected at regular intervals by its retraction from within the component. The EDM process was allowed to run for about 6 hours, but it was found that little or no further increase in the trepanned depth was achieved. At this point it was decided to halt the EDM process and a set of reference hole diameter measurements taken.

Measurement of the reference hole diameter revealed that at depths between 43 and 55mm the walls of the reference hole had been eroded away by the EDM process. Closer inspection of the extracted core and the hole within the component revealed that the first electrode tip had fallen off inside the component and eroded half way through the core and reference hole. Therefore the deformations of the reference hole were only measured up to a depth of 43mm for location 1. After a depth of 55mm the release of residual stresses did not occur and so deformations of the reference hole also did not occur.

Due to the incomplete measurement at location 1, a second attempt (location 2) was made to measure the residual stresses. Location 2 was carried out from the non-welded side of the flange, through the HAZ of the second weld, see Figure 7.38. Without the access restrictions at location 2, the standard set-up was used and the DHD technique succeeded in measuring the residual stresses completely through the 100mm thickness of the flange plate.

The axis notation used for both measurement locations 1 and 2 is also shown in Figure 7.38.

Results

Figures 7.39 and 7.40 show the measured normalised radial distortions of the reference hole, following core extraction, in the transverse and longitudinal directions for locations 1 and 2 respectively. The normalised radial distortions of the

reference hole following core extraction were converted to residual stresses using a Young's modulus, E, of 212GPa. The measured residual stress distributions for locations 1 and 2 are shown in Figures 7.41 and 7.42 respectively. The residual stresses are shown for the transverse and longitudinal directions as well as the associated in-plane shear. The residual stresses are shown as functions of depth from the weld root.

At location 1, it can be seen that the transverse and longitudinal residual stresses were essentially equi-biaxial for depths up to approximately 24mm. Therefore both residual stresses were found to be at a maximum tensile value of 260MPa near the front face before decreasing to a compressive value of –120MPa at 24mm. The transition from tension to compression occurred at a depth of about 14mm. At depths greater than 24mm the transverse and longitudinal residual stresses separated. The transverse residual stress continued decreasing to a maximum compressive value of –150MPa at 29mm before increasing slightly to reach –140MPa at 43mm. The longitudinal residual stress also continued decreasing but to a maximum compressive value of only –125MPa at 28mm before increasing to reach –70MPa at 43mm. At depths between 43 and 55mm the residual stresses were undetermined. For reference hole depths greater than 55mm (i.e. where the core had not been trepanned and residual stresses not released) the measured residual stresses were zero as expected.

At location 2, it can be seen that the transverse and longitudinal residual stresses were only equi-biaxial for depths up to approximately 11mm. Therefore both residual stresses were found to be at a maximum tensile value of 220MPa near the front face before decreasing to a value of 75MPa at 11mm. At depths greater than 11mm the transverse residual stress continued decreasing to a maximum compressive value of –160MPa at 28mm. The transverse residual stress then increases passing 0MPa at 74mm before reaching a maximum tensile value of 105MPa near the rear face. At depths greater than 11mm the longitudinal residual stress also continued decreasing to a maximum compressive value of –120MPa at 27mm. The longitudinal residual stress then increases passing 0MPa at 56mm before reaching a maximum tensile value of 45MPa near the rear face.

Discussion

Locations 1 and 2 were measured at the same state of manufacture of the component and so are able to provide information about the repeatability of the DHD residual stress measurement technique. Therefore, the transverse residual stresses at locations 1 and 2 are compared in Figure 7.43 and the longitudinal residual stresses at locations 1 and 2 are compared in Figure 7.44. It can be seen that overall there is excellent agreement between the repeated transverse and longitudinal residual stress measurements. Obviously the residual stresses at the depths greater than 43mm are not taken into account. The main discrepancy occurs near the front face where the residual stresses at location 2 are lower by about 40MPa. This discrepancy could be due to a combination of measurement errors. It could also be due to the fillet of weld not trepanned at the end of the EDM process for location 2. The small fillet was not trepanned because the glue attaching the rear bush prevented the electrode from eroding the final filaments of fillet weld. The glue provides no electrical conduction and so prevents any further advancement of the electrode. The remaining filament of weld could be responsible for preventing the full release of residual stresses at these depths. Location 1 was carried out from the welded side and so this did not occur at location 1.

Residual stress measurements were also made using the ND technique [Wimpory et al, 2003]. Due to the limited penetration of the ND technique, the slice of T-section measured using ND was only 12.5mm thick, instead of 100mm thick as used for DHD. Figure 7.45 shows the transverse residual stress measurements carried out using the ND technique as well as the DHD technique. It can be seen that there is excellent agreement between the DHD and ND measurements of the transverse residual stress providing confidence in the accuracy of both techniques. Figure 7.46 shows the longitudinal residual stress measurements carried out using the ND technique as well as the DHD technique. Unfortunately the ND and DHD longitudinal residual stress measurements do not agree. The ND results show near zero longitudinal residual stresses throughout the thickness of the T-section, except near to the weld. These comparisons suggest that the transverse residual stress distribution has not been affected by the smaller slicing of the T-section for the ND measurements. However the same cannot be said for the measurement of the

longitudinal residual stresses where the smaller slicing of the T-section does have a large effect. Therefore the DHD technique has presented as the most credible technique, when compared to ND, for the measurement of both the transverse and longitudinal residual stresses in thick section components.

7.4 Alternative Materials

The last two components measured using the DHD technique were manufactured from aluminium and titanium alloys. This application was unusual because the DHD technique had thus far been developed for and used on steel components. The measurements carried out on these components provided tests of the sensitivity, sampling volume and material applicability of the DHD technique.

7.4.1 Aluminium punched plate

Concurrent research at the University of Bristol is being undertaken to explore the effects of residual stresses on crack growth within a component [Mahmoudi et al, 2003]. The interaction of both tensile and compressive residual stresses is being researched. The compressive residual stresses are generated within the component by punching the surface and introducing localised plastic deformation. The punching of the surface and the generation of compressive residual stresses is an experimental process for which the parameters are still being defined. Therefore a punched component was supplied for the measurement of the generated compressive residual stresses using the DHD technique.

Component Design

The component supplied was a 60mm square aluminium plate with a thickness of 15mm, see Figure 7.47. The plate was manufactured from aluminium alloy AL2650 used heavily throughout the aerospace industry. The punching process was carried out between the jaws of a servo-hydraulic test machine containing two 25mm diameter, flat-nosed punches. The localised deformation of the plate following punching was such that the thickness of the plate was reduced by 1.6%.

Measurement Location

The measurement location used for the DHD technique was through the centre of the deformed area through the thickness of the plate, see Figure 7.47. The axis notation used for the measurement is also shown in Figure 7.47.

Due to the very localised deformation the residual stresses generated were presumed to also be very localised. Therefore a 1.5mm diameter reference hole and a 5mm diameter core was used to carry out the DHD measurement. The plate had previously been subjected to residual stress measurement using the CHD technique. The CHD measurement had already produced a 1.6mm diameter, 1.6mm deep centre-hole in the centre of the deformed area of the plate. Therefore the reference hole for the DHD technique was gundrilled through the centre of the CHD measurement location. The 1.5mm diameter gundrilling operation was sub-contracted out.

Results

Figure 7.48 shows the measured normalised radial distortions of the reference hole, following core extraction, in the *xx* and *yy* directions. The normalised radial distortions of the reference hole following core extraction were converted to residual stresses using a Young's modulus, E, of 72GPa. The measured residual stress distributions, σ_{xx}, σ_{yy} and σ_{xy}, are shown in Figure 7.49. The residual stresses are shown as functions of depth through the plate from the surface containing the centre-hole.

Residual stresses were not measured over the initial 2.5mm in depth due to the presence of the centre-hole and the inability of the air probe to measure the reference hole diameter near to its entrance and exit.

Figure 7.49 shows that the measured residual stresses were compressive, equi-biaxial and symmetric throughout the plate thickness as expected. At an initial measurement depth of 2.5mm the residual stresses have a compressive value of –128MPa and decrease to a maximum compressive stress of –236MPa at mid-thickness. The

residual stresses then increase to a minimum compressive value of –90MPa at the rear surface.

Discussion

The residual stress results shown are very smooth (i.e. no noise evident) and are the exact values calculated from the diameter deformations without smoothing. The diameter measurements of the reference hole show the incredibly smooth surface finish produced by gundrilling. Bell mouthing was present but the diameter of the reference hole through the thickness of the plate was still within ±3.5μm of a median diameter of 1.5025mm.

As already mentioned, CHD measurements were undertaken at the University [Mahmoudi et al, 2003] to provide an initial gauge on the residual stresses present within the plate. The residual stresses using CHD are also shown in Figure 7.49. It can be seen that there is excellent agreement between the CHD and DHD residual stress measurements. Again providing credibility to both measurements and techniques.

7.4.2 Titanium Friction Weld

Titanium is known to be highly reactive at elevated temperatures, therefore during fusion welding titanium is prone to the production of undesired oxides and a brittle weld. Research by Wallis and Wisbey [2001] has found that the friction welding of titanium alloys is a comparatively easier process and also achieves better results. Minimal research however has been carried out to quantify the residual stresses generated during the friction welding process. Therefore a titanium, friction welded pipe was subjected to residual stress measurement using the DHD technique.

Component Design

The component consisted of a friction butt-welded titanium alloy pipe with dimensions of 142mm long, 59mm OD and an average wall thickness of 19.5mm, see Figure 7.50. The composition of the titanium alloy pipe was defined as Ti-10V-

2Fe-3Al by percentage weight. The alloy is used heavily in the aerospace industry for the manufacture of landing gear and airframes.

The friction weld was a 4mm thick, full depth, fully circumferential weld at mid-length of the pipe. The welding process was carried out with one half of the pipe fixed and the other half spun at high speed before being rammed together creating friction, excessive heat build-up and the subsequent welding of the two halves.

Measurement Location

The measurement location was on the centre-line of the weld at an arbitrary position around the circumference. The axis notation used for this measurement location is shown in Figure 7.50. A 3.18mm diameter reference hole was gundrilled through the wall thickness along the radial line of the pipe and a 10mm core extracted. The hole location and axis is also shown in Figure 7.50.

Results

Figure 7.51 shows the measured normalised radial distortions of the reference hole, following core extraction, in the transverse and longitudinal directions. The normalised radial distortions of the reference hole following core extraction were converted to residual stresses using a Young's modulus, E, of 110GPa. The measured residual stress distribution is shown in Figure 7.52. The residual stresses are shown in the transverse, longitudinal and associated in-plane shear directions. The residual stresses are shown as functions of depth through the pipe thickness from the outer surface.

The transverse and longitudinal residual stresses are similar in shape, both compressive from the outer surface up to a depth of about 6.5mm before transforming into and remaining tensile thereafter.

The transverse residual stress starts at a maximum compressive value of -90MPa at the outer surface and then rises to a maximum tensile value of 220MPa at the inner

surface. The transition from compression into tension occurs at 7mm from the outer surface.

The longitudinal residual stress starts at a maximum compressive value of -45MPa at the outer surface and then rises to a maximum tensile value of 290MPa at the inner surface. The transition from compression into tension occurs at 6mm from the outer surface.

It can be seen that the magnitude of the in-plane shear stresses is small, hence the principal stresses are approximately equal to the transverse and longitudinal residual stresses.

Discussion

A "10mm" core containing a 3.18mm diameter reference hole was extracted successfully from the titanium pipe. The diameter of the extracted core was such that it contained weld, HAZ and parent material. Therefore the residual stresses released and measured were those experienced by the weld, HAZ and parent material. Hence the accuracy of the measured residual stresses relative to those experienced by the weld, HAZ and parent material is open to interpretation.

The large sampling area of the standard DHD technique was therefore unsuited to this application. The measurement should therefore be repeated with the miniaturised extraction of a "5mm" core containing a 1.5mm diameter reference hole.

Chapter 8: PORTABLE DHD MACHINE

8.1 Introduction

The DHD technique has its own place in the residual stress measurement field originating from its ability to penetrate to great depths. A problem arises however due to the nature of the large penetration depths. The components needing large depths of penetration also tend to be very large.

The 1 tonne "*mini*" mock-up discussed in Section 7.2.5 highlights this problem. The mock-up was at the limit of practical handling at the University's facility. Therefore the handling of real components, which weigh from 80 – 460 tonnes, would have been impossible. The problem also arises from the physical dimensions of the real components. During this research project a request was made for a DHD measurement to be carried out on a component that was two stories high (approximately 5m). To undertake the measurement the equipment and personnel were required to work on the inside of the component.

In principle, the DHD technique can be carried out away from the University but the machines discussed in Section 3.2, are very large and very heavy. The transportation and set-up of the DHD machinery would require craning facilities and an HGV lorry. Therefore to provide a solution to this size problem a portable DHD machine has been developed during this research project to carry out measurements away from the University and "on-site".

The following sections give an overview of the portable machine. Following the overview are the results of two DHD measurements undertaken with the portable machine. The specimens were chosen in order to test and validate the machine's

performance. The first measurement was undertaken at the University and the second measurement was undertaken "on-site" in Spain.

8.2 Machine Specifications

The machine has been designed and built using knowledge accumulated throughout this research project. For example, the investigation of alternative machining processes discussed in Section 4.2 was mainly carried out for the benefit of the design of the portable machine. Having found that gundrilling and EDM were the most suitable machining processes for the DHD technique, the design of the machine naturally evolved around them.

The machine is a modular design. The main structure of the machine is common to the whole DHD process whether it be laser alignment, gundrilling, hole diameter measurement or EDM. The different processes are then carried out with the attachment of process specific modules.

In order to remain portable, each module weighs less than 25kg. The 25kg limit was imposed as the maximum that was deemed suitable for a single person to lift and manipulate.

The machine is capable of working at any angle from just less than horizontal to vertical. The accurate alignment of the machine to the component at any of the above angles is carried out using a laser system. The laser system is attached to the machine using the "Measurement Module". During alignment of the machine, the laser system allows for the specification of a variable angle between the surface of the component and the axis of the reference hole. Such versatility is needed for components with a complex geometry such as the nozzle-pipe intersection discussed in Section 7.3.1, where the reference hole axis was at a 69° angle to the surface of the pipe.

The concentric machining of both reference hole and core is achieved by using a common "Machining Module" for both gundrilling and EDM. The portable machine

is capable of gundrilling reference holes with diameters ranging from 1.5mm to 3.18mm. Therefore the "Machining Module" is capable of supplying spindle speeds ranging from about 10,000rpm down to 5,000rpm respectively. When used for EDM however, the same "Machining Module" also supplies a spindle speed of only 90rpm. The "Machining Module" is capable of producing various diameters of core, only being limited by the practical manufacture of the electrode. The "Machining Module" also supplies gundrilling cutting oil and EDM dielectric fluid to the tool during the relavent processes.

Following machining, the "Measurement Module" is used to measure the reference hole diameter with an air probe. The "Measurement Module" is capable of using any size of air probe.

The constant velocity feeds (as used for machining) and the incremental steps (as used for measuring) are provided by the main structure of the machine. The feeds and steps are provided with dual encoder feedback ensuring accurate position and velocity movements.

The range of movement of the machine is limited to a maximum distance of 450mm which converts to a maximum penetration depth of 375mm when the bush configurations and gundrill guides are all taken into account.

Control and datalogging of the machine is carried out via serial link from a laptop computer. The control and datalogging software has been specifically designed and built for the machine using Delphi (Pascal machine code with a Windows skin). The software has been designed with a graphical user interface to lead the machine operator through the DHD process and allow the operator to set the machining and measurement parameters. Once the parameters have been set, the software automatically controls the machine and provides a real-time graphical display to show the progression of the process.

The measurements taken during the DHD technique are recorded to file in a generic ASCII format. The data can then imported into any standard Windows spreadsheet for analysis.

8.3 Portable Machine DHD Measurements

Having designed and built the machine, two DHD measurements were undertaken to test and validate its use. The first measurement was undertaken at the University in a controlled environment. The second measurement was undertaken "on-site" in Cartagena, Spain.

8.3.1 Measurement 1 (University)

A 50mm thick butt-welded plate was provided for the measurement of residual stresses using the DHD technique. The plate was supplied as part of a European research project called ELIXIR. The research project is concerned with investigations of the influence of PWHT on residual stresses. Three DHD measurements had been previously carried out on the plate using the laboratory based equipment [Stefanescu et al]. The plate was therefore well characterised in terms of the residual stress distribution present and was thus suitable for a fourth measurement using the portable machine.

Component Design

The component consisted of a steel butt-welded plate with dimensions 1000mm x 300mm x 50mm, see Figure 8.1. The plate was manufactured from S690 steel and butt-welded using a submerged arc welding procedure. After welding the root of the weld was machined flat with the parent material. The parent material and welding procedure are representative of those commonly used in off-shore applications.

Measurement Location

The measurement location was through the centre of the weld, at a distance of 162mm from one end. The measurement location and axis notation used is shown in Figure 8.1. The measurement was carried out using a 3.18mm diameter reference hole and 10mm diameter core. The machine was located above the plate and the DHD technique was carried out in a vertical position (i.e. the axis of the reference hole was vertical).

Complications were initially encountered during the manufacture of the reference hole. The feed rate programmed in and hence automatically controlled by the machine, was too fast. Hence the swarf produced was too large, leading to inadequate swarf clearance and packing, and the ultimate ceasing of rotation of the gundrill. The drill was therefore removed and discarded, and the measurement location was inspected. The initial process was found to have drilled to a depth of about 13mm before the complications were encountered. The front reference bush had also become detached. Therefore a new front reference bush was adhered to the measurement location and the initial hole packed with glue. A second attempt at the manufacture of the reference hole was carried out with a new gundrill and a slower feed rate. At the second attempt, the manufacture of the reference hole was successful. The remainder of the DHD technique was then carried out without complication.

Results

Figure 8.2 shows the measured normalised radial distortions of the reference hole, following core extraction, in the transverse and longitudinal directions. The normalised radial distortions of the reference hole following core extraction were converted to residual stresses using a Young's modulus, E, of 206.4GPa. The measured residual stress distributions are shown in Figure 8.3. The residual stresses are shown for the directions longitudinal and transverse to the weld as well as the associated in-plane shear. The residual stresses are shown as functions of depth through the plate from the weld-cap surface.

It can be seen that the residual stresses measured over the initial 13mm in depth are highly erratic when compared to the rest of the results. The calculated residual stresses at these depths correspond to the depths of the first unsuccessful attempt at reference hole manufacture. Figure 8.4 shows the measured diameter of the reference hole at 0° and 90° (i.e. longitudinal and transverse to the weld, respectively). It can be seen that the measured diameter of the reference hole over the initial 13mm in depth was found to be large and outside the calibration range of the air probe. The accuracy of the calibration curve and hence the diameter measurements outside of the calibration range is unknown. The calculated residual

stresses over these depths are therefore assumed to be inaccurate and have thus been omitted from further discussions.

It can be seen that the longitudinal and transverse residual stress distributions are similar in shape, with the longitudinal residual stresses being larger in magnitude. Both directions show peak residual stresses near to the front and rear surfaces of the plate and a minimum at a depth of 33mm. Whilst the longitudinal residual stress remains tensile throughout the thickness, the transverse residual stress is only tensile over the first 21mm and last 13mm in depth.

The longitudinal residual stress starts at a peak tensile value of 540MPa after the initial 13mm in depth and then decreases to a minimum of 330MPa at 33mm. After 33mm the longitudinal residual stress then increases to reach a maximum of 475MPa near the rear surface.

The transverse residual stress starts at a tensile value of 245MPa after the initial depth of 13mm and gradually decreases to a minimum compressive value of –140MPa at 33mm. The transition between tension and compression occurs at a depth of 21mm. After 33mm the transverse residual stress then increases to reach a maximum of 460MPa near the rear surface with the transition between compression and tension occurring at a depth of 42mm.

It can be seen that the magnitude of the in-plane shear stresses is small, hence the principal stresses are approximately equal to the longitudinal and transverse residual stresses.

Discussion

The fourth measurement location, carried out using the new portable machine, was chosen to provide similar results to locations 1 and 3, previously carried out using the laboratory based equipment [Stefanescu et al]. Locations 1, 3 and 4 were all located on the weld centre-line. Figures 8.5 and 8.6 respectively show the longitudinal and transverse residual stresses measured at locations 1, 3 and 4 for comparison. It can be seen that there is excellent agreement between the residual stresses measured at

the different locations. This demonstrates the excellent repeatability of the DHD technique. However, more importantly, it also shows that the new portable machine is able to successfully carry out the DHD technique.

8.3.2 Measurement 2 (Cartagena, Spain)

Following the successful residual stress measurement carried out within the laboratory, the next measurement was undertaken "on-site" in Cartagena, Spain. The component for residual stress measurement was a circular section of a submarine hull weighing 17 tonnes. This "on-site" measurement was also carried out as part of the European ELIXIR project.

A single DHD measurement had been previously carried out using the laboratory equipment on a small, straight coupon of part of the hull section [Kingston et al, 2004]. A similar measurement had therefore already been carried out, and could be used for comparison.

Transportation of the whole machine and operators to Cartagena was by a family estate car, providing evidence of its portability.

Component Design

The component consisted of a circular, steel section of a submarine hull with dimensions 2360mm long, 6600mm OD and average wall thickness 30.6mm. Inside the hull section was welded four T-section ribs to provide stiffness. Figure 8.7 shows the design of the hull section for clarification. The material used for the manufacture of the whole hull section was a high yield strength steel, 80 HLES.

The T-section ribs comprise of a web and flange plate fillet-welded together before being fillet-welded again to the inside of the hull. All the fillet-welds are deposited using the automatic submerged arc (ASA) welding process.

Measurement Location

The hull section was laid on its side and raised above floor level to allow easy access to the inside surface, see Figure 8.8.

The axis of the reference hole was through the thickness of the hull at the point of intersection with the weld root. This location was chosen in order to measure the residual stresses generated in the HAZ between the weld and the hull material. The measurement was carried out on the second rib down from the top, with the entrance of the reference hole located on the outer surface of the hull at an arbitrary position around its circumference. The portable machine was positioned horizontally on the outside of the hull section, at a height of about 2.5m off the ground. The DHD technique was therefore carried out in a horizontal position (i.e. the axis of the reference hole was horizontal). The measurement and machine locations are shown in Figure 8.8, along with the axis notation used. A 3.18mm diameter reference hole and a 10mm core were used to carry out the DHD technique at this location.

Results

Figure 8.9 shows the measured normalised radial distortions of the reference hole, following core extraction, in the transverse and longitudinal directions. The normalised radial distortions of the reference hole following core extraction were converted to residual stresses using a Young's modulus, E, of 210GPa. The measured residual stress distributions are shown in Figure 8.10. The residual stresses are shown for the directions transverse and longitudinal to the weld as well as the associated in-plane shear. The residual stresses are shown as functions of depth through the hull from the welded surface.

The longitudinal and transverse residual stress distributions were found to be similar in shape, both exhibiting an oscillatory distribution about 0MPa. The longitudinal residual stress was found to be the larger of the two throughout the majority of the thickness. The maximum longitudinal and transverse residual stresses were found to occur near the welded surface as expected.

The longitudinal residual stress starts at a maximum tensile value of 525MPa at the welded surface, before decreasing to a compressive value of –150MPa at a depth of 11.5mm. The longitudinal residual stress then increases to a tensile value of 210MPa at 20mm before decreasing again to reach –125MPa at the outer surface. The transitions between tension and compression occur at depths of 7.5mm, 15mm and 27mm.

The transverse residual stress starts at a maximum tensile value of 220MPa at the welded surface, before decreasing to a compressive value of –185MPa at a depth of 10mm. The transverse residual stress then increases to a tensile value of 135MPa at 20mm before decreasing again to reach –40MPa at the outer surface. The transitions between tension and compression occur at depths of 6mm, 16mm and 29mm.

It can be seen that the magnitude of the in-plane shear stresses is small, hence the principal stresses are approximately equal to the longitudinal and transverse residual stresses.

Discussion

The coupon manufactured for the laboratory DHD technique was a 1m straight length of a T-section rib. The overall design of the weld region between the web and flange of the rib is almost identical to the design of the weld region between the web and outer hull. Therefore the laboratory and "on-site" residual stress measurements carried out at these two locations, see Figure 8.7, should exhibit similar distributions. Figures 8.11 and 8.12 therefore respectively show the longitudinal and transverse residual stresses measured "on-site" and in the laboratory for comparison.

It can be seen that there is good agreement only over the initial 7mm in depth (i.e. closest to the weld). At depths greater than 7mm, the oscillatory distribution of the "on-site" measured residual stresses is not evident in the laboratory measured residual stresses. In comparison the laboratory measured residual stresses remain constant at near zero values at depths greater than 10mm. Further analysis reveals that the difference between the measurements is an oscillatory distribution, which is 180° rotationally symmetric about mid-depth, see Figure 8.12. The symmetric,

oscillatory distribution is consistent with the residual stresses generated due to the plastic bending of a plate to form a curve. The laboratory measurement was carried out on a straight coupon and the "on-site" measurement was carried out on a curved hull section. Therefore the difference in distributions is justified and the ability of the new portable machine is demonstrated.

8.3.3 Conclusions

The new portable machine has been shown to carry out the measurement of residual stresses as accurately as the already established laboratory equipment using a 3.18mm reference hole and 10mm core.

The new portable machine has been shown to be able to carry out residual stress measurements along the vertical and horizontal axes.

The difference between the "on-site" and laboratory residual stress measurements for the submarine components highlights the need for real component measurements using portable machines.

Chapter 9: DISCUSSION

9.1 Introduction

A wide variety of topics have been presented within this thesis detailing the advancement of the DHD residual stress measurement technique. The topics have been presented in self-contained sections, which included relevant discussions and conclusions. The aim of this section is not to repeat this work but to present a generic discussion about the DHD technique with particular emphasis on its comparative abilities. The discussion therefore presents the state of the DHD technique and provides a comparison with the four most widely used residual stress measurement techniques.

The four most widely used residual stress measurement techniques were identified by NPL (Kandil et al [2001]) through an industrial market survey on residual stress measurement techniques. The four residual stress measurement techniques were identified as centre-hole drilling, X-ray diffraction, neutron diffraction and layer removal (LR).

The detailed abilities of each technique have been reviewed with reference to Kandil et al [2001], Withers and Bhadeshia [2001], Toten et al [2002] and Buttle [2000].

9.2 Comparison of DHD and Other Measurement Techniques

Prior to this research the DHD technique was limited to laboratory applications on coupons/mock-ups of moderate size, (e.g. weight < 2 tonnes). With the development of the new portable machine however, the DHD technique can now be carried out either in the laboratory or "on-site". This enables the DHD technique to be applied to very large structures and components (e.g. complete piping systems and pressure

vessels, bridges, large machinery). Of the other 4 techniques, ND and LR are restricted to the lab, but CHD and XRD can also be carried out "on-site" with portable machinery. The portability of the DHD, CHD and XRD machines also enable the residual stress measurements to be carried out at almost any location on the components. For ND the location of residual stress measurement may have a constricted access for the fixed machinery, either requiring significant modification of the component for access or making the measurement location impossible. LR is only applicable to plates and so constricted access is not an issue.

Although DHD, CHD and XRD are available for "on-site" measurements and can therefore measure the residual stresses within large components, the penetration of the different techniques is very different. DHD has been shown to be successful at measuring residual stresses at depths between 10 – 433mm. CHD can measure residual stresses at depths equal to the depth of drilling, which tends to be approximately equal to the diameter of the drill used, usually 1.6 – 3.2mm. XRD however can only measure residual stresses at depths below the surface of 5μm for titanium, 15μm for steel and 50μm for aluminium. Therefore for large components, which usually means large thicknesses, DHD is the only portable technique to be able to measure the residual stress distribution through the full thickness. For "on-site" applications the order of technique applicability with respect to the depth of penetration is XRD, CHD and DHD. The penetration depths of the portable techniques do not change when they are applied in the laboratory. However in the laboratory environment, ND and LR are also available. ND can measure residual stresses at depths below the surface of 4mm for titanium, 37mm for steel and 250mm for aluminium. LR however can measure the residual stresses completely through the component, independent of thickness. Therefore for laboratory based applications the order of technique applicability with respect to the depth of penetration is XRD, CHD, ND, DHD and LR.

Like CHD, the penetration of the DHD technique is equal to the depth at which machining is carried out. For CHD it is equal to the depth of drilling, for DHD it is equal to the depth of the drilled reference hole or trepanned core, whichever is the smaller. Therefore in order to carry out the DHD technique a small hole (i.e. 5 - 10mm OD) is made in the component. The size of the hole is comparatively small

compared to the size of the component and so the DHD technique is classed as a semi-invasive technique. The CHD technique is also classed as semi-invasive due to its manufacture of a small hole in the component during measurement. CHD also requires that the surface of the component is smooth and so light abrasion of the surface is usually carried out in preparation of the measurement. XRD and ND can carry out their residual stress measurements without modifying the component and so are generally classed as non-invasive techniques. For ND it is sometimes necessary to manufacture large holes in the specimen to allow the incident and emergent beams access. Therefore ND can also be classed as a semi-invasive technique depending on its application. LR however is classed as an invasive technique due to the complete destruction of the component during residual stress measurement. Complete destruction of the component only allows for one set of residual stress measurements to be carried out. In comparison, the DHD, CHD, XRD and ND techniques allow for repeated sets of measurements to be carried out on the same component and at different stages in its life (e.g. different stages in heat treatment, ageing and repair). Being semi-invasive, DHD and CHD only allow for a finite number of measurements to be carried out until the component is also destroyed. Generally however, the increments in destruction are small and so the cycle of testing on any component is satisfied before complete destruction occurs.

The DHD technique was originally developed for steel components. However, application of the technique is widening and it has already been used successfully on aluminium alloys, titanium alloys and graphite. The DHD technique is applicable to most materials in principle, however, minor modifications may be required. For example, extraction of the core using EDM would not work for ceramics, polymers and plastics due to their electrically non-conductive properties, but other machining processes could be carried out instead. Composite materials pose another obstacle due to the measurement of the step changes in generated residual stress between the matrix phase and the dispersed phase. Obviously calibration/validation experiments would have to be carried out to the test the application of the DHD technique on the different materials. The material based applicability of the different techniques depends upon the method by which the distortion of the material generated by residual stresses is measured. DHD, CHD and LR measure the macro-distortions of the material following the release of residual stresses by machining. Therefore these

methods are applicable to most materials and composites. XRD and ND however measure the micro-distortions of the material by comparing the atomic interplanar spacing between regions with and without residual stresses. Therefore for XRD and ND, the materials measured need to conform to a crystalline structure and hence are only applicable to metals, ceramics and composites of the two.

The identification of the type of distortion measured by the different techniques generally also identifies the type of residual stresses calculated. Macro residual stresses are calculated from macro-distortions and micro residual stresses from micro-distortions. Micro-distortions can also be used to calculate macro residual stresses but not vice versa. Macro residual stresses are the residual stresses that vary within the body of the component over a range much larger than the grain size. Micro residual stresses however operate at the atomic or grain-size level. Therefore DHD, CHD and LR calculate macro residual stresses, and XRD and ND can calculate both macro and micro residual stresses.

During the DHD technique, the macro normalised radial distortions are measured along the entire length of the reference hole. The measured normalised radial distortion are then used to calculate the biaxial residual stresses acting in a plane normal to the axis of the reference hole. Also, during the trepanning operation the axial strain of the core can be measured and used for the estimation of the axial residual stresses. Therefore the triaxial state of residual stresses acting within a component can be estimated using the DHD technique. The possible error in the estimated axial residual stresses is large when compared to the biaxial residual stresses and so, typically only the accurate biaxial residual stresses are usually specified. ND is the only technique able to accurately calculate the triaxial state of residual stress. CHD, XRD and LR are limited to determining the biaxial state of residual stress.

The depth resolution of the biaxial residual stresses calculated using the DHD technique was found to be dependent on the size of air probe used for the reference hole diameter measurement. For the 3.18mm diameter air probe the depth resolution was found to be approximately 0.8mm and for the 1.5mm diameter air probe inferred to be approximately 0.4mm. When calculating the triaxial residual stresses the

measured axial and normalised radial distortions of the core are combined. Due to the slow progression of the EDM process and the time interval between axial strain measurements, the resolution of the measured axial strains is of the order of 0.05mm. Therefore the measured axial and normalised radial distortions of the core are combined at the higher depth resolutions of 0.4 and 0.8mm. The triaxial residual stresses are therefore calculated with a depth resolution of 0.4 and 0.8mm depending on whether the 1.5mm or 3.18mm diameter air probes are used, respectively. The biaxial and triaxial residual stresses are both specified as functions of depth through the thickness of the component and as such the residual stress gradients present within the component can be found. Of the other four techniques, CHD, ND and LR are also able to measure residual stress gradients, however XRD cannot. The measurement of the residual stress gradients using CHD is carried out using a refinement thereof called ICHD, where the hole is drilled, and strains measured and analysed in 0.05 – 0.1mm depth increments. Like DHD, the increments in ICHD strain measurement define the depth resolution. For XRD and ND the depth resolutions are 0.02mm and 0.5mm respectively. For LR the depth resolution is dependent on the resolution of the strain measurement equipment used and the material being tested.

During the trepanning operation of the DHD technique, the triaxial residual stresses are released from the extremities of the core and hence the whole volume of the core deforms to reach a new equilibrium state of negligible stress. Therefore the sampling area is the area enclosed within the core diameter. Hence, for the standard and specialised applications of the DHD technique the sampling area relates to a diameter of 10mm and 5mm respectively. For CHD there exists a similar relationship between the diameter of the drilled hole and the sampling area (i.e. sampling area enclosed by 1.6 – 3.2mm drilled diameter). For XRD the sampling area varies from 0.1 – 1mm^2 and for ND a sampling volume of 1mm^3 is typical. Again, the sampling volume of LR is dependent on the resolution of the strain measurement equipment used and the material being tested.

When putting all these issues into practice, the time taken to carry out a DHD residual stress measurement is heavily dependent on the total depth at which the residual stresses are to be measured. When applied to a 10mm thick component the

DHD technique could be completed in as little as three working days, however when applied to a 433mm thick component the DHD technique would be completed in about 11 working days. The DHD technique is therefore considered to be a slow technique when measured against time. However when measured against quantity of residual stress measurements carried out, the DHD technique could be considered fast.

Chapter 10: CONCLUSIONS AND FUTURE WORK

10.1 Conclusions

- A review of the available machining processes found that gundrilling was still most suited for the manufacture of the deep, precision reference hole. The review also found that EDM was still the most suitable machining process for the trepanning operation and the extraction of the deep-hole core.

- Redesign of the EDM equipment and measurement system has enabled the standardised extraction of a 10mm OD core containing a 3.18mm diameter reference hole. Also, the specialised extraction of a 5mm OD core containing a 1.5mm diameter reference hole has been introduced.

- The extraction of smaller diameter cores has reduced the scale of destruction of the DHD technique.

- The smaller diameter cores have also enabled the DHD technique to measure residual stresses in thinner components. The redesign of the EDM equipment has enabled the DHD technique to increase its depth of penetration, hence measuring residual stresses in thicker components. The DHD technique can now measure residual stresses at depths from 10 – 433mm.

- The inclusion of noise within the reference hole diameter measurement signal has been eliminated through using a serial port link, thereby increasing the accuracy of the residual stresses calculated and the DHD technique.

- The automatic datalogging of the temperature of the core during EDM has been implemented, increasing the efficiency of the DHD technique and a reduction in human error.

- The calculated 2D residual stresses (i.e. the stresses acting in a plane normal to the reference hole axis) were found to be accurate to within ±30MPa. The error in estimation of the axial residual stresses was improved, however it still remains large when compared to the measured biaxial residual stresses.

- FE analyses and parameter updating have been carried out to refine the theoretical analysis used for the calculation of residual stresses. The theoretical analysis had been previously modified by the inclusion of parameters *A(z)* and *B(z)*. During this research, parameters *A(z)* and *B(z)* were found to vary with the applied biaxial loading, and vary with the dimensions of component height and width. Equations for *A(z)* and *B(z)* were found for implementation into the analysis. Exclusion of parameter *A(z)* results in a maximum error of 0.3% (i.e. the effects of *A(z)* are negligible). Exclusion of parameter *B(z)* results in a maximum error of 4.8% for a component under uni-axial loading and 0% for equi-biaxial loading.

- The frequencies of variation of the normalised radial distortions of the reference hole were investigated using a power spectral density analysis. A frequency of two was found to be dominant as predicted by the theoretical analysis. All other frequencies present were found to be equal in magnitude to that of random noise incurred by the inaccuracy of the air probe. Therefore the theoretical analysis is fully defined (i.e. frequency = 2) with respect to the current accuracy of the experimental measurement system.

- The subsequent "state of the art" of the DHD technique has been presented. The equipment used, the process followed, the analysis applied and the sources of experimental error were described.

- Calibration experiments were carried out on aluminium plates with applied uniaxial tensile stresses, aluminium shrink-fit specimens containing step changes in residual stress and a graphite cube with applied uniaxial compressive stresses. The aluminium plates validated the use of a 1.5mm diameter reference hole. The aluminium shrink-fit specimens showed the ability of the DHD technique to measure step changes in residual stress. The graphite cube showed the ability of the DHD technique to measure stresses in a porous material with low resistance to wear.

- A depth resolution of about 0.8mm was found for the DHD measurements carried out using the 3.18mm diameter air probe. The depth resolution for the 1.5mm diameter air probe was inferred to be about 0.4mm.

- DHD residual stress measurements were carried out on real components with different geometries, different origins of residual stress generation and different material compositions. The ability of the DHD technique to measure the residual stresses in such varied components was proven.

- The first portable machine for carrying out the DHD technique was designed, built and tested. The tests, both in the laboratory and "on-site", proved the ability of the portable machine to accurately measure residual stresses.

- Advantages of the DHD technique:
    i. Penetration depth up to 433mm,
    ii. Applicable to a wide range of materials,
    iii. Applicable to a wide range of component geometries,
    iv. Measurement of stress gradients due to depth profiling,
    v. Measurements can be carried out "on-site" using a portable machine,
    vi. The semi-invasive technique enables repeated measurement to be made,
    vii. Fast process in relation to the quantity of measurements.

- Limitations of the DHD technique:
    i. Material is removed during the technique,

ii. Not yet applicable to thin components (i.e. less than 10mm),
iii. Only macro residual stresses measured,
iv. The sampling area is large,
v. Slow process in relation to time,
vi. Specialist equipment and knowledge required.

10.2 Future Work

- The manufacture of through-holes during DHD is not permitted in certain applications (e.g. an in-service pipe). Therefore the manufacture and use of blind holes for both the reference hole and extracted core need investigation. This would allow a wider spectrum of components to be examined.

- The technique is usually applied to mock-ups and so the presence of the final small hole is not critical. However investigations into the plugging of the hole with parent/weld material would allow the measurements to be carried out on usable components.

- Refinements in machining to permit the extraction of smaller diameter cores (minimum currently 5mm) to decrease the sampling volume, and increase the resolution and accuracy of the technique.

- The application of the DHD technique to thinner components (currently less than 10mm thick) and thicker components (currently greater than 433mm thick) would be an obvious development.

- The analysis used for the calculation of the residual stresses relies upon the assumption that the deformation of the core following residual stress release by trepanning is completely linear-elastic. Investigations into the effects of plasticity during core deformation are needed.

- Work is needed on the development of analyses for a complete 3D elasticity solution to reconstruct the residual stresses from the measured distortions.

Therefore further analysis is needed to improve the measurement and calculation of the mechanical axial deformation of the core.

- Tests are required to show the applicability of the technique to different materials (e.g. composites, ceramics, polymers and plastics).

- Further analysis is needed to calculate the full spectrum of updated parameters $A(z)$ and $B(z)$ and implementation thereof.

- The time taken to carry out the measurement technique is relatively long and so resources should be applied to improve efficiency. The minimum number of angles at which the diameter of the hole is measured should be the first area to be examined.

REFERENCES

Abaqus – 2001 – Finite Element Analysis Code, Hibbit Karlson And Sorrensen (Hks) Uk Ltd., Warrington, Cheshire.

Abuku S. – 1977 – Jpn J. Appl. Phys., **16**, Pp1161-1170.

Asm Handbook – 1989 – "*Vol. 16, Machining*", Asm International.

Bainbridge A. T. - 1969 - "*Residual Stresses Arising From Machining And Fabrication*", Agard Conf. Proc. No. 53, Symposium On Engineering Practice To Avoid Scc, Istanbul, Turkey, Pp 8-1 To 8-21.

Baldwin W.M. Jr. - 1949 - "*Residual Stress In Metals*", Proc. Astm, Technical Papers, Vol. 49, Pp 539-583.

Bates S.K., Leggatt R.H., George D., Youtssos A.G. And Bouchard P.J. – 2000 – "*Measurement And Modelling Of Residual Stresses In Thick Section Type 316 Stainless Steel Welds*", 6th International Conference On Residual Stresses, Oxford, Uk.

Beaney E.M. – 1978 – "*Measurement Of Sub-Surface Stress*", Cegb Report No. Rd/B/N4325, Unclassified.

Bonner N.W., Smith D.J. And Leggatt R.H. – 1994 - "*Measurement Of Residual Stresses In Thick Section Steel Welds*", Proceedings Of The 10th International Conference On Experimental Mechanics, A.A. Balkema, Pp 767-772.

Bonner N.W. – 1996a - "*Measurement Of Residual Stresses In Thick Section Steel Welds*", Phd Thesis, University Of Bristol.

Bonner N.W. And Smith D.J. – 1996b - "*Measurement Of Residual Stresses Using The Deep-Hole Method*", Pvp, Vol. 327, Pp 53-65.

Boothroyd G. And Knight W.A. – C1989 – "*Fundamentals Of Machining And Machine Tools*", Dekker, 2nd Edition.

Borland D.W. – 1994 – "*Residual Stress Measurement – Methods, Limitations And Significance*", Proc. 2nd Australian Int. Conf. On Surface Engineering, Pp114-121.

Bouchard P.J., Holt P. And Smith D.J. – 1997 - "*Prediction And Measurement Of Residual Stresses In A Thick Section Stainless Steel Weld*", Proc. Asme-Pvp Conf., Vol. 347, Pp 77-82.

Bouchard P.J., Leggatt R.H., George D., Bates S.K. And Youtssos A.G., "*Thermal Relaxation Of Residual Stresses In Thick Section Type 316 Stainless Steel Girth Welds*", 6th International Conference On Residual Stresses, Oxford, UK.

Bouchard P.J. – 2002 – "*TRAINSS Project Final Report: Residual Stresses Near Repairs In A 19.6mm Thick, 412mm Diameter Stainless Steel Pipe Girth Weld*", British Energy report E/REP/ATEC/0034/GEN/01.

Bray D.E., Pathak N. And Srinivasan M.N. – 1997 – Materials Science Forum, **210**, Pp317-324.

Bsebsu F.M. And Bede G. – 2002 – "*Theoretical Study In Single-Phase Forced-Convection Heat Transfer Characteristics For Narrow Annuli Fuel Coolant Channels*", Periodica Polytechnica Ser. Mech. Eng., Vol 46, No. 1, Pp 15-27.

Buchanan W. – 1998 – "*Mastering Pascal And Delphi Programming*", Macmillan.

Buttle D.J. And Scruby C.B. – 2001 – Encyclopedia Of Materials Science And Technology, Pergamon.

Buttle D.J., Dalzell W., Hutchings M.T. And Allen A.J. – 2000 – "*Residual Stress In Butt Weldments Of 50d Steel Measured Using Neutron Diffraction And Magnetic Techniques*", Icrs-6 Conf. Proc., Pp923-931.

Callister W.D. – 1994 – "*Materials Science And Engineering – An Introduction*", John Wiley & Sons Inc., 3rd Edition.

Clyne T.W. And Gill S.C. – 1996 – J. Therm. Spray Technol., **5**, (4), 1-18.

De Angelis V. And Sampietri C. – 1990 - "*Report On The State Of The Art Regarding The Problem Of Residual Stresses In Welds Of Lmfbr Components*", Cise Technologie Innovative, Report No. 5495.

Edwards L., Santisteban J.R., Stelmukh V., Bouchard P.J. and Daymond M.R. – 2001 – "Measurement of the residual stresses near a short 20 degree repair in a 19mm thick stainless steel pipe girth weld", Journal of Neutron Research, 9:173-181.

Ericsson T. And Hildenwall B. – 1981 – "*Thermal And Transformational Stresses*", 28th Sagamore Army Materials Research Conf., Pp19-38.

Garcia-Granada A.A., George D. And Smith D.J. – 1998 - "*Assessment Of Distortions In The Deep-Hole Technique For Measuring Residual Stresses*", Proceedings Of The 11th International Conference On Experimental Mechanics, Pp1301-1306, Oxford.

George D. – 2000a – "*Determination Of Residual Stresses In Large Section Stainless Steel Welds*", PhD Thesis, University Of Bristol.

George D., Bouchard P.J. And Smith D.J. – 2000b – "*Evaluation Of Through Wall Residual Stresses In Stainless Steel Weld Repairs*", Materials Science Forum, Vol. 347-349, Pp 646-651.

George D. And Smith D.J. – 2000c – "*The Application Of The Deep-Hole Technique For Measuring Residual Stresses In Autofrettahed Tubes*", Pvp High Pressure Technology, Vol. 406, Pp 25-31.

George D. And Smith D.J. – 2000d – "*Residual Stress Measurement In Thick Section Components*", Pvp Assessment Methodologies For Preventing Failure: Deterministic And Probabilistic Aspects And Weld Residual Stress, Vol. 410-1, Pp 275-282.

Gere J.M. And Timoshenko S.P. – 1995 – "*Mechanics Of Materials*", Chapman & Hall, 3rd Edition.

Gerhardt J. And Tekkaya A.E. – 1987 – "*Advanced Technology Of Plasticity*", Vol. Ii, Springer-Verlag, Pp841.

Glyn J., Burley D., Clements D., Dyke P., Searl J. And Wright J. – 1996 – "*Modern Engineering Mathematics*", Addison-Wesley, 2nd Edition.

Glyn J., Burley D., Clements D., Dyke P., Searl J. And Wright J. – C1999 – "*Advanced Modern Engineering Mathematics*", Addison-Wesley.

Golub G.H. And Van Loan C.F. – 1983 – "*Matrix Computations*", North Oxford Academic.

Gong B. And Wang Z. – "*Investigation Of Cold-Drawing Process – Mechanical Property Relationship Of High C Steel Wires*", Unpublished Technical Report, University Of Toronto.

Grant P.V., Lord P.D. And Whitehead P.S. – 2002 – "*The Measurement Of Residual Stresses By The Incremental Hole Drilling Technique*", Measurement Good Practice Guide No. 53, National Physics Laboratory, Uk.

Green R.E. – 1973 – "*Treatise On Materials Science And Technology*", Academic Press, Vol. 3, 73.

Greening P.D. – 1999 – "*Dynamic Finite Element Modelling And Updating Of Loaded Structures*", Phd Thesis, University Of Bristol.

Hall-Stephens J. – 2001 – "Kempe's Engineers Year-Book", United Business Media.

Hicks J.G. – 1979 – "*Welded Joint Design*", Granada.

Holmes C. – 2003 – "*The Mechanical Behaviour And Ultrasonic Measurement Of Graphite Joints*", PhD Thesis, University Of Bristol.

Horn G. – 1991 – "*Modern Section Straightening Technology*", Proc. Of Straightening Of Long Products.

Jesensky M. And Vargova J. - 1981 - "*Calculation And Measurement Of Stresses In Thick-Walled Welded Pressure Vessels*", Svaracske Spravy, Part 4, Pp 79-87.

Kandil F.A., Lord J.D., Fry A.T. And Grant P.V. – 2001 – "*A Review Of Residual Stress Measurement Methods – A Guide To Selection*", Npl Report Matc(A)04.

Keil S. - 1993 - "*Experimental Determination Of Residual Stresses With The Ring-Core Method And An On-Line Measuring System*", Experimental Techniques, The Soc. For Exp. Mech. Inc., Issn 0732-8818, Pp 17-24.

Keller H.P., Kerkoff H., Giffeler R. And Meinhardt J. - 1989 - *"Residual Stresses And Their Influence On The Integrity Of Pressure Vessel*", T&V Rheinland Institute For Material Testing, Report No. Sb 203/89.

Kingston E.J., Stefanescu D., Mahmoudi A.H., Truman C.E. And Smith D.J. – 2004 – *"Novel Applications Of The Deep-Hole Drilling Technique For Measuring Through-Thickness Residual Stress Distributions"*. Journal Of Testing And Evaluation. ASTM International. Paper submitted.

Kuroda S., Kukushima T. And Kitahara S. – 1987 – J. Vac. Sci. Technol., **A5**, Pp72-87.

Lacarac V. – 2000 – "*Residual Stresses And Fatigue Crack Growth From Cold Expanded Holes In Al 2650 At Room And High Temperature*", Phd Thesis, University Of Bristol.

Leggatt R.H., Smith D.J., Smith S.D. And Faure F. – 1996 - "*Development And Experimental Validation Of The Deep-Hole Method For Residual Stress Measurements*", J. Strain Analysis, Vol. 31, Pp 177-186.

Li K.Y. – 1997 – Opt. Lasers Eng., **27**, Pp125-136.

Lin Y.C. And Chou C.P. – 1995 – *"Error Induced By Local Yielding In Hole Drilling Method For Measuring Residual Stress Of Materials"*, Materials Science And Technology, Vol. 11, Pp 600-604.

Liu J. – 1997 - "*Handbook Of Measurement Of Residual Stresses*", Society For Experimental Mechanics Inc., Fairmont Press Inc.

Lord J.D., Fry A.T. and Grant P.V. – 2002 – *"A UK residual stress intercomparison exercise – an examination of the XRD and hole drilling techniques"*, NPL Report MATC(A)98.

Macherauch E. And Wohlfahrt H. - 1977 - "*Different Sources Of Residual Stress As A Result Of Welding*", Residual Stresses In Welded Construction And Their Effects, Vol. 1, ISBN 0-85300119-7, Paper 11, Pp 267-282.

Macherauch E. And Klaus K.H. – 1986 – "*Origin, Measurement And Evaluation Of Residual Stresses*", Residual Stresses In Science And Technology, Vol. 1, ISBN 3-88355-099-X, Pp3-26.

Mahmoudi A.H., Hadidi-Moud S., Truman C.E. and Smith, D.J. – 2003 – *"Measurement And Prediction Of Residual Stress Generated By Local Compression"*, 5th Euromech Solid Mechanics Conference: ESMC-5, Greece.

Makino A. And Nelson D. – 1997 – J. Eng. Mater. Technol., **119**, Pp95-103.

Mathar J. – 1934 – "*Determination Of Initial Stresses By Measuring Deformation Around Drilled Holes*", Trans. Asme, Vol. 56 (No. 4), Pp249-254.

Mayr P. – 1987 – "*Dimensional Alteration Of Parts Due To Heat Treatment*", Residual Stresses In Science And Technology, Vol. 1, Pp57-77.

Mcguid S.A., Shagal G. And Stranart J.C. – 1999 – "*Finite Element Modelling Of Shot Peening Residual Stresses*", J. Materials Processing Technology, Vol. 92-93, Pp401-404.

Megson T.H.G., 1996 – "*Structural And Stress Analysis*", Arnold.

Misra A. And Peterson H.A. - 1982 - "*Examination Of The Ring Method For Determination Of Residual Stress*", Experimental Mechanics, Proc. Soc. For Exp. Stress Analysis, Vol. 38, Pp268-72.

Mori K.I. And Osada K. – 1994 – "*Application Of Dynamic Viscoplastic Finite Element Method To Shot Peening Process*", Trans. Namri/Sme, Vol. Xxii, Pp29-34.

Morris S. – 1997 – "*Delphi Made Simple*", Made Simple Books.

Nelson D.V., Makino A. And Fuchs E.A. – 1997 – Opt. Lasers Eng., **27**, Pp3-23.

Noyan I.C. And Cohen J.B. - 1981 - "*The Nature Of Residual Stress And Its Measurement*", Residual Stress And Stress Relaxation, Isbn 0-306-41102-4, Pp 1-17.

Noyan I.C. And Cohen J.B. - 1987 - "*Residual Stress - Measurement By Diffraction And Interpretation*", Springer-Verlag, Isbn 0-387-96378-2.

Ott H.W. – 1976 – "*Noise Reduction Techniques In Electronic Systems*", Wiley.

Parlane A.J.A. - 1981 - "*Origin And Nature Of Residual Stresses In Welded Joints*", Twi Report, Residual Stresses And Their Effect, Isbn 0-85300141-3, Pp 1-4.

Perry A.J., Sue J.A. And Martin P.J. – 1996 – "*Practical Measurement Of The Residual Stresses In Coatings*", Surface And Coatings Technology, 81, Pp17-28.

Procter E. And Beaney E.M. – 1987 – "*Advances In Surface Treatments: Technology-Application-Effects*", International Guidebook On Residual Stresses, Pergamon, Vol. 14, Pp 165-198.

Qing M.A. And Clarke D.R. – 1993 – "*Measurement Of Residual Stresses In Sapphire Fibre Composites Using Optical Fluorescence*", Acta. Met. Mater., Vol. 41, Pp1817-1823.

Qing M.A., Liang L.C., Clarke D.R. And Hutchinson – 1994 – Acta Metall. Mater., **42**, Pp3299-3308.

Rebelo J.C., Morao Dias A., Kremer D. And Lebrun J.L. – 1998 – "*Influence Of Edm Pulse Energy On The Surface Integrity Of Martensitic Steels*", Journal Of Materials Processing Technology, 84, Pp 90-96.

Rees D.W.A. – C1990 – "*The Mechanics Of Solids And Structures*", Mcgraw-Hill.

Rogers G.F.C. And Mayhew Y.R. – 1992 – "*Engineering Thermodynamics : Work And Heat Transfer*", Longman Scientific & Technical, 4th Edition.

Rudd C.O. – 1992 – "*Residual Stresses And Their Measurement*", Proc. 1st Int. Conf. On Quenching & Control Of Distortion, Pp193-198.

Sachs, G. – 1927 - "*Der Nachweis Innerer Spannungen In Stangen And Rohren*", Zeitschrift Fur Metallkunde, 19, Pp. 352-357.

Schadler L.S. And Galiotis C. – 1995 – "*Fundamentals And Applications Of Micro-Raman Spectroscopy To Strain Measurements In Fibre-Reinforced Composites*", Int. Mater. Reviews, Vol. 40, 116-134.

Schajer G.S. – 1988a – "*Measurement Of Non-Uniform Residual Stresses Using The Hole Drilling Method. Part I – Stress Calculation Procedures*", J. Of Eng. Materials. Technology, **110**, Pp338-343.

Schajer G.S. – 1988b – "*Measurement Of Non-Uniform Residual Stresses Using The Hole Drilling Method. Part Ii – Practical Application Of The Integral Method*", J. Of Eng. Materials. Technology, **110**, Pp344-349.

Schajer G.S., Roy G., Flamen M.T. And Lu J. – 1996 – "*Handbook Of Measurement Of Residual Stresses*", Society For Experimental Mechanics, 5-34.

Schajer G. And Tootoonian M. – 1997 – Exp. Mech., **37**, Pp299-306.

Schiffner K. And Droste Gen Helling C. – 1999 – "*Simulation Of Residual Stresses By Shot Peening*", Computers And Structures, Vol. 72, Pp329-340.

Scholtes B. – 1987 – "*Residual Stresses Introduced By Machining*", Advances In Surface Treatments, Vol. 4, Pp59-71.

Scholtes B. – 1991 – "*Residual Stresses In Mechanically Surface Deformed Materials*", Dgm Informationsgesellschaft Verlag.

Smith D.J. And Bonner N.W. – 1994 - "*Measurement Of Residual Stresses In Thick Section Steel Welds*", Engineering Integrity Assessment, J.H. Edwards, J. Kerr And P. Stanley Edited, (Emas Chameleon Press), Pp 259-274.

Smith D.J. And Bonner N.W. - 1996 - "*Measurement Of Residual Stresses Using The Deep Hole Method*", Asme Pressure Vessels And Piping Conference, Florida, Usa.

Smith D.J., George D., Bouchard P.J. And Watson C. – 1999 – "*Prediction And Measurement Of Residual Stress In Thick-Section Stainless Steel Welds*", I.Mech.E Seminar, London, Uk.

Smith D.J., George D. And Bouchard P.J. – 2000 - "*Measurement And Prediction Af Through Thickness Residual Stresses In Thick Section Welds*", Journal Of Strain Analysis, Special Issue, Vol. 35, No. 4, Pp 287-305.

Smith D.J. And Hossain S. – 2002 – *"Measurement Of Residual Stresses In A Nozzle-To-Cylinder Weld After Thermal Ageing At 550°C"*, University Of Bristol Report, Contract Reference BWD40033000.

Stefanescu D., Truman C.E. And Smith D.J. – *"Measurement And Prediction Of Welding Residual Stresses In Components Made From High Resistance Steels"*, American Society Of Mechanical Engineers, Pressure Vessels And Piping Division (Publication), In Preparation.

Thomas, A., Ehrlich, R., Kingston, E., and Smith, D. J. – 2002a – *"Measurement Of Residual Stresses In Steel Nozzle Intersections Containing Repair Welds"*. American Society Of Mechanical Engineers, Pressure Vessels And Piping Division (Publication) PVP, Vol. 434, Pp 67-72

Thomas A. – 2002b – *"Residual Stress Measurements With Hole-Drilling Method On Repair Welded P91-Pipe"*, EU INTEGRITY Project, Internal Document Reference 10886/WG6/054, Issue 1.

Thompson R.B., Lu W.Y. And Clark A.V. – 1996 – "*Handbook Of Measurement Of Residual Stresses*", Society For Experimental Mechanics, Pp149-178.

Timoshenko S. And Goodier J.N. – 1951 - "*Theory Of Elasticity*", Mcgraw-Hill, 2nd Edition.

Totten G., Howes M. And Inoue T. – 2002 – "*Handbook Of Residual Stress And Deformation Of Steel*", Asm International.

Ueda Y., Fukuda K. And Endo S. – 1975 - "*A Study On The Accuracy Of Estimated Residual Stresses By The Existing Measurement Methods*", Trans. Jap. Weld. Res. Inst., Vol. 4, No. 2, Pp 13-27.

Wallis I.C. And Wisbey A. – 2001 – "*Welding Of Ti-10v-2fe-3al: A Comparison Of Techniques*", Proc. Titanium Alloys At Elevated Temperature Conf., Iom Communications Ltd, Pp133-150.

Webster G.A. And Webster P.J. - 1985 - "*Measurement Of Residual Stress Using High Resolution Neutron Diffraction*", Twi Seminar, Newcastle : Residual Stresses In Welded Construction.

Wimpory R.C., May P.S., O'Dowd N.P., Webster G.A., Smith D.J. and Kingston E. – 2003 – *"Measurement Of Residual Stresses In T-Plate Weldments"*. Journal Of Strain Analysis, Vol. 38, No. 4, Pp 349-365

Withers P.J. And Bhadeshia H.K.D.H. – 2001a – *"Residual Stress: Part 1 - Measurement Techniques"*, Materials Science And Technology, Vol. 17, Pp355-365.

Withers P.J. And Bhadeshia H.K.D.H. – 2001b – *"Residual Stress: Part 2 – Nature And Origins"*, Materials Science And Technology, Vol. 17, Pp366-375.

Withers P.J. And Webster P.J. – 2001c – Strain, **37**, Pp19-33.

Wolf H. And Sauer D.C. – 1974 – "*New Experimental Technique To Determine Residual Stresses In Large Turbine-Generator Components*", American Power Conf.

Wong Y.S., Lim L.C. And Lee L.C. – 1995 – "*Effects Of Flushing On Electro-Discharge Machined Surfaces*", Journal Of Materials Processing Technology, 48, Pp 229-305

Zhdanov I.M. And Gonchar A.K. – 1978 - "*Determining The Residual Welding Stresses At A Depth In Metals*", Automatic Welding, Vol. 31, No. 9, Pp 22-24.

WWW references:

[W1] http://webware.princeton.edu/weicourses/che199/Lec5.pdf

[W2] http://math.nist.gov/~JDevaney/CommKnow/mar2001/washio.mar2001.ppt

FIGURES

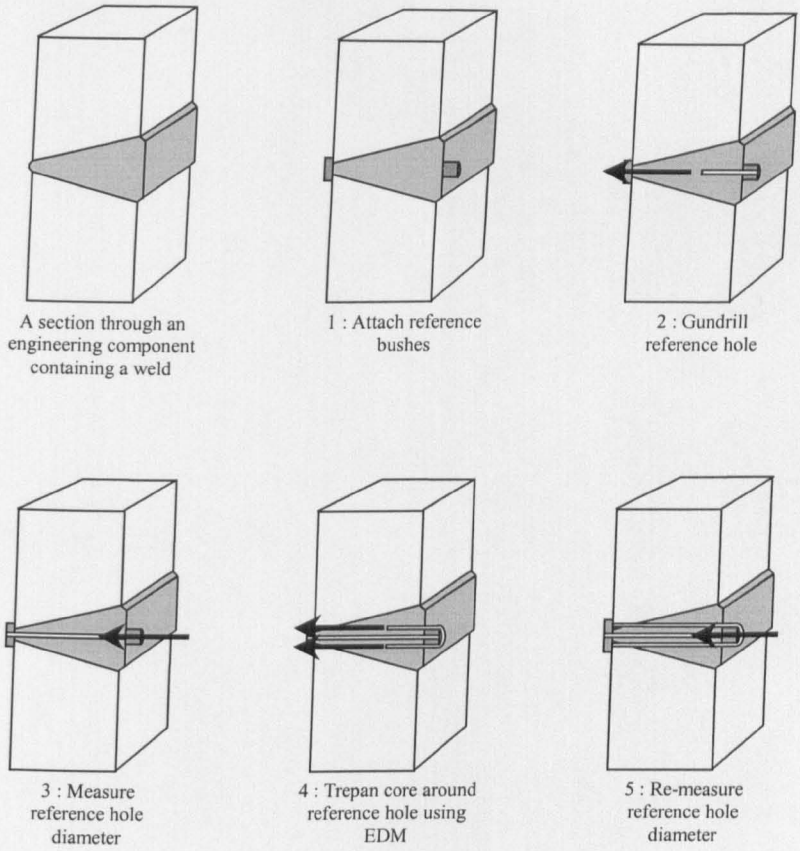

Figure 1.1. The 5 stages of the DHD residual stress measurement technique

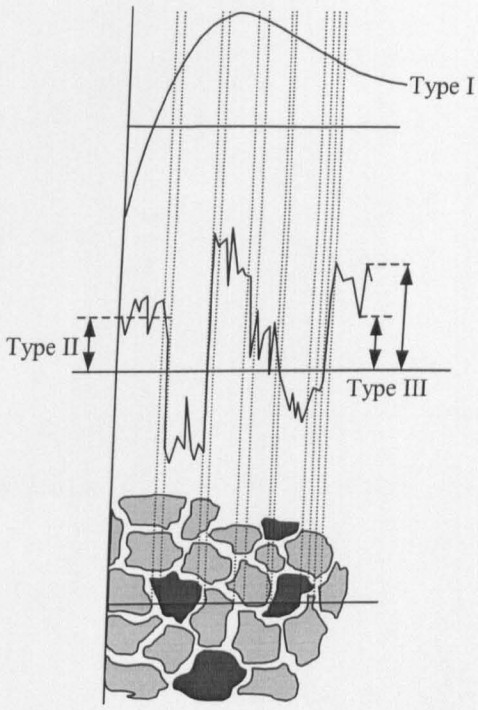

Figure 2.1. Categorisation of residual stresses according to length scales

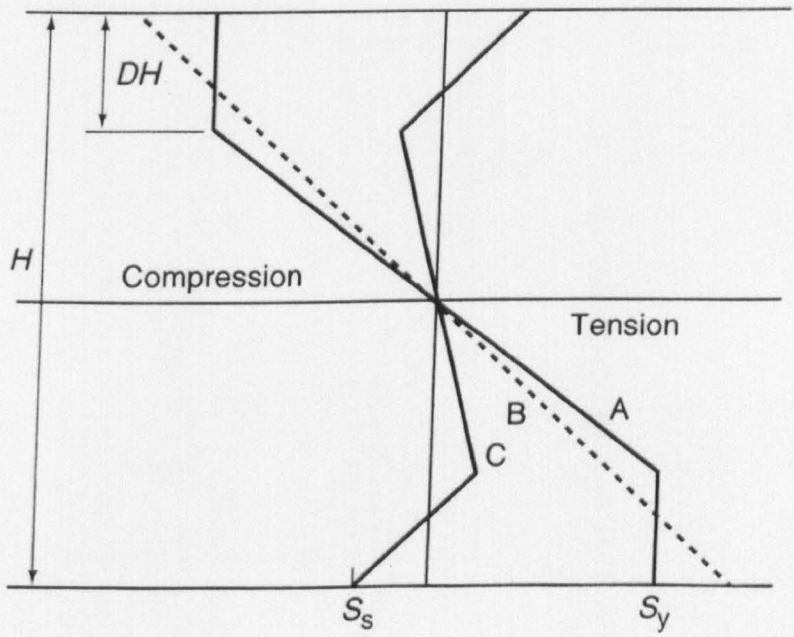

Figure 2.2. Stress distribution in a rectangular bar during plastic yielding to a depth DH (curve A); the elastic recovery (curve B); and the resulting residual stress (curve C) (Source: Totten et al [2002])

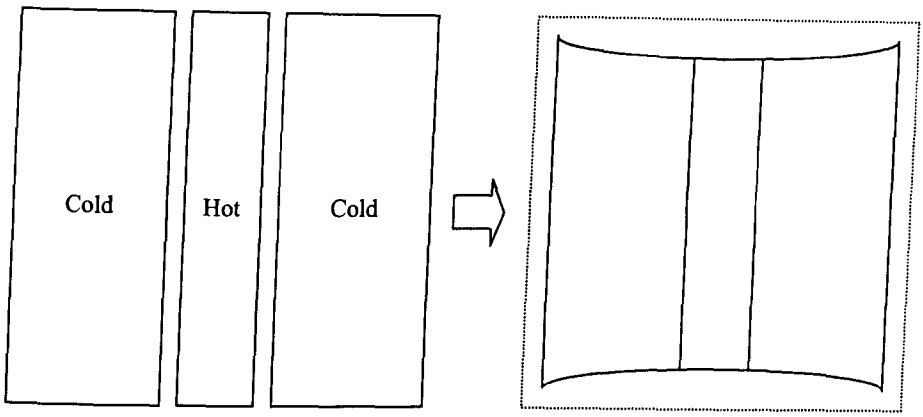

Figure 2.3. Schematic distortion of a butt-welded plate due to shrinkage of hot weld metal

(Source: Parlane [1981])

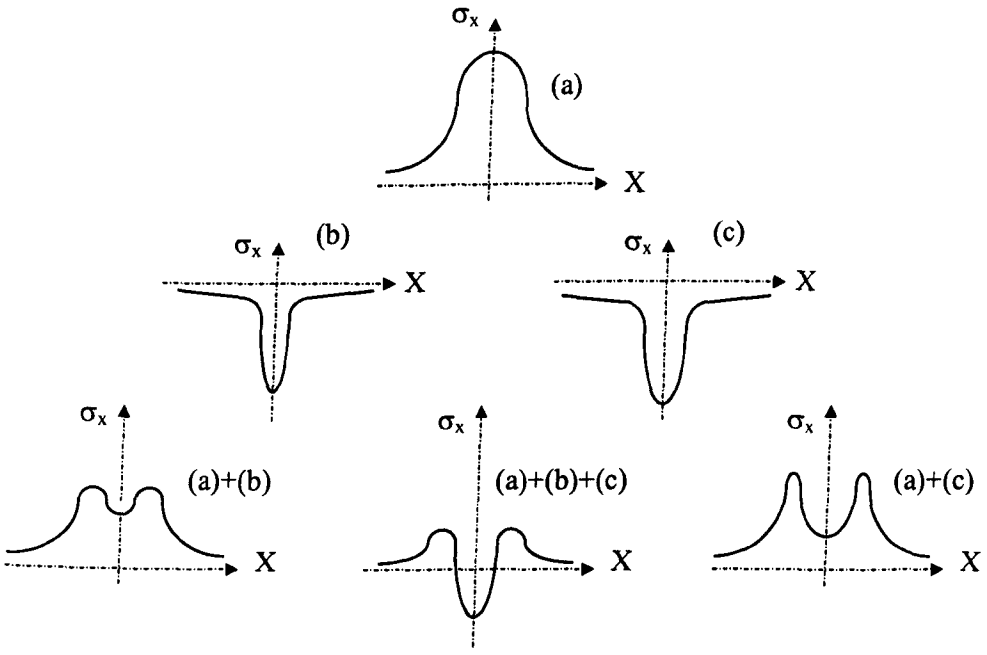

Figure 2.4. Schematic superimposition of transverse residual stresses due to (a) shrinkage, (b) quenching and (c) phase transformation

(Source: Macherauch et al [1977])

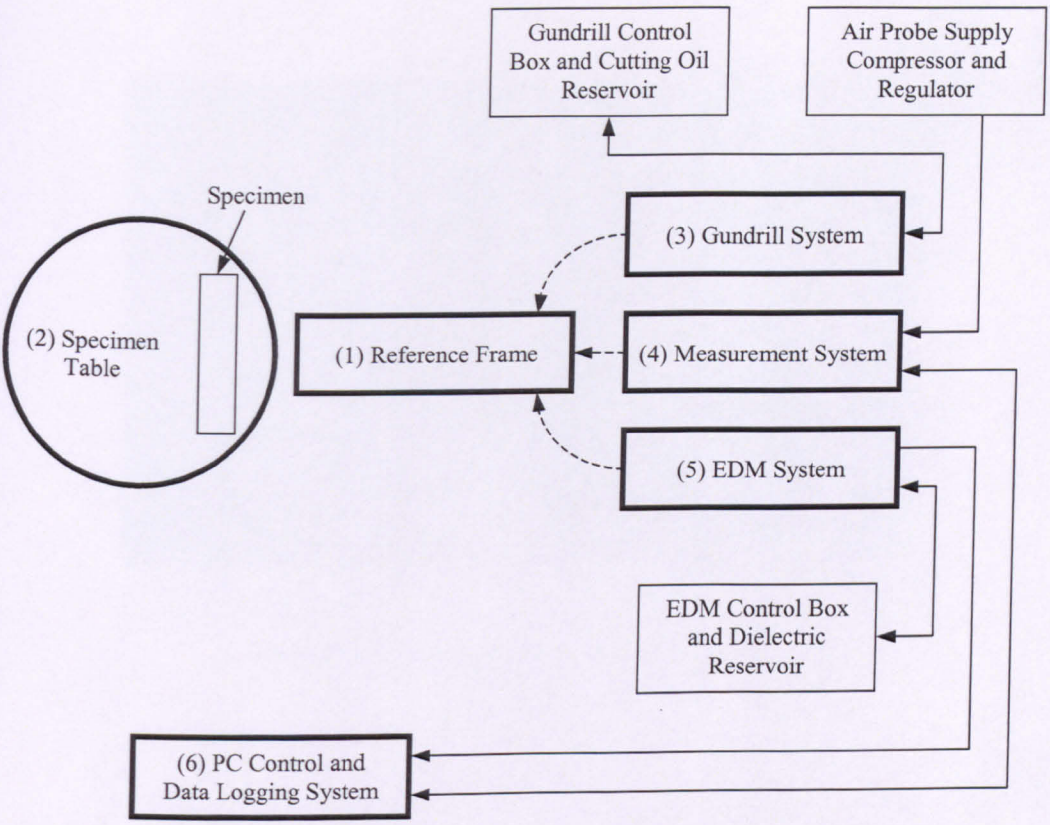

Figure 3.1. Schematic of the DHD equipment

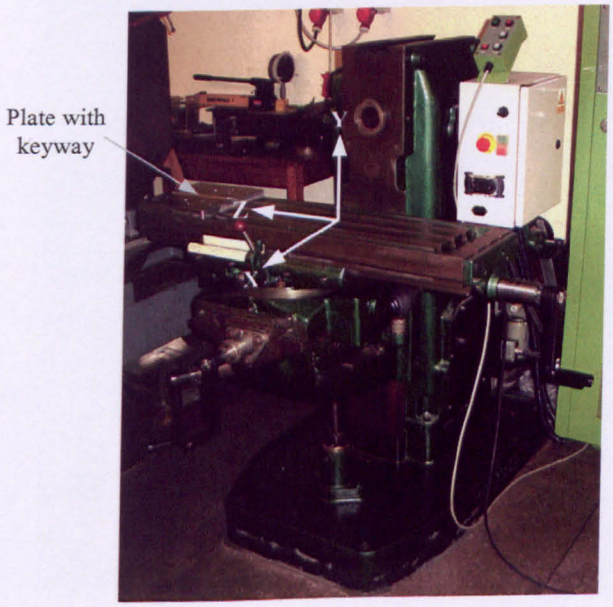

Figure 3.2. Photograph of the reference frame

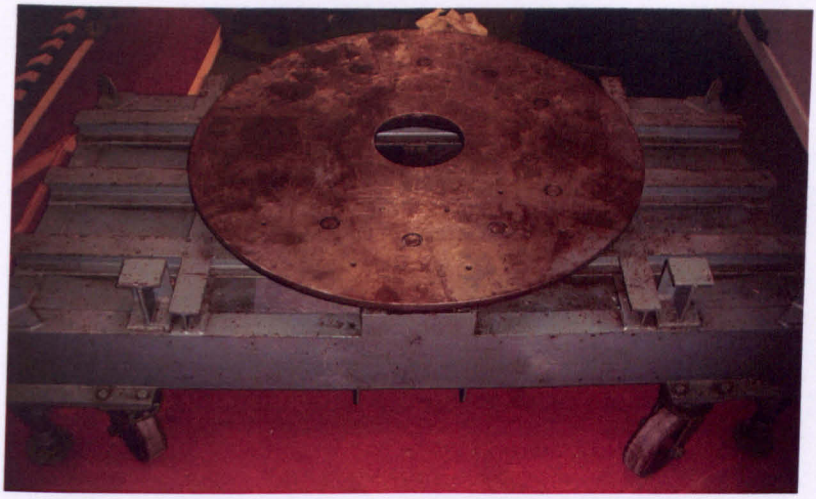

Figure 3.3. Photograph of the specimen table

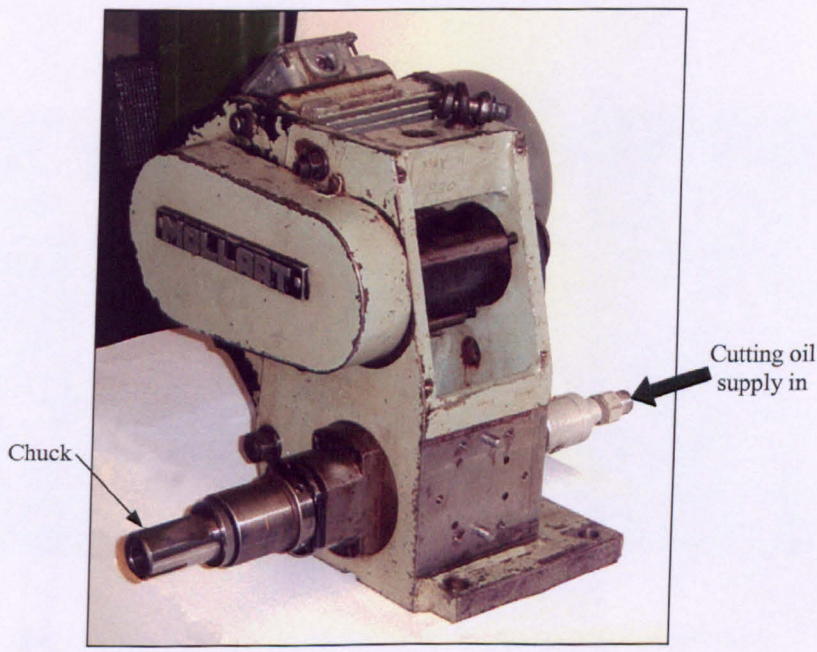

Figure 3.4. Photograph of the gundrill head

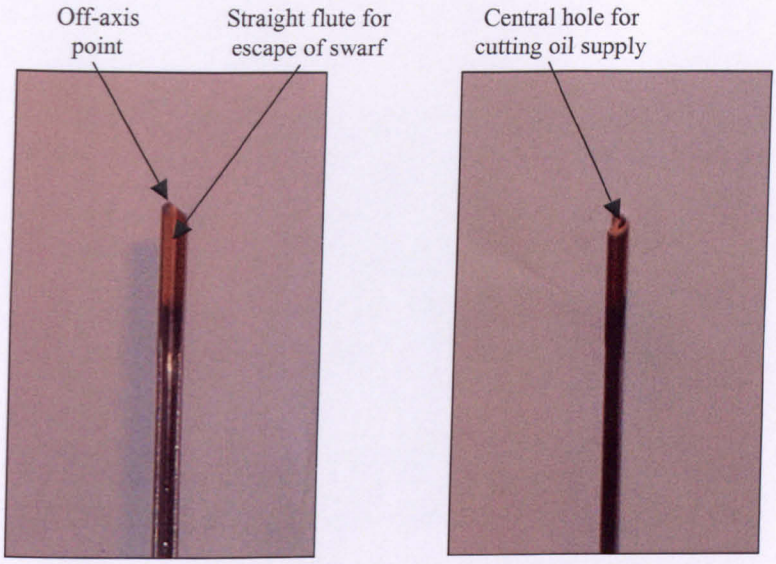

Figure 3.5. Photograph of a gundrill tip

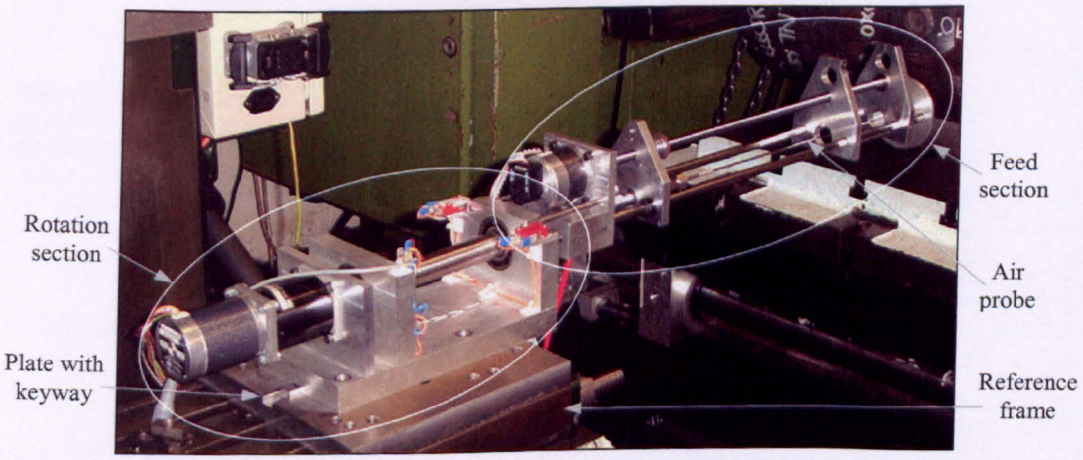

Figure 3.6. Photograph of the air probe measurement system

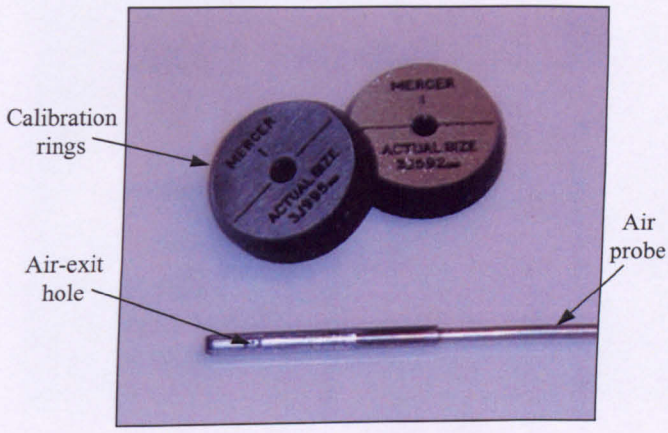

Figure 3.7. Photograph of the tip of an air probe and calibration rings

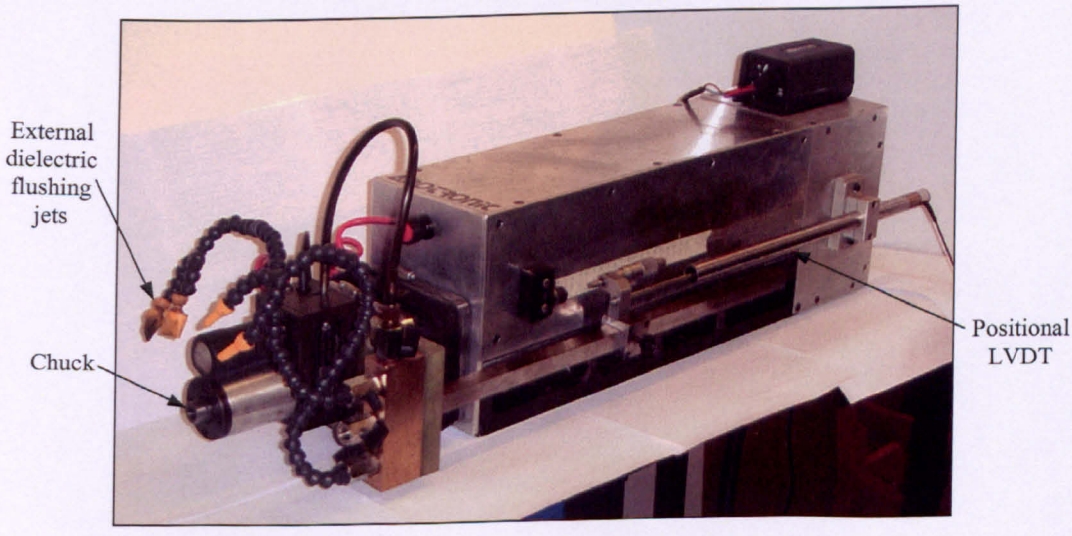

Figure 3.8. Photograph of the EDM head

Figure 3.9. Photograph of the PC control and datalogging system

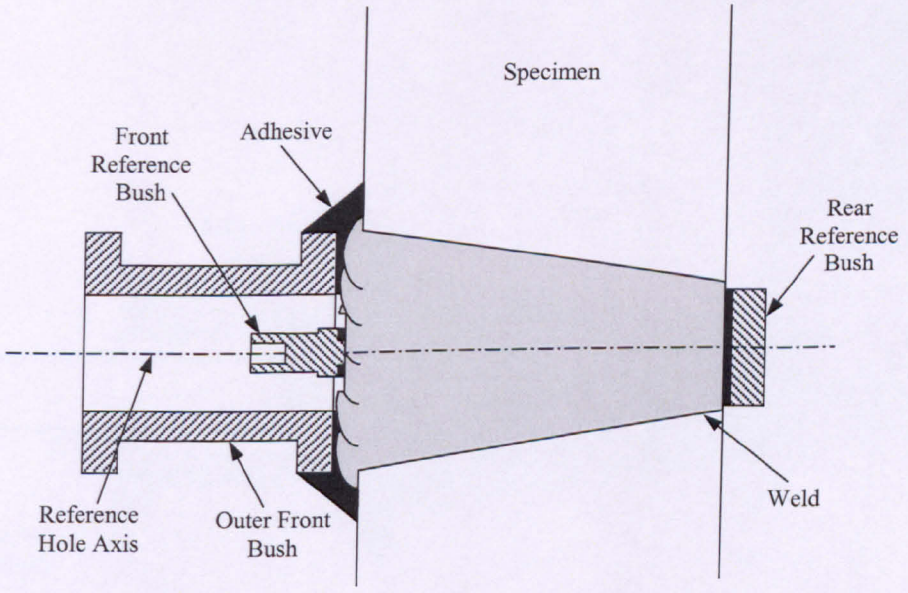

Figure 3.10. Cross-sectional schematic view of the reference bush arrangement

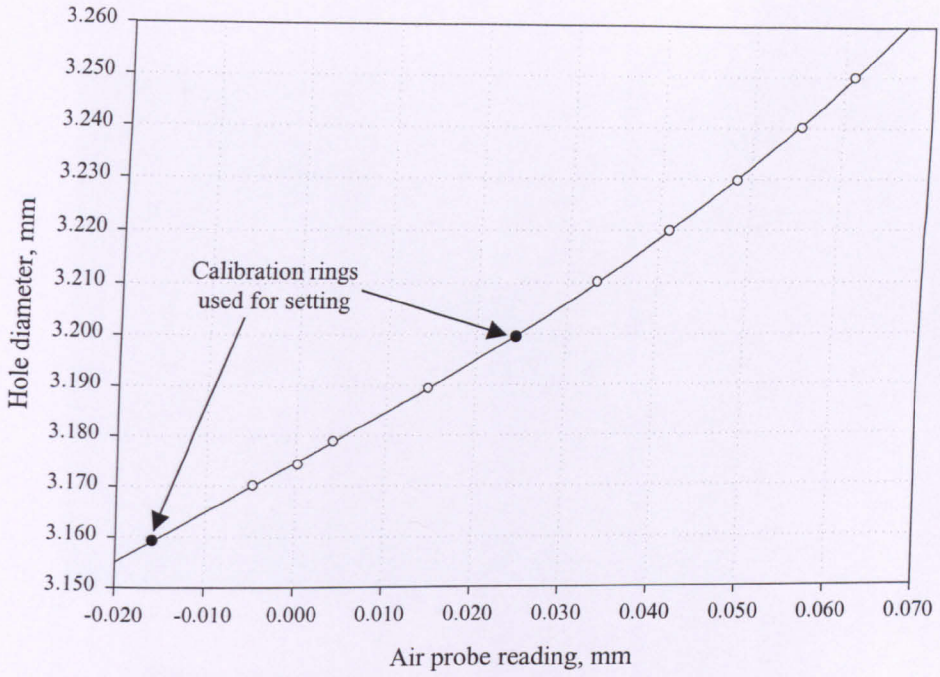

Figure 3.11. Example of an air probe calibration curve

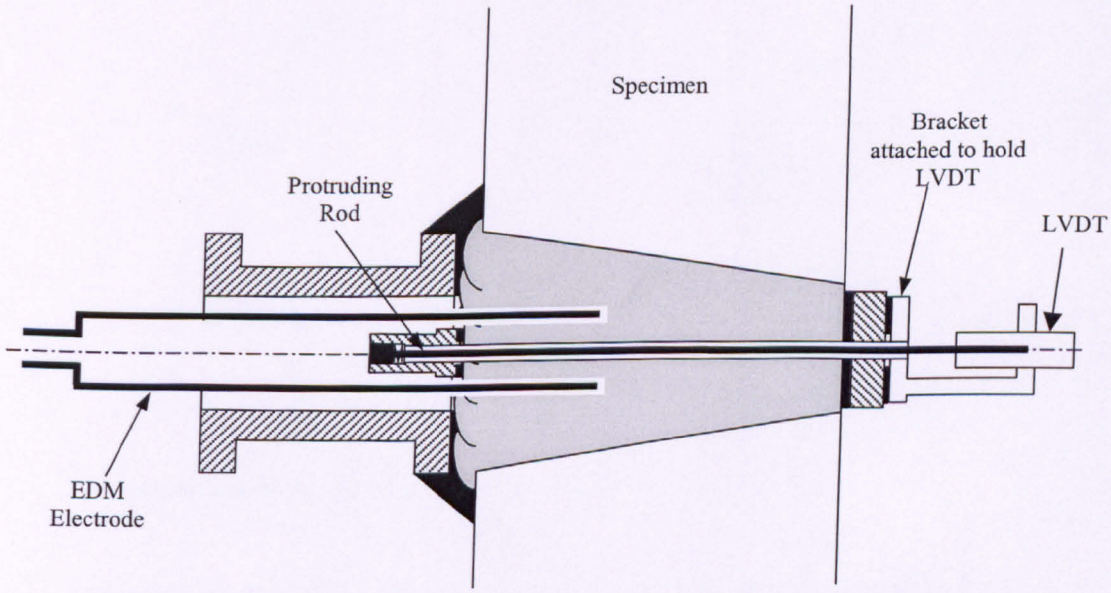

Figure 3.12. Cross-sectional schematic view of the LVDT set-up during EDM

Figure 3.13. Photograph of an extracted "10mm" core

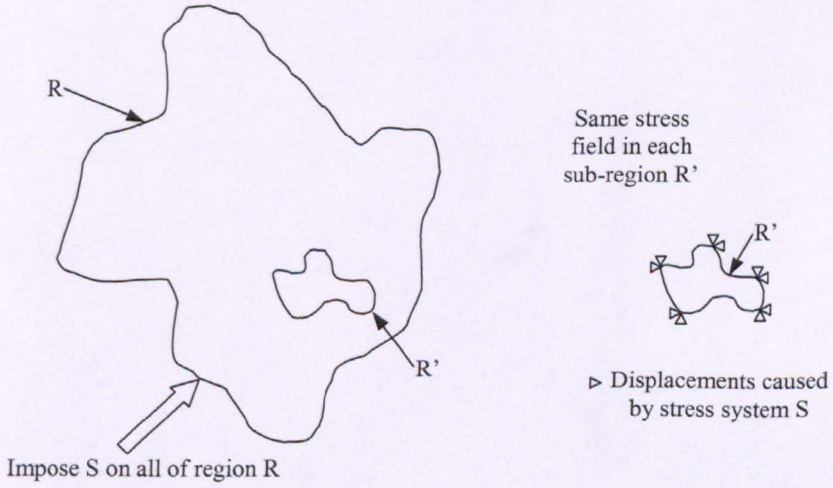

Figure 3.14. Sketch showing the equivalence of stress states and prescribed displacements

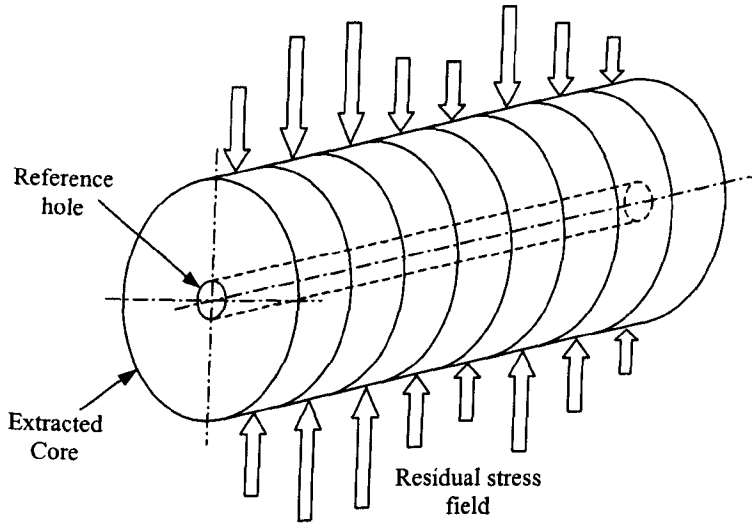

Figure 3.15. Extracted core comprising of many blocklengths

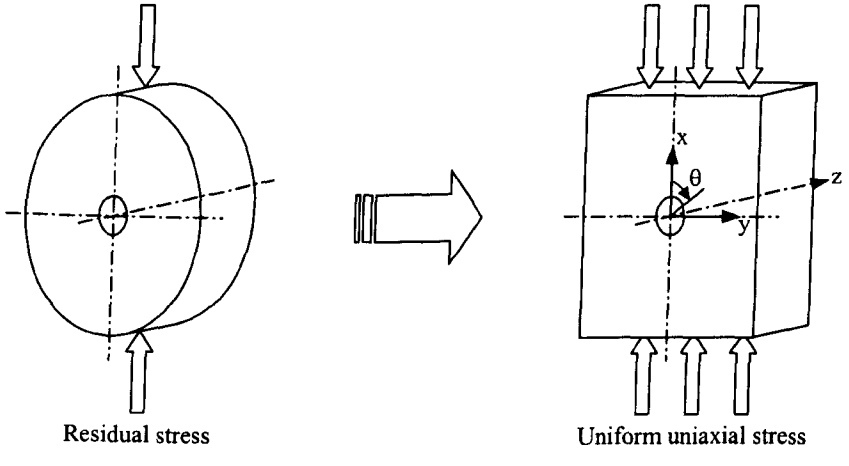

Figure 3.16. Single blocklength simplified to a plate with a hole

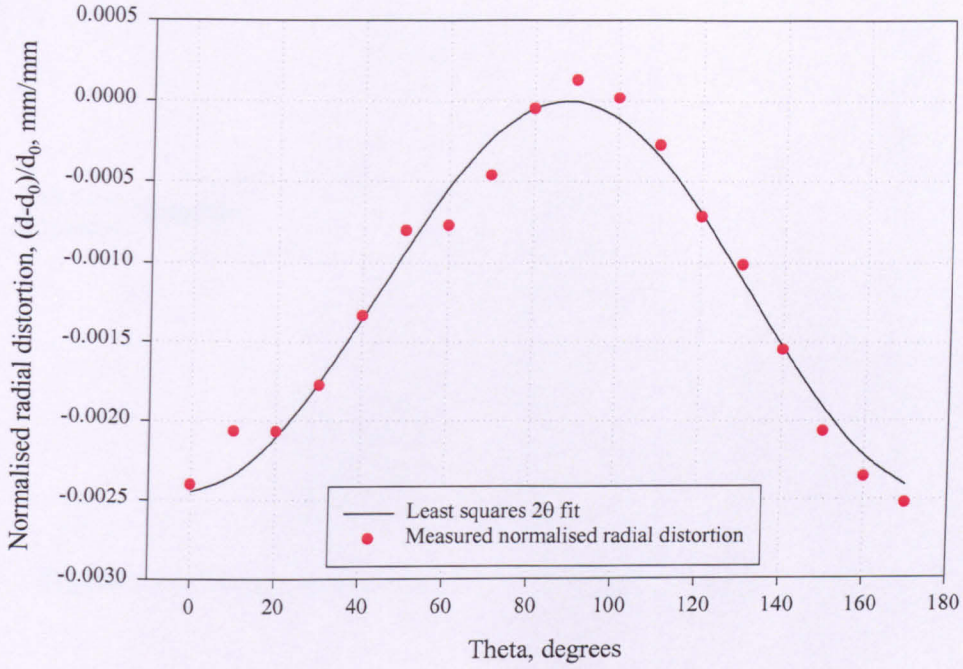

Figure 3.17. Least squares fit to the measured normalised radial distortion

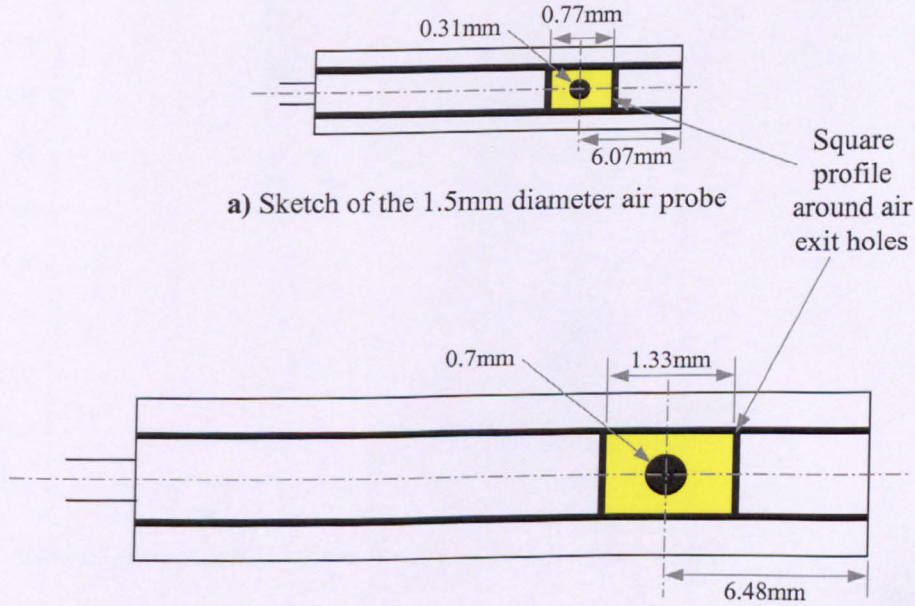

a) Sketch of the 1.5mm diameter air probe

b) Sketch of the 3.16mm diameter air probe

Not to scale

Figure 3.18. Dimensions of the air probe tips

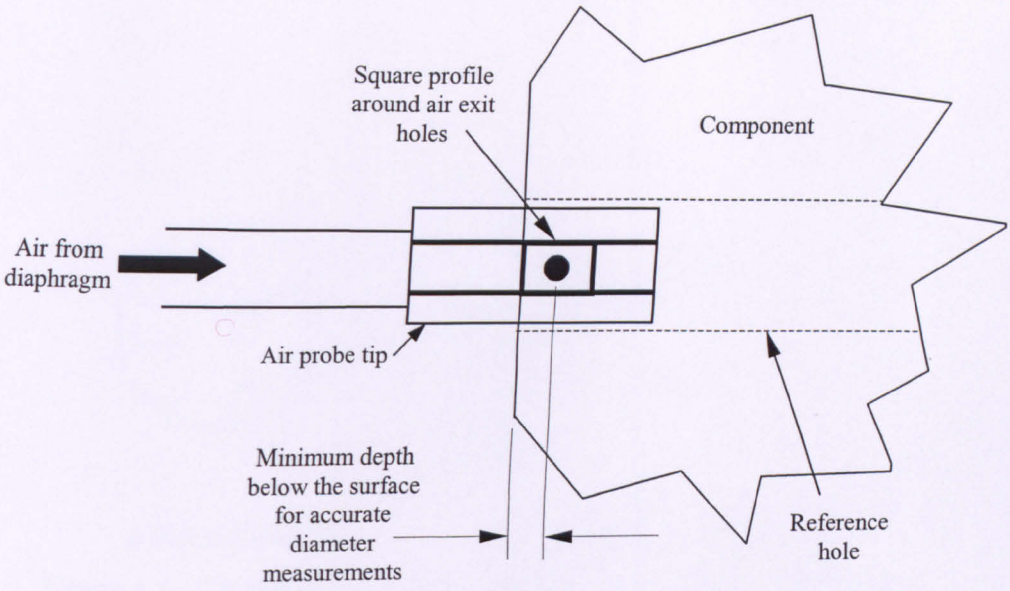

Figure 3.19. Minimum depth for accurate air probe diameter measurements

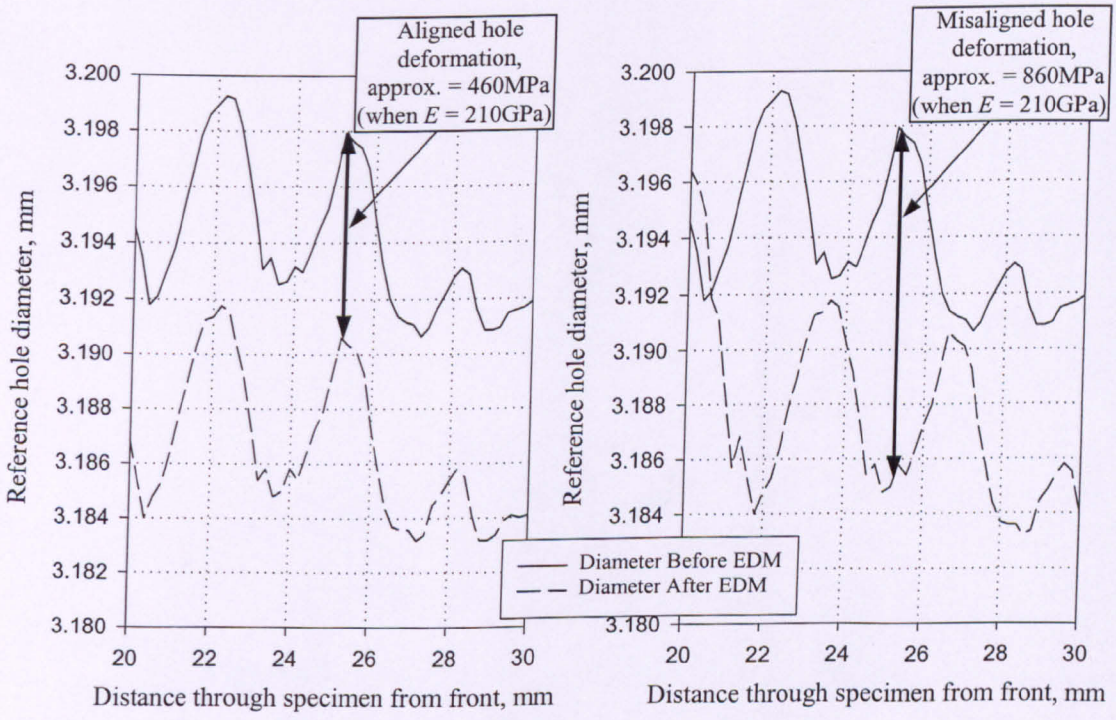

a) Aligned measurements

b) Misaligned measurements

Figure 3.20. Error due to depth misalignment between before and after EDM

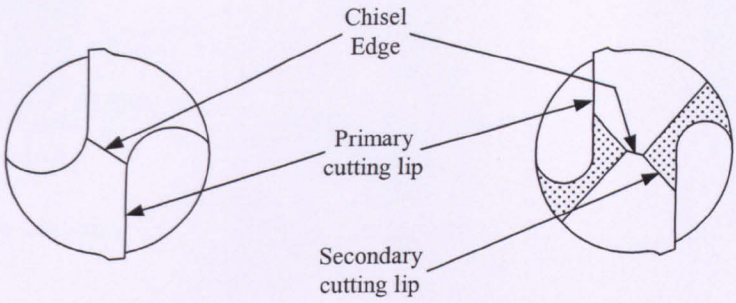

a) Normal drill bit b) Split-point drill bit

Figure 4.1. Comparison of the tips of a normal and a split-point drill bit

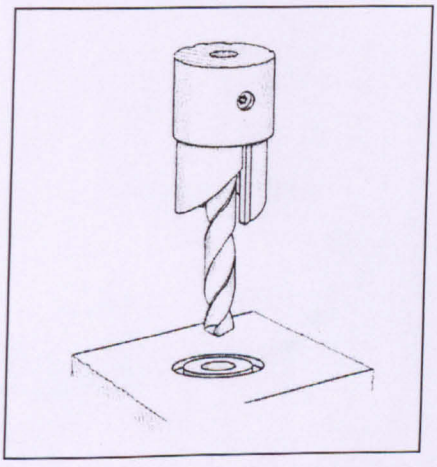

Figure 4.2. Conventional combination tool for trepanning

(Source: American Society for Metals [1989])

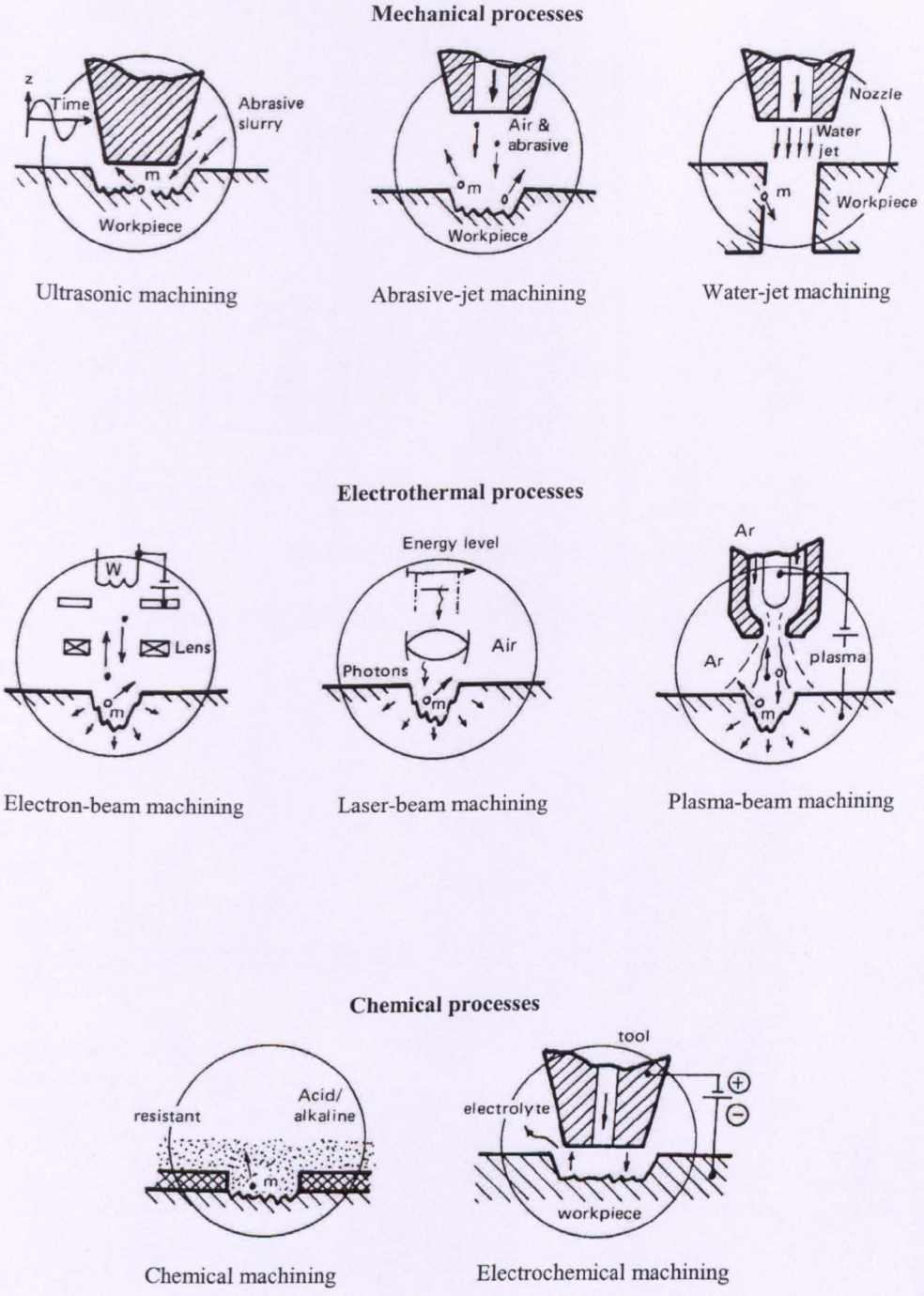

Figure 4.3. Schematics of various non-conventional machining processes (Source: Boothroyd et al [1989])

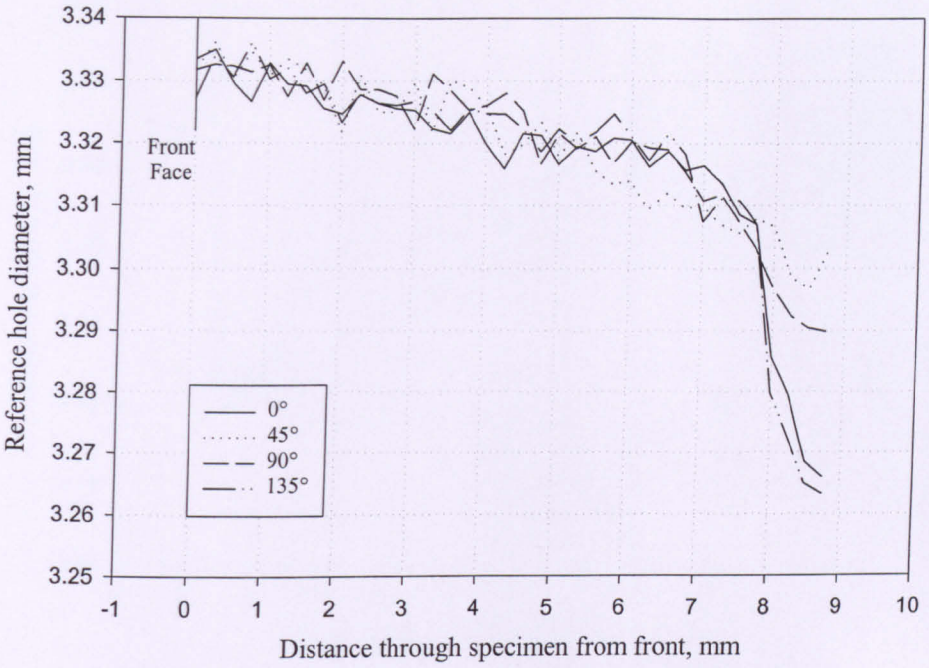

Figure 4.4. Diameter measurements of reference hole 4

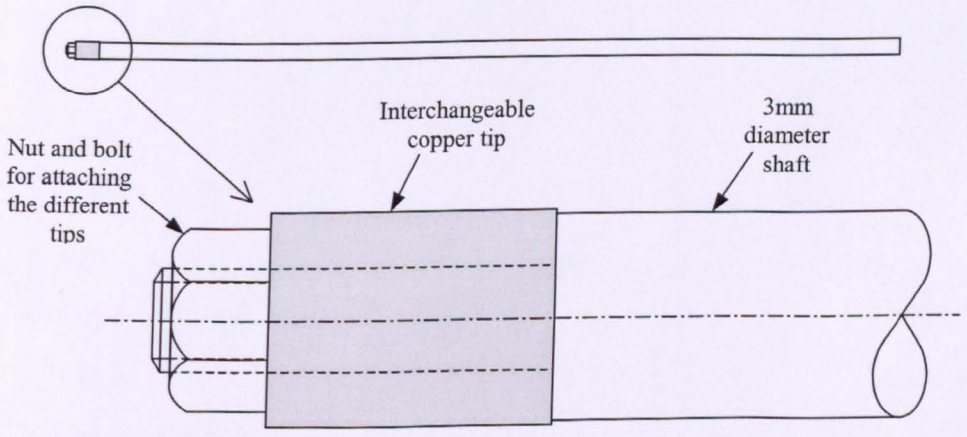

Figure 4.5. Sketch of the finishing electrode

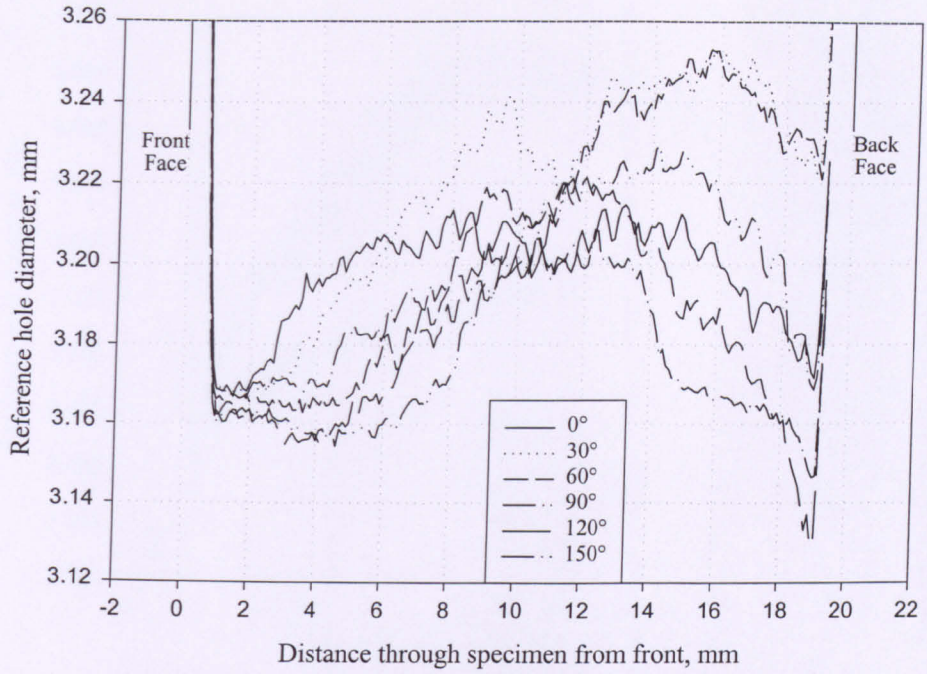

Figure 4.6. Diameter measurements of reference hole 6

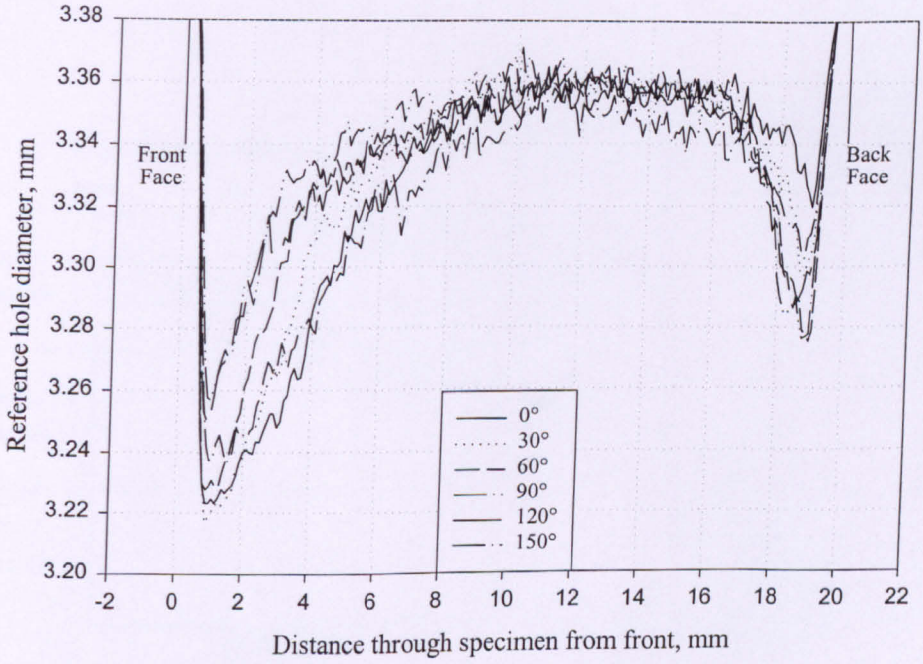

Figure 4.7. Diameter measurements of reference hole 7

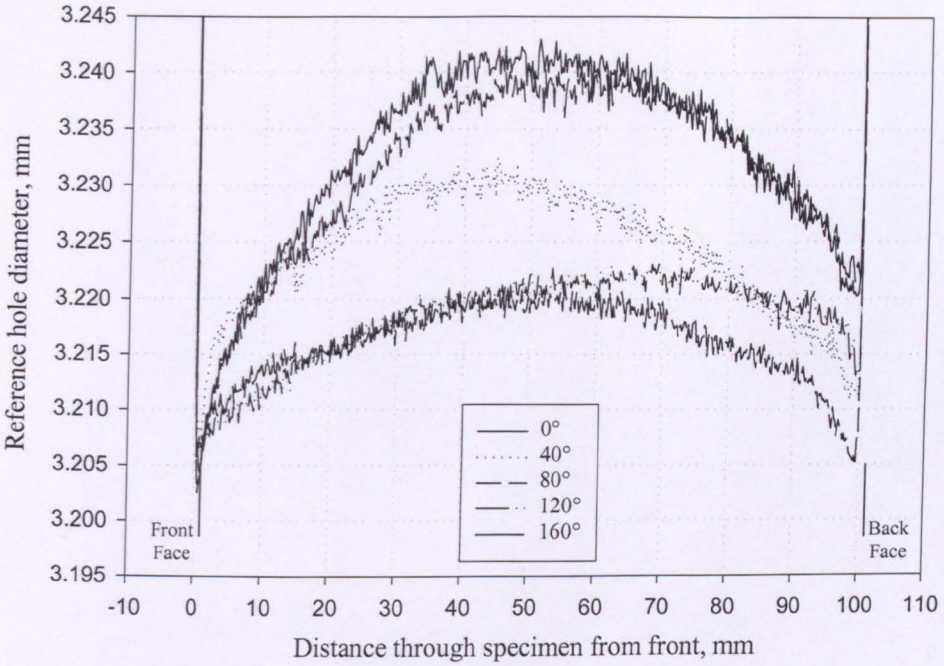

Figure 4.8. Diameter measurements of reference hole 8

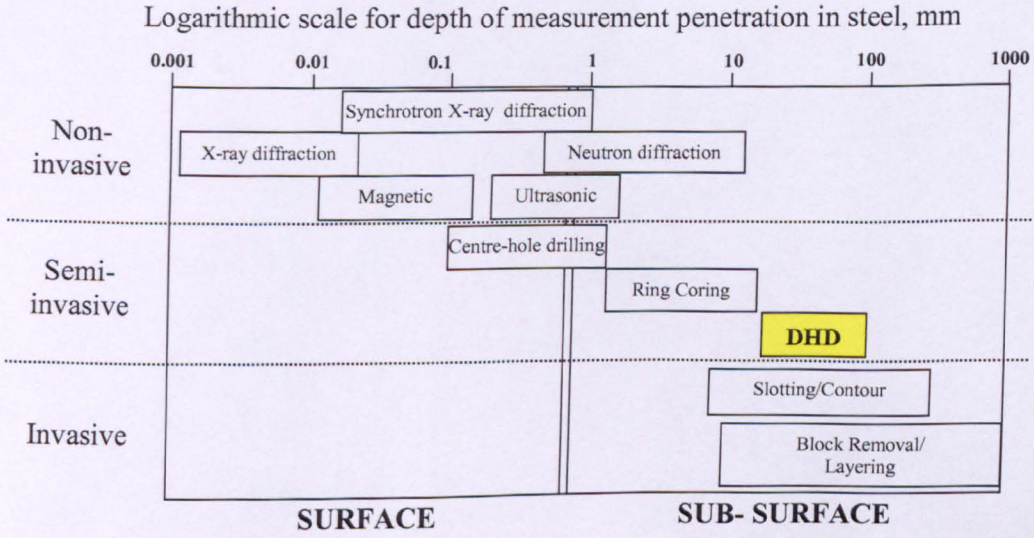

Figure 4.9. Penetration depths of standard residual stress measurement techniques

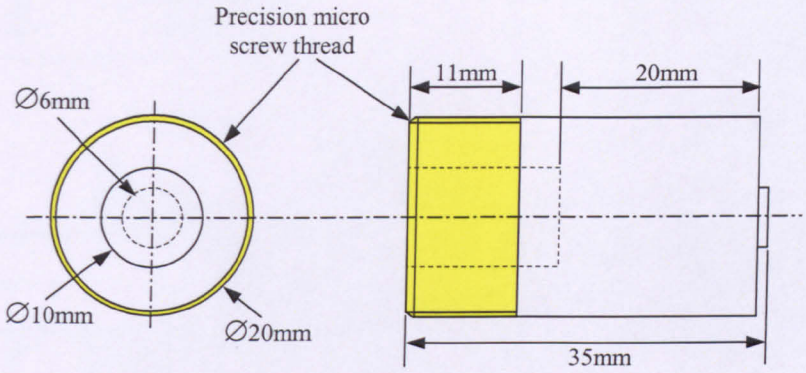

Figure 4.10. "20mm" front reference bush design

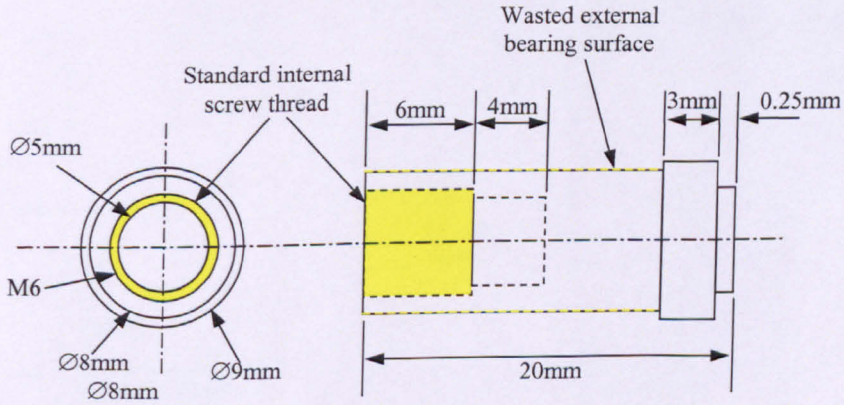

Figure 4.11. "10mm" front reference bush design

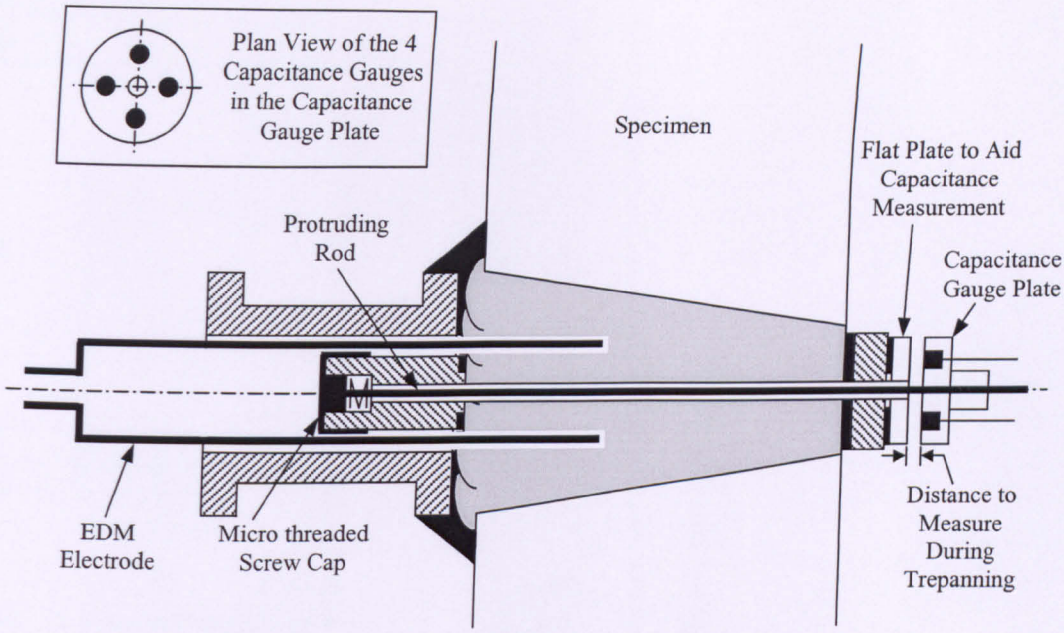

Figure 4.12. Cross-sectional schematic of the capacitance gauge set-up during EDM

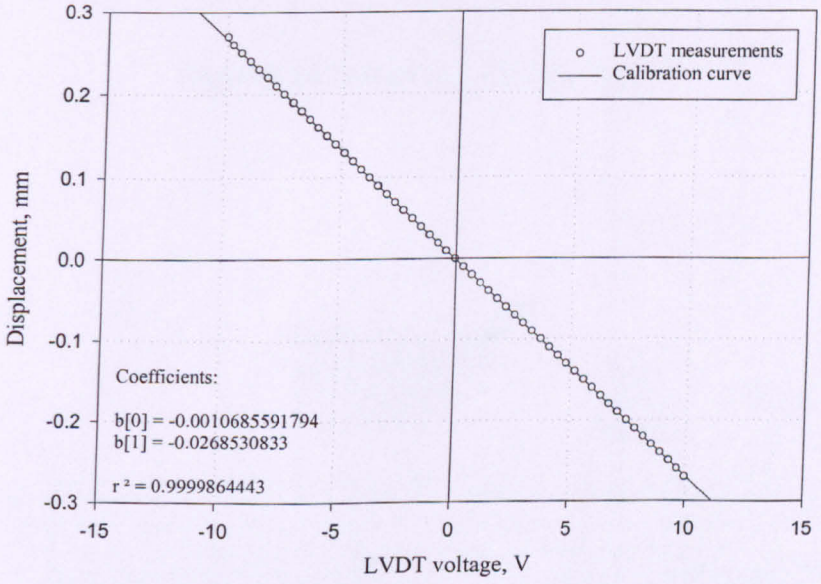

Figure 4.13. Calibration curve of the axial deformation LVDT

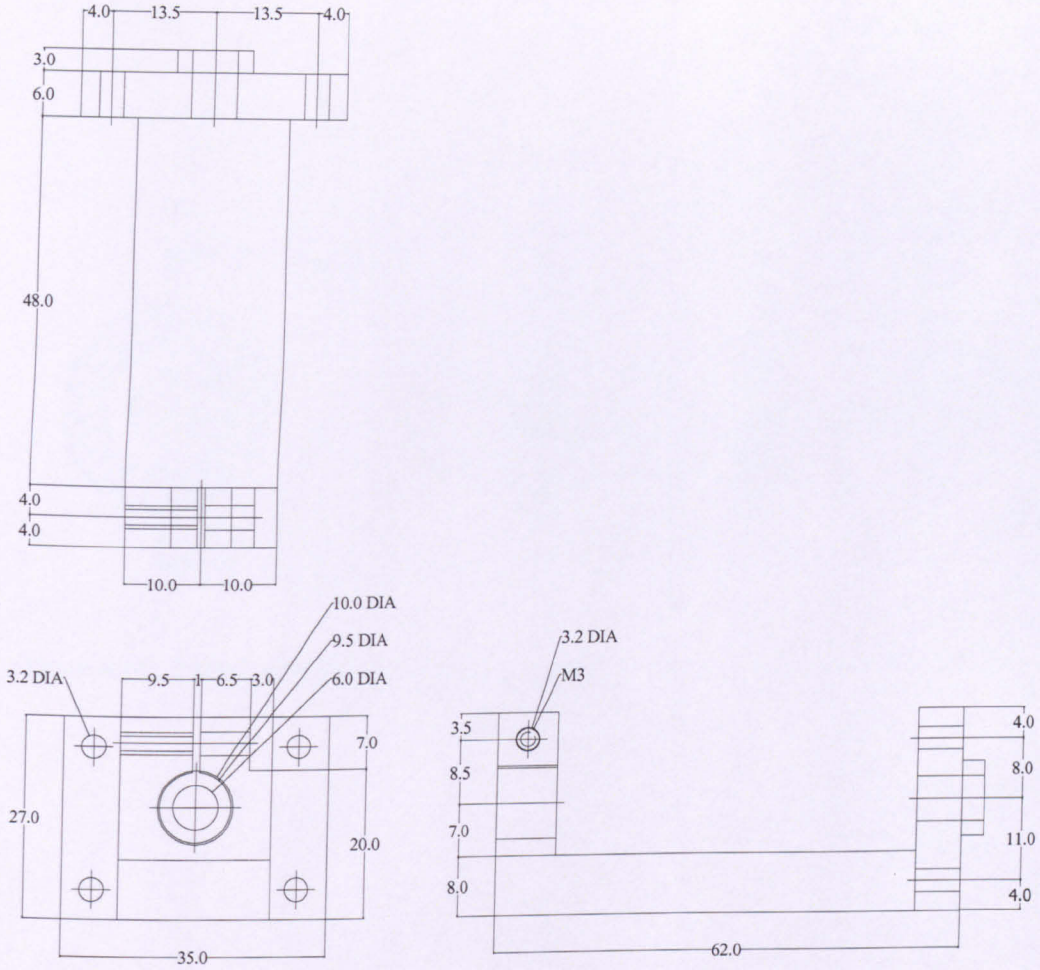

Figure 4.14. Design of the LVDT bracket

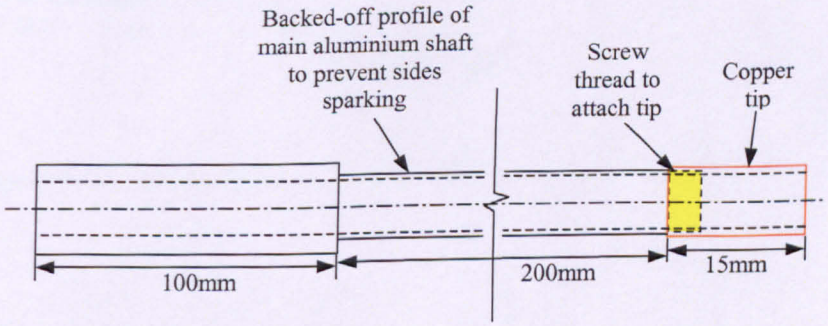

Figure 4.15. Sketch of the aluminium and copper extended length electrode

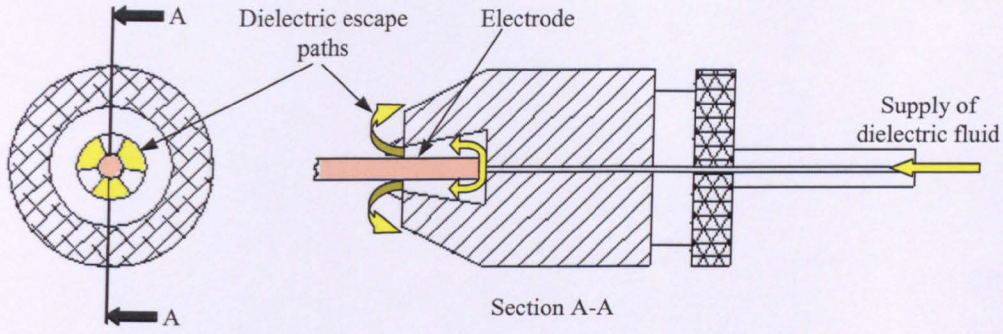

Figure 4.16. Sketch of the old EDM chuck, mounted electrode and dielectric escape paths

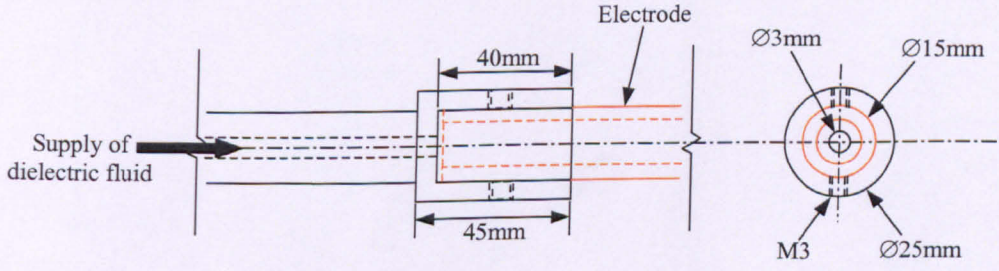

Figure 4.17. Sketch of the enclosed EDM chuck and mounted electrode

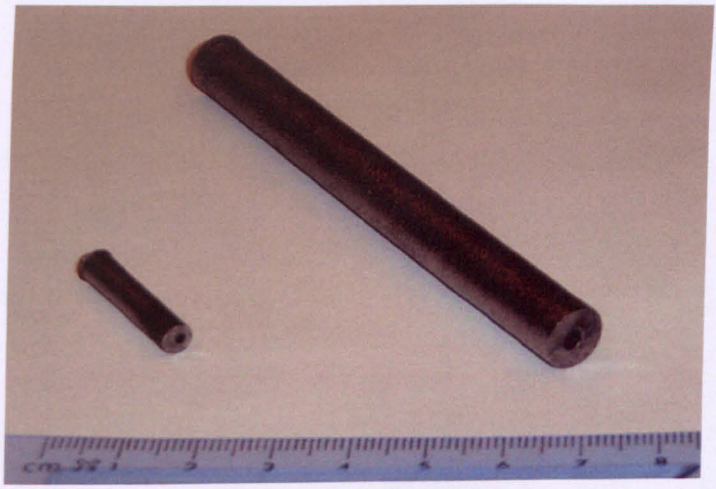

Figure 4.18. Photograph of a "5mm" and "10mm" deep-hole core

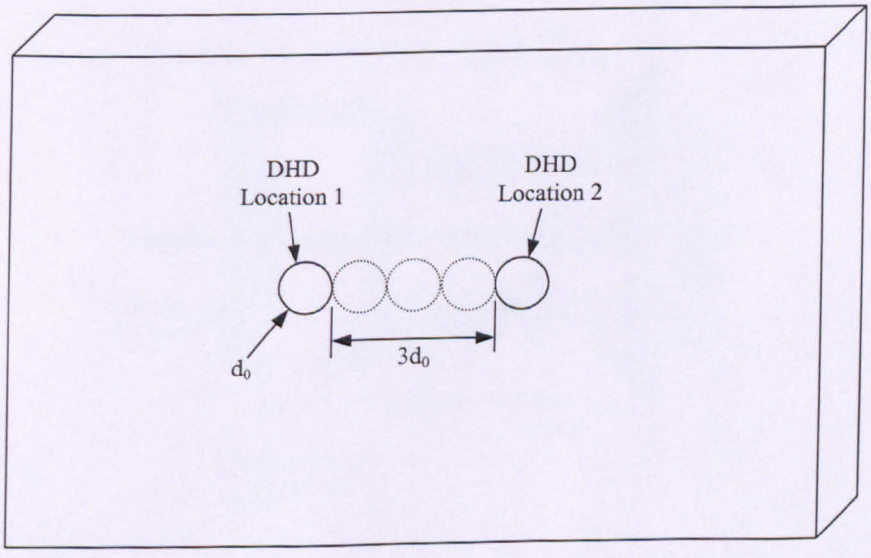

Figure 4.19. Minimum distance between DHD measurement locations

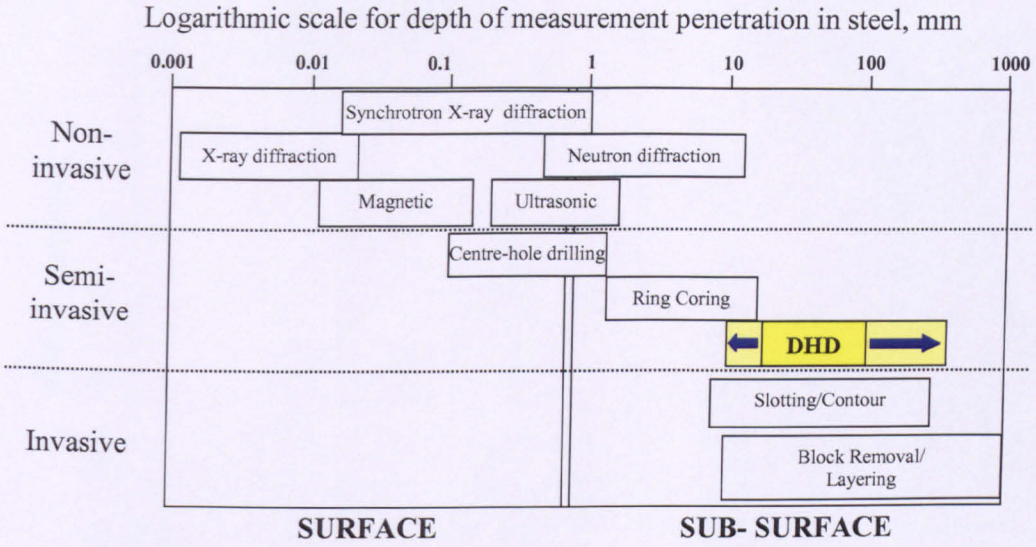

Figure 4.20. Increased applicability of the DHD technique

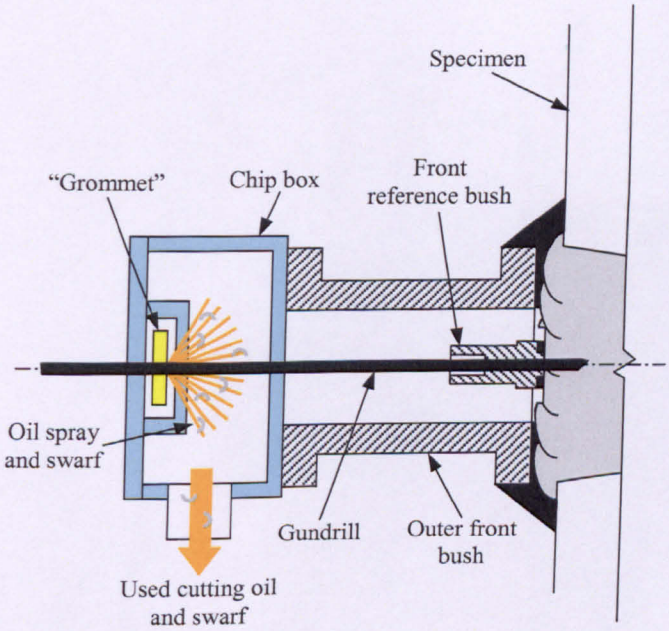

Figure 4.21. Cross-sectional schematic of the chip box and "grommet" during gundrilling

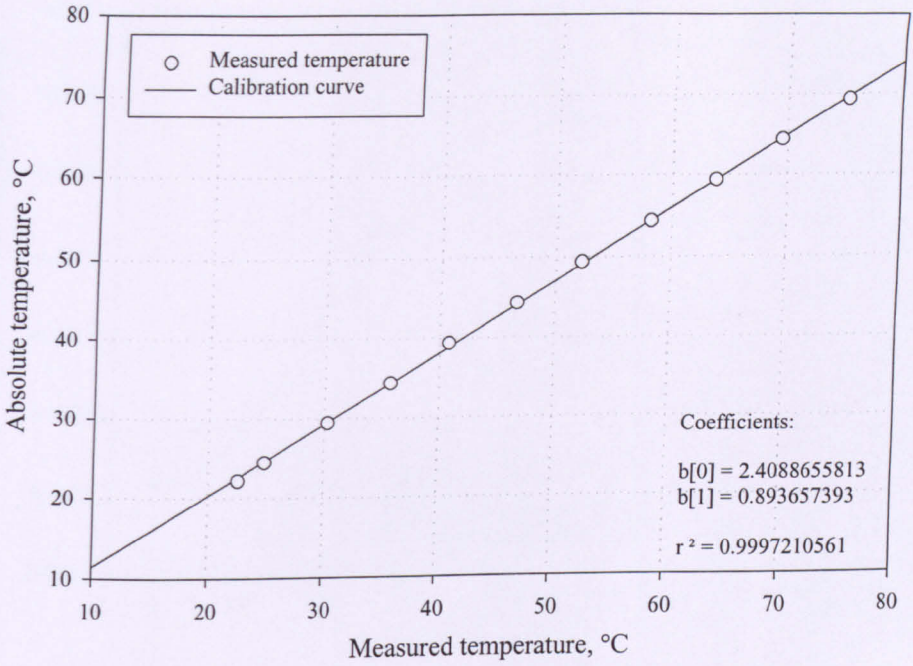

Figure 4.22. Shielded thermocouple calibration curve

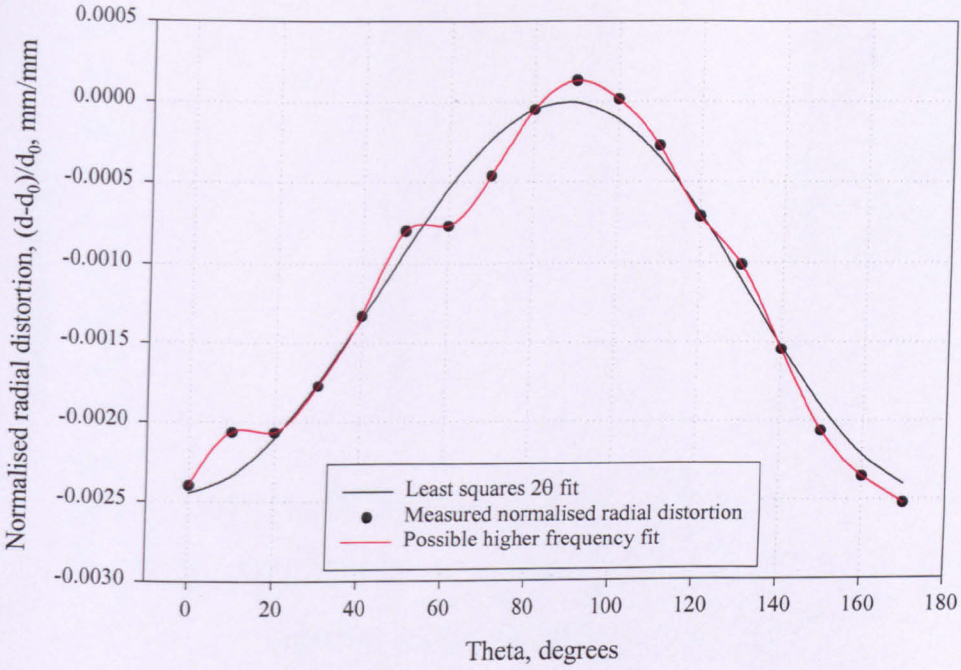

Figure 5.1. Possible curve fits to the measured normalised radial distortion

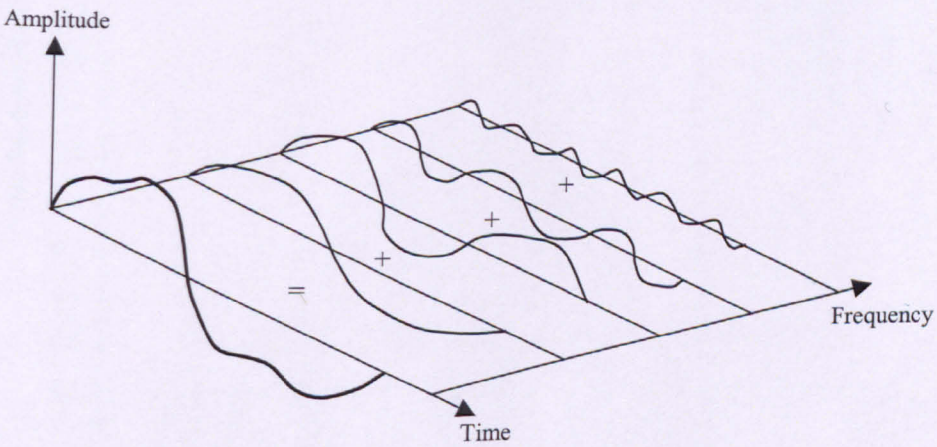

Figure 5.2. Signal amplitude in both time and frequency domains

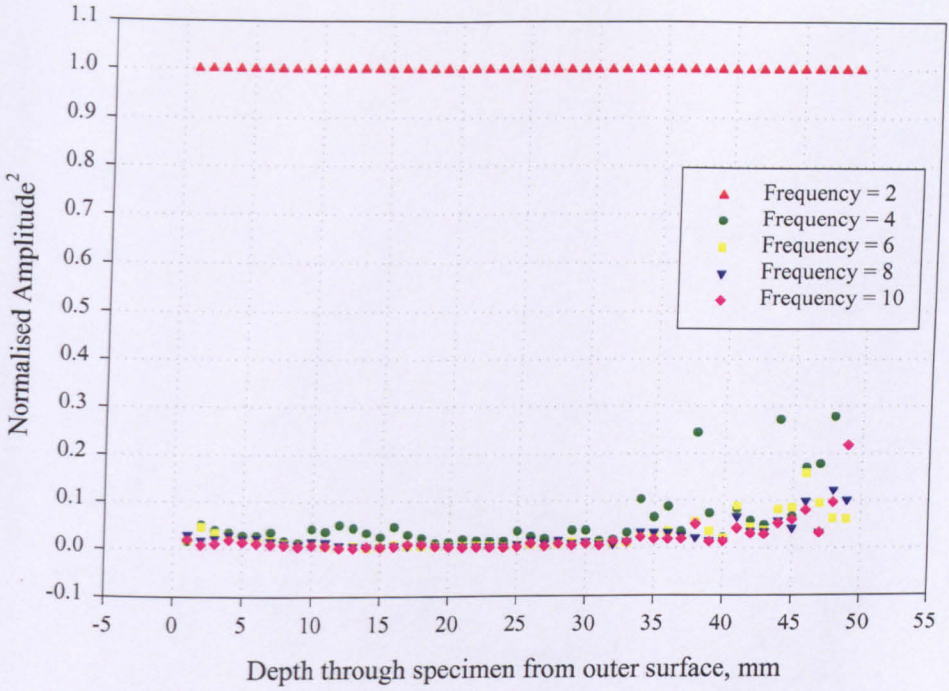

a) Frequencies 2 to 10

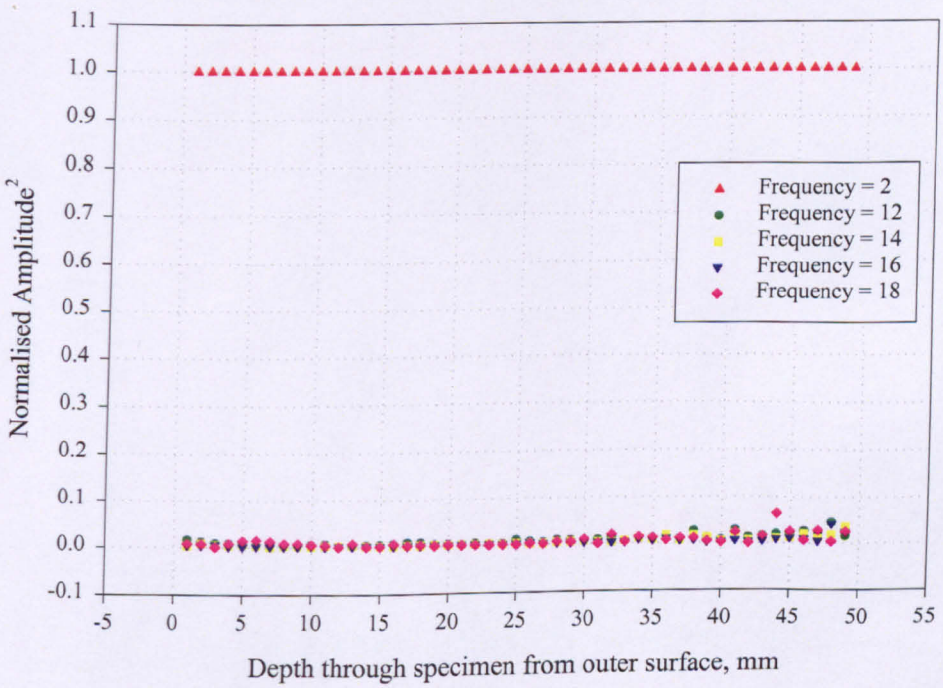

b) Frequencies 2 and 12 to 18

Figure 5.3. Normalised PSD of measured normalised radial distortion

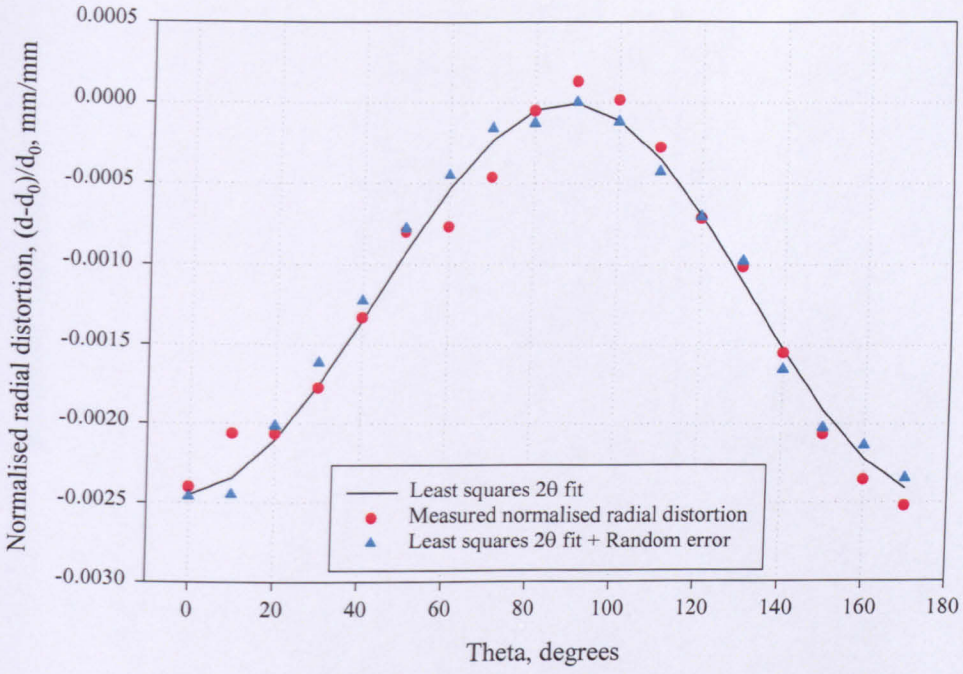

Figure 5.4. Normalised radial distortion data used for the PSD analysis

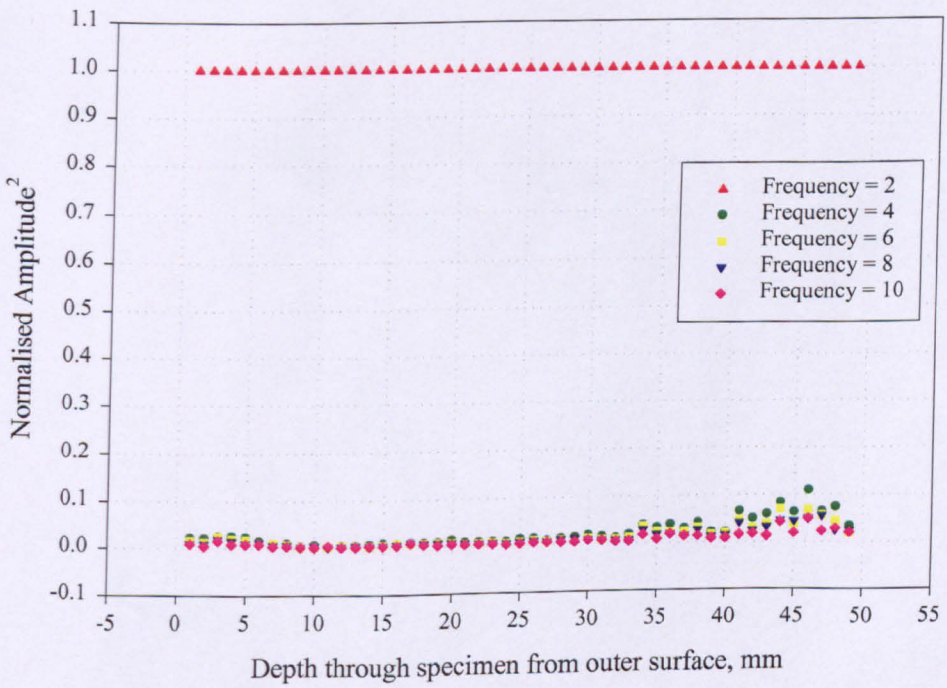

a) Frequencies 2 to 10

Figure 5.5. Normalised PSD of least squares 2θ fit + random error

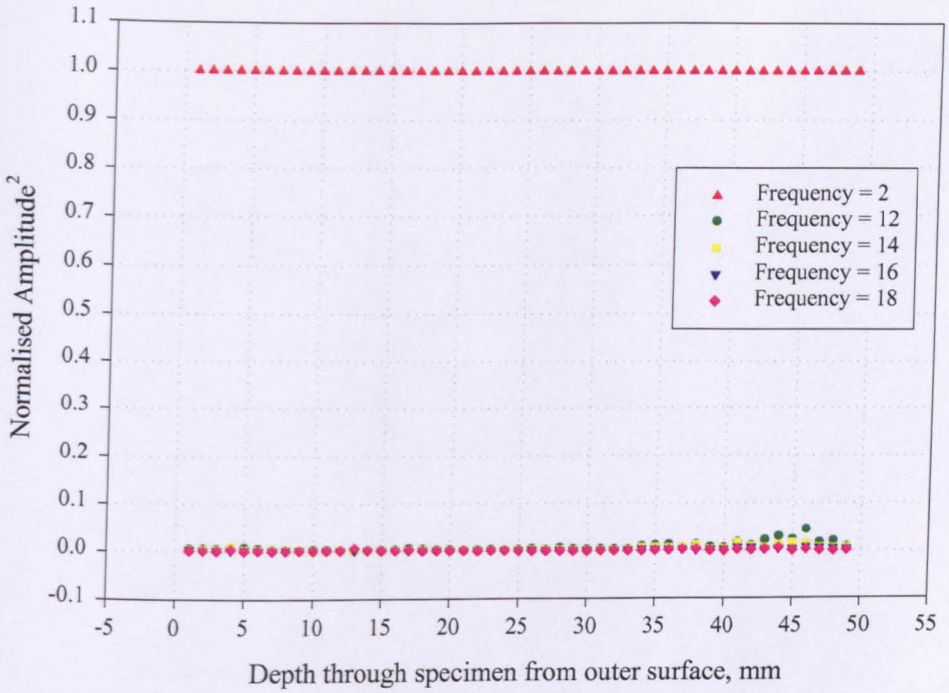

b) Frequencies 2 and 12 to 18

Figure 5.5. Normalised PSD of least squares 2θ fit + random error

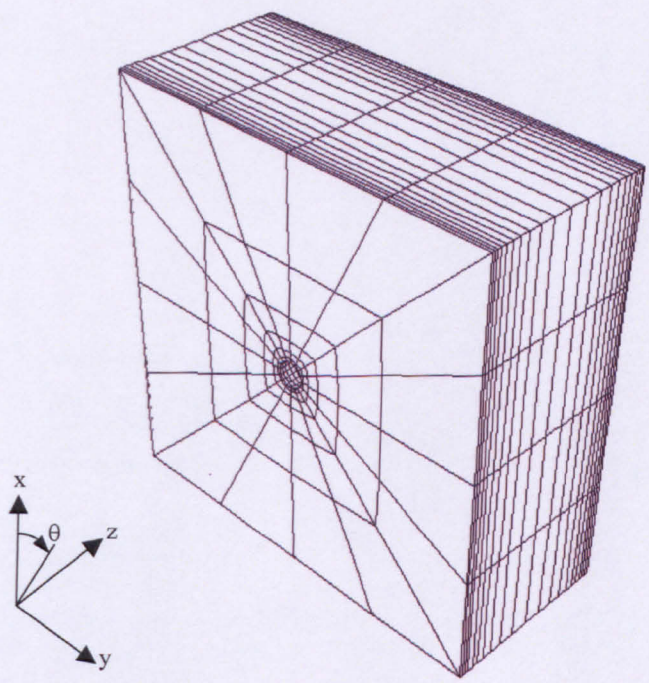

Figure 5.6. Finite element model for parameter updating analysis

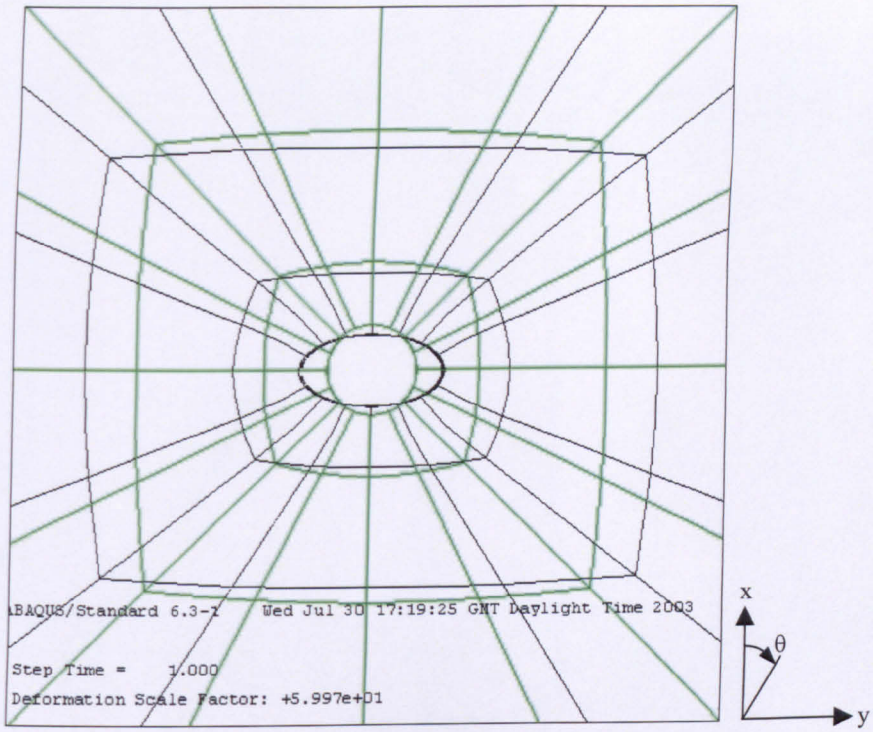

Figure 5.7. Exaggerated FE model showing the original and elliptically deformed reference hole

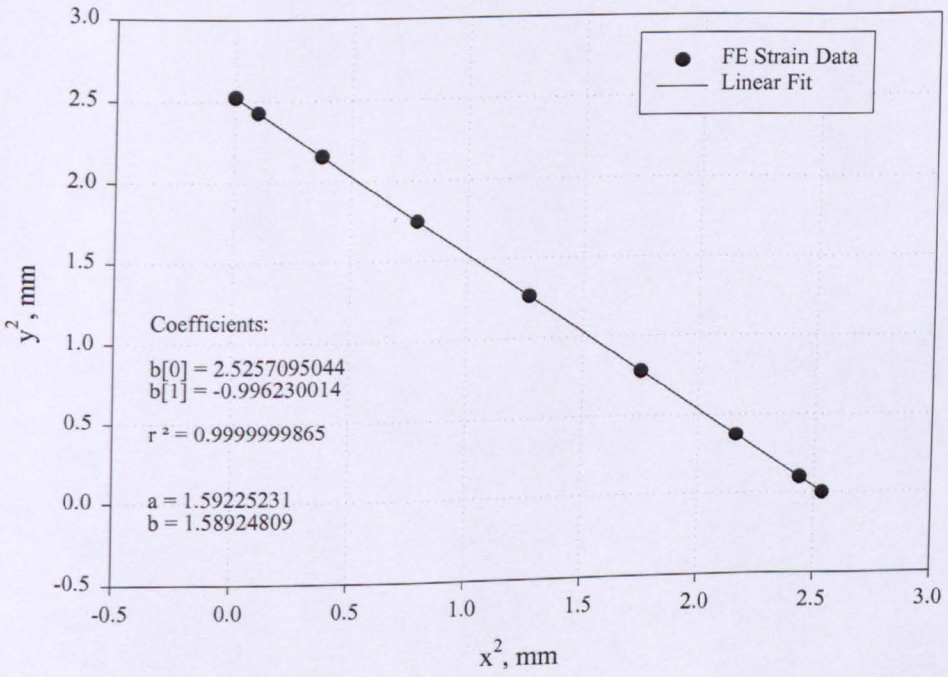

Figure 5.8. Linear fit to elliptically deformed hole

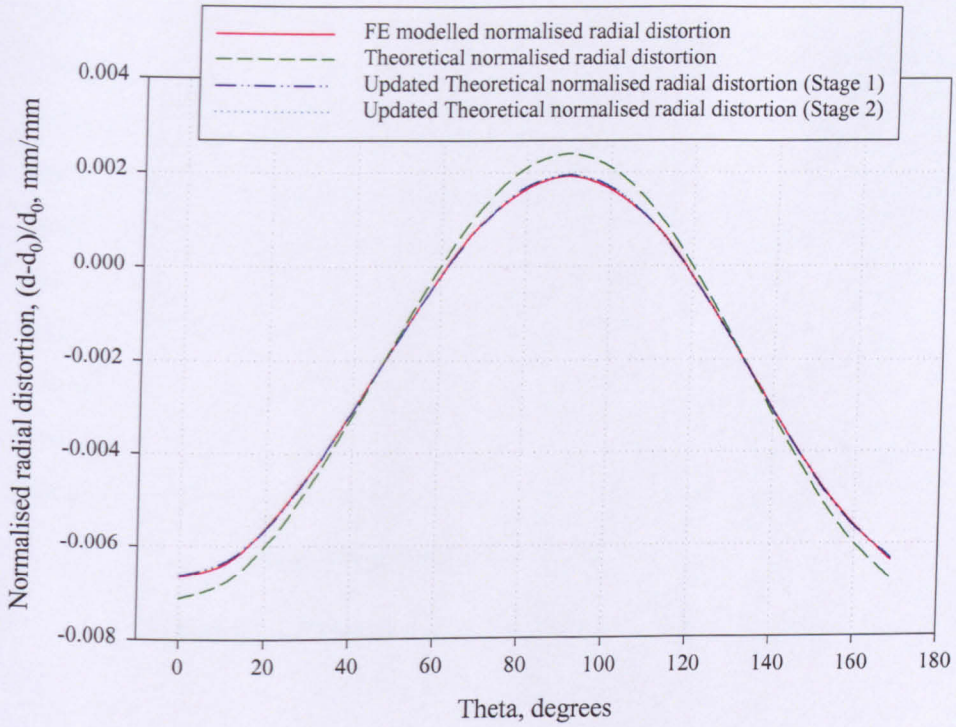

Figure 5.9. Updated theoretical to match FE modelled normalised radial distortions

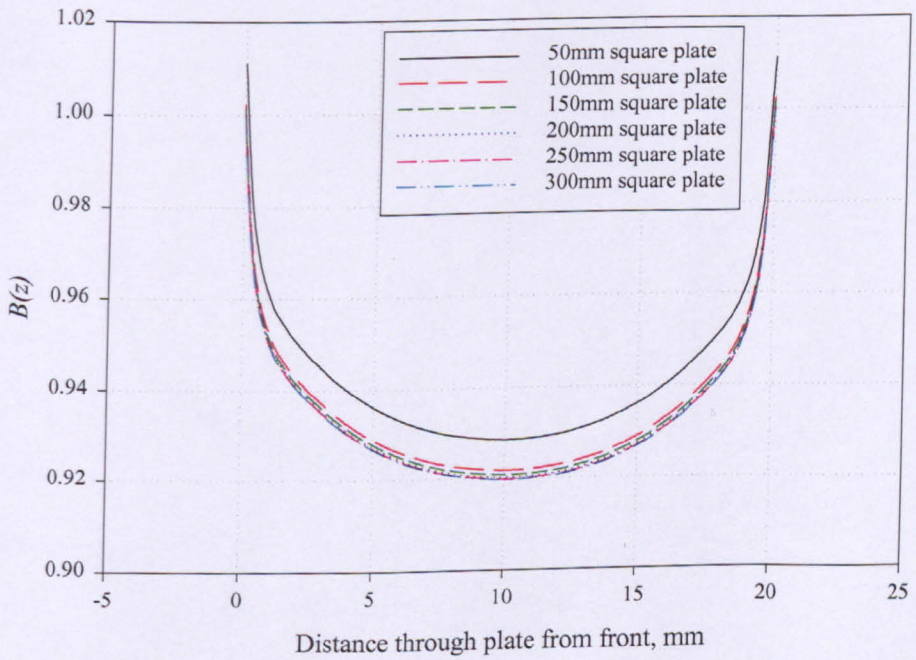

Figure 5.10. Parameter *B(z)* for different sized plates

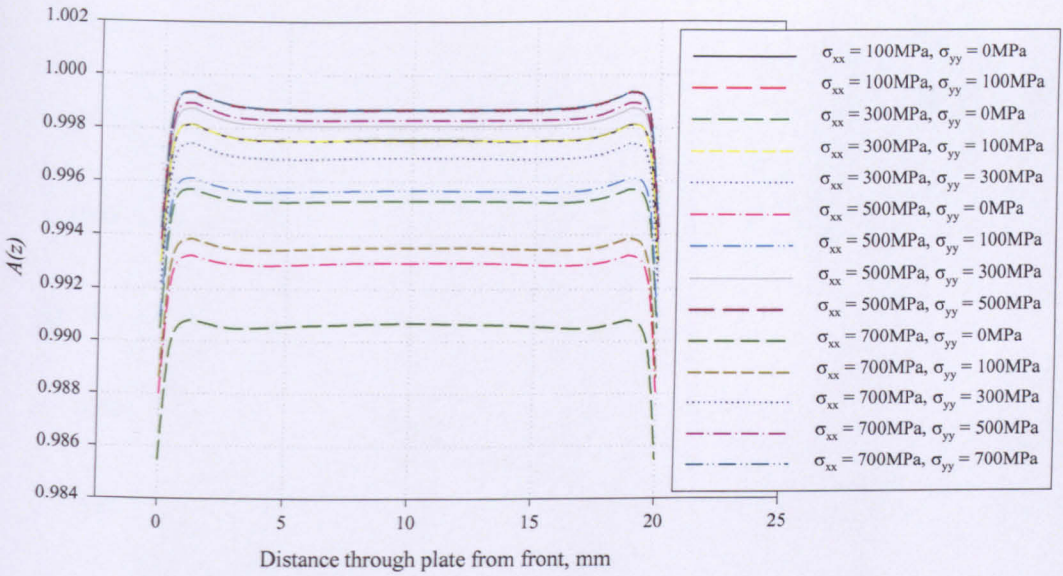

Figure 5.11. Parameter *A(z)* for different applied stresses

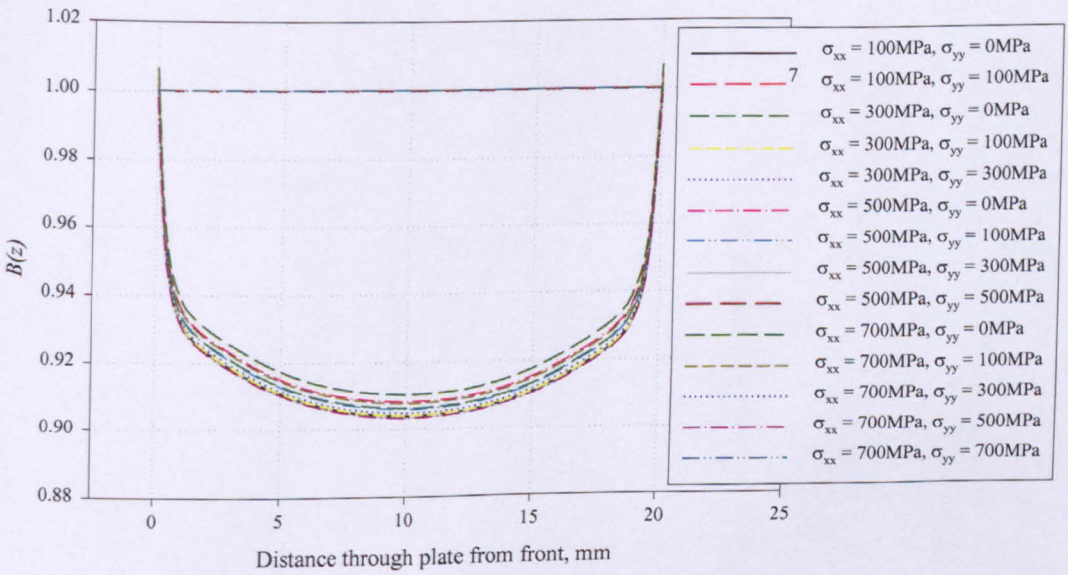

Figure 5.12. Parameter *B(z)* for different applied stresses

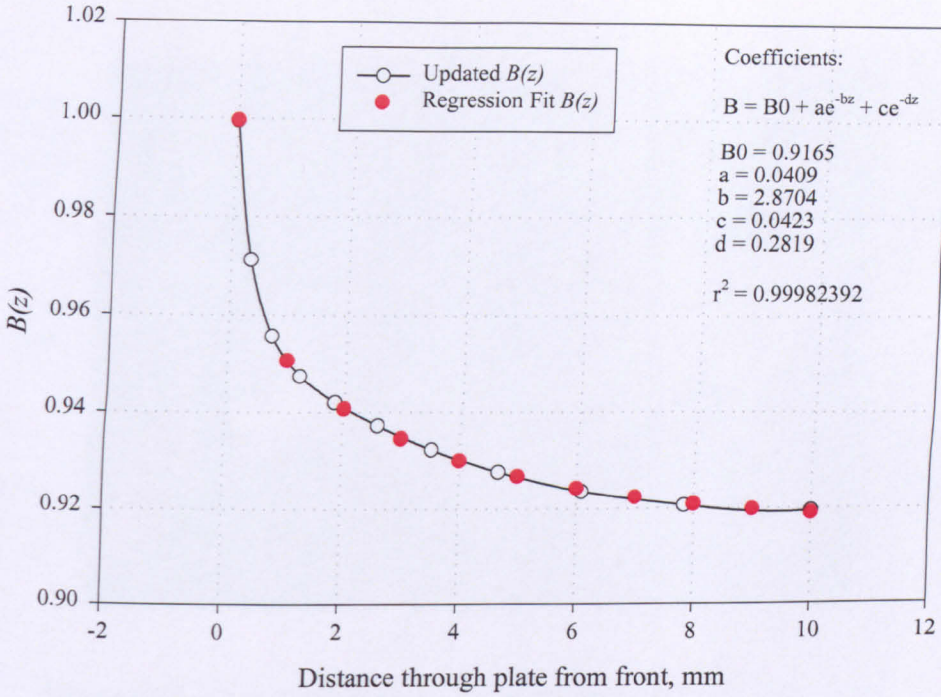

Figure 5.13. Regression fit through half of *B(z)* data

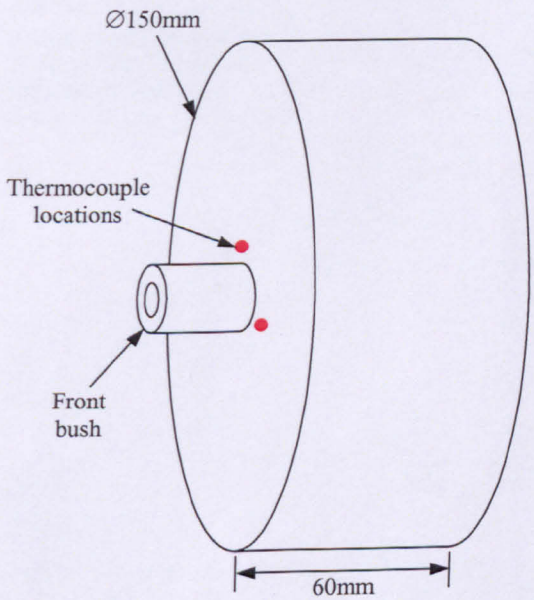

Figure 5.14. Stainless steel sample used for core temperature measurement experiments

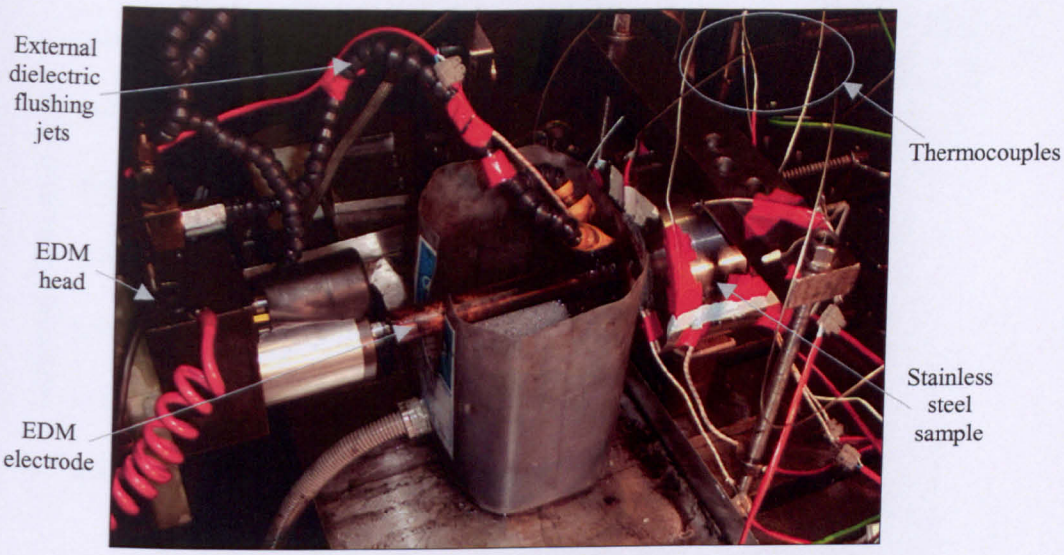

Figure 5.15. Photograph showing the experimental set-up during EDM

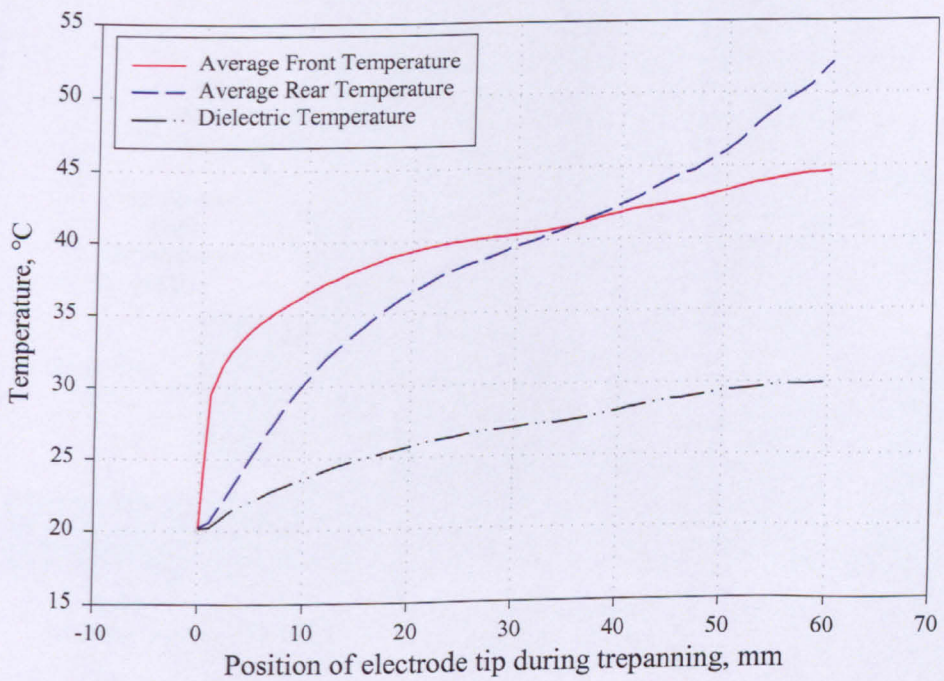

Figure 5.16. Measured temperatures of the sample and dielectric fluid during EDM

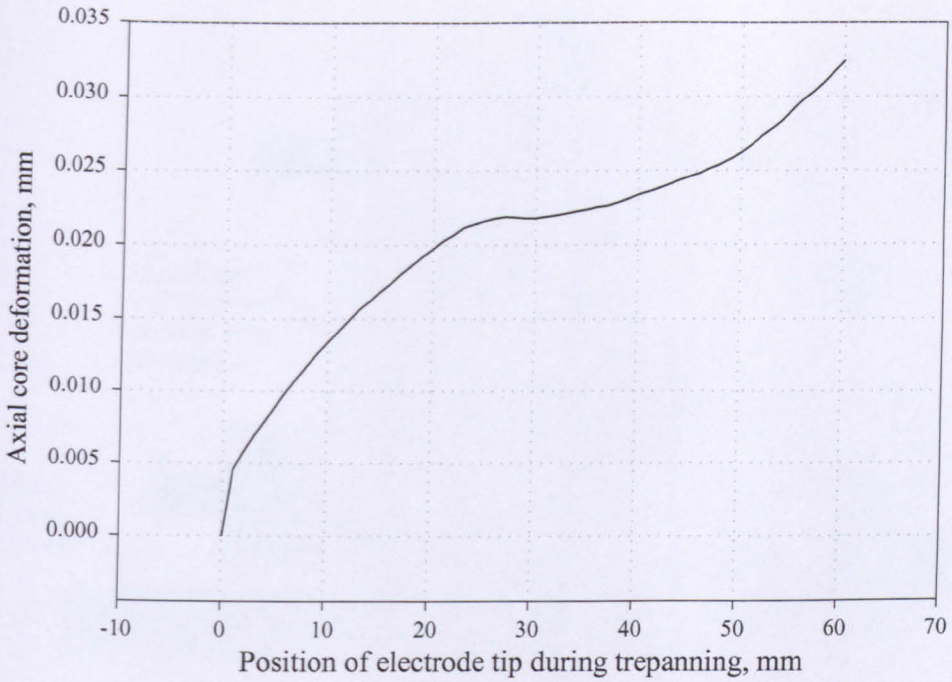

Figure 5.17. Measured axial deformation of the core during EDM

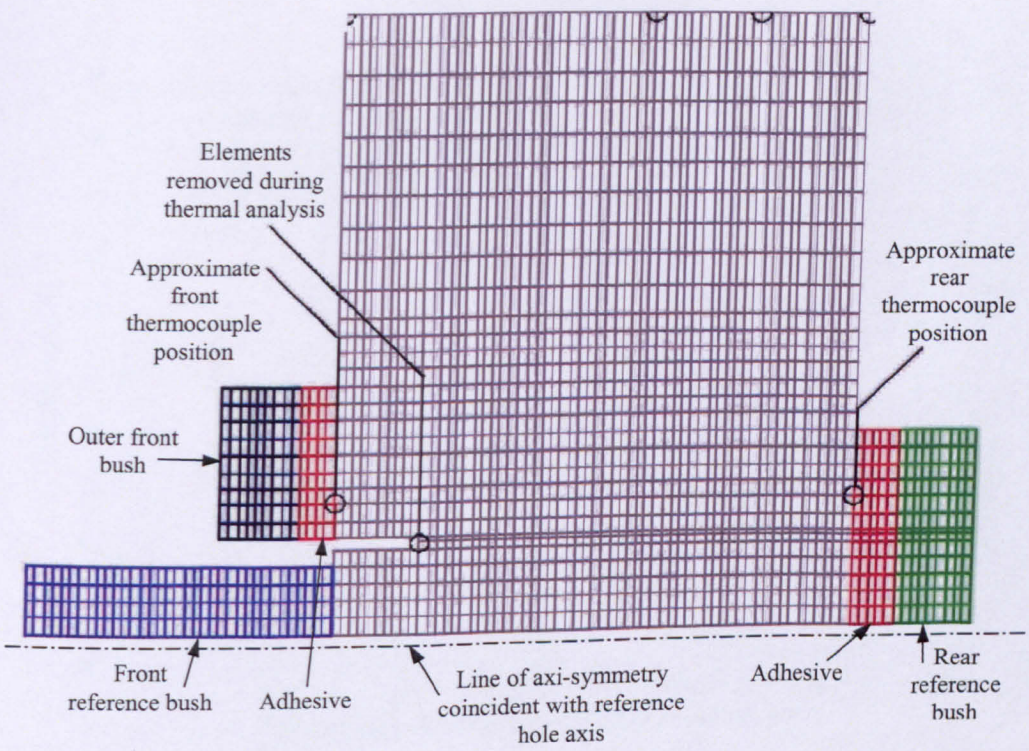

Figure 5.18. Axi-symmetric FE model for thermal analysis

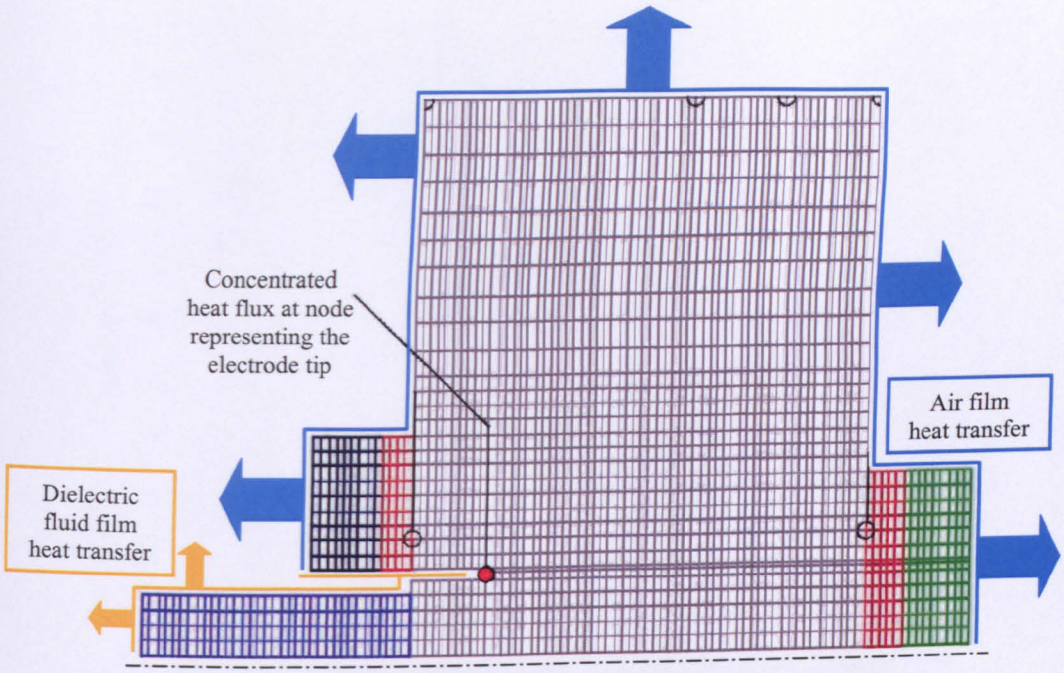

Figure 5.19. Axi-symmetric FE model with boundary conditions applied

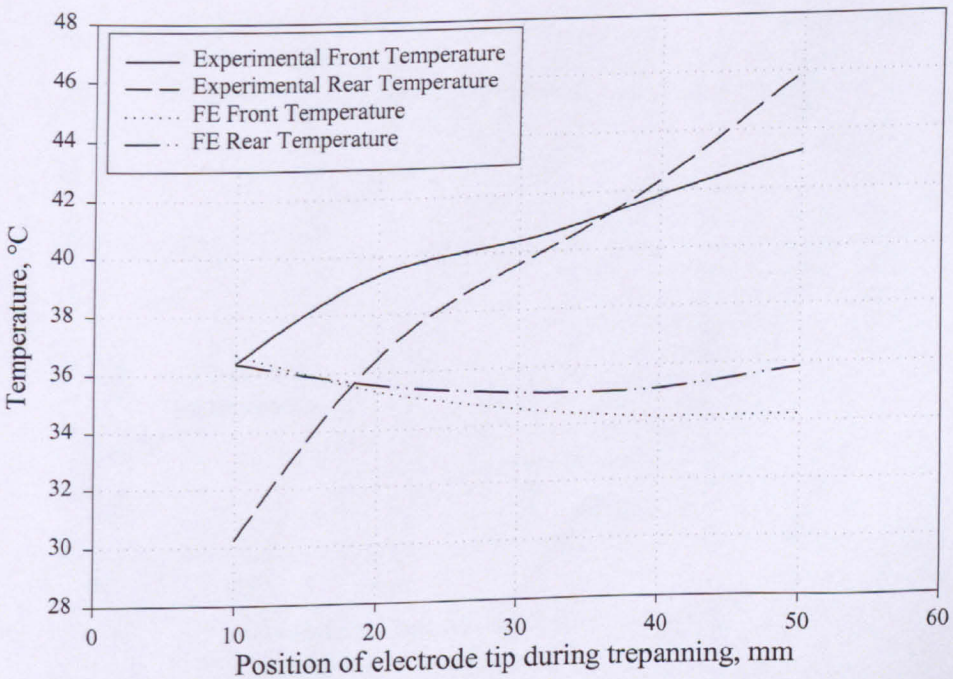

Figure 5.20. Comparison between initial FE and experimental temperatures

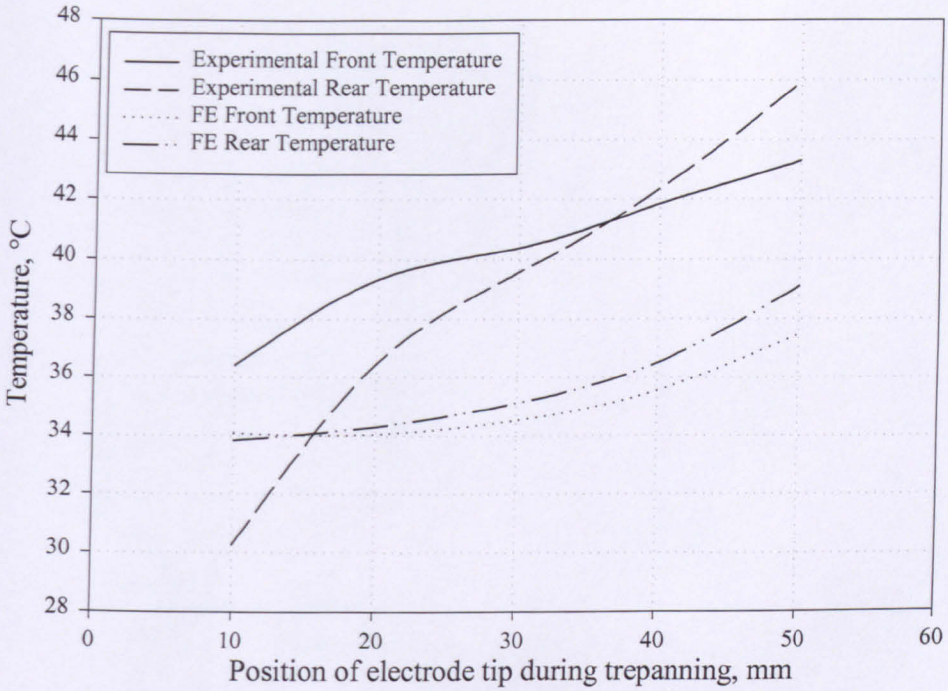

Figure 5.21. Comparison between refined FE and experimental temperatures

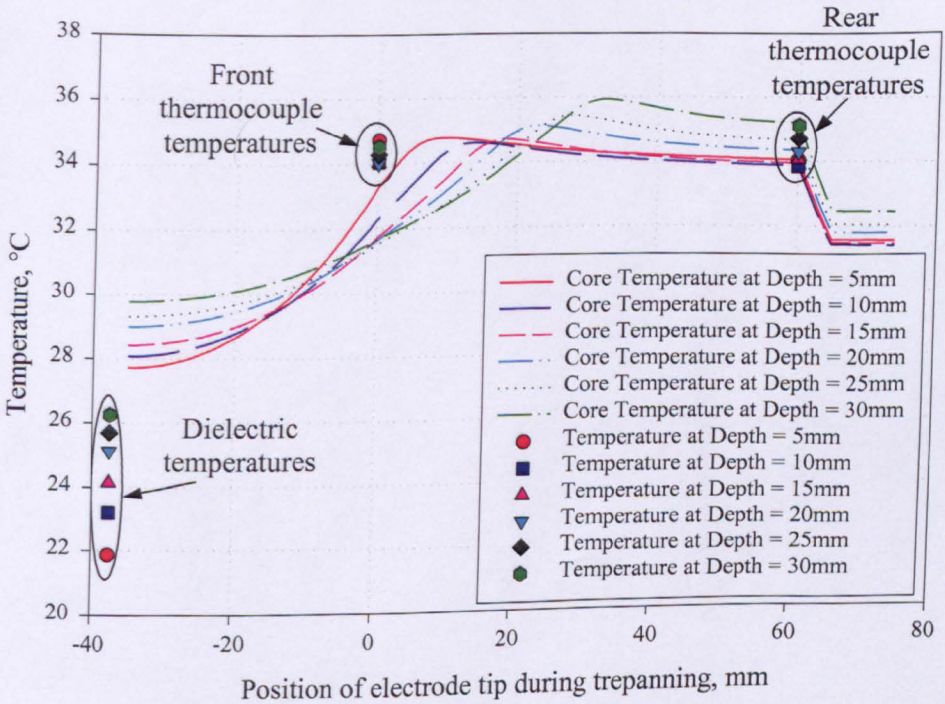

a) Electrode tip positions of 5 – 30mm

Figure 5.22. Experimental dielectric temperature and FE predicted temperature distributions throughout the core and at the front and rear thermocouple positions

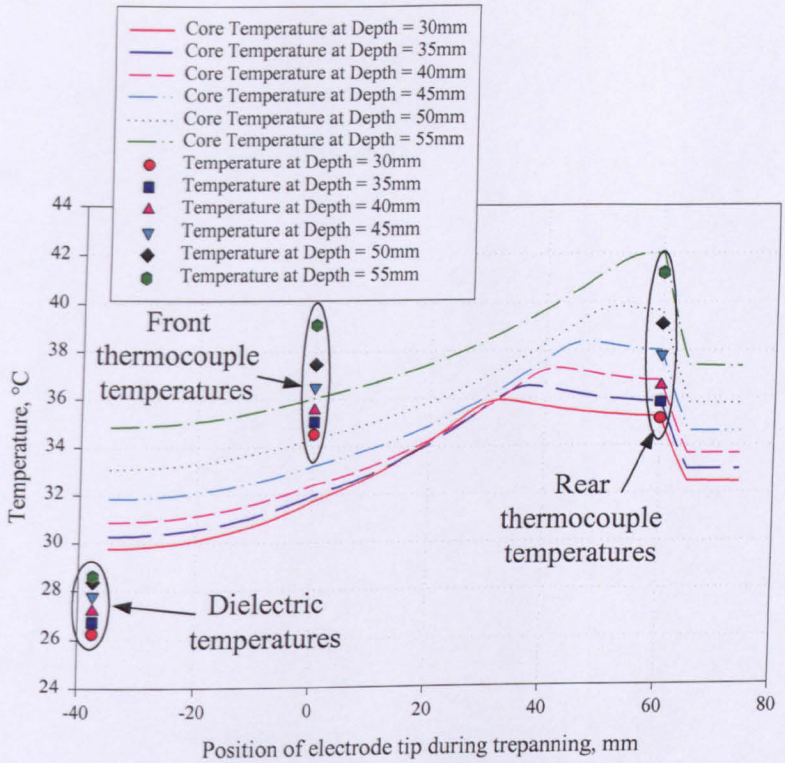

b) Electrode tip positions of 30 – 55mm

Figure 5.22. Experimental dielectric temperature and FE predicted temperature distributions throughout the core and at the front and rear thermocouple positions

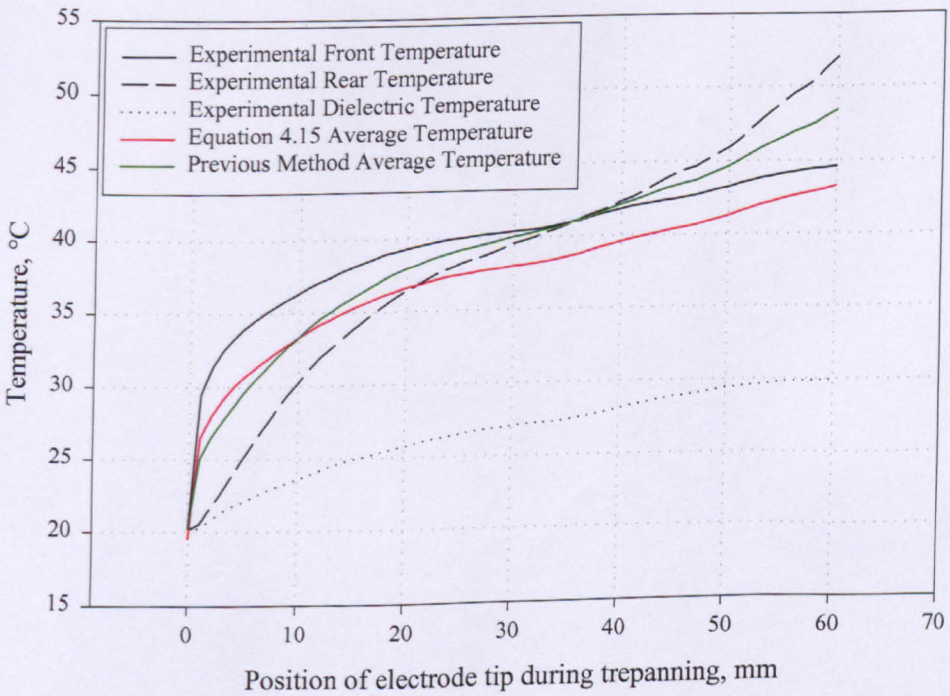

Figure 5.23. Comparison between predicted and experimental temperatures

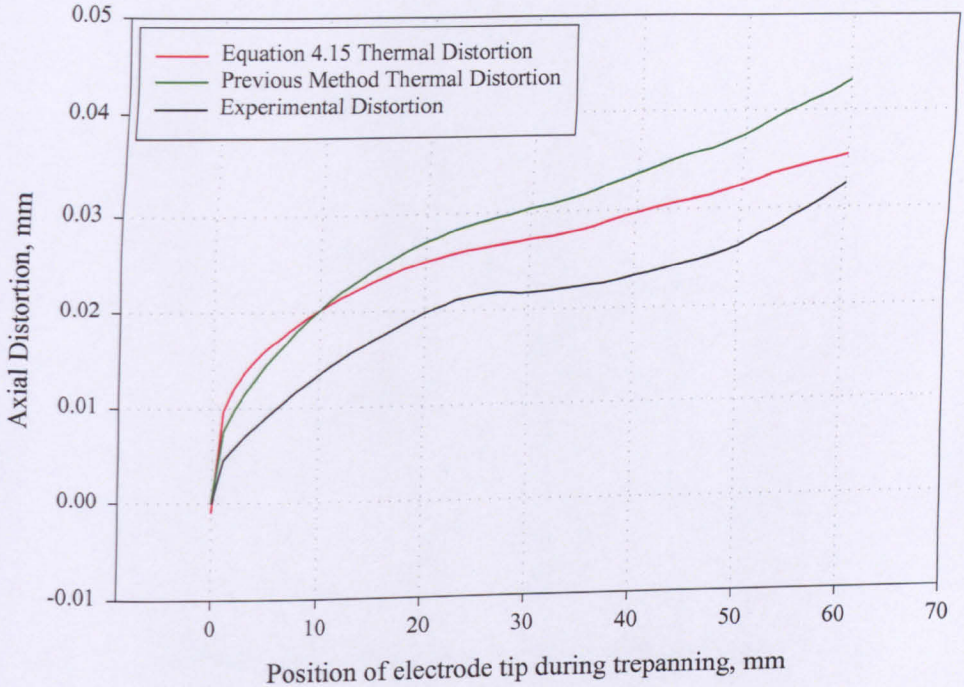

Figure 5.24. Comparison between predicted and experimental axial distortions

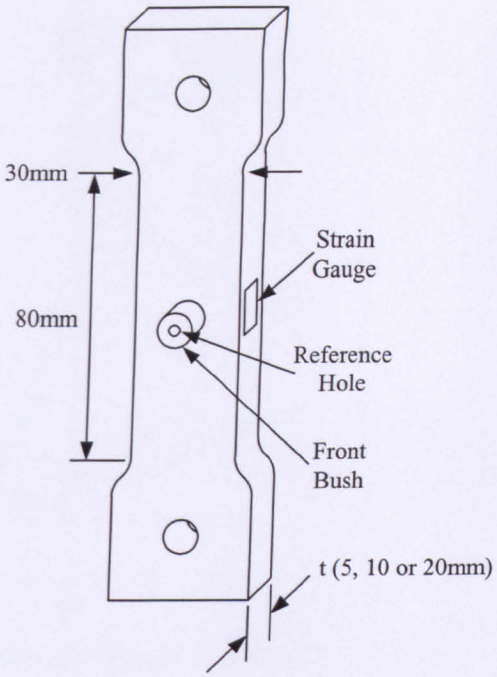

Figure 6.1. Design of uniaxial loading specimen

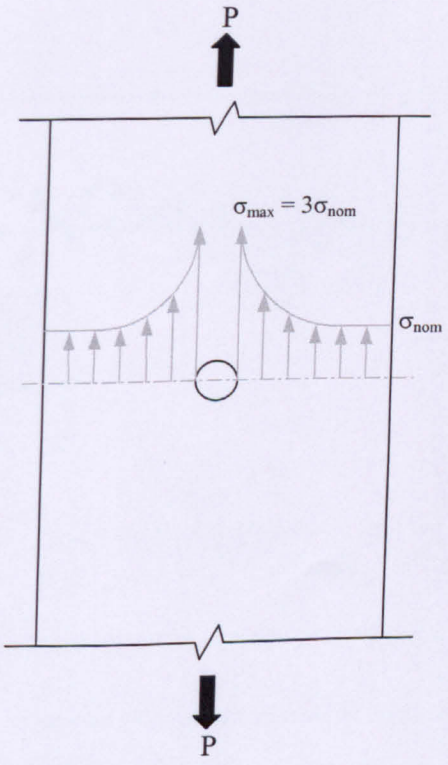

Figure 6.2. Induced stress concentration around a hole

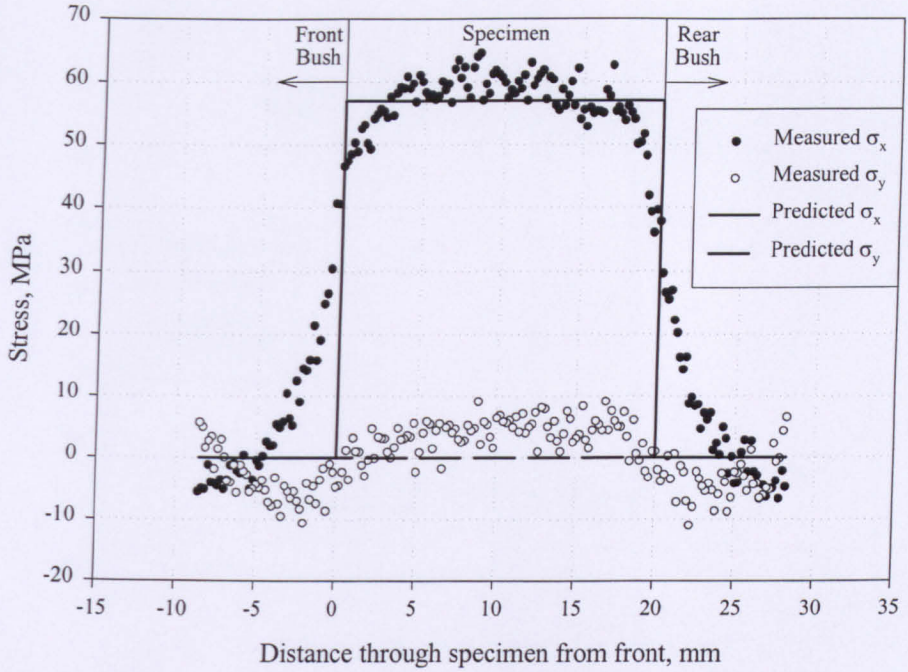

Figure 6.3. Measured stress distribution for specimen 1 with bushes at 57MPa (t=20mm, d_0=3.18mm)

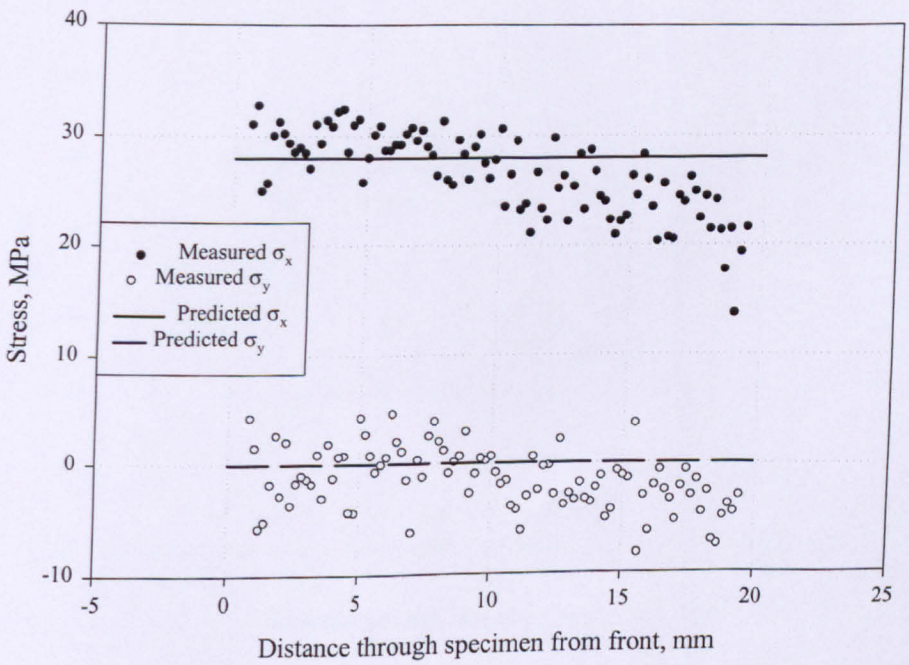

Figure 6.4. Measured stress distribution for specimen 1 without bushes at 28MPa (t=20mm, d_0=3.18mm)

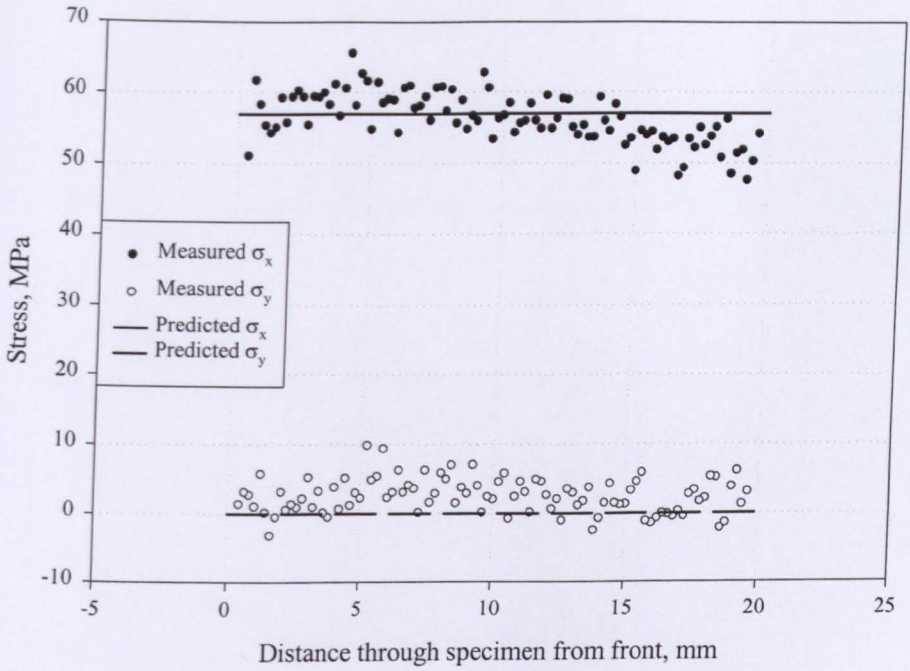

Figure 6.5. Measured stress distribution for specimen 1 without bushes at 57MPa (t=20mm, d_0=3.18mm)

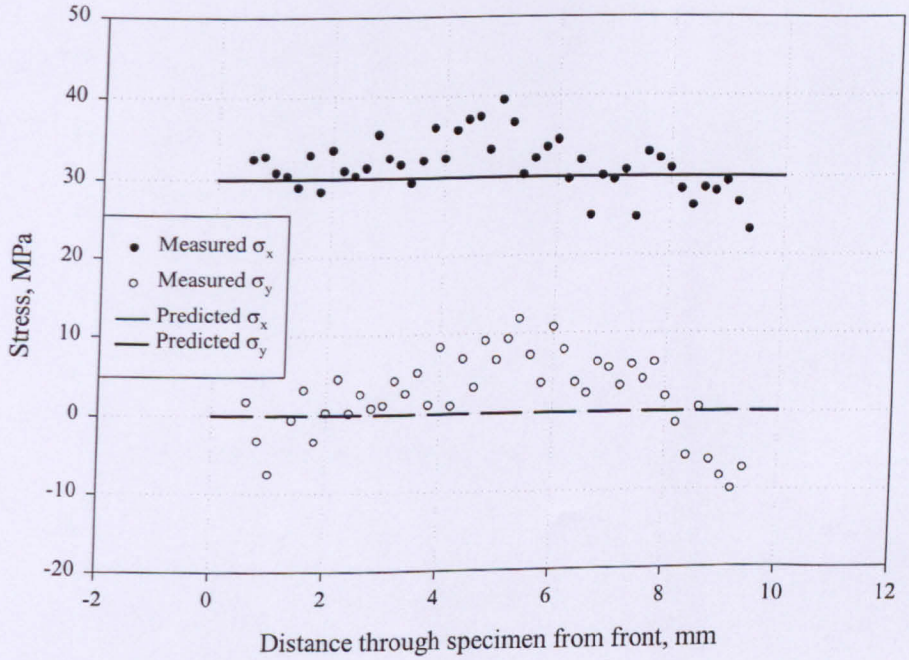

Figure 6.6. Measured stress distribution for specimen 2 without bushes at 30MPa (t=10mm, d_0=3.18mm)

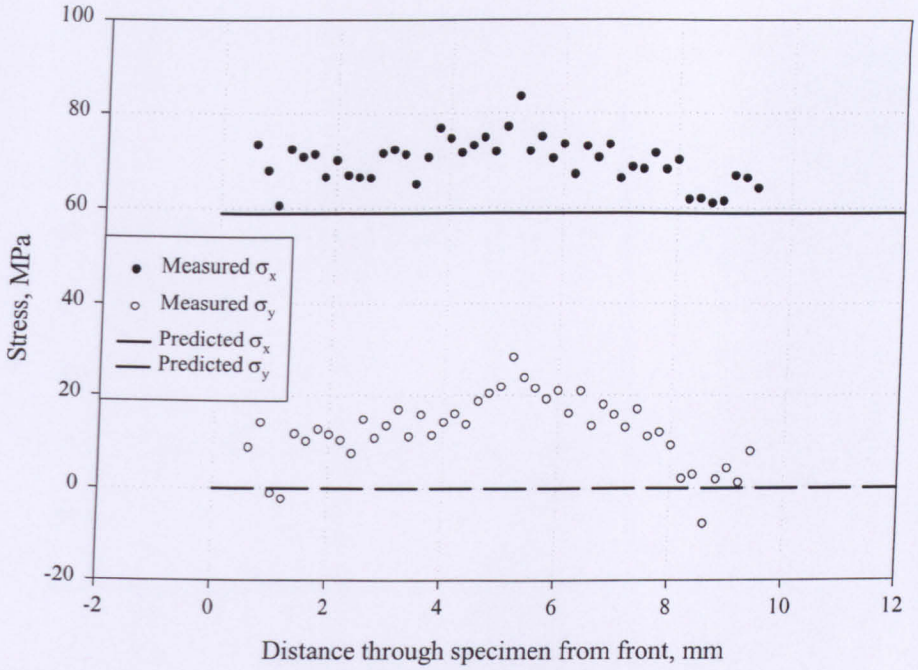

Figure 6.7. Measured stress distribution for specimen 2 without bushes at 59MPa (t=10mm, d_0=3.18mm)

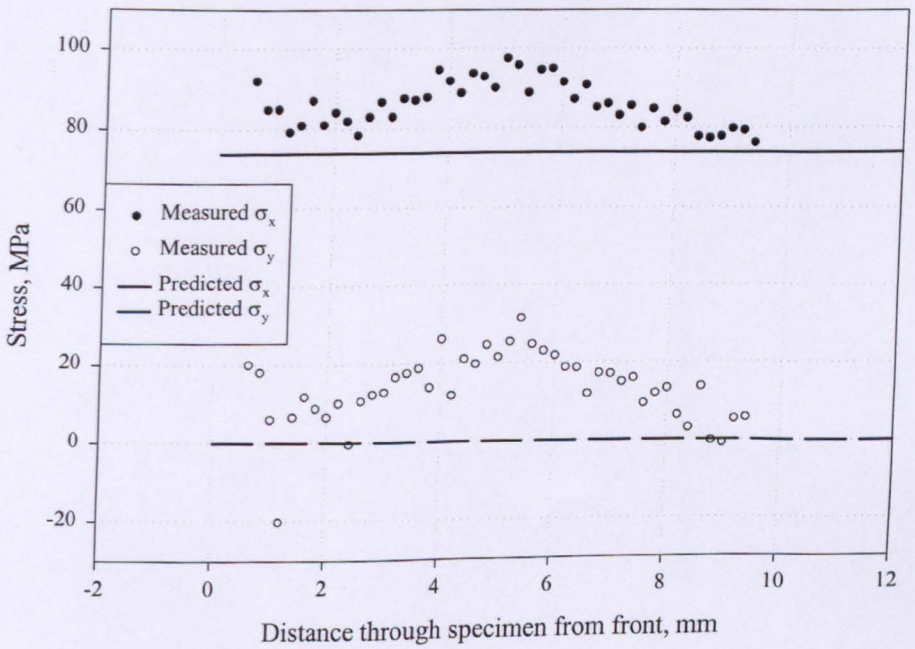

Figure 6.8. Measured stress distribution for specimen 2 without bushes at 74MPa (t=10mm, d_0=3.18mm)

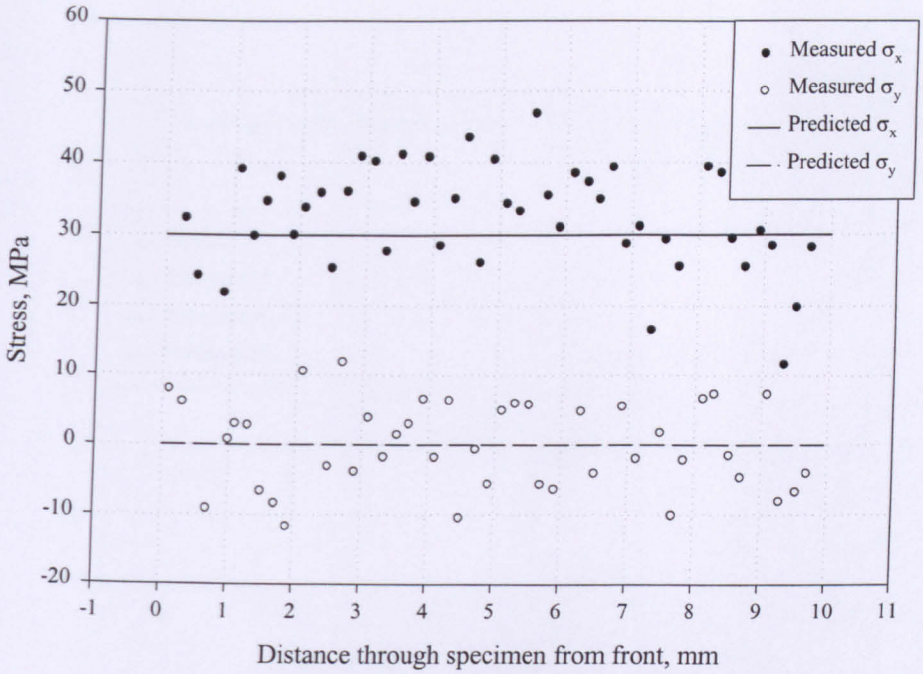

Figure 6.9. Measured stress distribution for specimen 3 without bushes at 30MPa (t=10mm, d_0=1.5mm)

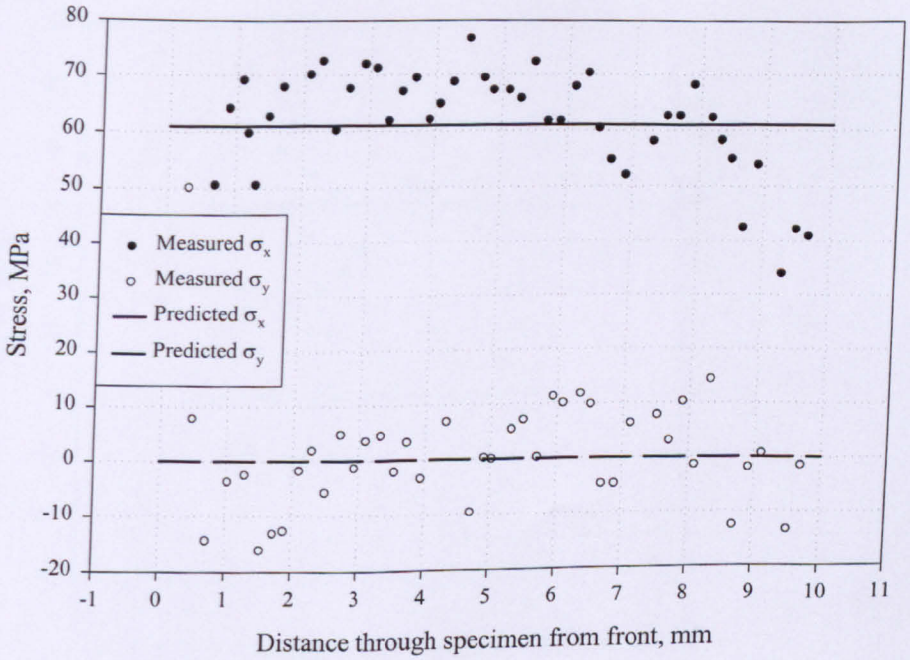

Figure 6.10. Measured stress distribution for specimen 3 without bushes at 61MPa (t=10mm, d_0=1.5mm)

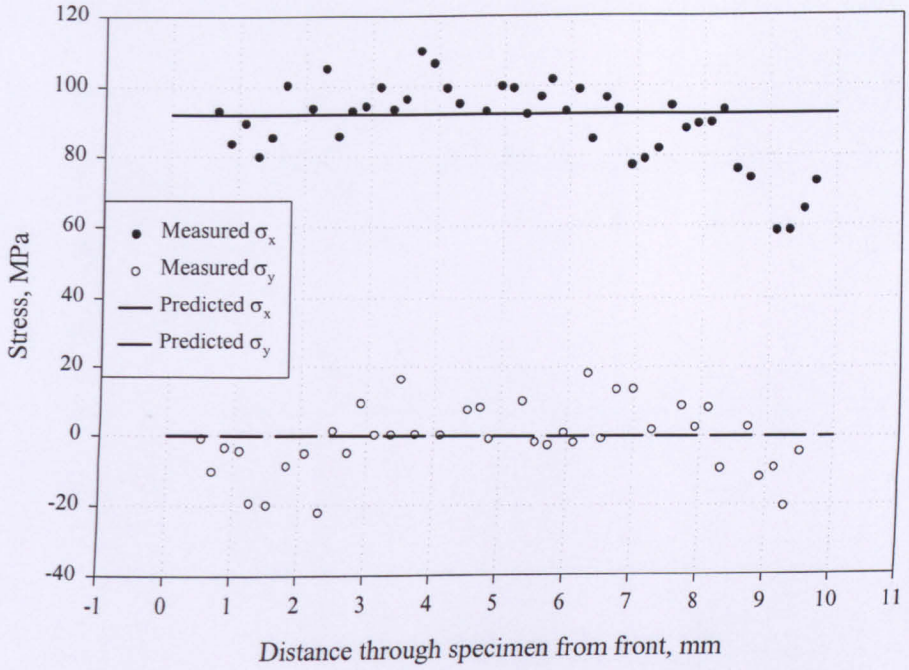

Figure 6.11. Measured stress distribution for specimen 3 without bushes at 92MPa (t=10mm, d_0=1.5mm)

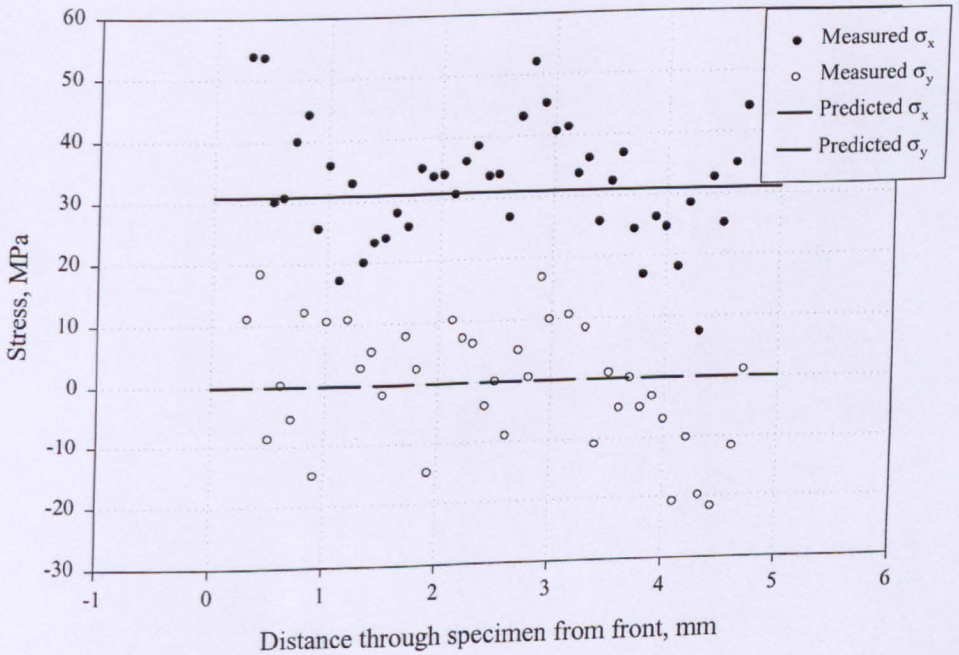

Figure 6.12. Measured stress distribution for specimen 4 without bushes at 31MPa (t=5mm, d_0=1.5mm)

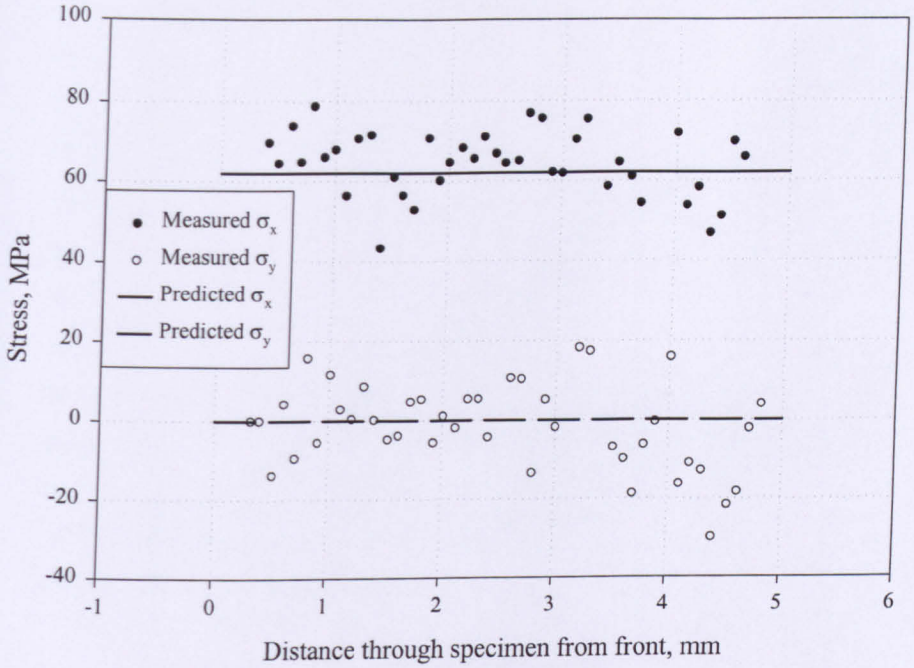

Figure 6.13. Measured stress distribution for specimen 4 without bushes at 62MPa (t=5mm, d_0=1.5mm)

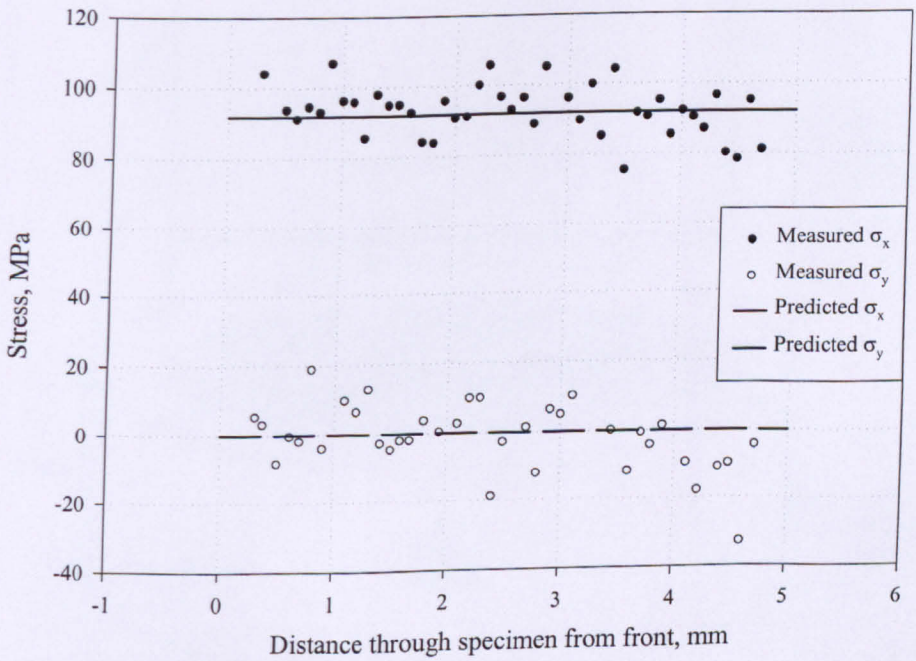

Figure 6.14. Measured stress distribution for specimen 4 without bushes at 92MPa (t=5mm, d_0=1.5mm)

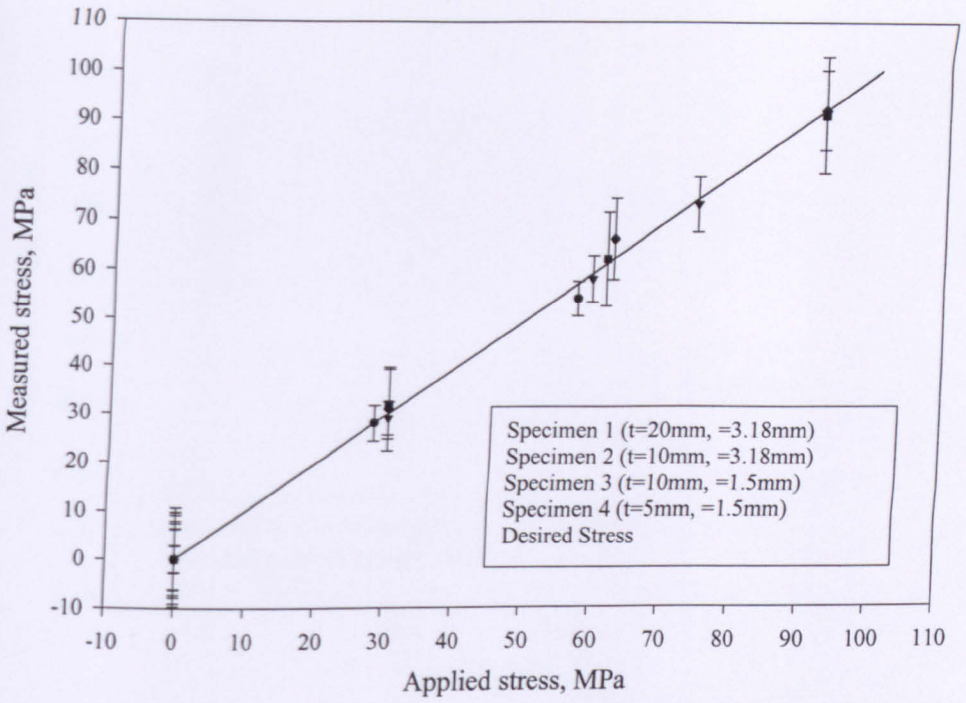

Figure 6.15. Calibration curve for aluminium specimens 1 to 4.

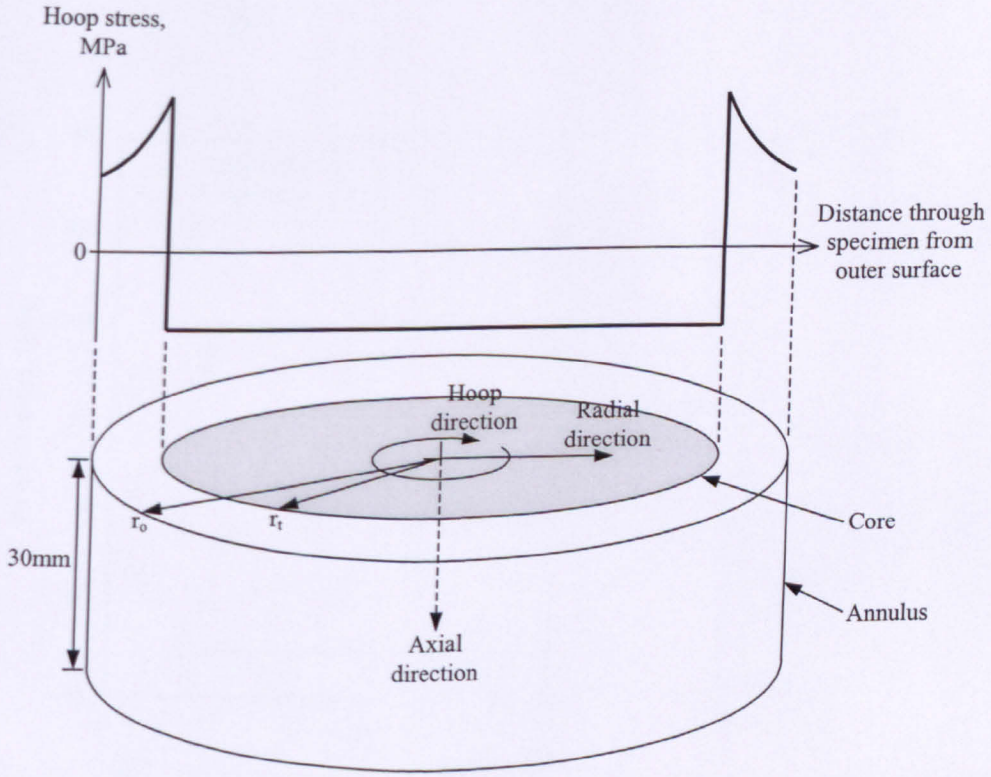

Figure 6.16. Sketch of a shrink fit specimen and the hoop stress step change

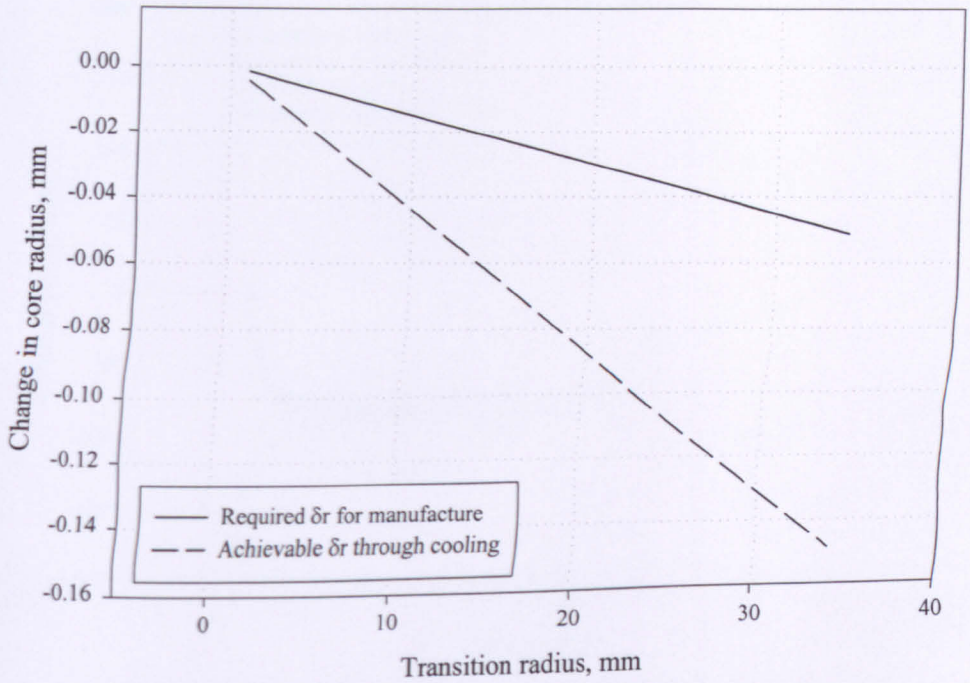

Figure 6.17. Comparison of the required and achievable contractions of the core ($r_0 = 35$mm, $E = 70$GPa, $P = 150$MPa)

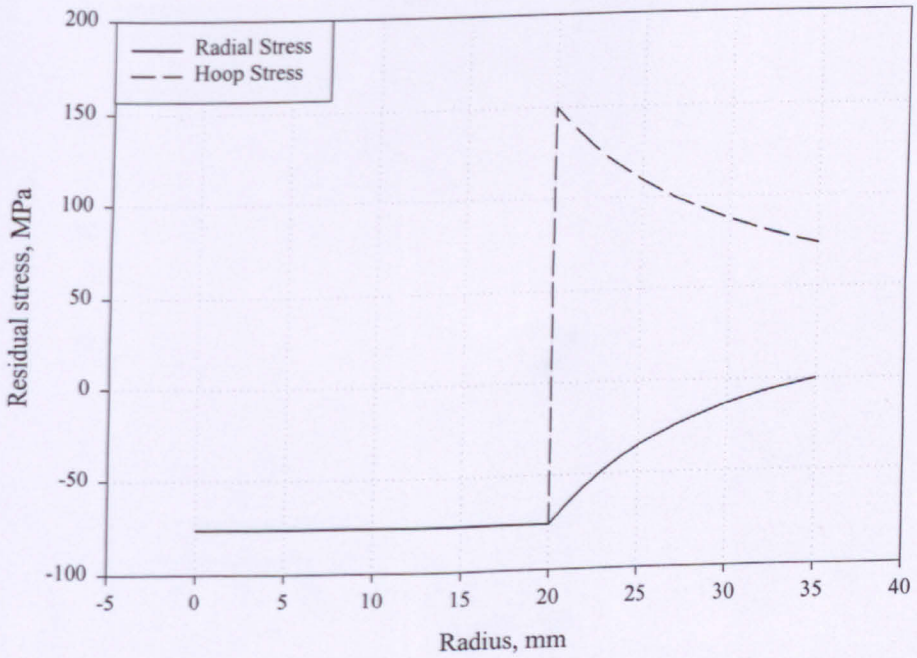

Figure 6.18. Predicted residual stress distribution in shrink-fit specimen 1

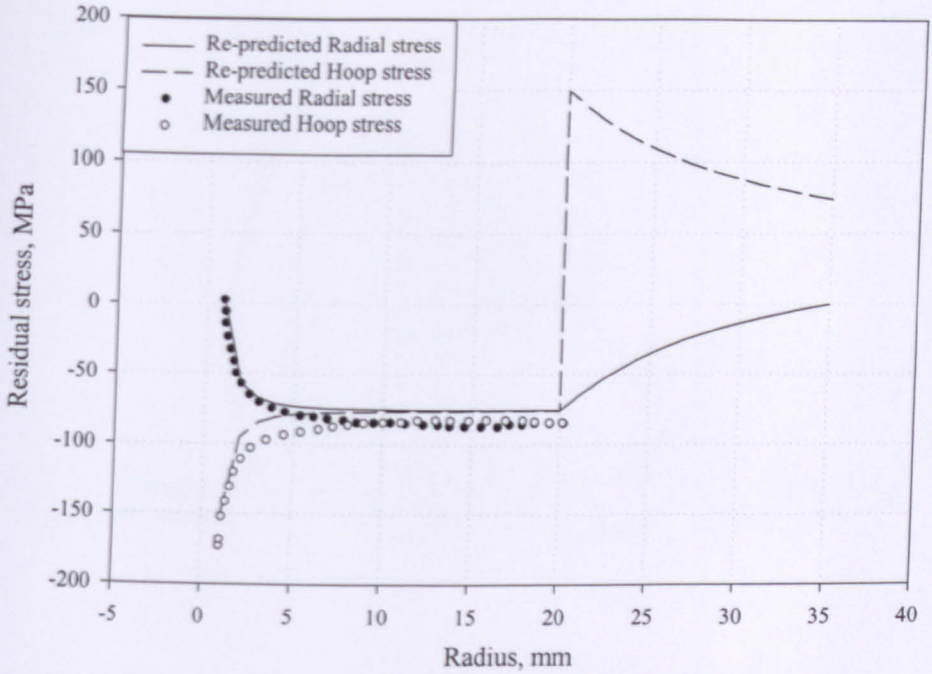

Figure 6.19. Re-predicted and Sachs measured residual stress distribution in shrink-fit specimen 1

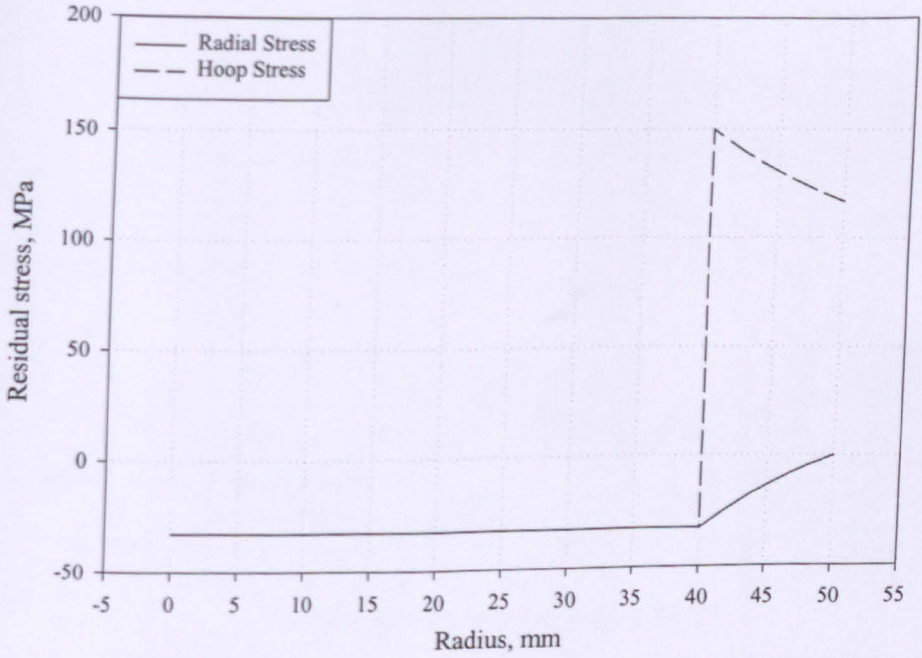

Figure 6.20. Predicted residual stress distribution in shrink-fit specimen 2

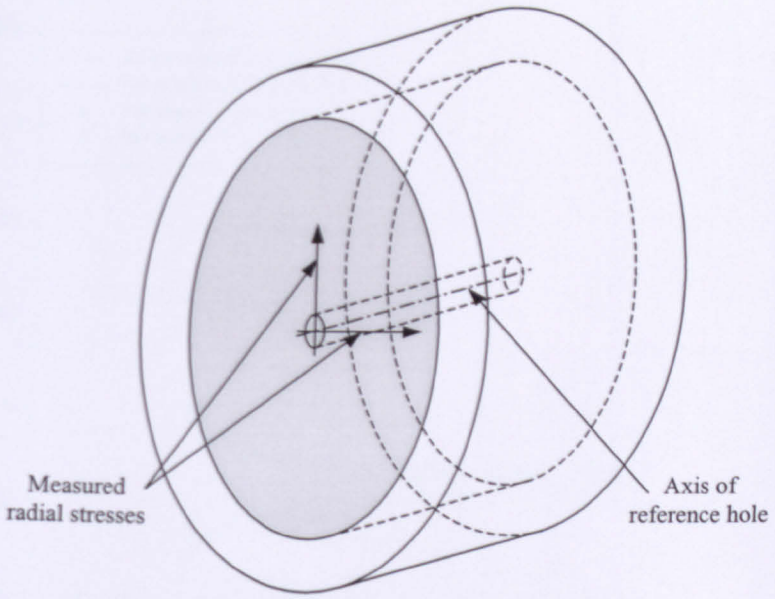

Figure 6.21. Location of the reference hole for the DHD measurement in shrink-fit specimen 2

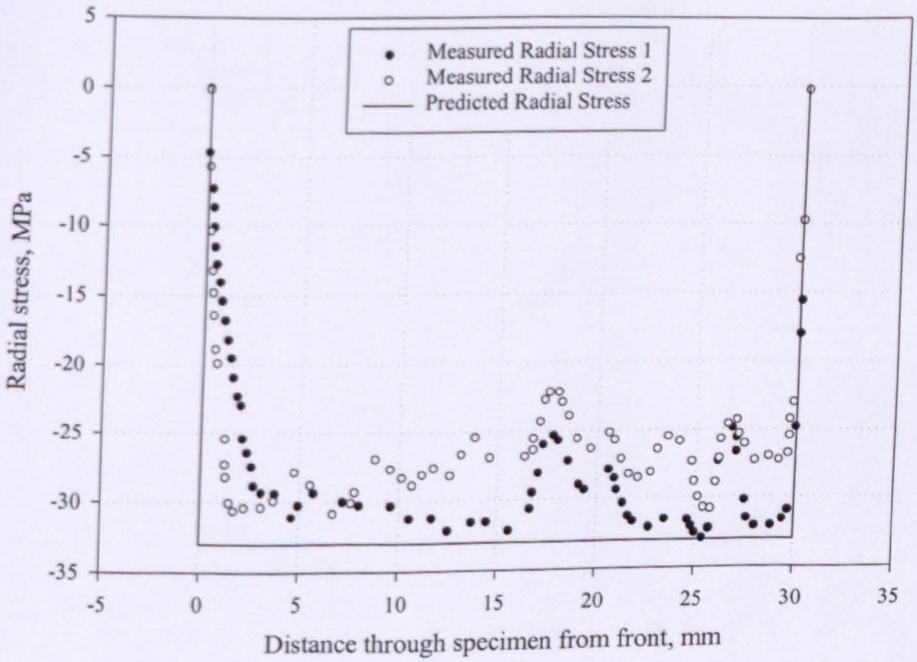

Figure 6.22. Predicted and deep-hole measured radial residual stress distributions in shrink-fit specimen 2

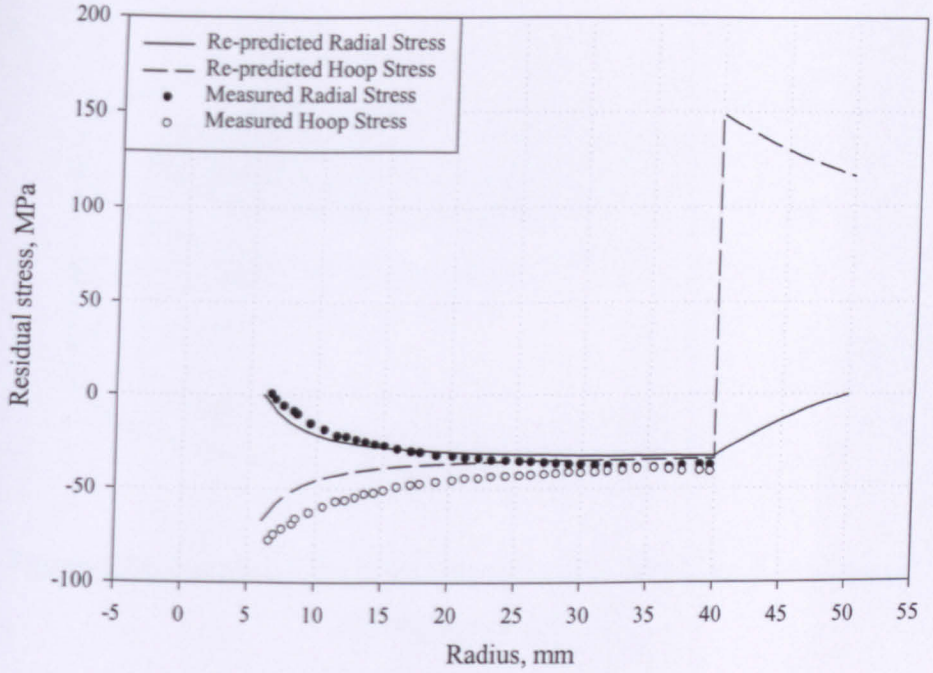

Figure 6.23. Re-predicted and Sachs measured residual stress distributions in shrink-fit specimen 2

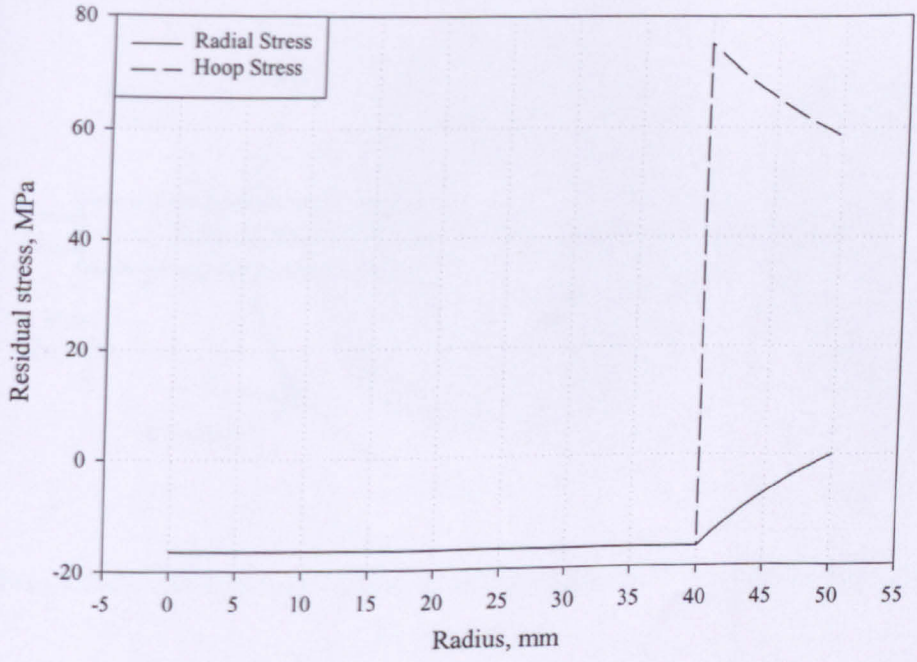

Figure 6.24. Predicted residual stress distribution in shrink-fit specimen 3

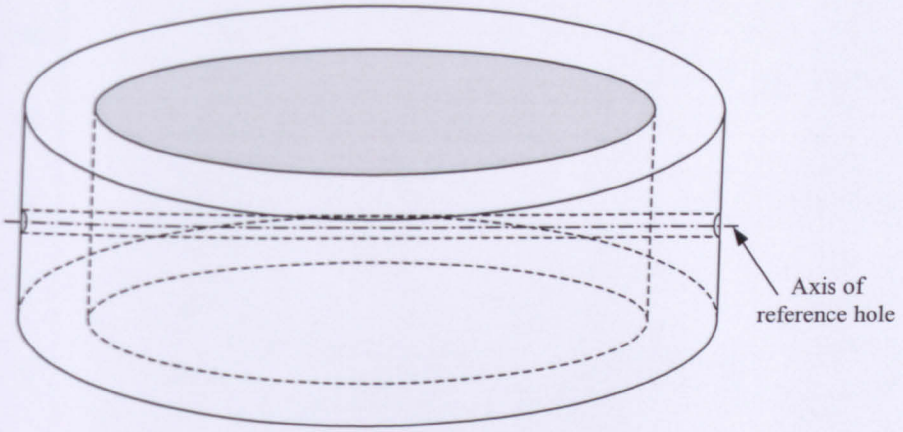

Figure 6.25. Location of the reference hole for the deep-hole measurement in shrink-fit specimen 3

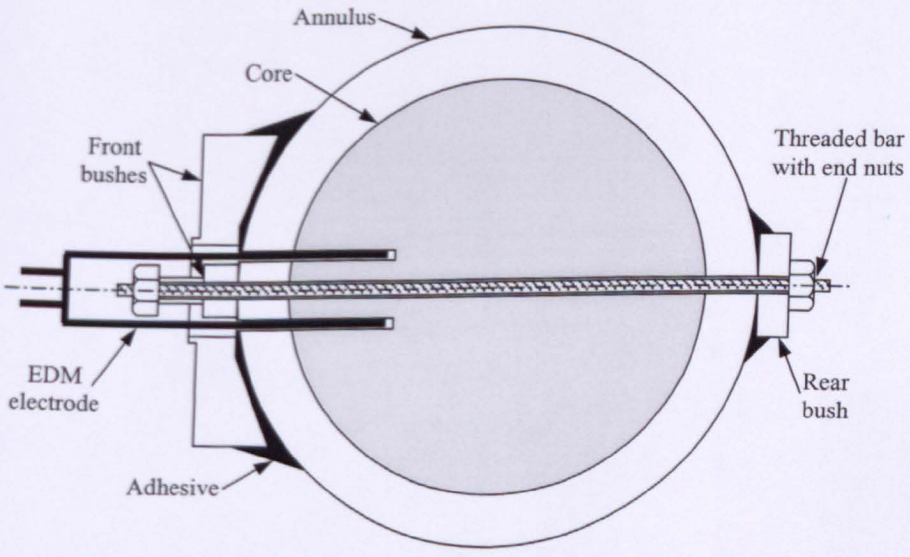

Figure 6.26. Cross-sectional view of the set-up of shrink-fit specimen 3 during the EDM process

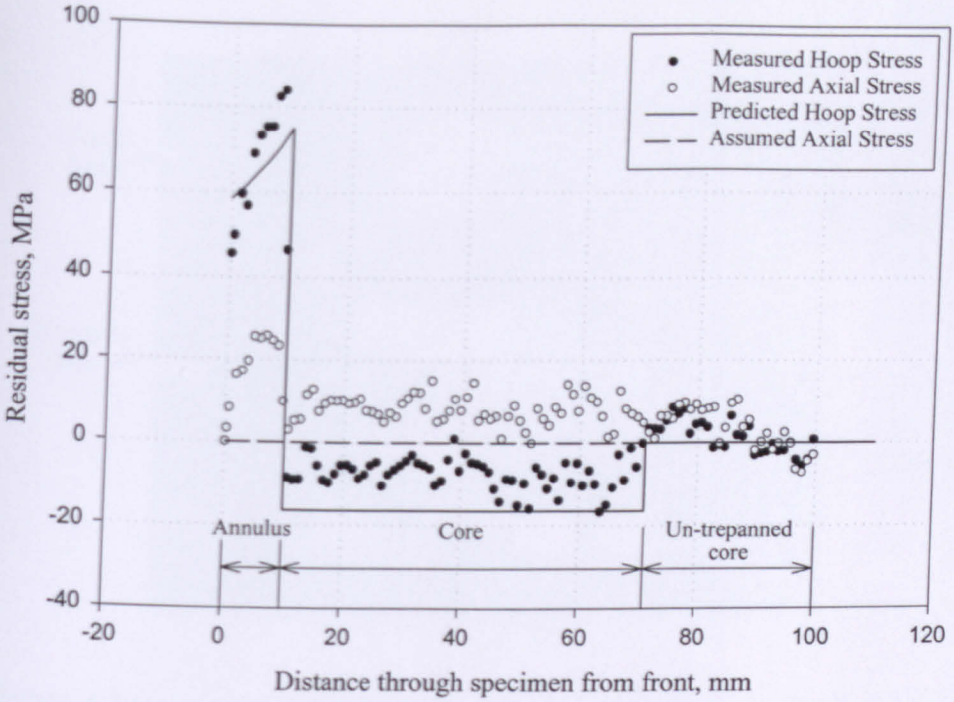

Figure 6.27. Predicted/assumed and deep-hole measured residual stress distributions in shrink-fit specimen 3

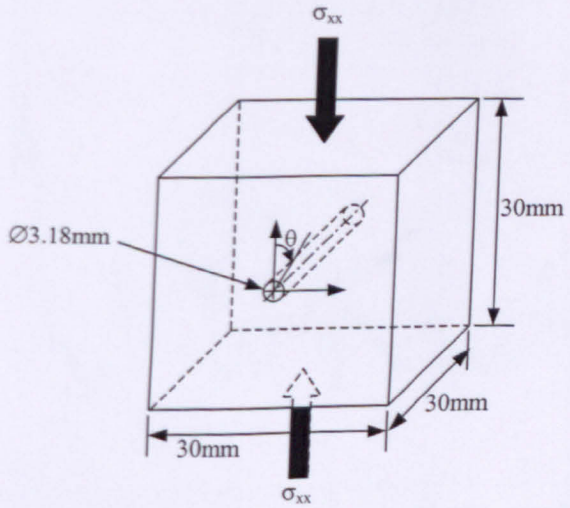

Figure 6.28. Schematic of the graphite block containing a reference hole under load

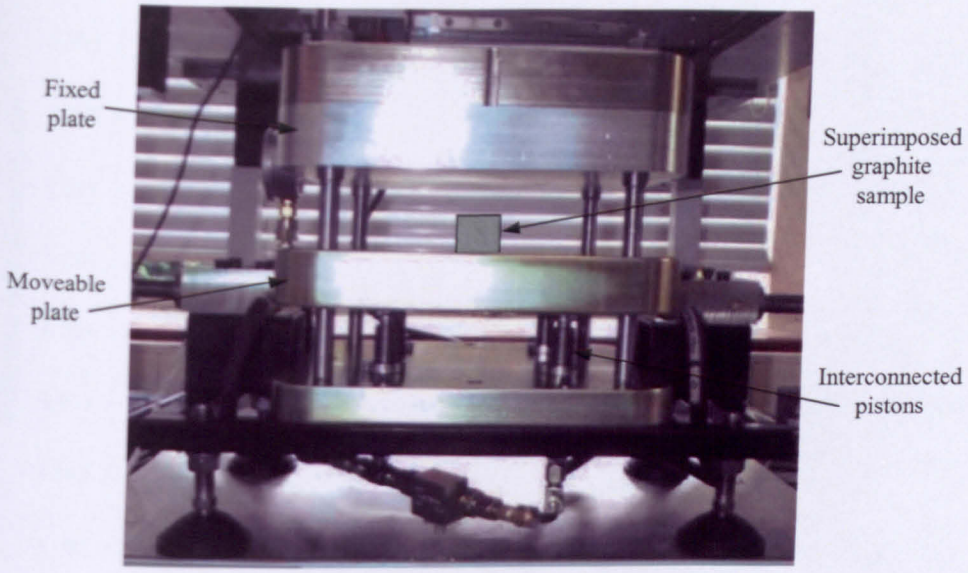

Figure 6.29. Machine used to apply the compressive loads on the graphite sample

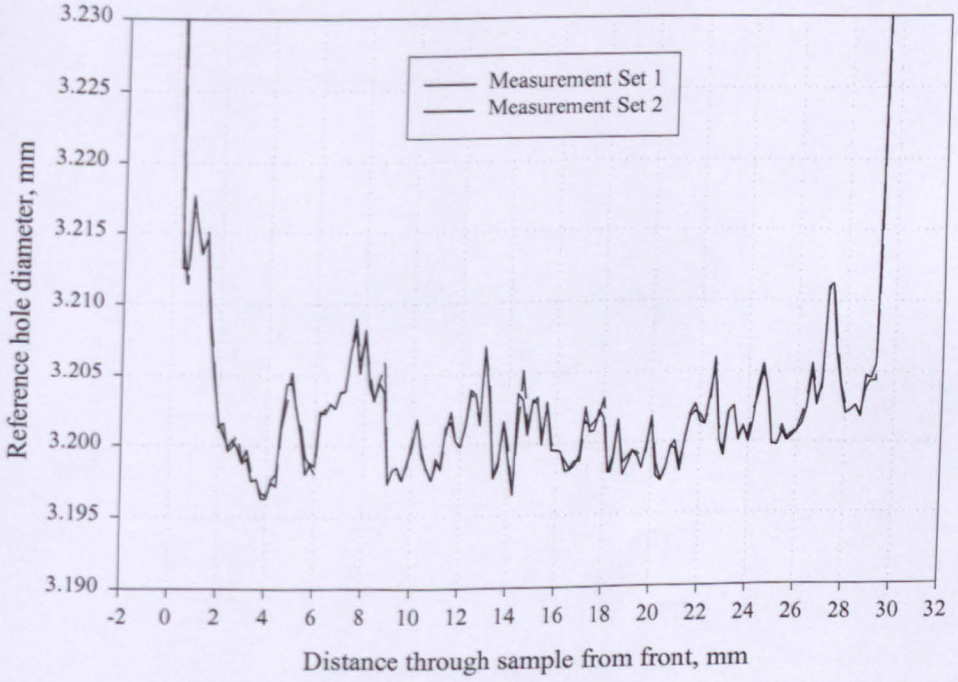

Figure 6.30. Repeated measurement of the reference hole diameter at 0°

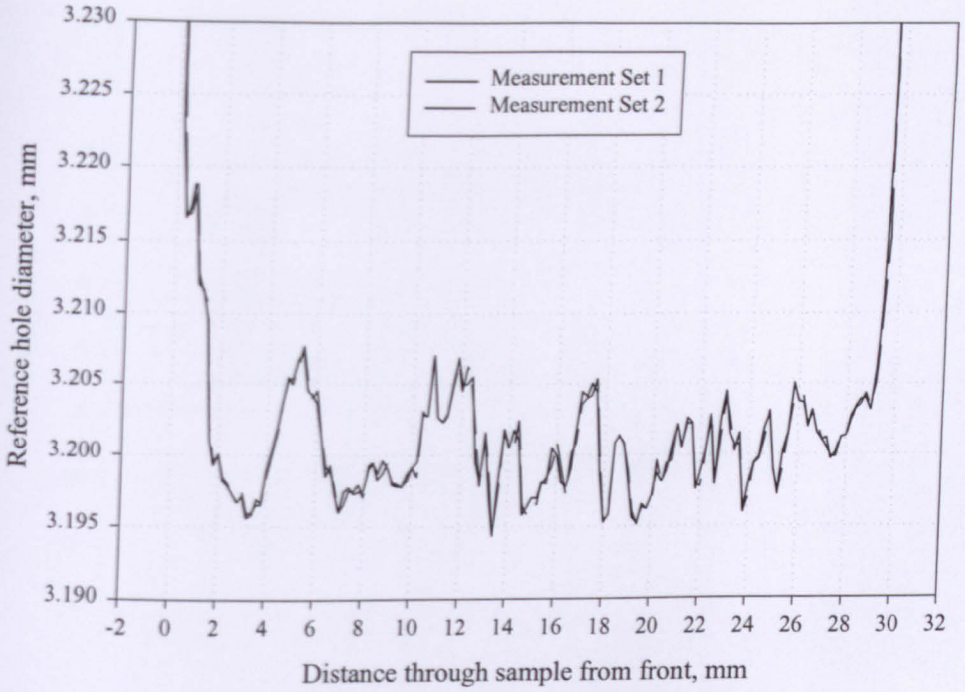

Figure 6.31. Repeated measurement of the reference hole diameter at 90°

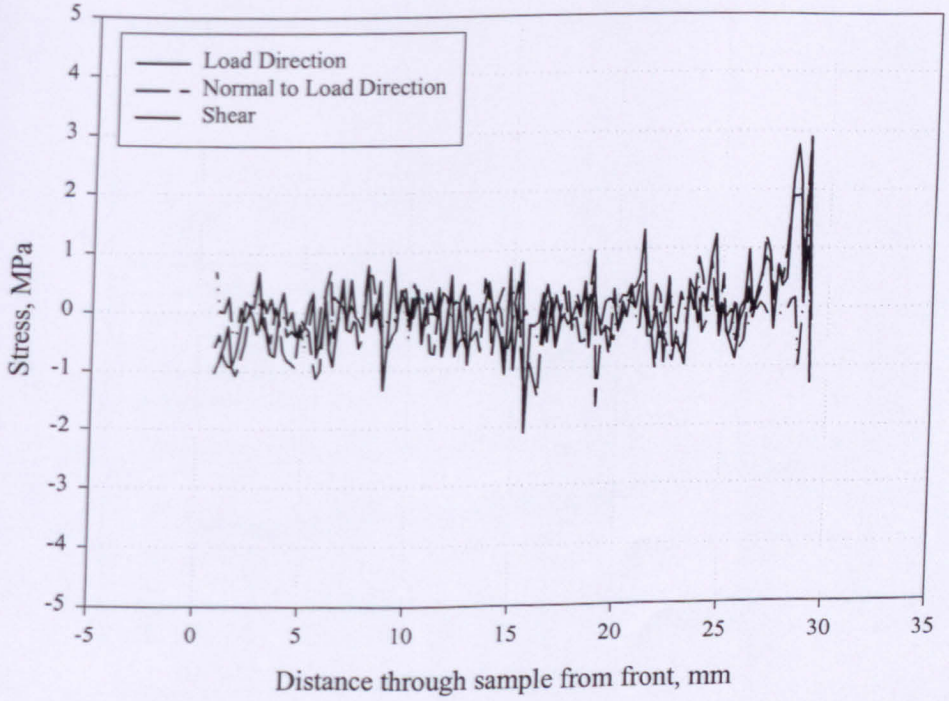

Figure 6.32. Calculated stress error associated with measurement sets 1 and 2

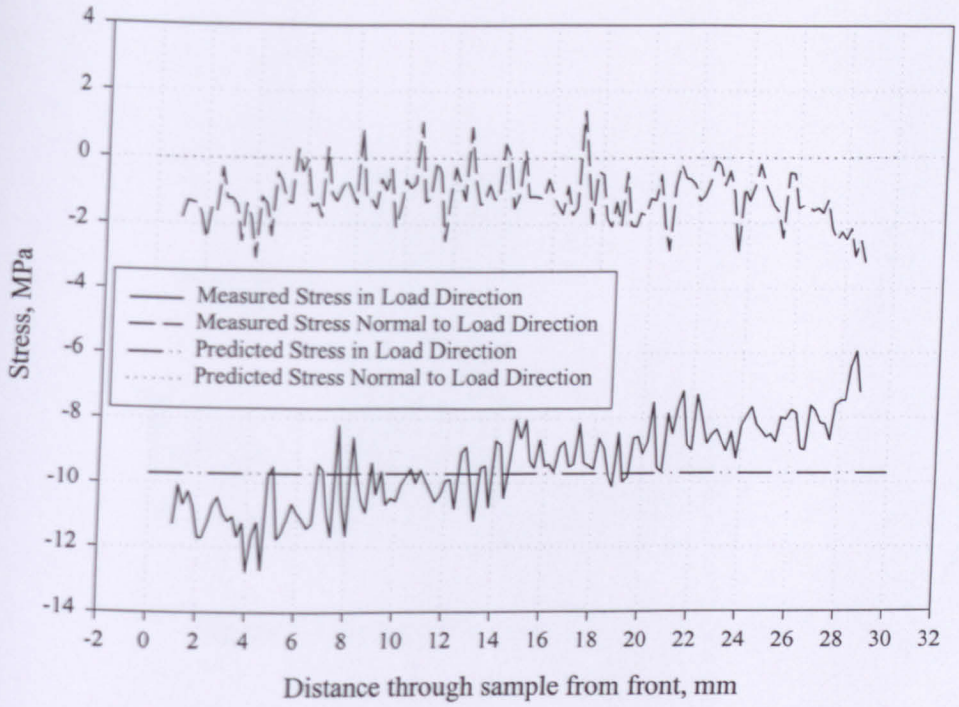

Figure 6.33. Measured and predicted stress for test 2

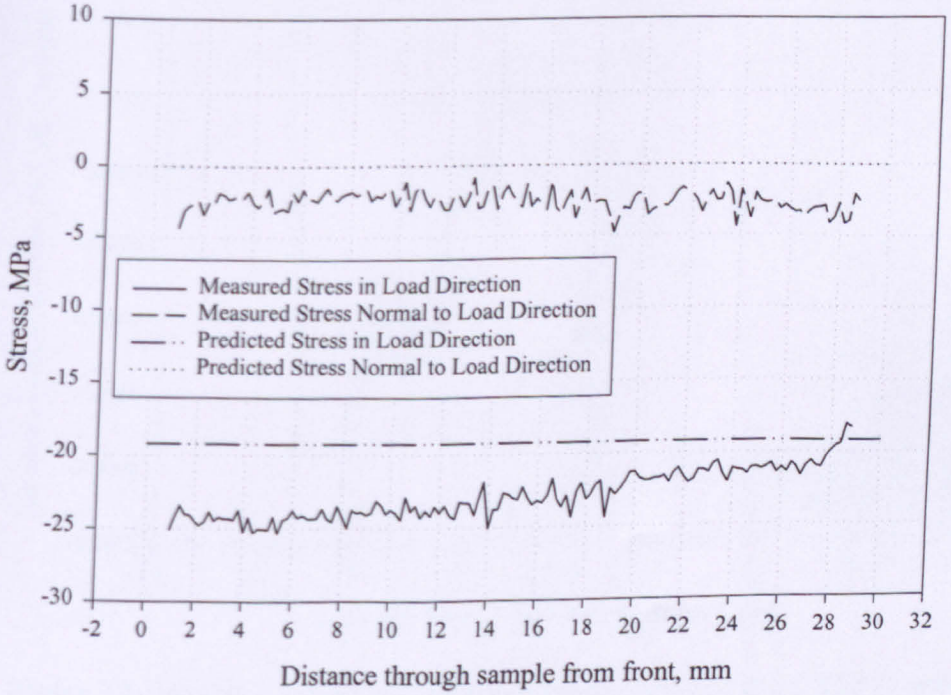

Figure 6.34. Measured and predicted stress for test 3

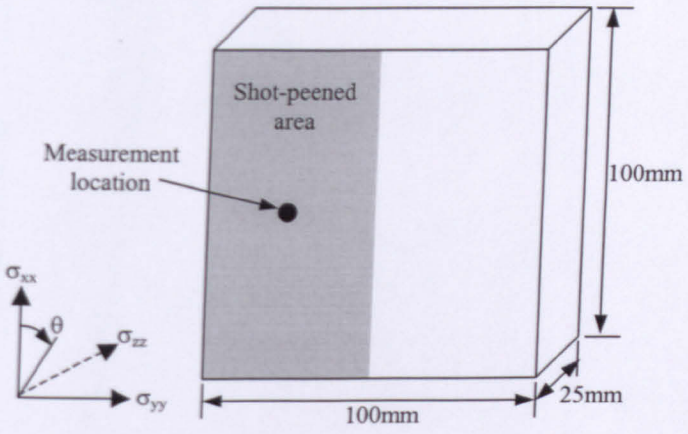

Figure 7.1. Design of the shot-peened component

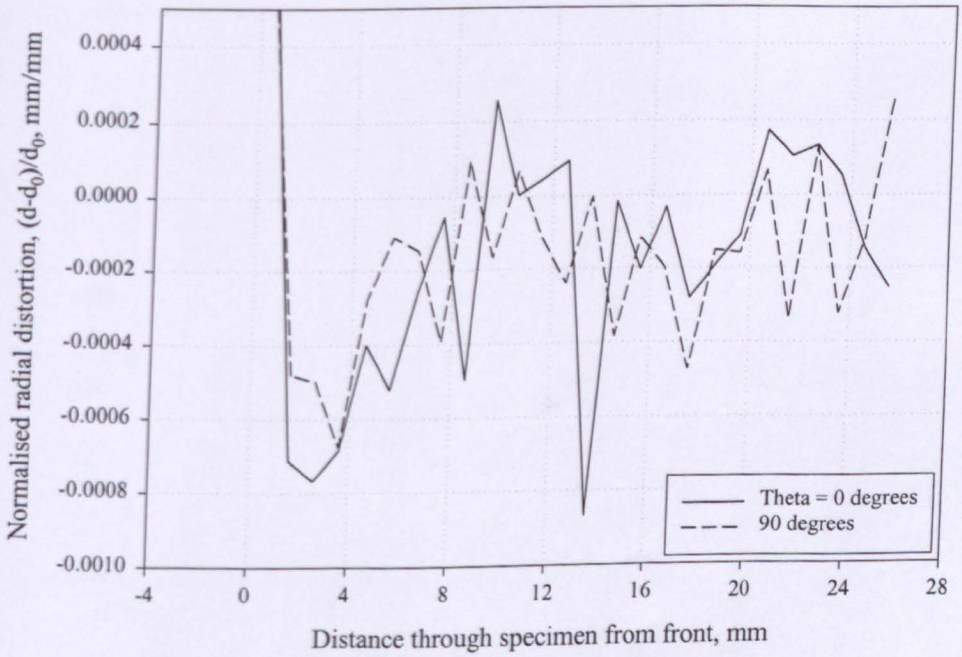

Figure 7.2. Smoothed normalised radial distortions measured in the shot-peened component

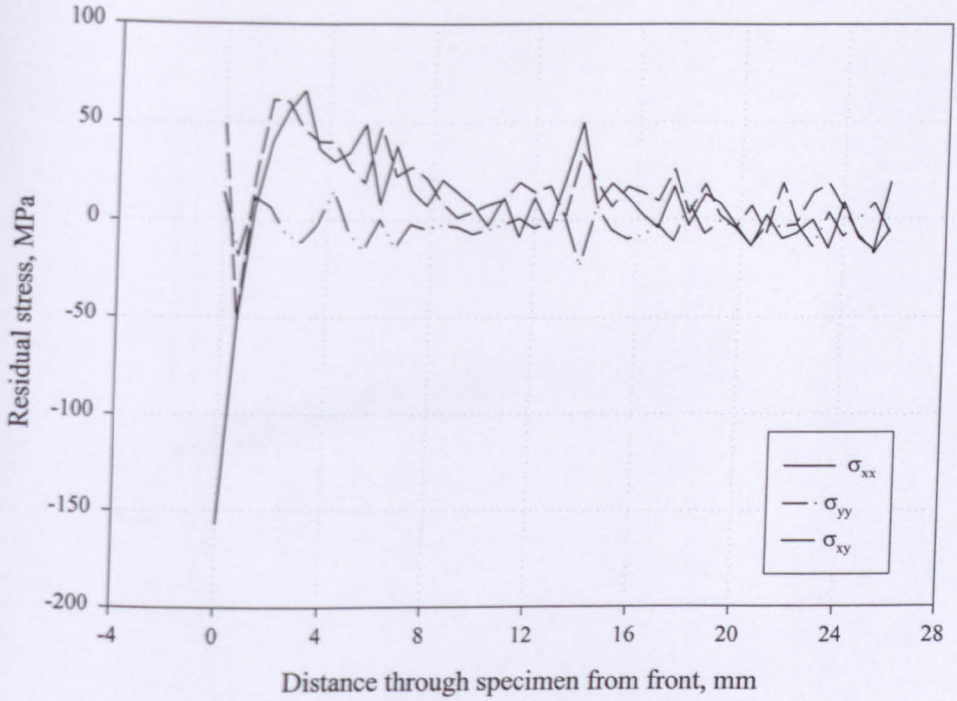

Figure 7.3. Smoothed residual stresses measured in the shot-peened component

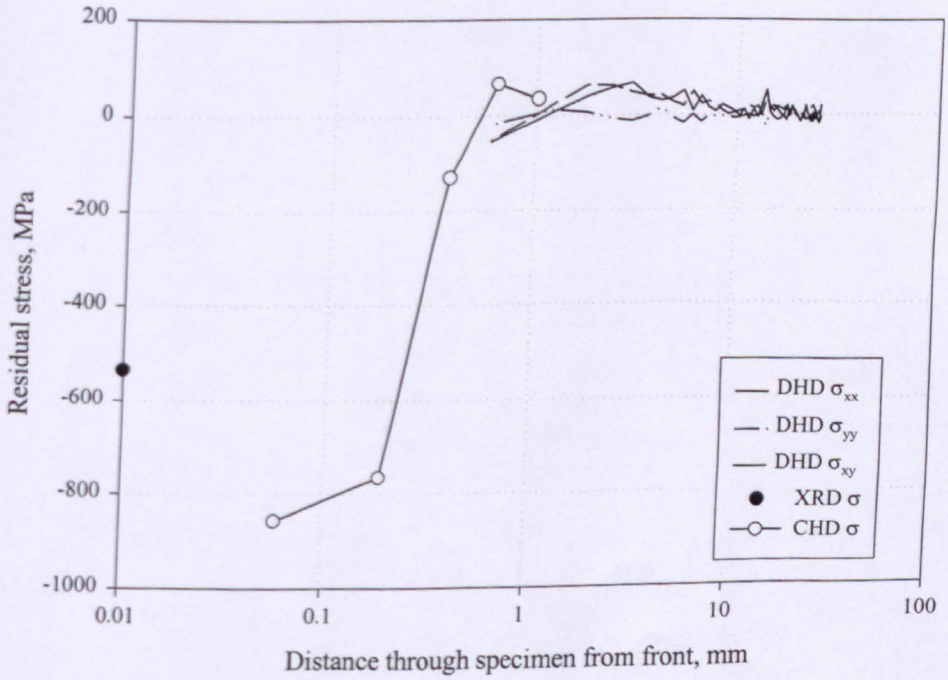

Figure 7.4. Residual stresses measured using DHD, XRD and CHD in the shot-peened component

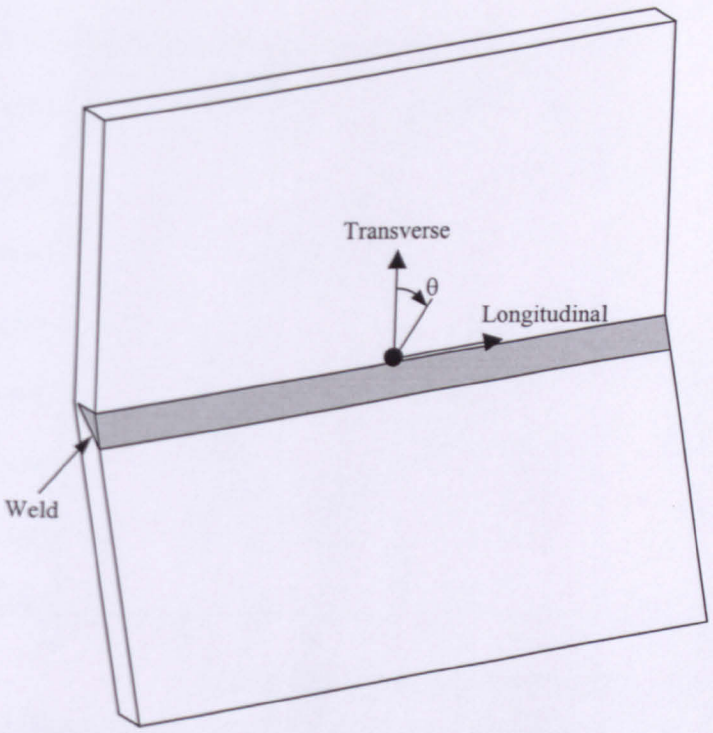

Figure 7.5. Design of the partial depth welded plate

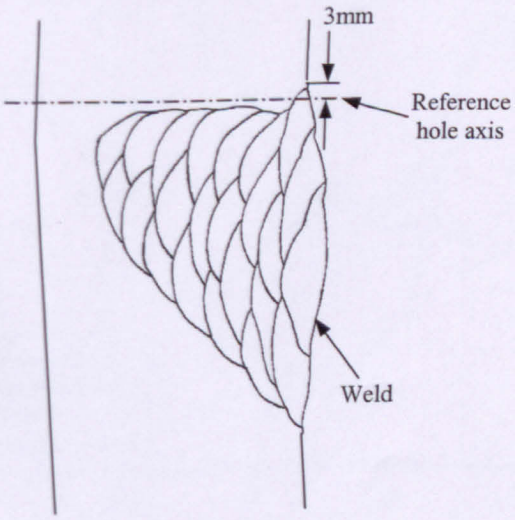

Figure 7.6. Axis of reference hole through partial depth welded plate

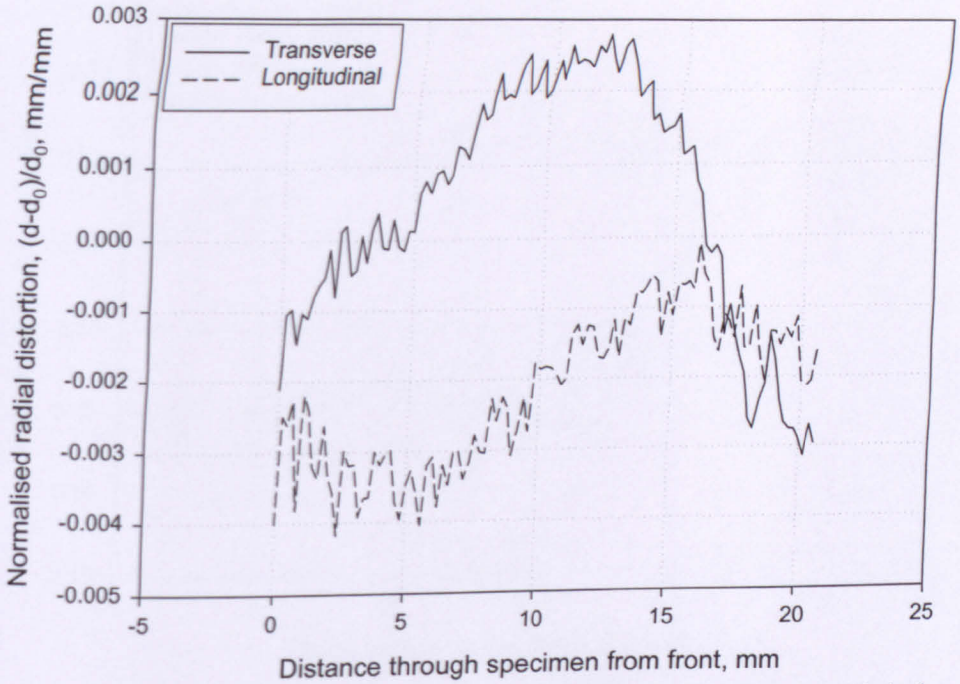

Figure 7.7. Normalised radial distortions measured in the partial depth welded plate

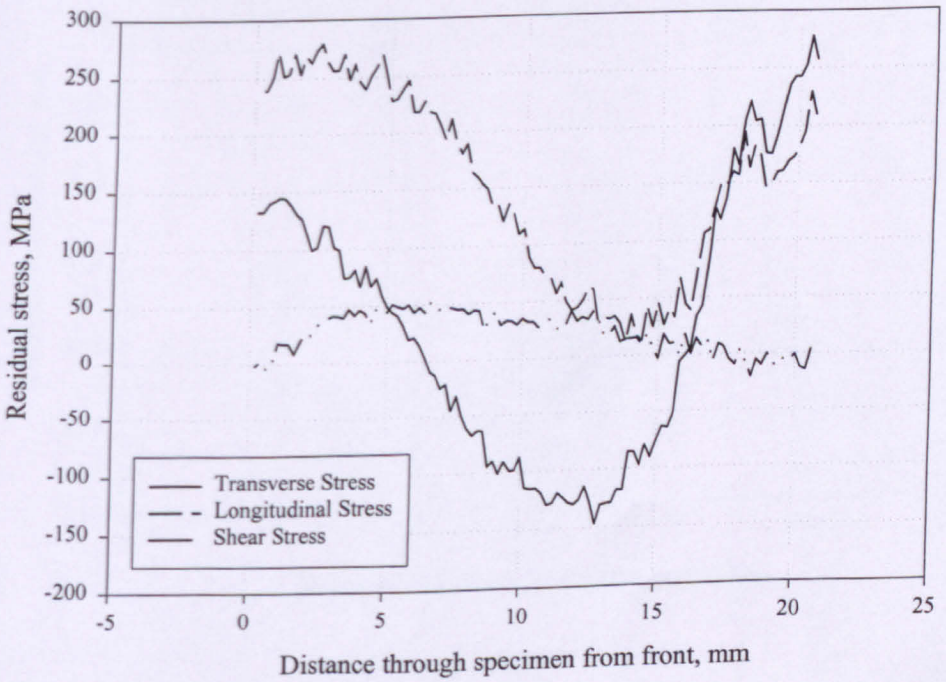

Figure 7.8. Residual stresses measured in the partial depth welded plate

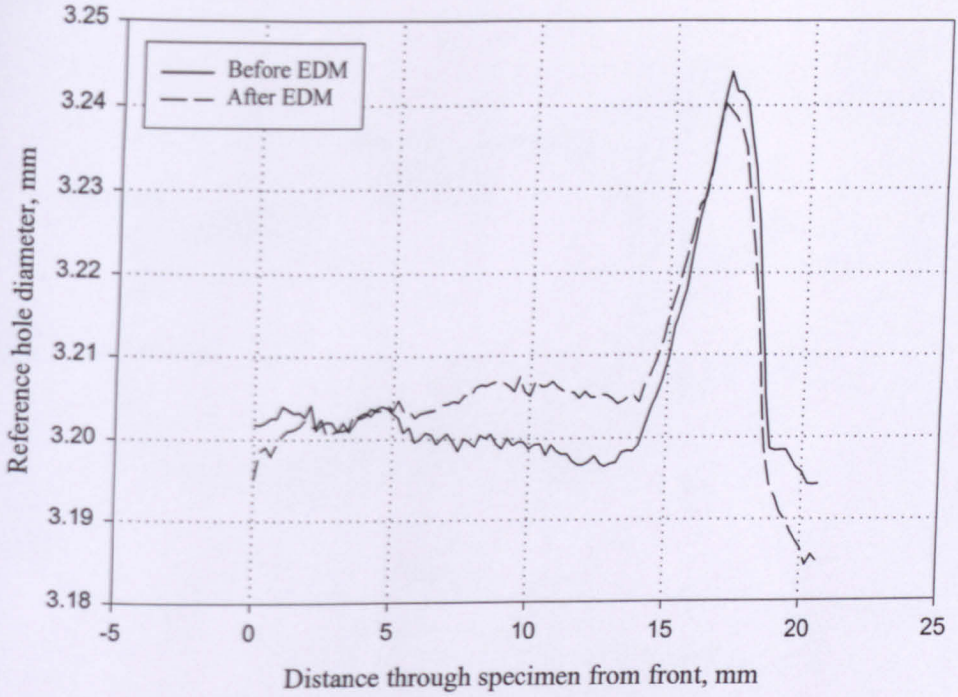

a) Diameter at $\theta = 0°$

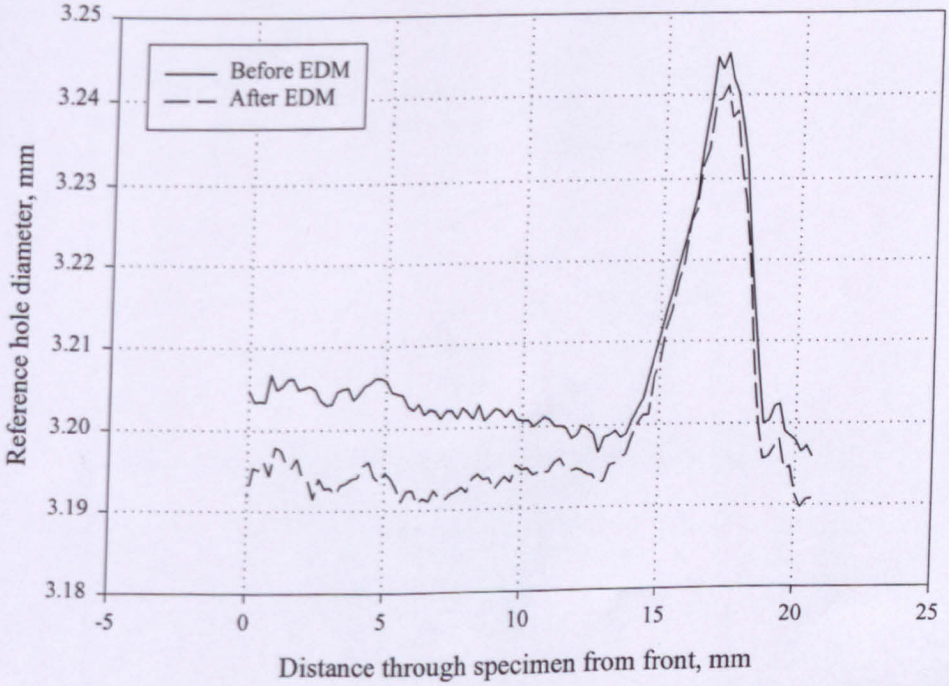

b) Diameter at $\theta = 90°$

Figure 7.9. Measured reference hole diameter in the partial depth welded plate

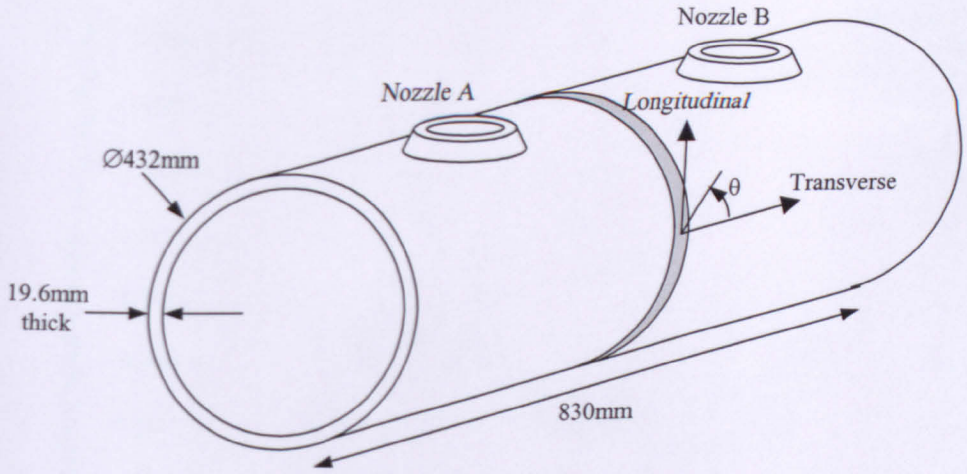

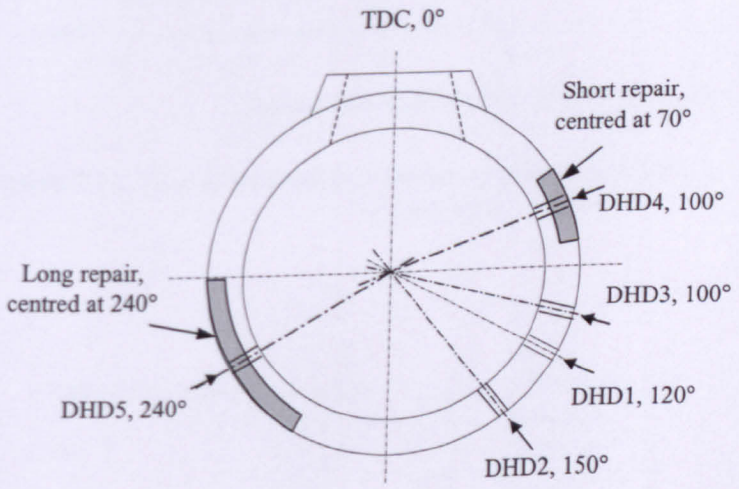

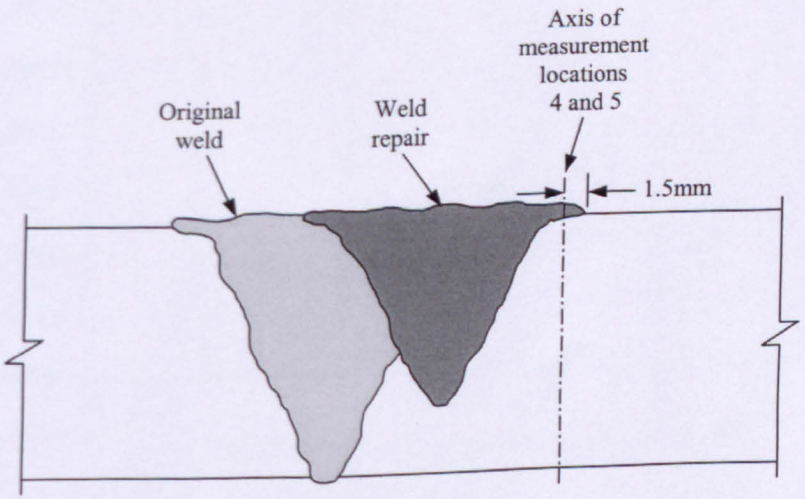

Figure 7.10. Design of the butt-welded pipe, 19mm wall thickness

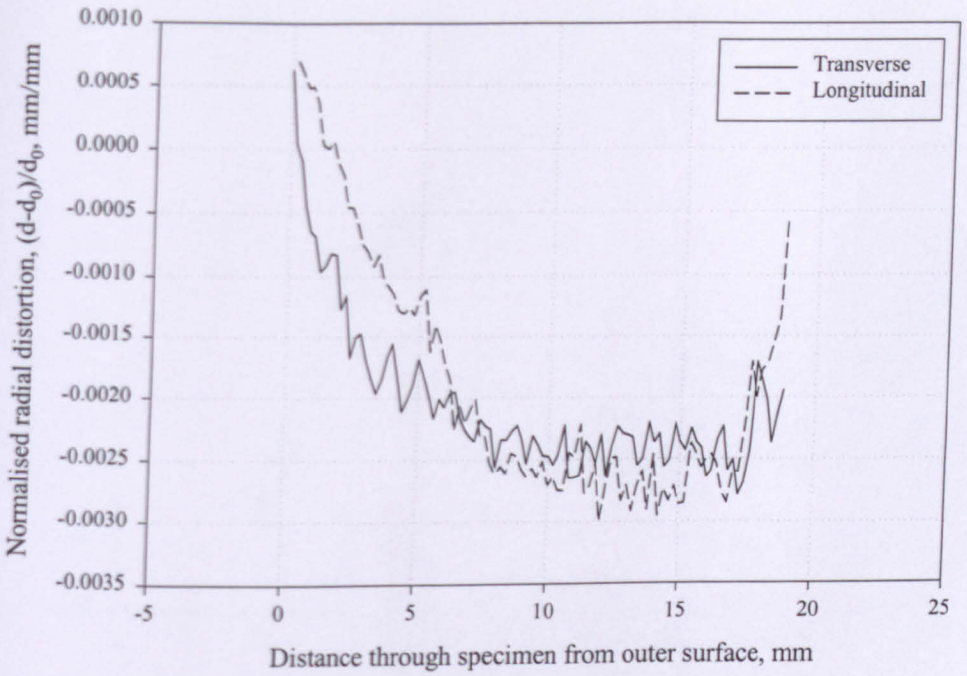

Figure 7.11. Normalised radial distortions measured in the butt-welded pipe at location 4

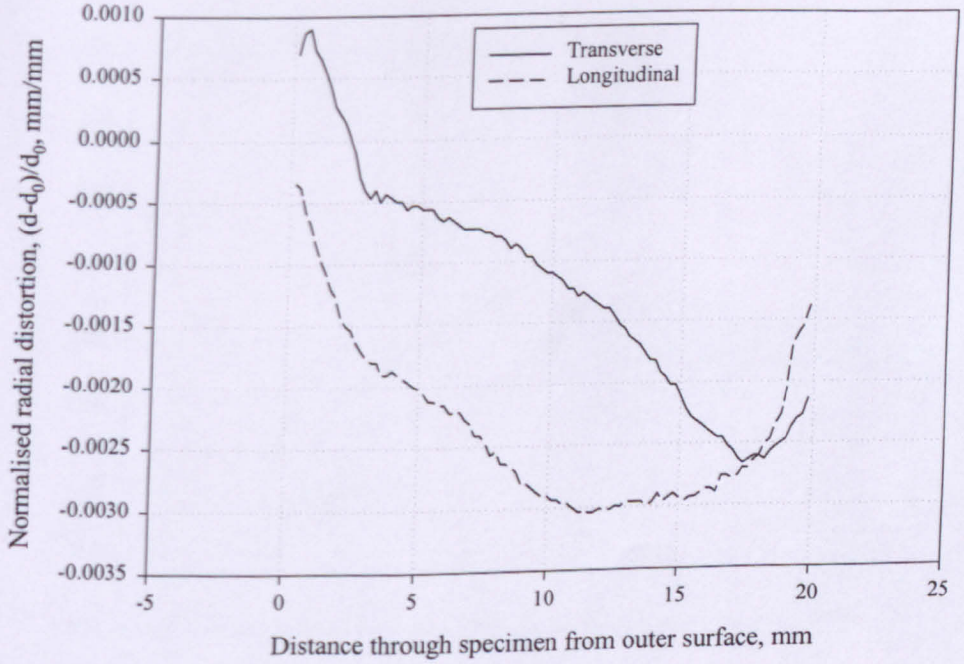

Figure 7.12. Normalised radial distortions measured in the butt-welded pipe at location 5

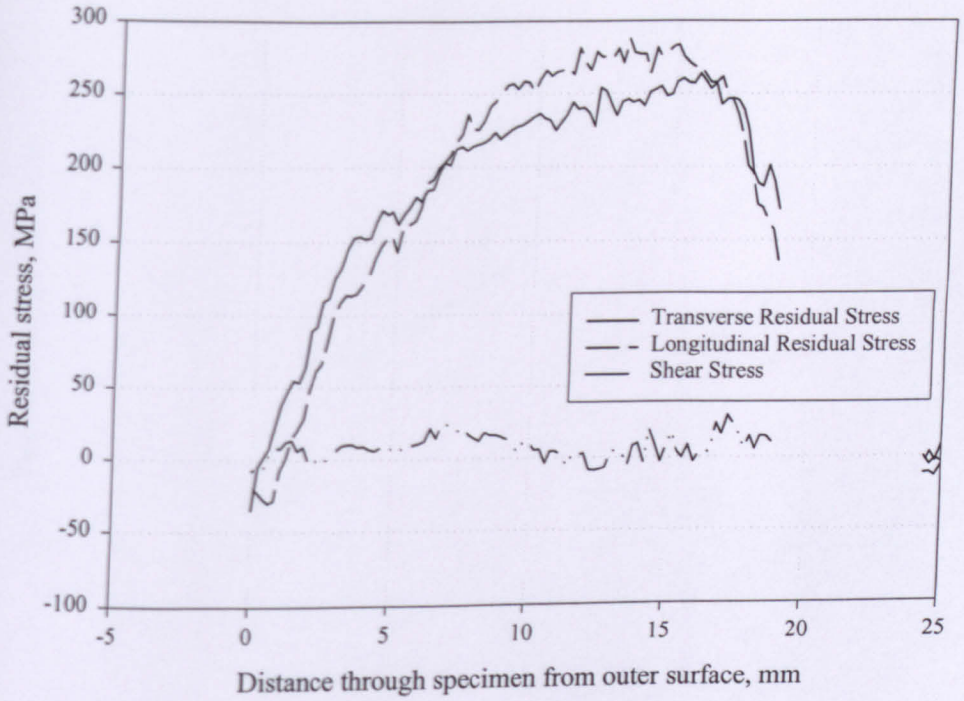

Figure 7.13. Measured residual stresses in the butt-welded pipe at location 4

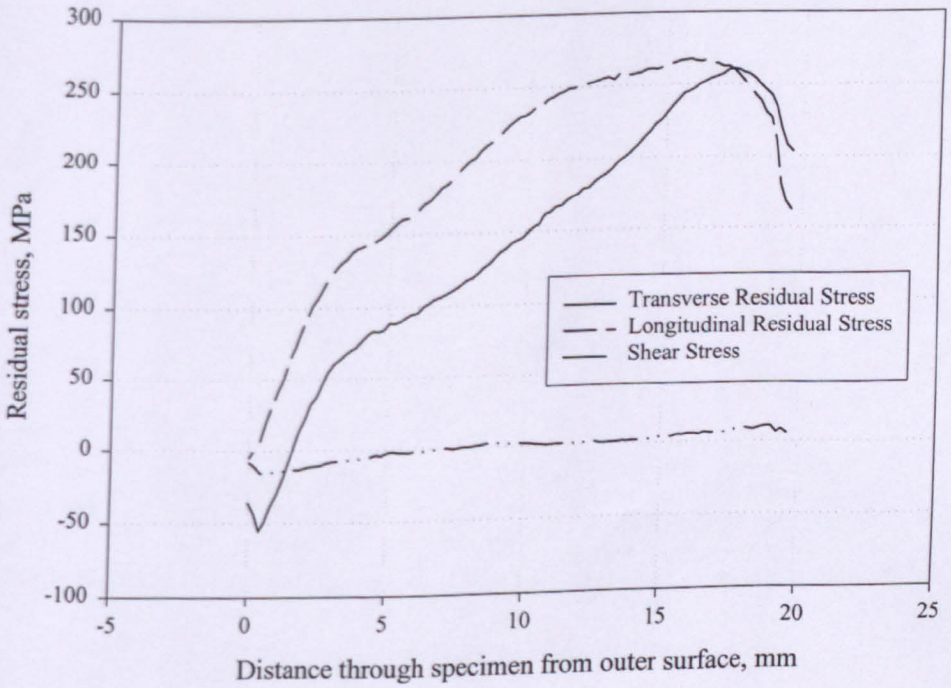

Figure 7.14. Measured residual stresses in the butt-welded pipe at location 5

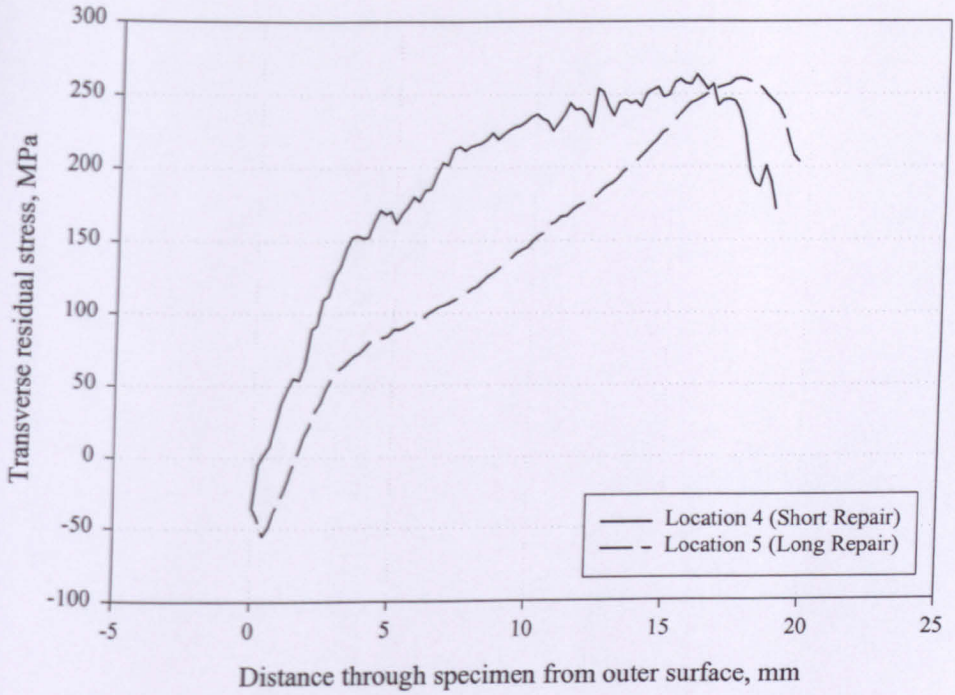

Figure 7.15. Measured transverse residual stresses in the butt-welded pipe

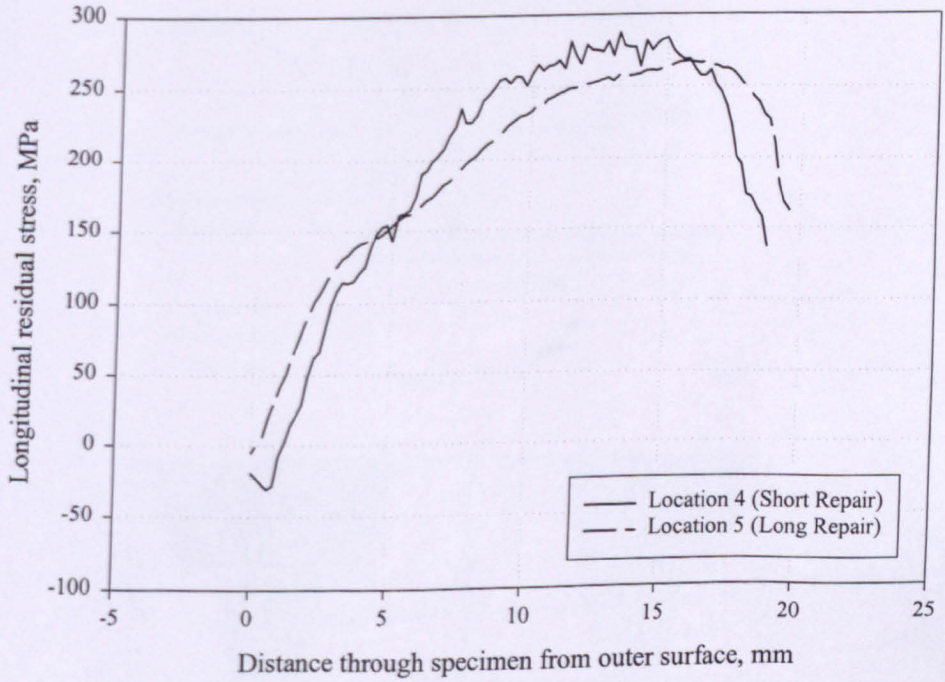

Figure 7.16. Measured longitudinal residual stresses in the butt-welded pipe

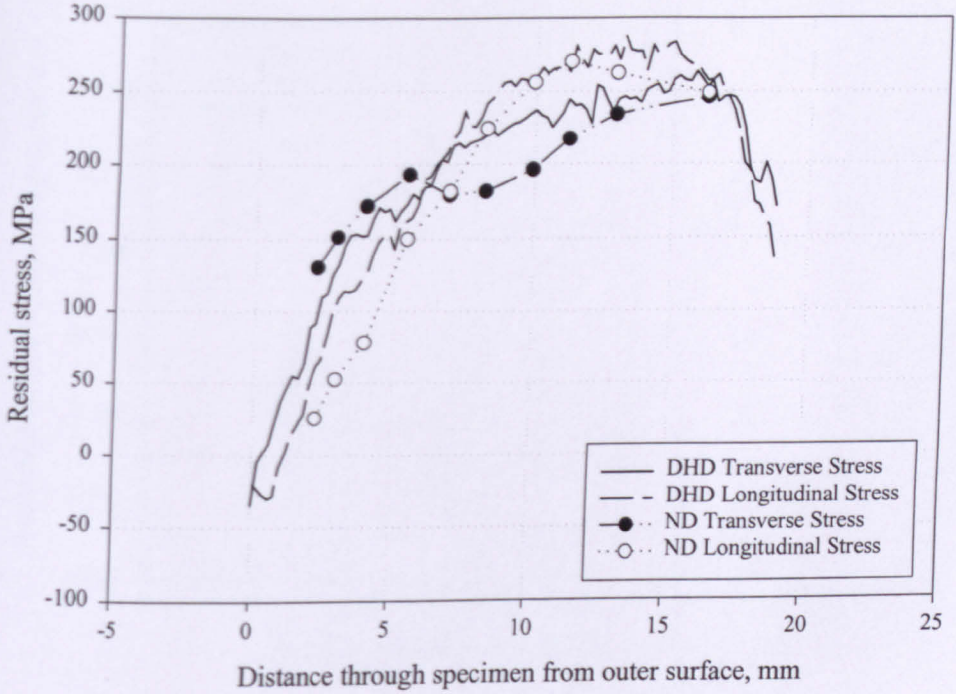

Figure 7.17. Measured residual stresses using DHD and ND in the butt-welded pipe at location 4

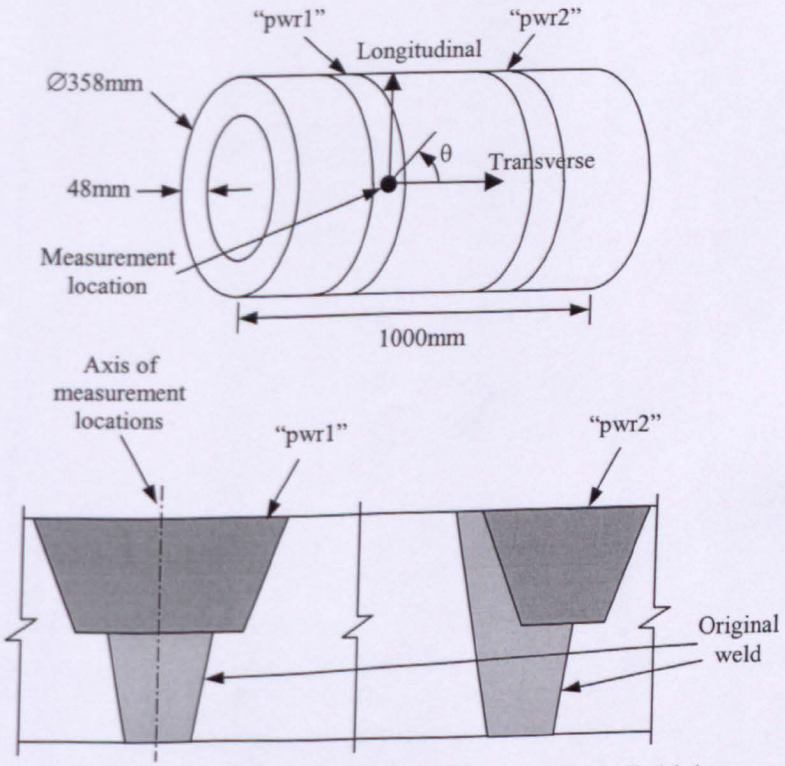

Figure 7.18. Design of the butt-welded pipe, 48mm wall thickness

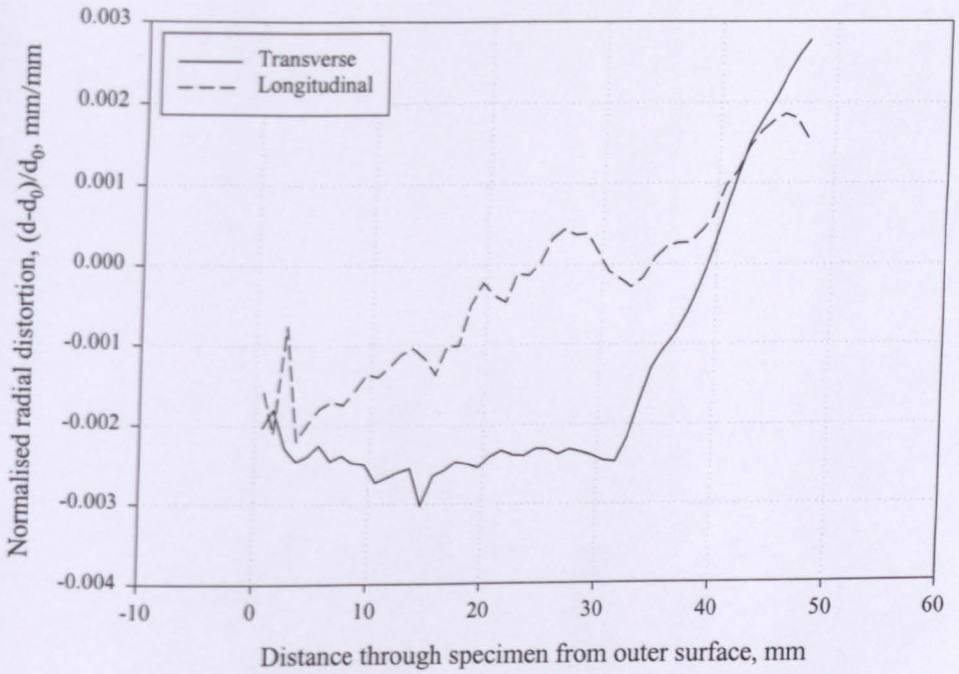

Figure 7.19. Smoothed normalised radial distortions measured in "pwr1" of the butt-welded pipe

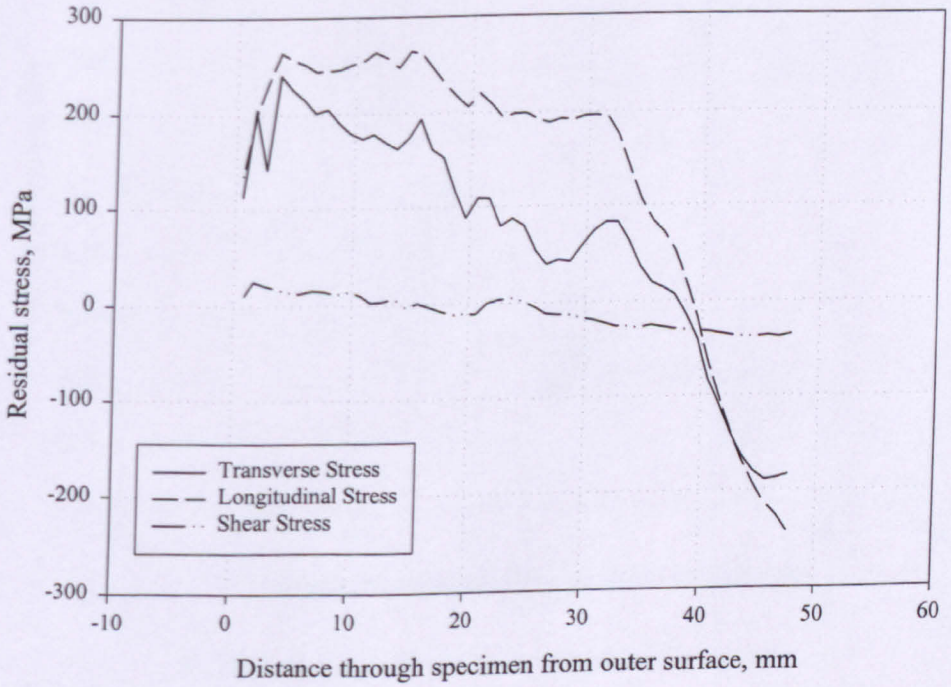

Figure 7.20. Smoothed residual stresses measured in "pwr1" of the butt-welded pipe

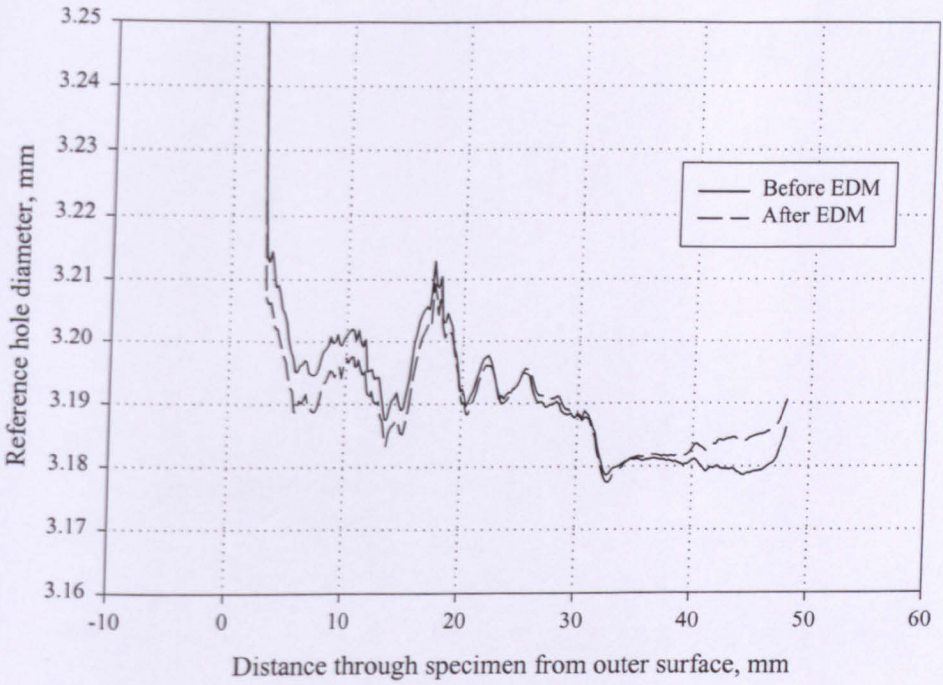

a) Diameter at $\theta = 0°$ (i.e. transverse direction)

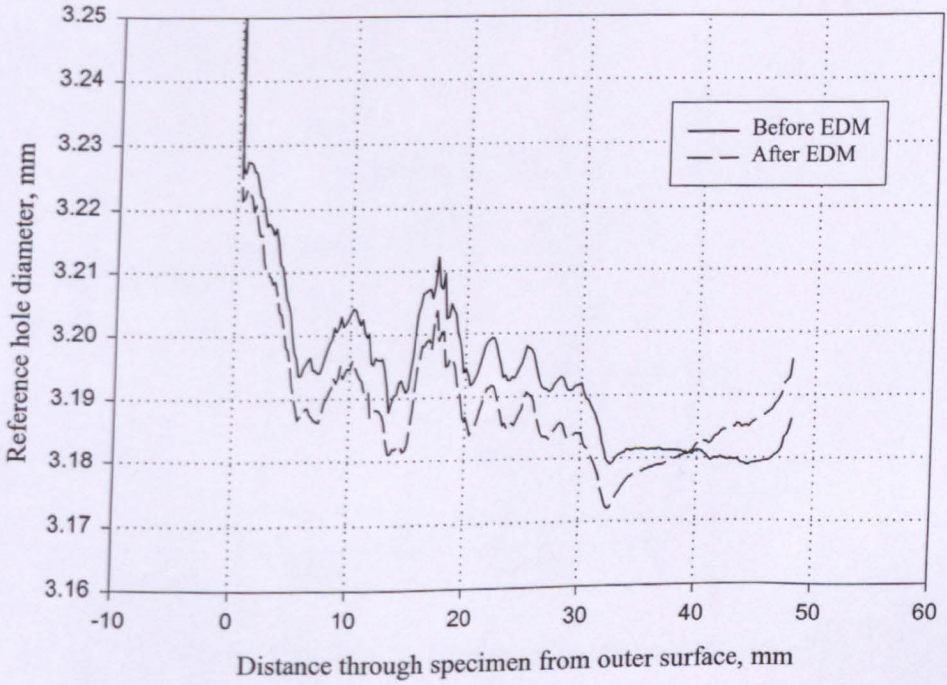

b) Diameter at $\theta = 90°$ (i.e. longitudinal direction)

Figure 7.21. Measured reference hole diameter of the butt-welded pipe

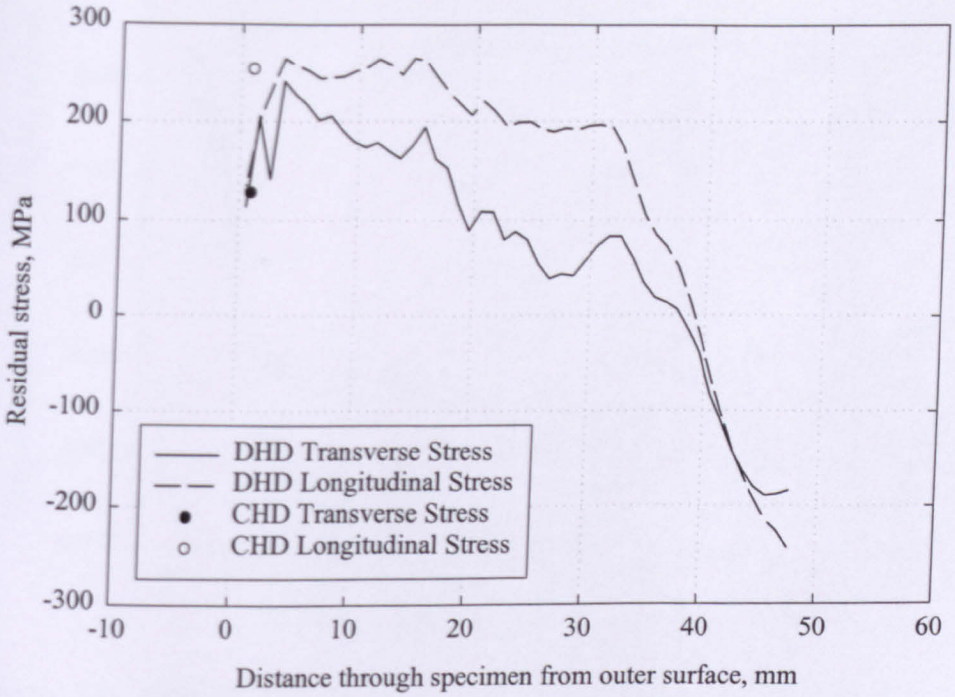

Figure 7.22. Measured residual stresses in "pwr1" using DHD and CHD

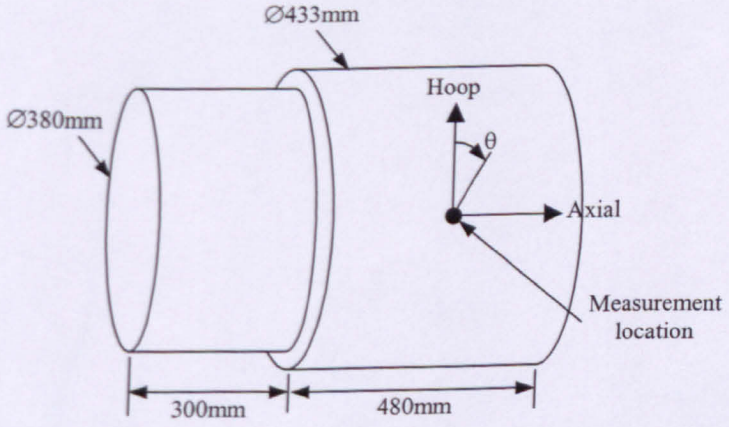

Figure 7.23. Design of the mini mock-up steel roll

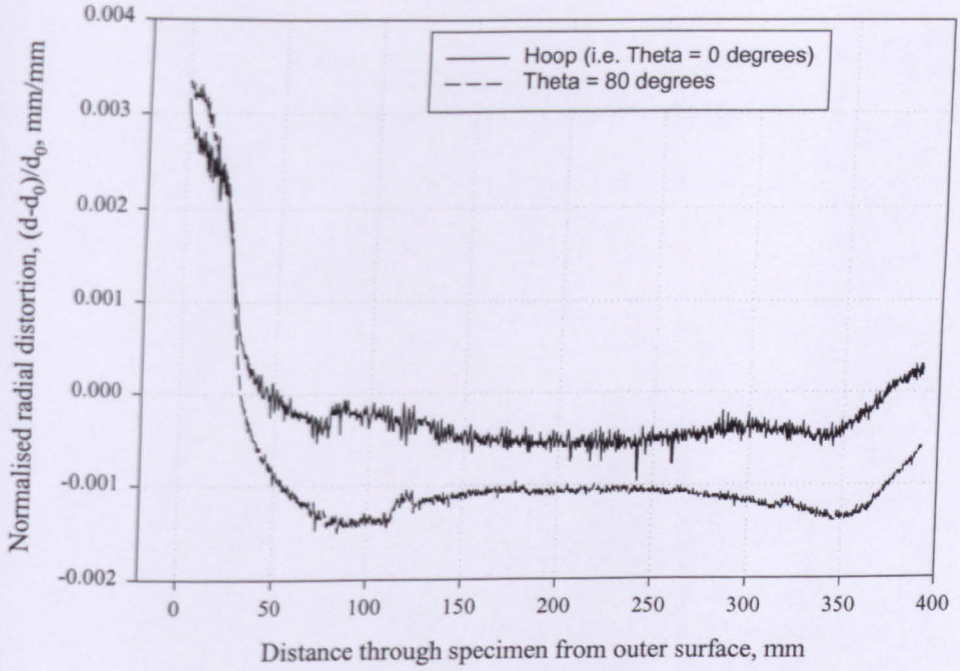

Figure 7.24. Measured normalised radial distortions in the mini mock-up steel roll

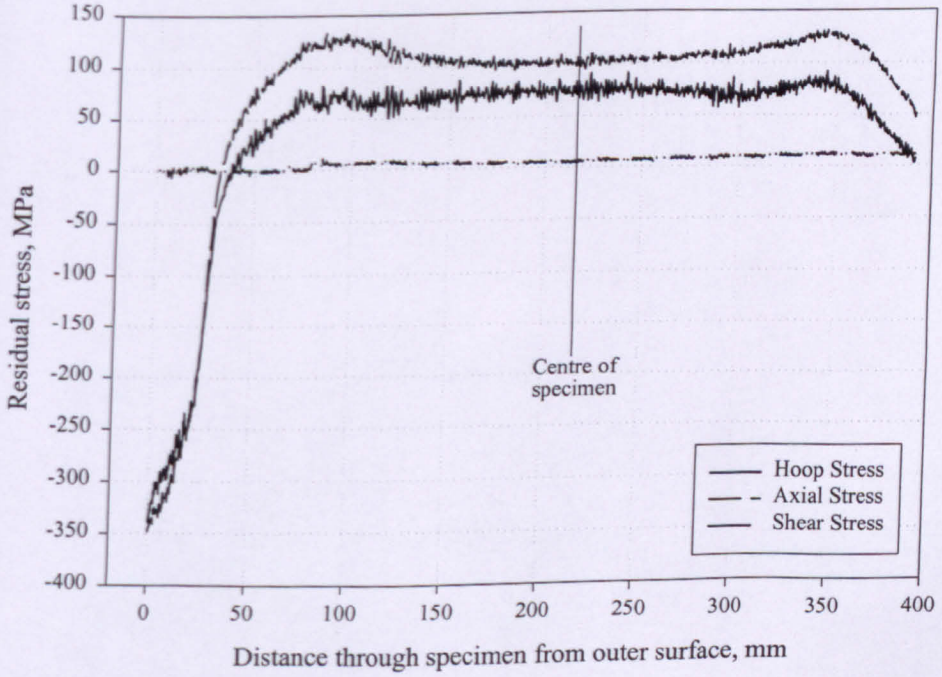

Figure 7.25. Measured residual stresses in the mini mock-up steel roll

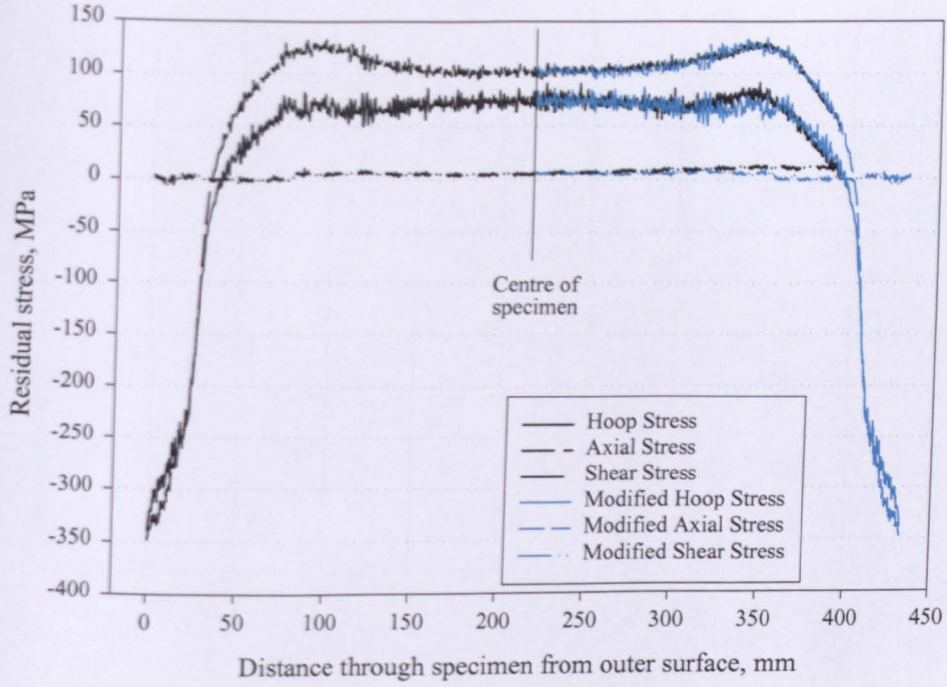

Figure 7.26. Symmetrically modified residual stresses in the mini mock-up steel roll

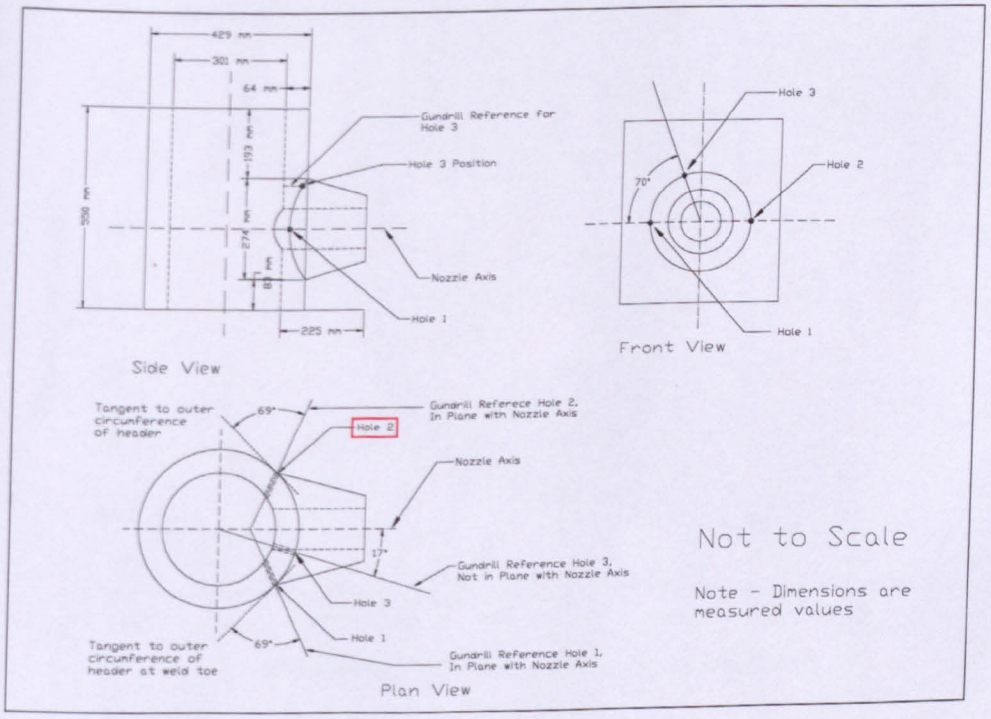

Figure 7.27. Design of nozzle-pipe T-section (S4) (Source: Smith et al, [2002])

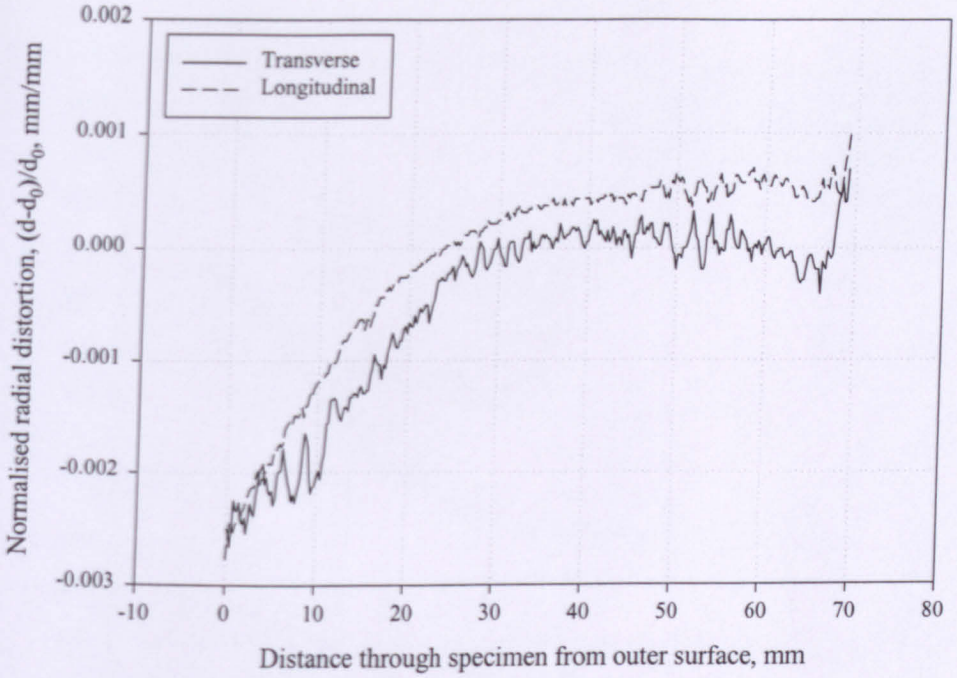

Figure 7.28. Measured normalised radial distortions in hole 2 of the nozzle-pipe T-section (S4)

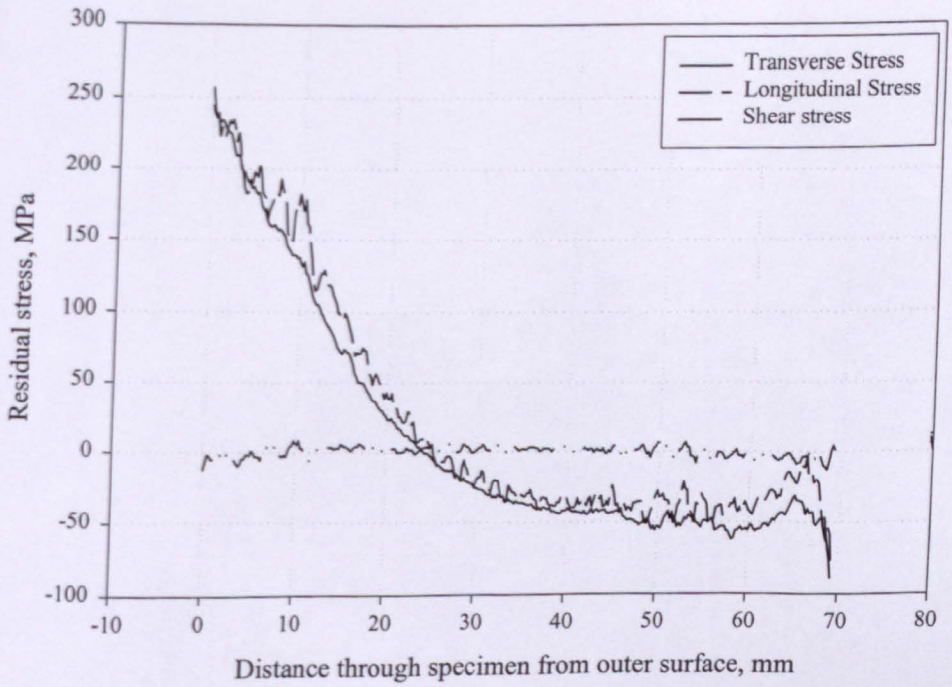

Figure 7.29. Measured residual stresses in hole 2 of the nozzle-pipe T-section (S4)

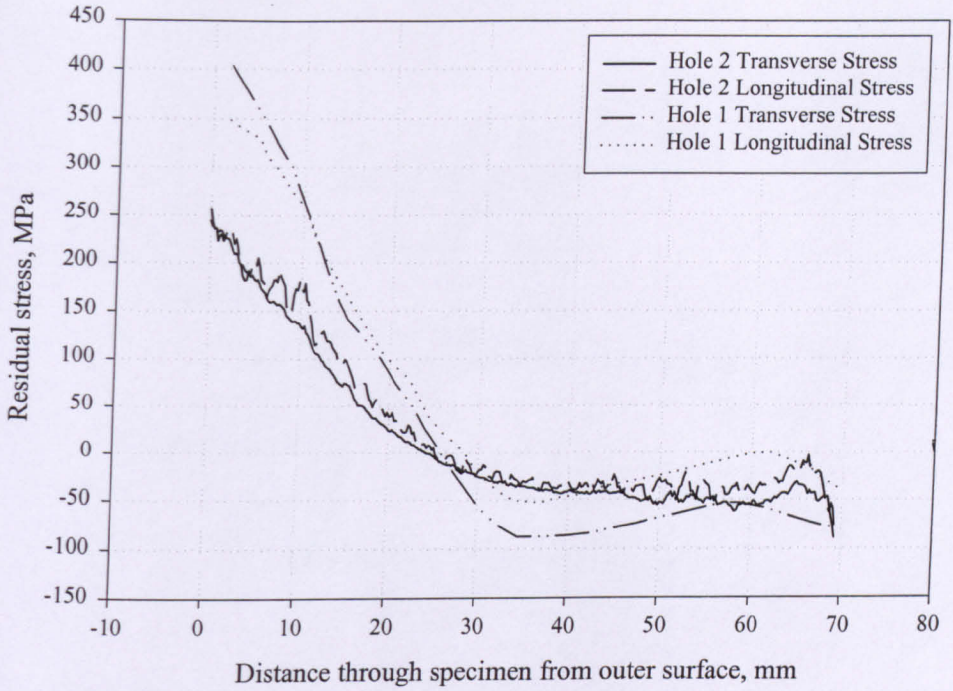

Figure 7.30. Measured residual stresses in nozzle-pipe T-section at holes 1 and 2

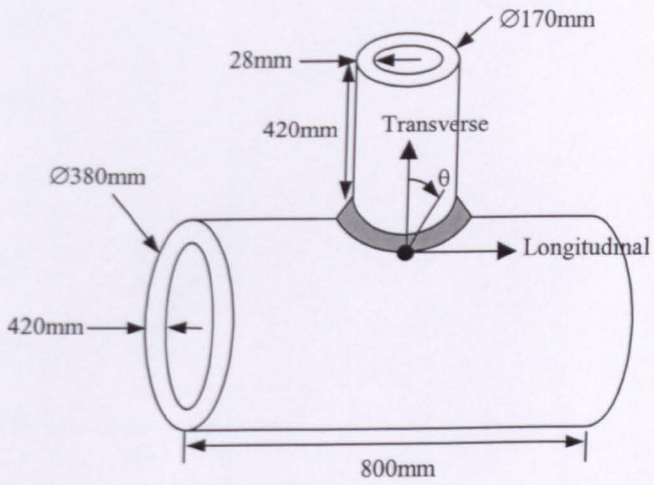

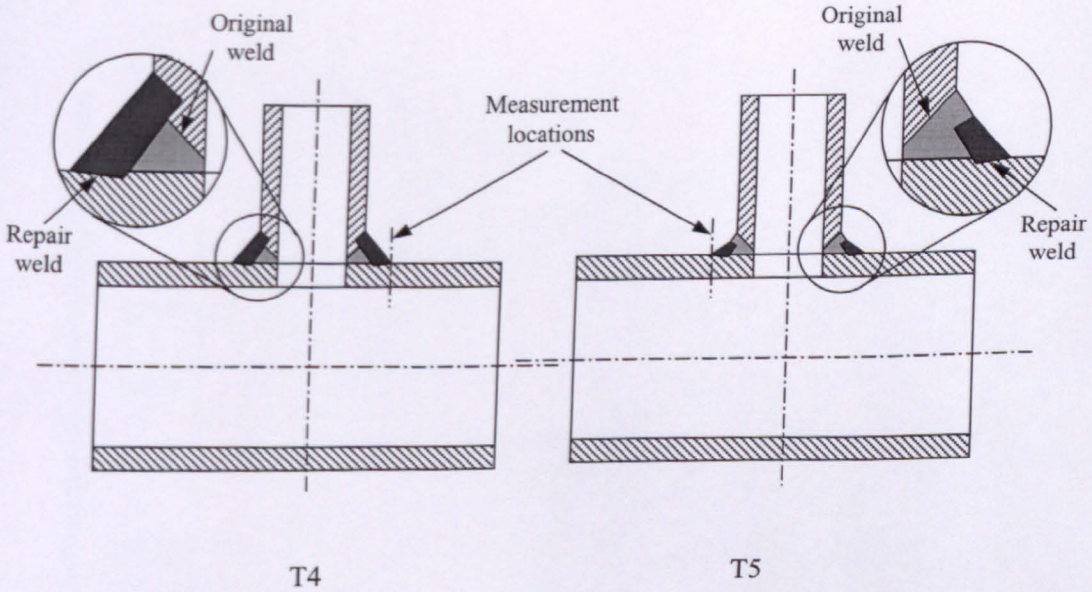

Figure 7.31. Design of the nozzle-pipe T-section (P22)

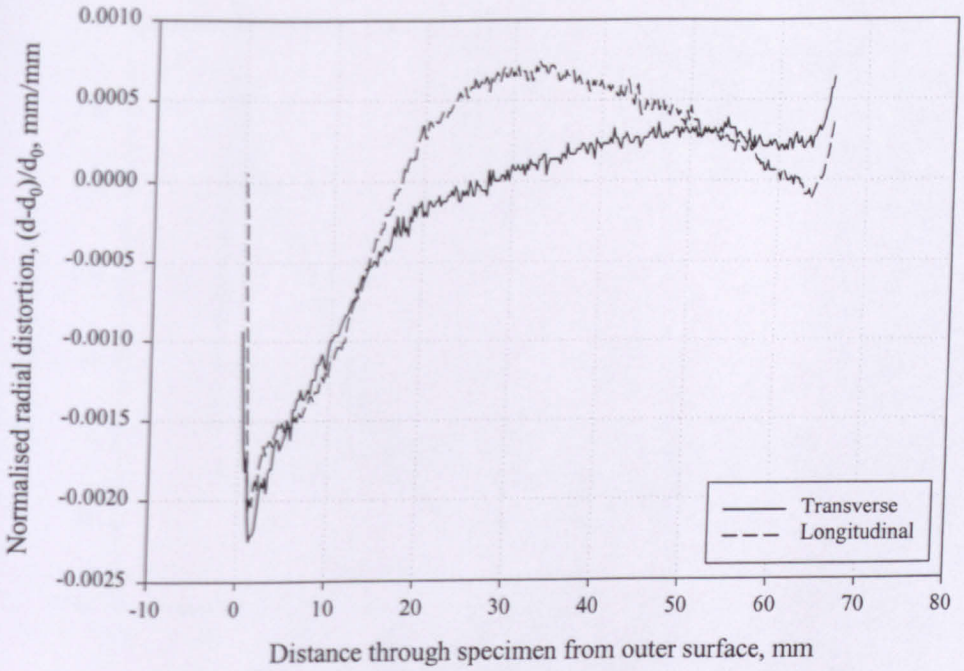

Figure 7.32 Measured normalised radial distortions in "pwr1" of the nozzle-pipe T-section T4

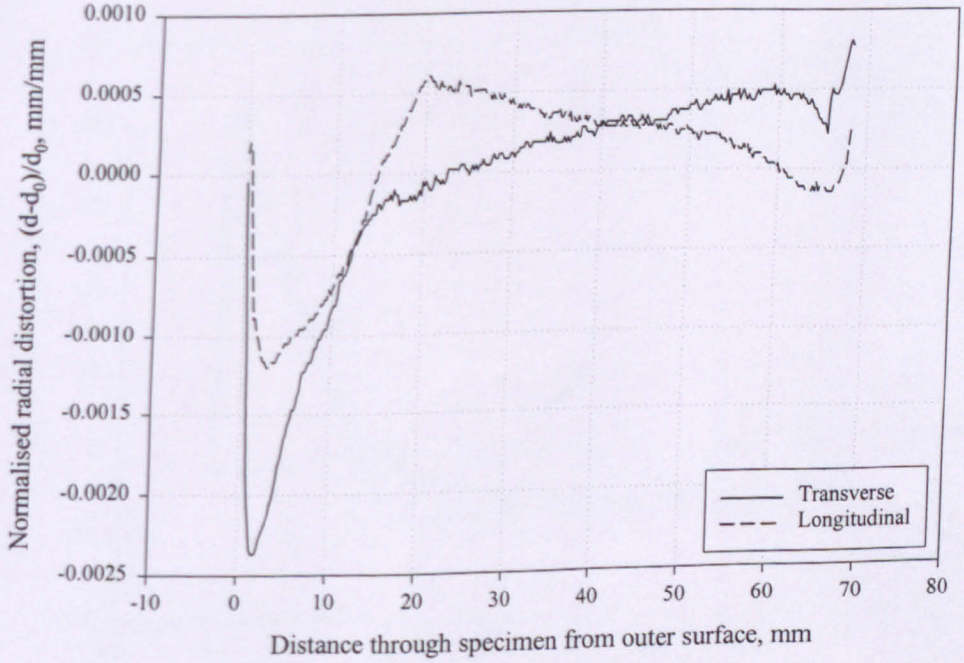

Figure 7.33. Measured normalised radial distortions in "pwr2" of the nozzle-pipe T-section T5

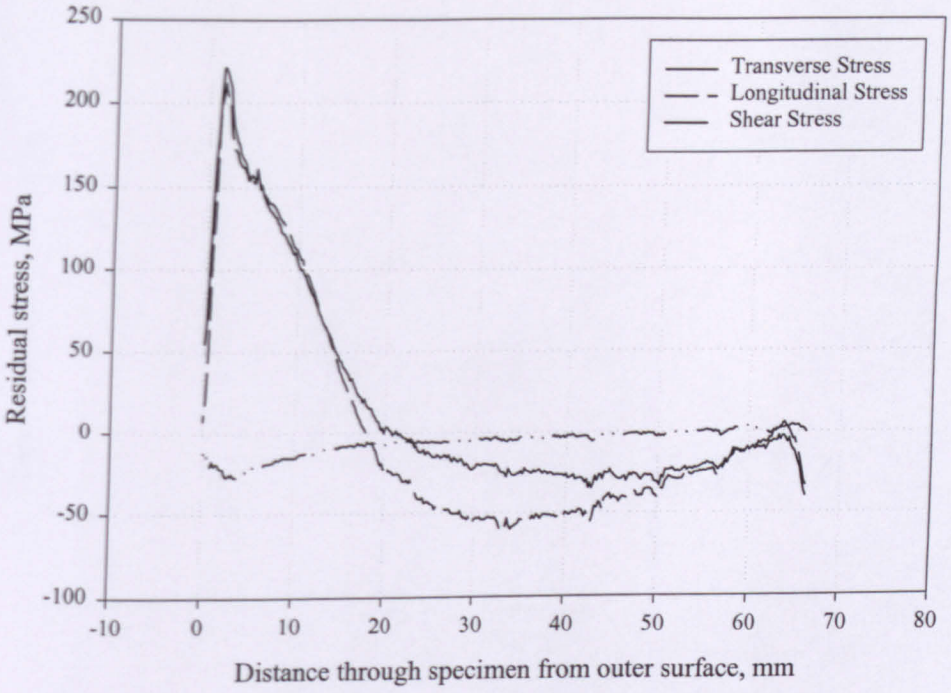

Figure 7.34. Measured residual stresses in "pwr1" of the nozzle-pipe T-section T4

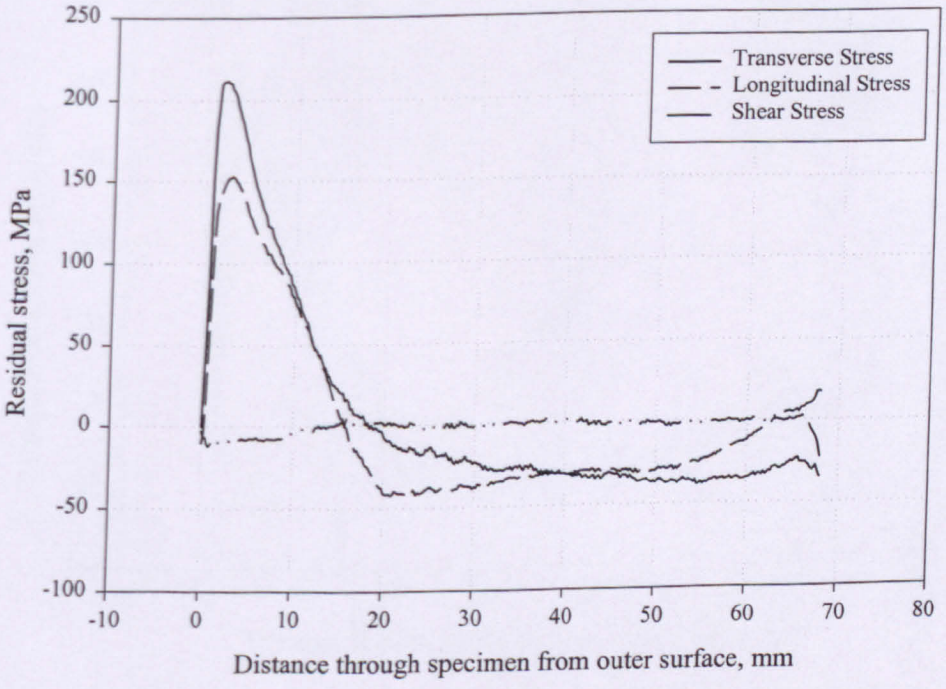

Figure 7.35. Measured residual stresses in "pwr2" of the nozzle-pipe T-section T5

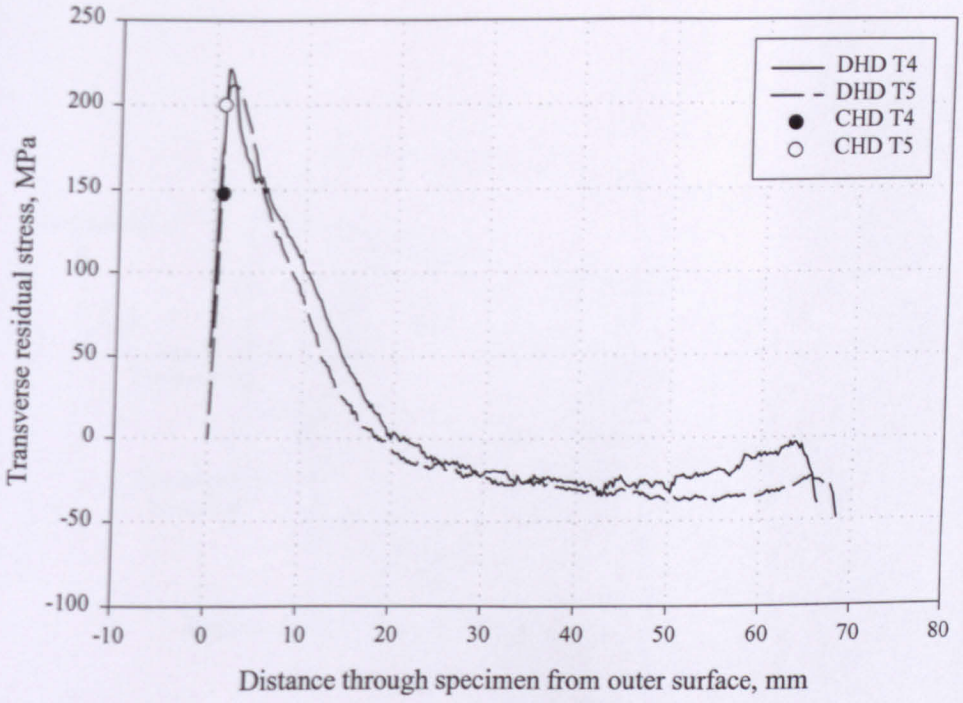

Figure 7.36. Measured transverse residual stresses using DHD and CHD in "pwr1" and "pwr2" of the nozzle-pipe T-sections, T4 and T5

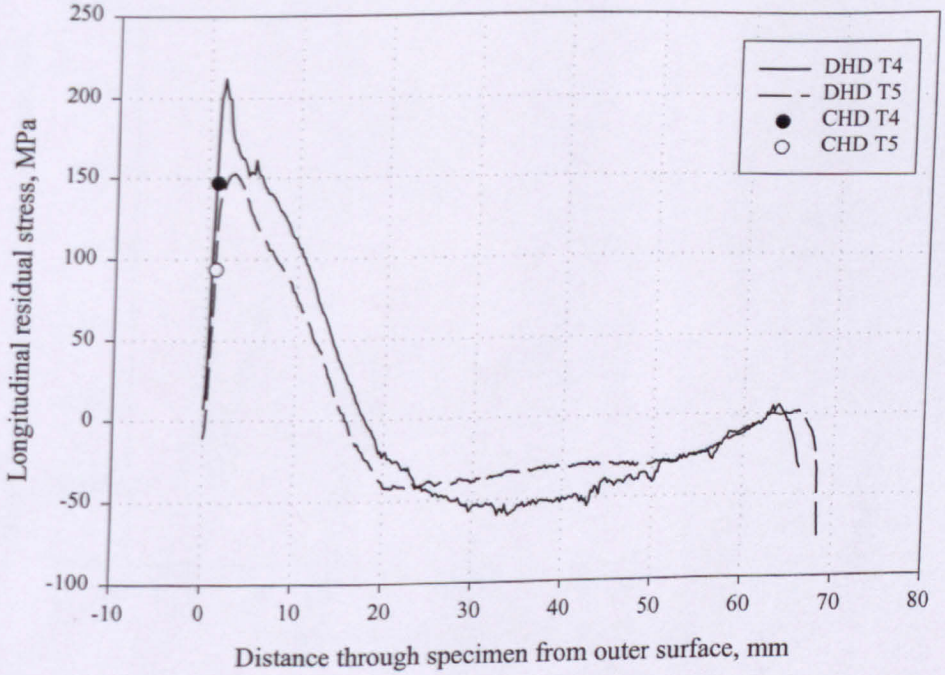

Figure 7.37. Measured longitudinal residual stresses using DHD and CHD in "pwr1" and "pwr2" of the nozzle-pipe T-sections, T4 and T5

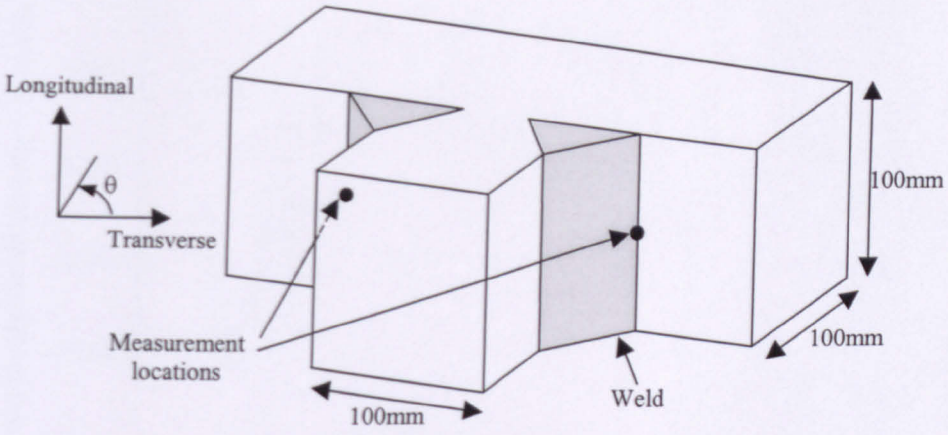

Figure 7.38. Design of the butt-welded T-section

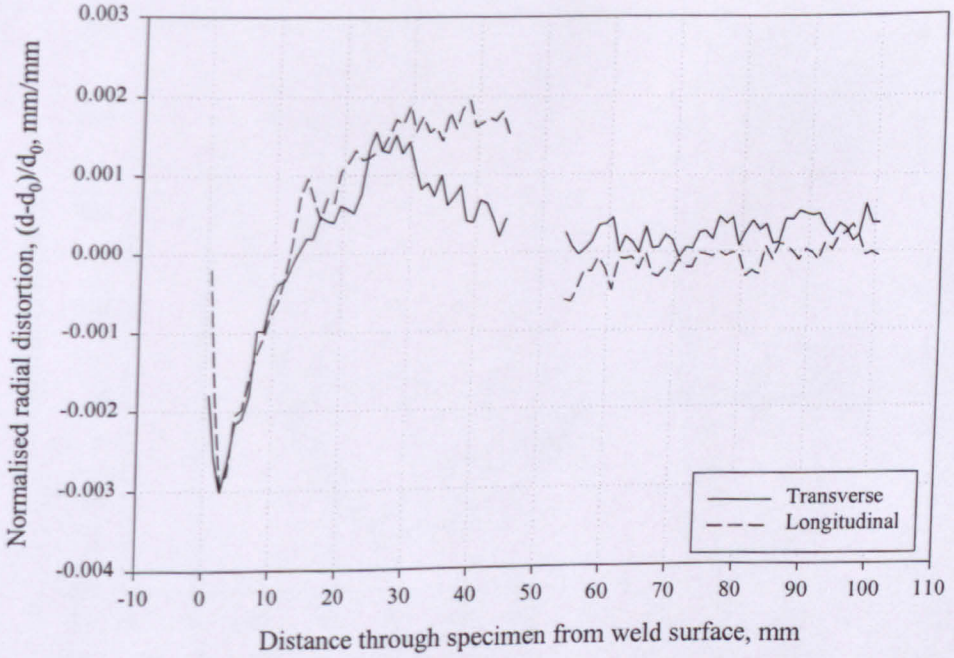

Figure 7.39. Smoothed normalised radial distortions measured in the butt-welded T-section at location 1

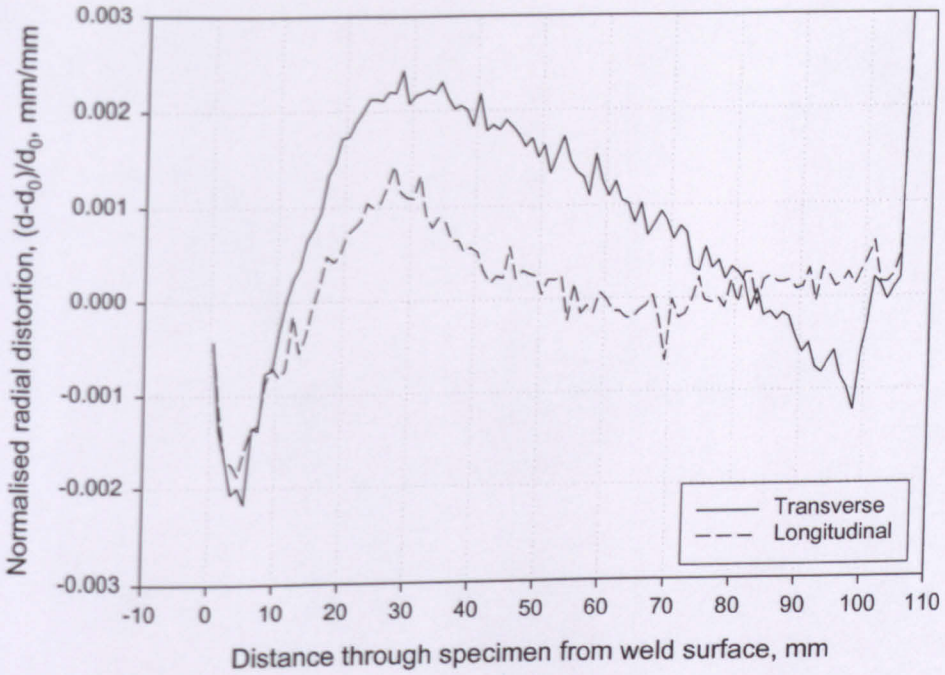

Figure 7.40. Smoothed normalised radial distortions measured in the butt-welded T-section at location 2

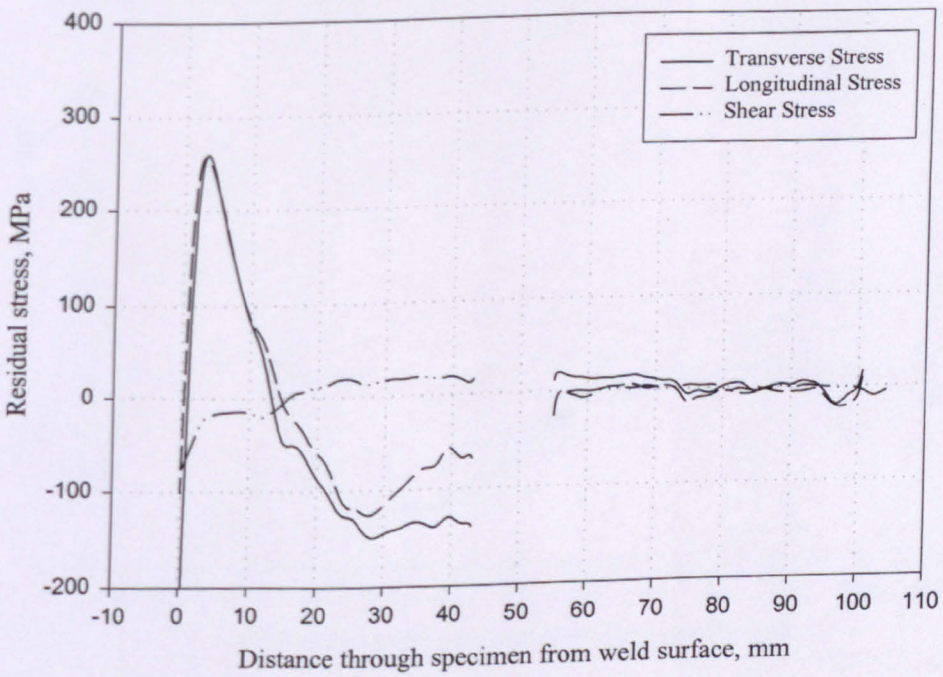

Figure 7.41. Smoothed residual stresses measured in the butt-welded T-section at location 1

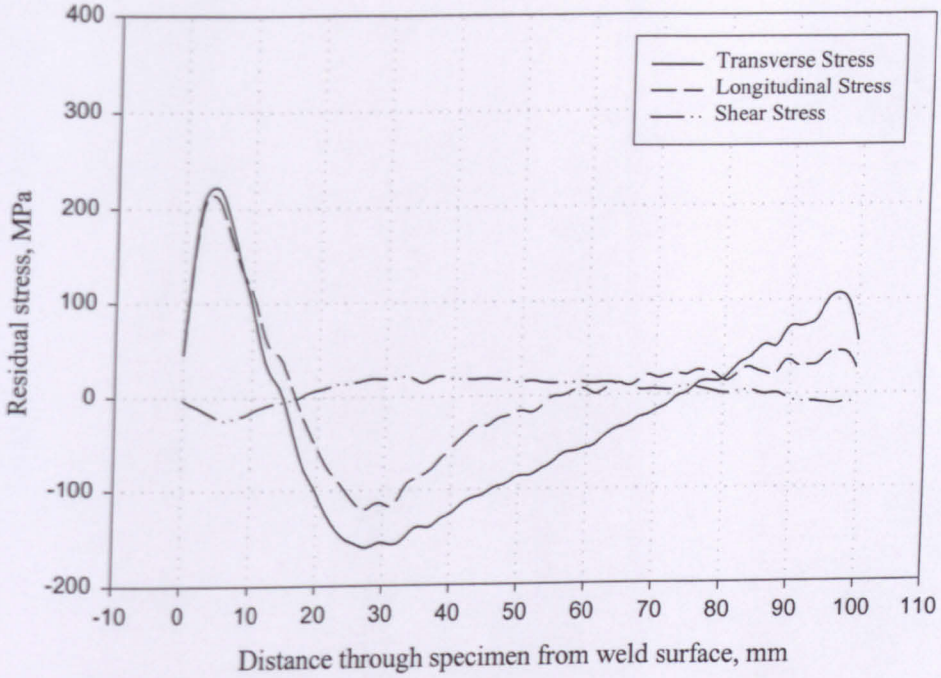

Figure 7.42. Smoothed residual stresses measured in the butt-welded T-section at location 2

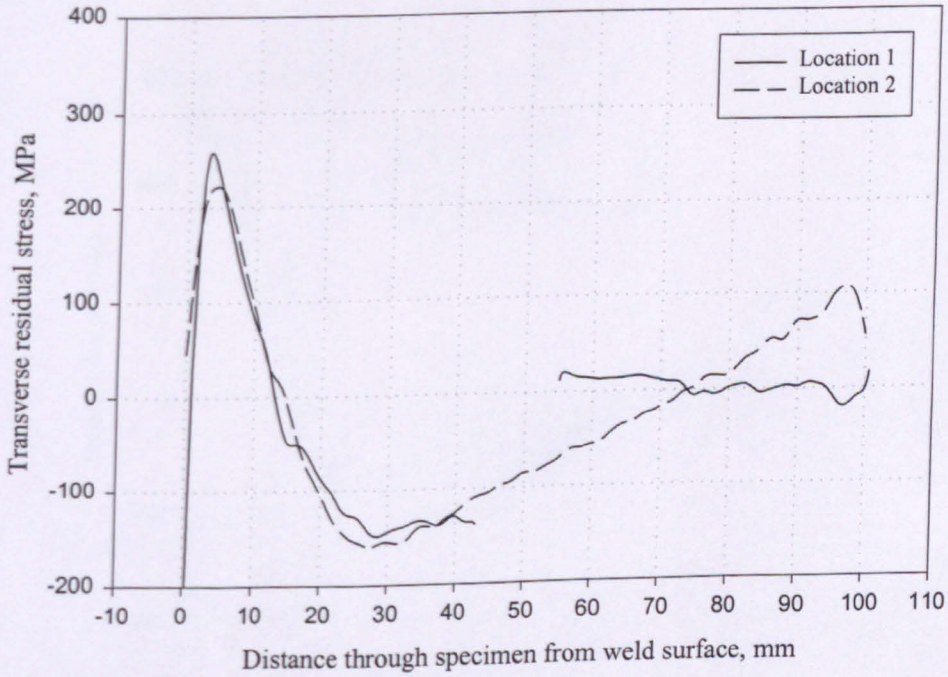

Figure 7.43. Measured transverse residual stresses in the butt-welded T-section at locations 1 and 2

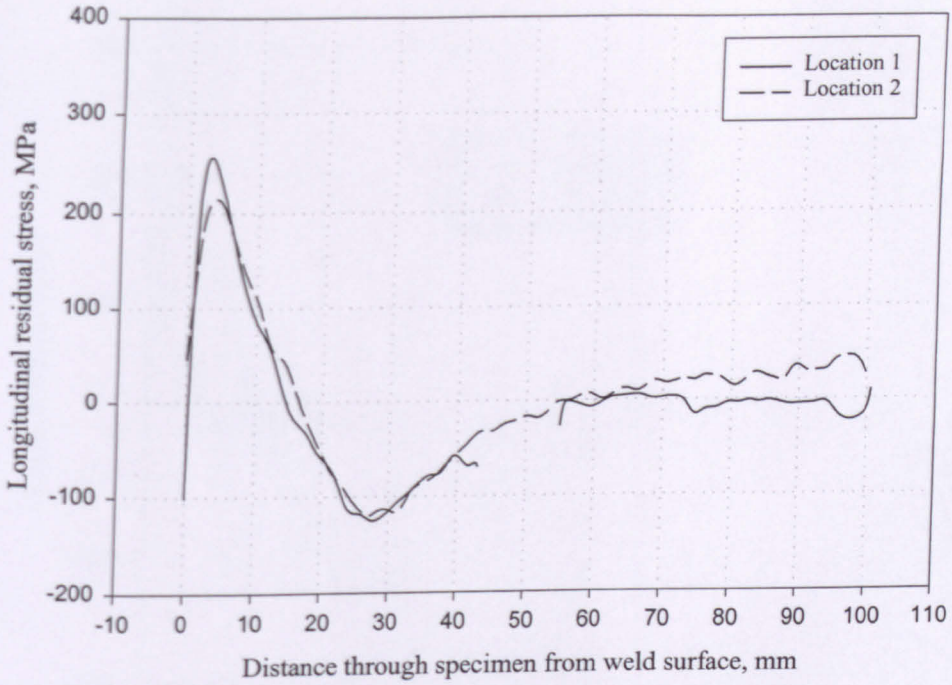

Figure 7.44. Measured longitudinal residual stresses in the butt-welded T-section at locations 1 and 2

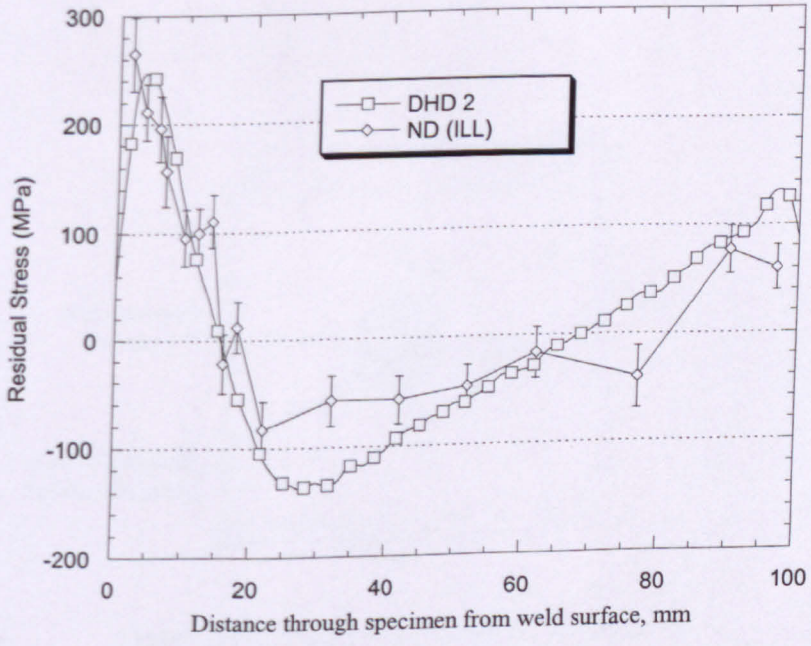

Figure 7.45. Measured transverse residual stresses in the butt-welded T-section using DHD and ND (Source: Wimpory et al [2003])

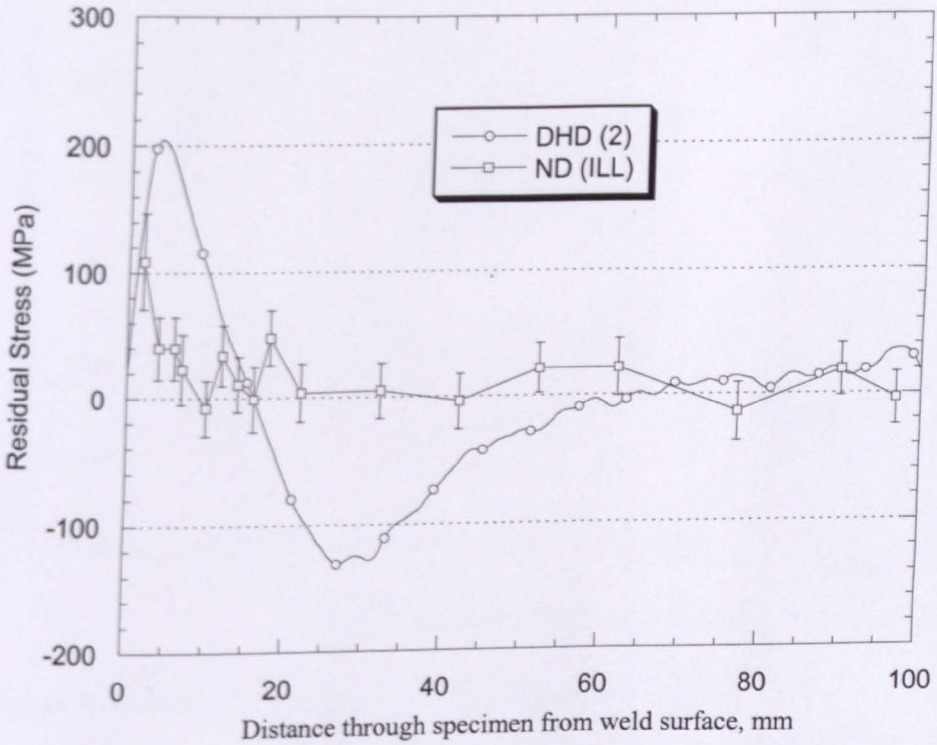

Figure 7.46. Measured longitudinal residual stresses in the butt-welded T-section using DHD and ND (Source: Wimpory et al [2003])

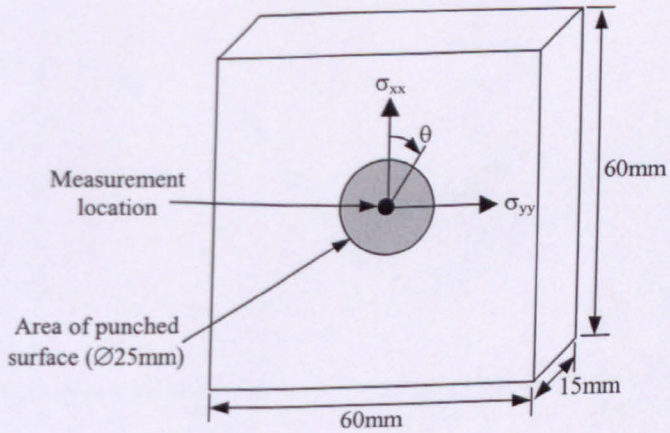

Figure 7.47. Design of aluminium punched plate

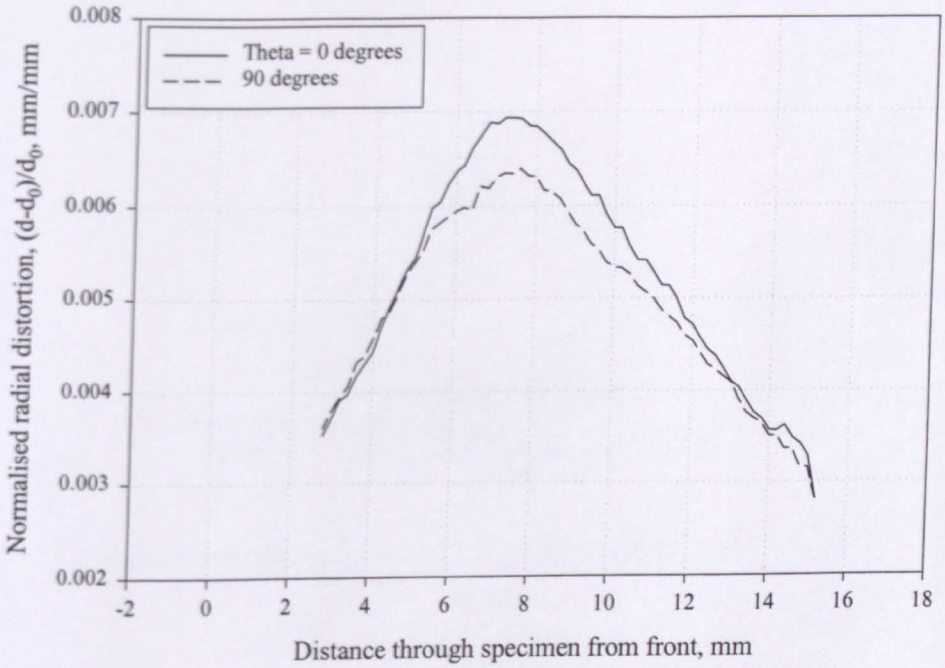

Figure 7.48. Measured normalised radial distortions in aluminium punched plate

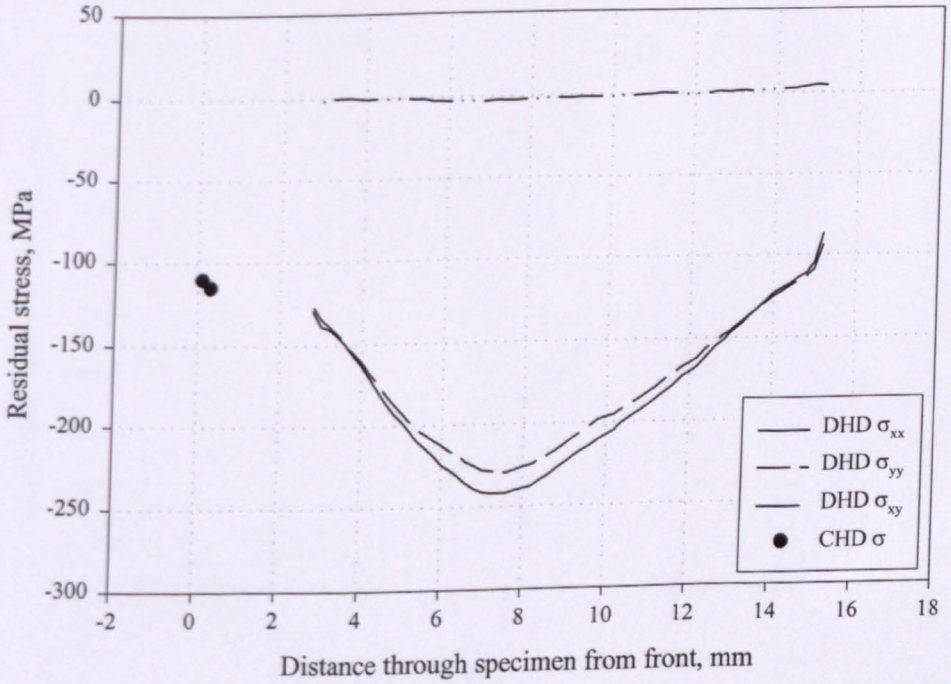

Figure 7.49. Measured residual stresses in aluminium punched plate using DHD and CHD

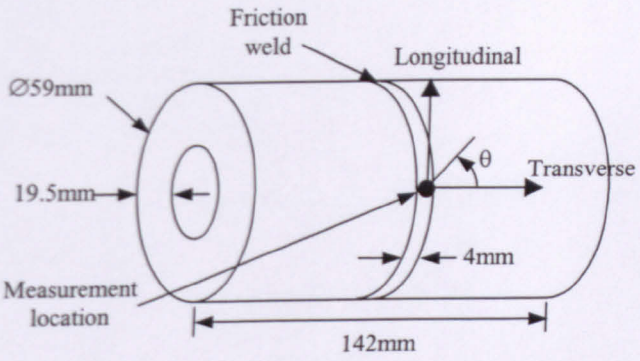

Figure 7.50. Design of the titanium friction welded component

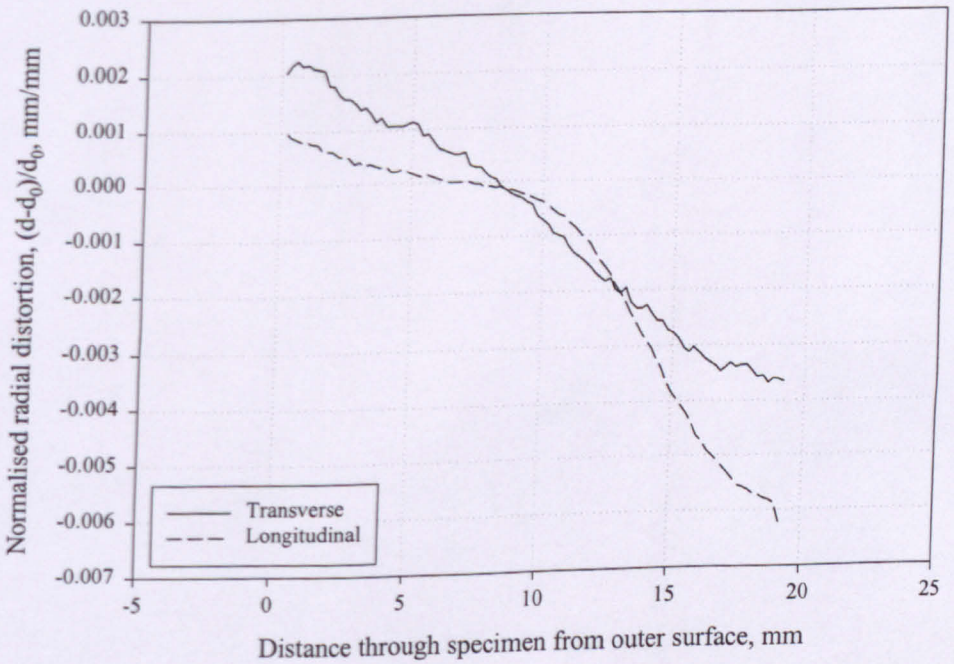

Figure 7.51. Measured normalised radial distortions in the titanium friction welded component

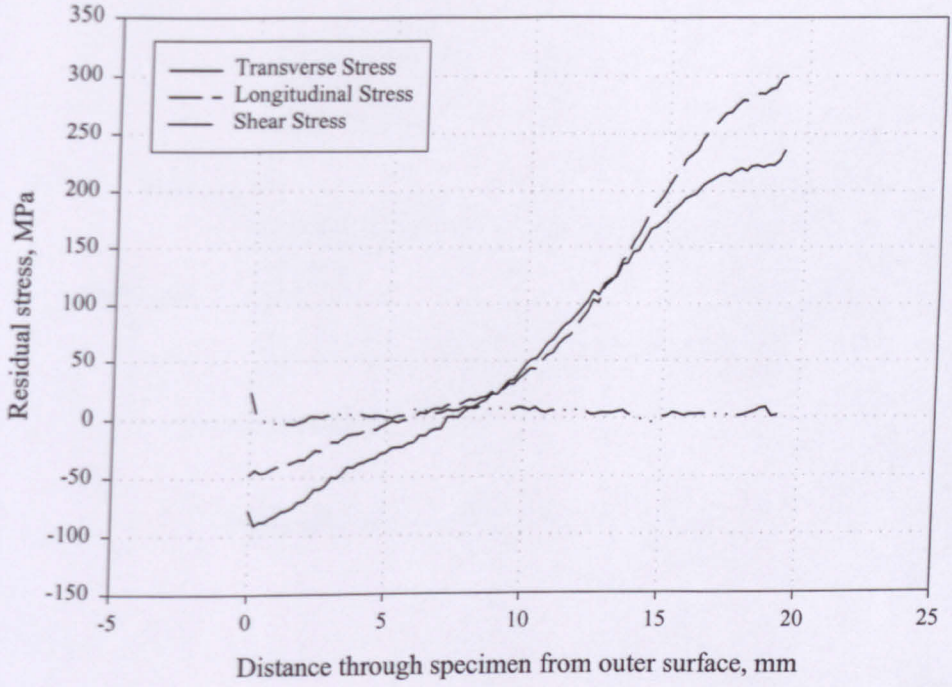

Figure 7.52. Measured residual stresses in the titanium friction welded component

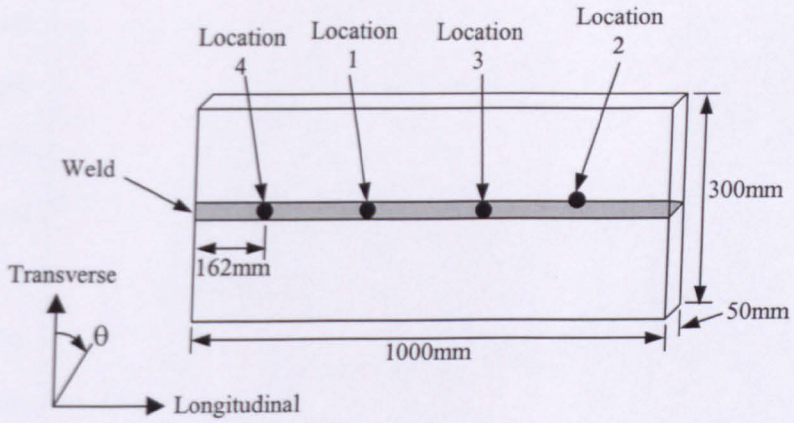

Figure 8.1. Design of the butt-welded plate

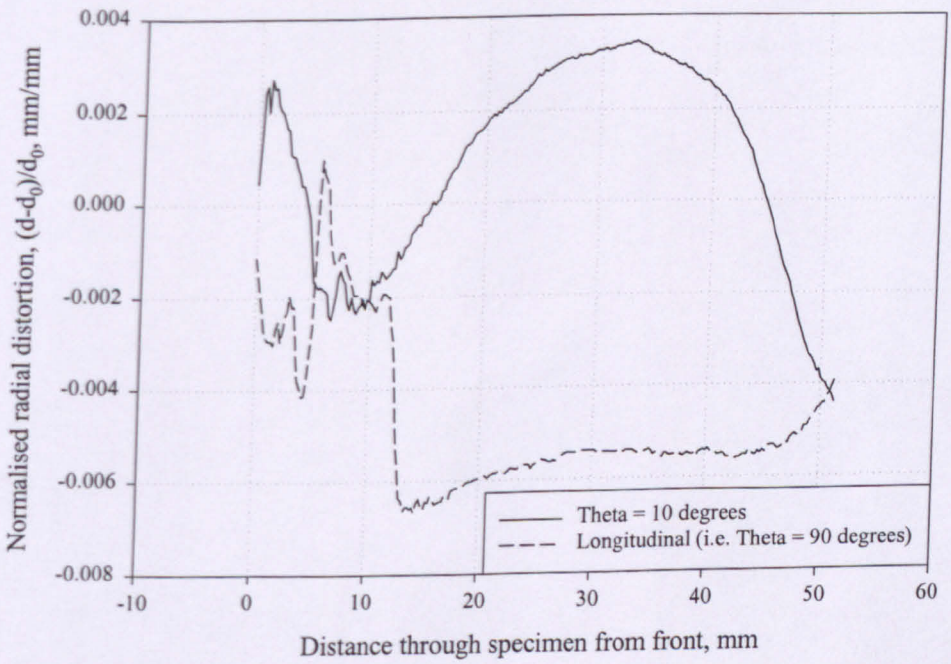

Figure 8.2. Normalised radial distortions measured in the butt-welded plate at location 4

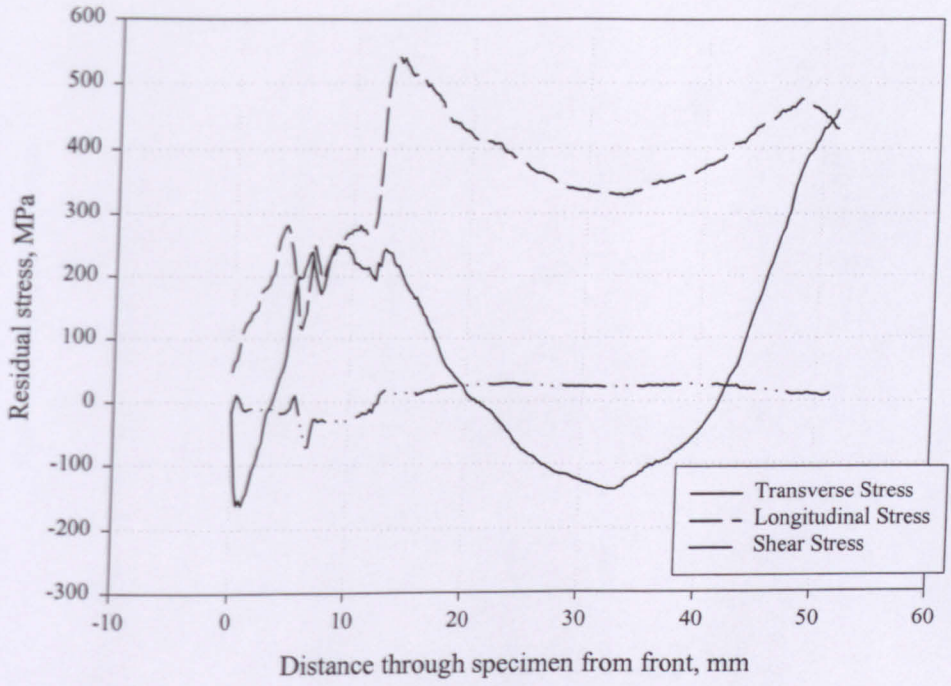

Figure 8.3. Measured residual stresses in the butt-welded plate at location 4

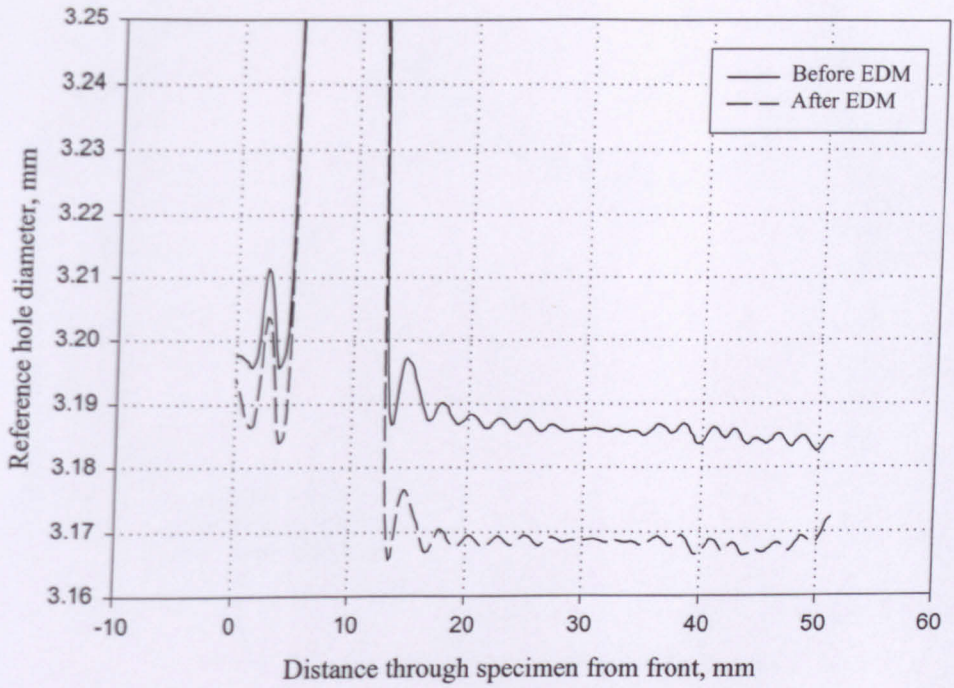

a) Longitudinal to the weld

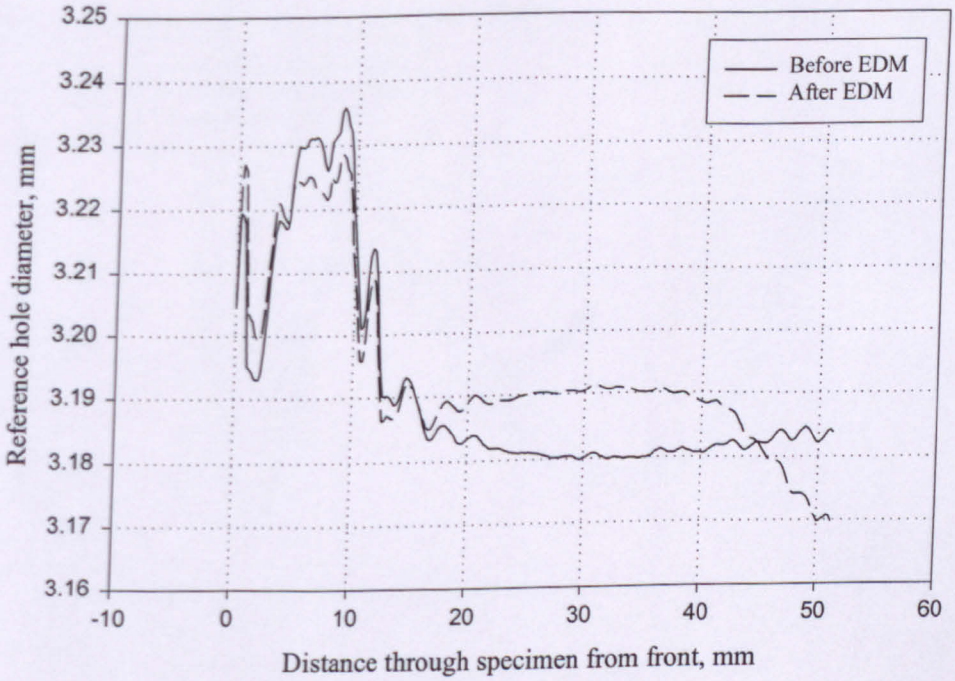

b) Transverse to the weld

Figure 8.4. Measured reference hole diameter at location 4

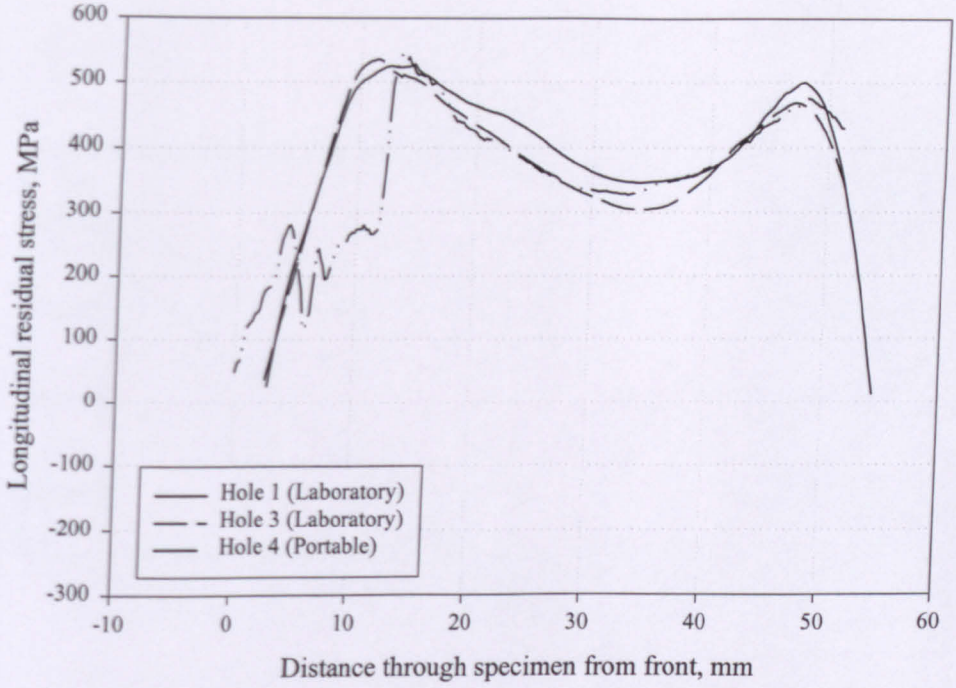

Figure 8.5. Measured longitudinal residual stresses at holes 1, 3, and 4

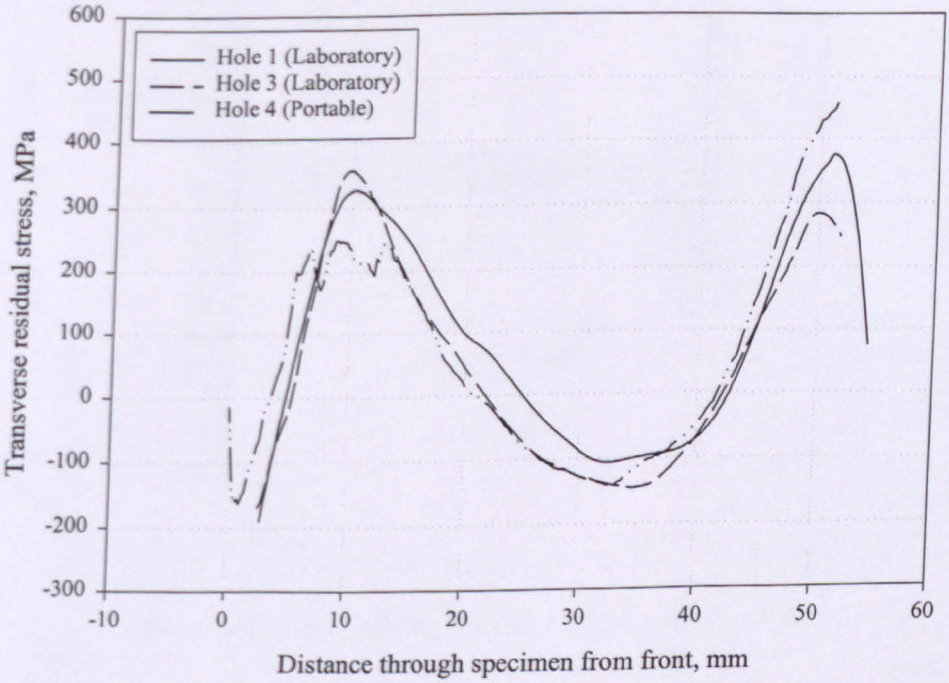

Figure 8.6. Measured transverse residual stresses at holes 1, 3, and 4

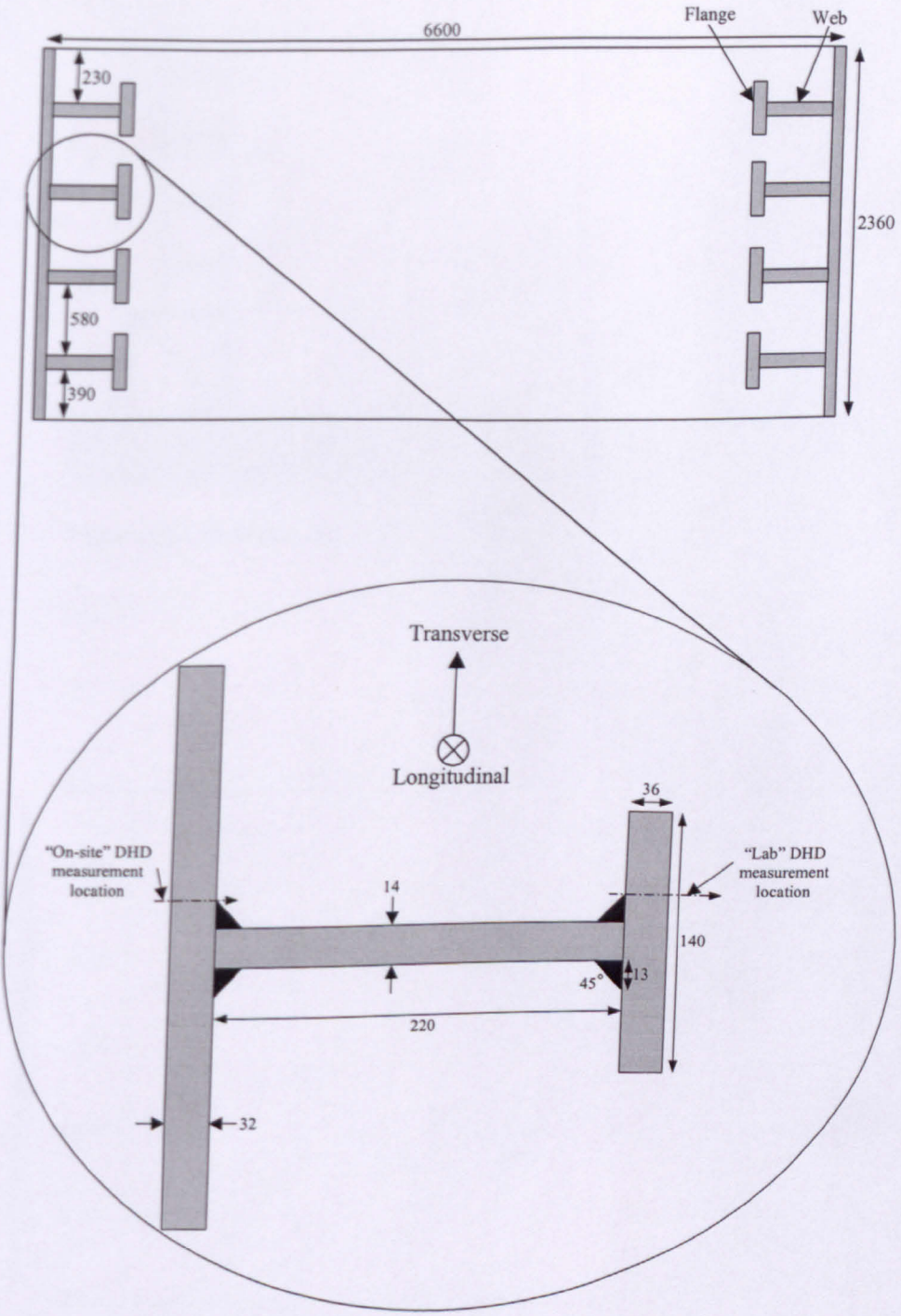

Figure 8.7. Cross-section and detail of the submarine hull

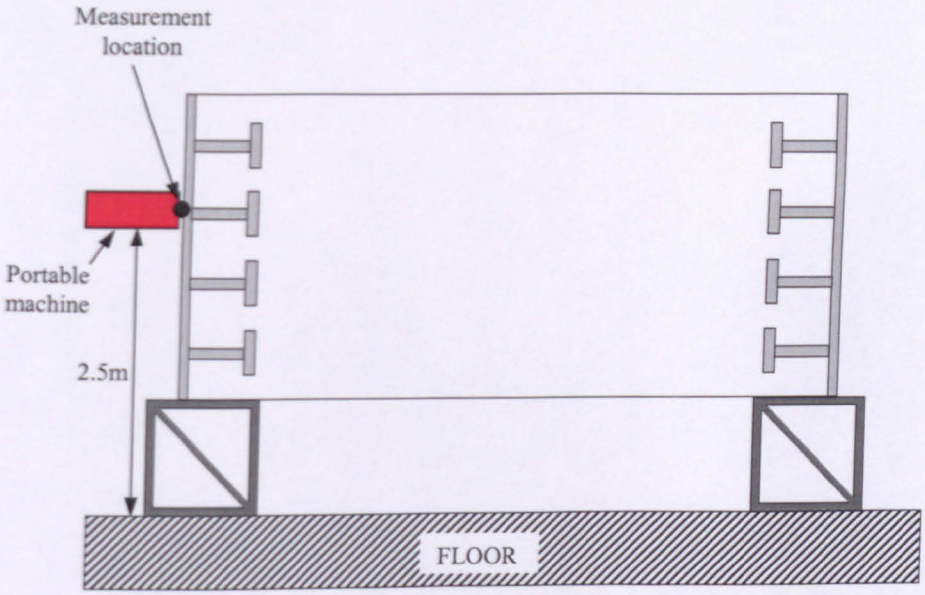

Figure 8.8. Machine and measurement locations on the submarine hull

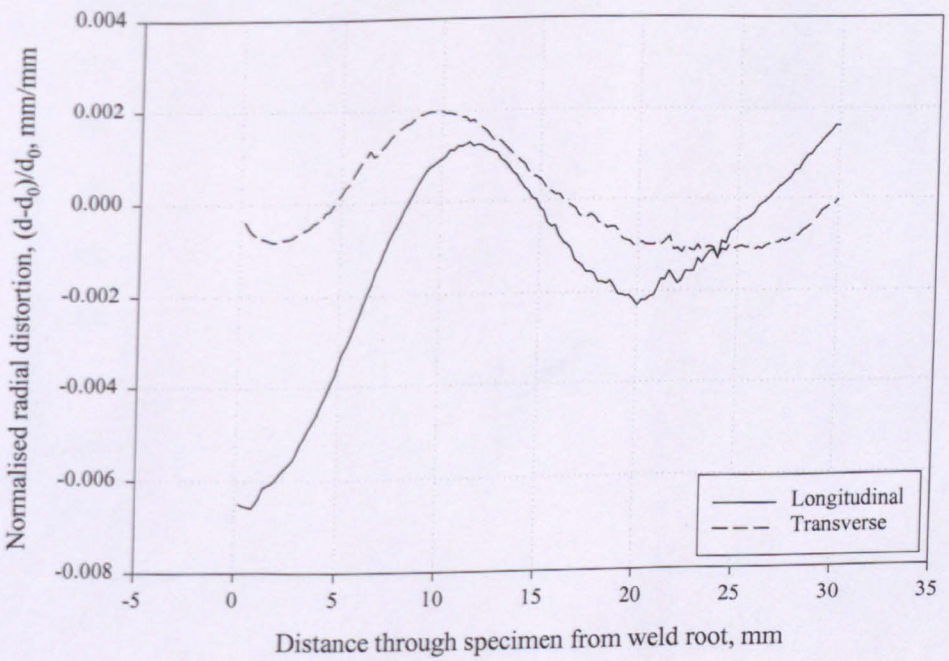

Figure 8.9. Normalised radial distortions measured in the full-scale submarine hull

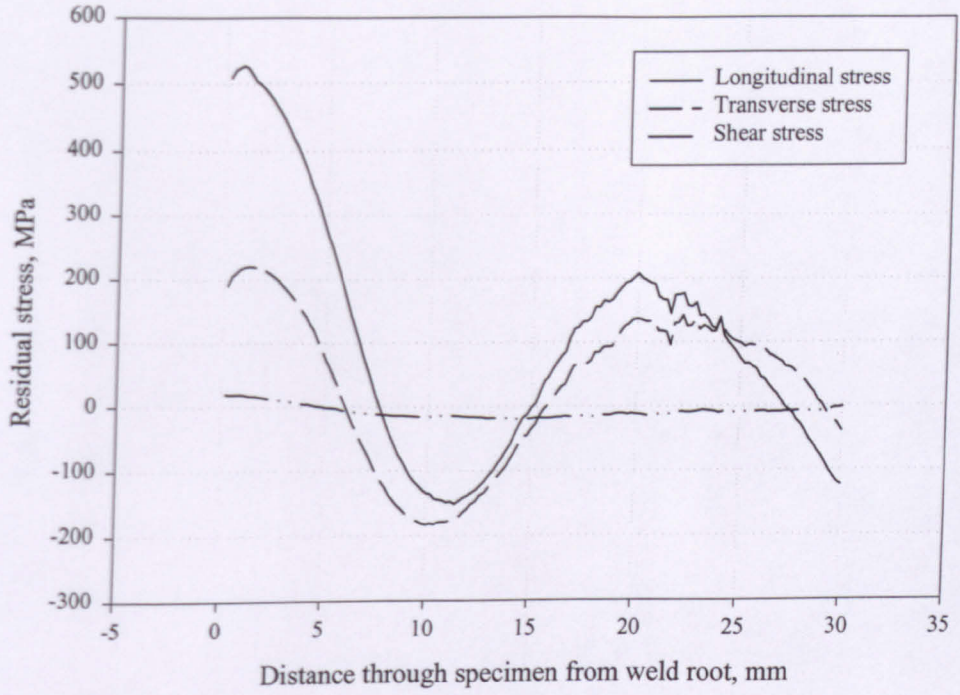

Figure 8.10. Residual stresses measured in the full-scale submarine hull

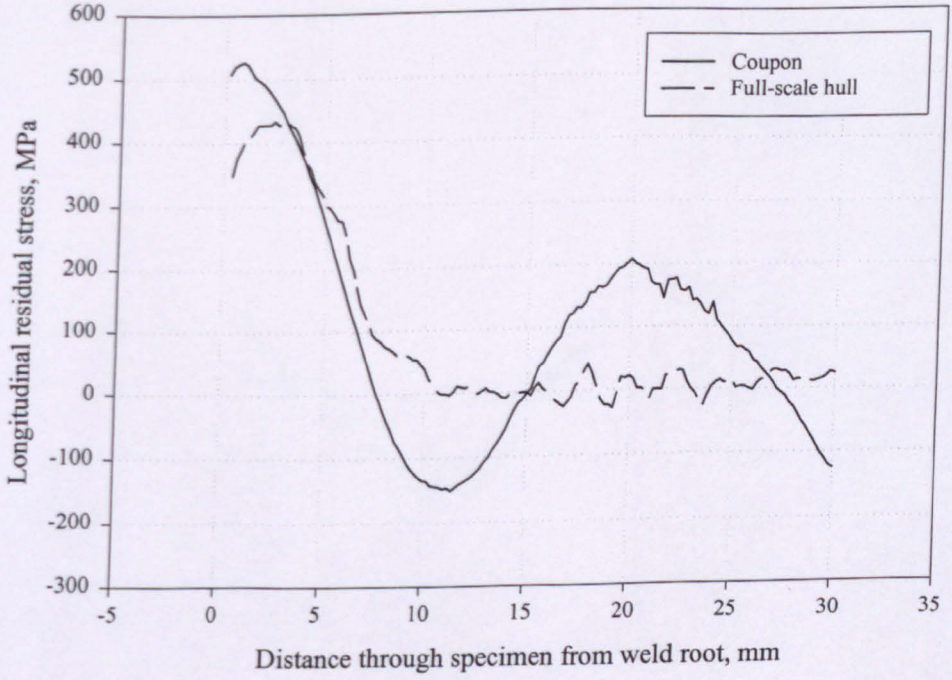

Figure 8.11. Longitudinal residual stresses measured in the coupon and full-scale submarine hull

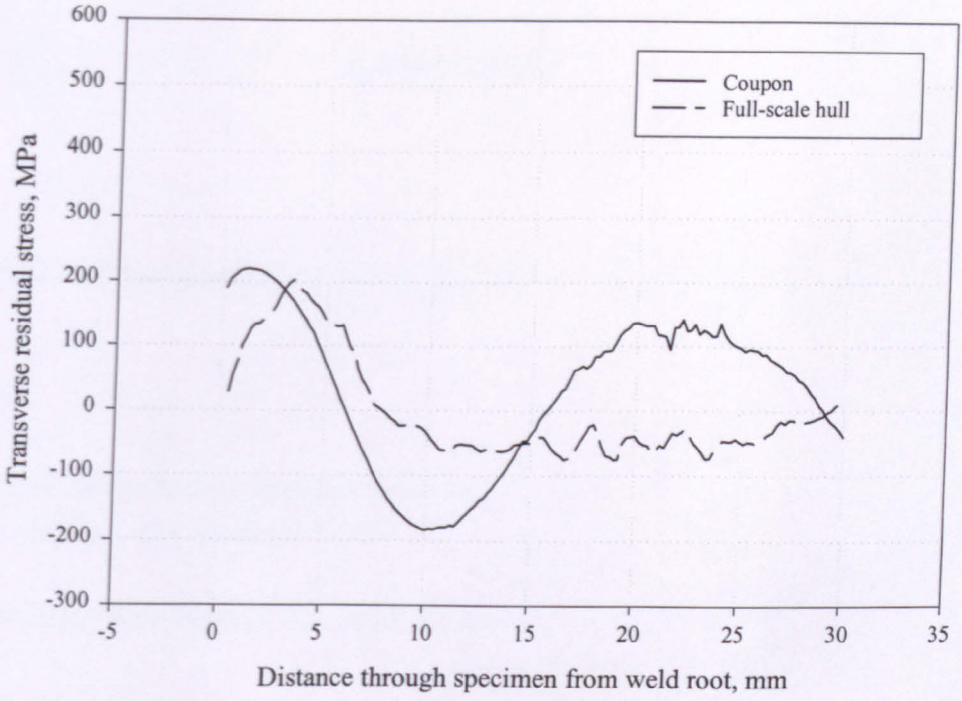

Figure 8.12. Transverse residual stresses measured in the coupon and full-scale submarine hull

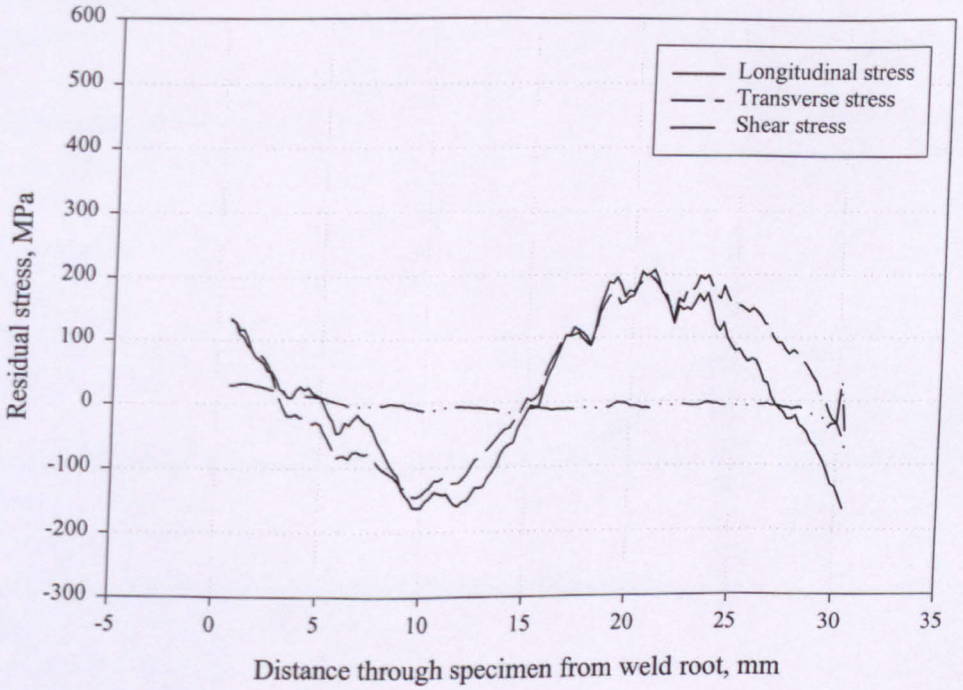

Figure 8.13. Difference between the residual stresses measured in the coupon and the full-scale submarine hull (i.e. full-scale hull – coupon)

APPENDIX A

MATLAB parameter updating procedure, used for Section 5.3.

Start

```
% Update the theoretical to fit the experimental data
%    using 3 parameters named A and B
%
% Saved as:- "E:\PhD\MatLab\DHD_Updating_z.m"
%
% User input parameters ------------------------------------------------
%
% Thickness of specimen
t=20
%
% Material properties
E=210000
%
% Angles measured
theta=(0:11.25:168.75)'
%
% Stresses acting
sx=500;
sy=0;
sxy=0;
%
% Experimental strain data in "16" rows x n columns format (n=(total depth/0.2) + zero depth column)
%
% Set-up depth vector using pBias (if linear depth settings then set pB=1)
pB=0.9;
%
% Temporary delta parameters for Sens matrix calculation
tempDelta=10
```

```
%
% End of "User input parameters" ------------------------------------------------
%
%
% Initialise parameters A and B
A=1
B=1
%
params=[A;B];
%
% M matrix including z
Miz=[A*(1+2*B*cos(2*pi*theta/180))          A*(1-2*B*cos(2*pi*theta/180))          A*(-
4*B*sin(2*pi*theta/180))];
%
% Set-up experimental strain matrix
eX=strain;
%
% Number of columns in strain matrix
n=size(strain,2);
%
% Set-up depth vector using pBias
d=ones(floor(n/2),1);
depth=zeros(n,1);
for i=2:floor(n/2)
  d(i,1)=d(i-1,1)+pB^(2*(i-1));
end
dz=(t/2)/d(floor(n/2),1);
depth(floor(n/2)+1,1)=t/2;
for j=1:floor(n/2)
  depth(floor(n/2)-j+1,1)=t/2-d(j,1)*dz;
  depth(floor(n/2)+j+1,1)=t/2+d(j,1)*dz;
end
%
% Set-up stress vector
stress=[sx;sy;sxy]
%
% Calculate initial analytical strain data
eA=-(Miz*stress)/E;
%
%Initialise recording matrices
```

```
allupparams=zeros(n,3);
allupparams(:,1)=depth;
allres=zeros(n,7);
allres(:,1)=depth;
cumupeA1=[eX(:,1) eA];
cumupeA2=[eX(:,6) eA];
cumupeA3=[eX(:,11) eA];
%
%
% For each 1mm increment in depth
for z=1:n
  % Initialise analytical strain data
  upeA=eA;
  %
  % Initialise parameters A and B
  upparams=params;
  %
  A=upparams(1);
  B=upparams(2);
  %
  % 3 iterations of updating
  for k=1:5
    % Calculate the difference between the experimental and analytical strain
    Deltae=(eX(:,z)-upeA);
    %
    % Calculate the absolute residual - its the amount by which the two sets of strain don't match
    allres(z,k+1)=sum(abs(Deltae));
    %
    % Create the sensitivity matrix
    tempMizA=[(A+(A/tempDelta))*(1+2*B*cos(2*pi*theta/180))  (A+(A/tempDelta))*(1-
2*B*cos(2*pi*theta/180)) (A+(A/tempDelta))*(-4*B*sin(2*pi*theta/180))];
    tempeAA=-(tempMizA*stress)/E;
    Sens(:,1)=(tempeAA-upeA)/(A/tempDelta);
    %
    tempMizB=[A*(1+2*(B+(B/tempDelta))*cos(2*pi*theta/180))  A*(1-
2*(B+(B/tempDelta))*cos(2*pi*theta/180)) A*(-4*(B+(B/tempDelta))*sin(2*pi*theta/180))];
    tempeAB=-(tempMizB*stress)/E;
    Sens(:,2)=(tempeAB-upeA)/(B/tempDelta);
    %
    Sens;
```

```
    %
    % SVD decomposition of Sens: Sens=U*W*V'
    [U,W,V]=svd(Sens);
    %
    % Modifies W if zero columns found
    if W(2,2)<(W(1,1)/1000)
      modW=zeros(16,1);
      modW(:,1)=W(:,1);
      W=modW;
      modV=zeros(3,1);
      modV(:,1)=V(:,1);
      V=modV;
   elseif W(3,3)<(W(2,2)/1000)
      modW=zeros(16,2);
      modW(:,1)=W(:,1);
      modW(:,2)=W(:,2);
      W=modW;
      modV=zeros(3,2);
      modV(:,1)=V(:,1);
      modV(:,2)=V(:,2);
      V=modV;
   end
   %
   % Create inverse of the singular value matrix (W)
   invW=inv(W'*W)*W';
   %
   % Create inverse of the Sens matrix
   invSens=V*invW*U';
   %
   % Calculate parameter changes
   Deltaupparams=invSens*Deltae;
   %
   % Update parameters
   upparams=upparams+Deltaupparams;
   %
   A=upparams(1);
   B=upparams(2);
   %
   % Update the M matrix
```

```
    upMiz=[A*(1+2*B*cos(2*pi*theta/180))        A*(1-2*B*cos(2*pi*theta/180))        A*(-
4*B*sin(2*pi*theta/180))];
    %
    % Calculate the updated analytical strain data
    upeA=-(upMiz*stress)/E;
    %
    % Store the updated analytical strain data
    if z==1
      cumupeA1=[cumupeA1 upeA];
    elseif z==(floor(n/4)+1)
      cumupeA2=[cumupeA2 upeA];
    elseif z==(floor(n/2)+1)
      cumupeA3=[cumupeA3 upeA];
    end
  end
  %
  % Calculate the final difference between the experimental and analytical strain
  Deltae=(eX(:,z)-upeA);
  %
  % Store the updated parameters and residuals for each 0.2mm depth increment
  allupparams(z,2)=A;
  allupparams(z,3)=B;
  %
  allres(z,7)=sum(abs(Deltae));
 end
 %
 allupparams
 allres
 %upStress
 cumupeA1
 cumupeA2
 cumupeA3
 %
 % Average parameter values
 Aave=0;
 Bave=0;
 z=0;
 for j=1:(size(allupparams,1)-0)
 Aave=Aave+allupparams(j,2);
 Bave=Bave+allupparams(j,3);
```

```
z=z+1;
end
Aave=Aave/z
Bave=Bave/z
%
subplot(2,2,1); plot(theta,cumupeA1)
xlabel('Theta, degrees')
ylabel('Strain')
title('Strain during parameter updating at 0mm')
legend('eX', 'eA', 'upeA 1', 'upeA 2', 'upeA 3', 'upeA 4', 'upeA 5',1)    % Position 1=upper right or
4=lower right
%
subplot(2,2,2); plot(theta,cumupeA2)
xlabel('Theta, degrees')
ylabel('Strain')
title('Strain during parameter updating at 1/4-thickness')
%
subplot(2,2,3); plot(theta,cumupeA3)
xlabel('Theta, degrees')
ylabel('Strain')
title('Strain during parameter updating at 1/2-thickness')
%
subplot(2,2,4); plot(depth,allupparams(:,2),depth,allupparams(:,3))
xlabel('Depth, mm')
ylabel('Parameter value')
title('Updated parameter values through the thickness of the specimen')
legend('A', 'B',0)
```

End